INTRACELLULAR CONSIDERATIONS IN THE DEVELOPMENT OF NON-VIRAL NUCLEIC ACID DELIVERY SYSTEMS FOR SYSTEMIC ADMINISTRATION

Thesis by

Swaroop Mishra

In Partial Fulfillment of the Requirements

for the Degree of

Doctor of Philosophy

California Institute of Technology

Pasadena, California

2006

(Defended September 19, 2005)

ACKNOWLEDGMENTS

My thanks go to all the teachers and mentors who have encouraged, supported, and inspired me, including Eleanor Metz, Joy McManus, Ray Brinjak, Steve Grimes, Bruce Hislop, Margaret Wildermann, Eileen Mattingly, Richard Houchens, Tom Shaffer, Dan Stack, Robert Pecora, Channing Robertson, and Ed Larenas.

My research accomplishments are due in large part to the encouragement and guidance of my advisor, Mark Davis. I appreciate his steadfast confidence in my abilities and his patience through the less productive periods. I also am deeply grateful for the guidance of Paul Webster, whose tutorials in electron microscopy have been central to my accomplishments and whose consistent and generous support has been invaluable to me. I appreciate the time and attention of my committee members: David Tirrell, Scott Fraser, and Anand Asthagiri. Given their busy schedules, it has been kind of them to play a role in my course of study.

It has been a pleasure to work with my colleagues in the Davis Laboratory and elsewhere at Caltech. Suzie Hwang Pun and Nathalie Bellocq kindly introduced me to conducting research in non-viral gene delivery. I have enjoyed working with Raj Kulkarni, Ryan Zeidan, and Jianjun Cheng, all of whom have been generous while making substantial and valuable contributions to my work. Much of my research was conducted in the company of John Murphy, Jeremy Heidel, Steve Popielarski, Derek Bartlett, and Greg Jensen, and I've enjoyed their advice, assistance, and good humor.

I appreciate the attention and responsiveness of everyone at the Caltech Biological Imaging Center, including Andy Ewald, Anita Gould, Dan Darcy, and Chris Waters. Also, I could not have completed my work in electron microscopy without the

kind assistance of Siva Wu. I am sure that her supervisor, Dr. Webster, must share my thorough appreciation of her pleasant disposition, diligent and organized efforts, and growing expertise.

My work has been made much easier thanks to many reliable and helpful staff members at Caltech, including Steve Gould, Lillian Kremar, Joe Drew, Moses Renteria, Terrance James, Cora Carriedo, and Carlos Hernandez. Kathy Bubash and Martha Hepworth are two of the chemical engineering department's most effective professionals as well as two of its most pleasant people. Finally, my thanks to Efrain Hernandez for the warmth and sincerity he brings to the basement of Spalding.

ABSTRACT

Non-viral nucleic acid delivery systems must condense nucleic acids into small particles, confer protection from degrading factors in serum and in cells, achieve uptake to targeted cells, direct nucleic acids to appropriate intracellular destinations, release this cargo to permit its action, and exhibit minimal toxicity. The nature of synthetic vectors allows for facile addition of new features, but these modifications can affect performance in unanticipated ways. The effective combination of functional components necessitates a systems approach, where the materials design simultaneously considers the functional environment of and the various barriers to delivery. This thesis facilitates and promotes a systems approach by undertaking development of an improved mechanistic understanding of non-viral gene transfer in vitro, emphasizing elucidation of delivery vehicles' interactions with and behavior within cells. Special attention is given to the gene delivery behavior of cyclodextrin-containing polycations.

Simple modifications to delivery systems can have unanticipated consequences. In Chapter 2, it is shown that greater distance between toxicity-reducing cyclodextrin moieties and amidine charge centers increases both the transfection efficiency and toxicity of a polycationic vector. Chapter 3 shows data demonstrating that modification with poly(ethylene glycol) for extracellular salt-stabilization alters non-viral gene delivery particles' intracellular trafficking and resulting gene expression. Taken together, the results reveal that non-viral gene delivery vehicles behave as assembled, multifunctional systems.

pH-buffering components exhibit complex behavior in non-viral gene delivery. In Chapter 4, the intracellular activity of such components is quantified using confocal

microscopy. Analysis of chloroquine and its chemical analogues demonstrates in Chapter 5 that chloroquine improves non-viral gene transfer through pH-buffering as well as through enhanced nucleic acid unpackaging and its own interactions with nucleic acids. Chapter 6 gives results that characterize delivery behavior of analogous vectors with and without pH-buffering capacity and show that factors beyond buffering activity contribute to improved transfection efficiency. Collectively, these results emphasize consideration of new system components' effects on all functions of a non-viral gene delivery system.

A systems approach requires comprehensive consideration of the gene delivery process. Chapter 7 reviews current understanding of intracellular barriers to non-viral gene delivery, and Chapter 8 offers recommendations for future work.

TABLE OF CONTENTS

LIST OF FIGURES, SCHEMES, AND TABLES

CHAPTER 1: INTRODUCTION

1.1 Introduction

Molecular conjugates are nanometer-sized entities consisting of synthetic materials (lipids, polycations, targeting agents, etc.) and nucleic acids. These composites are delivery vehicles that function to transport nucleic acids to sites of action. Such systems can avoid the DNA-size limitations and immunogenicity that are possible with some viral delivery vectors, and their straightforward formulation with easily-manufactured, relatively low-cost materials could be useful in preparing large-scale therapeutics at acceptable costs. If their therapeutic indices can be improved, non-viral gene delivery vectors will likely be used in a wide range of medical applications.

Non-viral gene delivery vectors must exhibit a variety of properties to achieve their function. First, they must condense nucleic acids into small particles (ca. 100 nm or less) and confer protection from degrading factors that exist in serum and in cells. The gene delivery particles must be taken up by cells that have been targeted, direct the nucleic acids to an appropriate intracellular destination (cytoplasm for small interfering RNA (siRNA) and nucleus for plasmid DNA (pDNA)), release the nucleic acids to allow for their action, and exhibit minimal toxicity (Figure 1.1). Although the limiting intracellular barrier(s) to non-viral gene delivery remain(s) poorly defined, many recent approaches have sought to better understand and enhance: (i.) escape from the endocytic pathway, (ii.) vector unpackaging, (iii.) cytoplasmic persistence of nucleic acids, and (iv.) nuclear delivery. A further intracellular barrier that has not been extensively addressed is the poor cytoplasmic mobility of large nucleic acids.

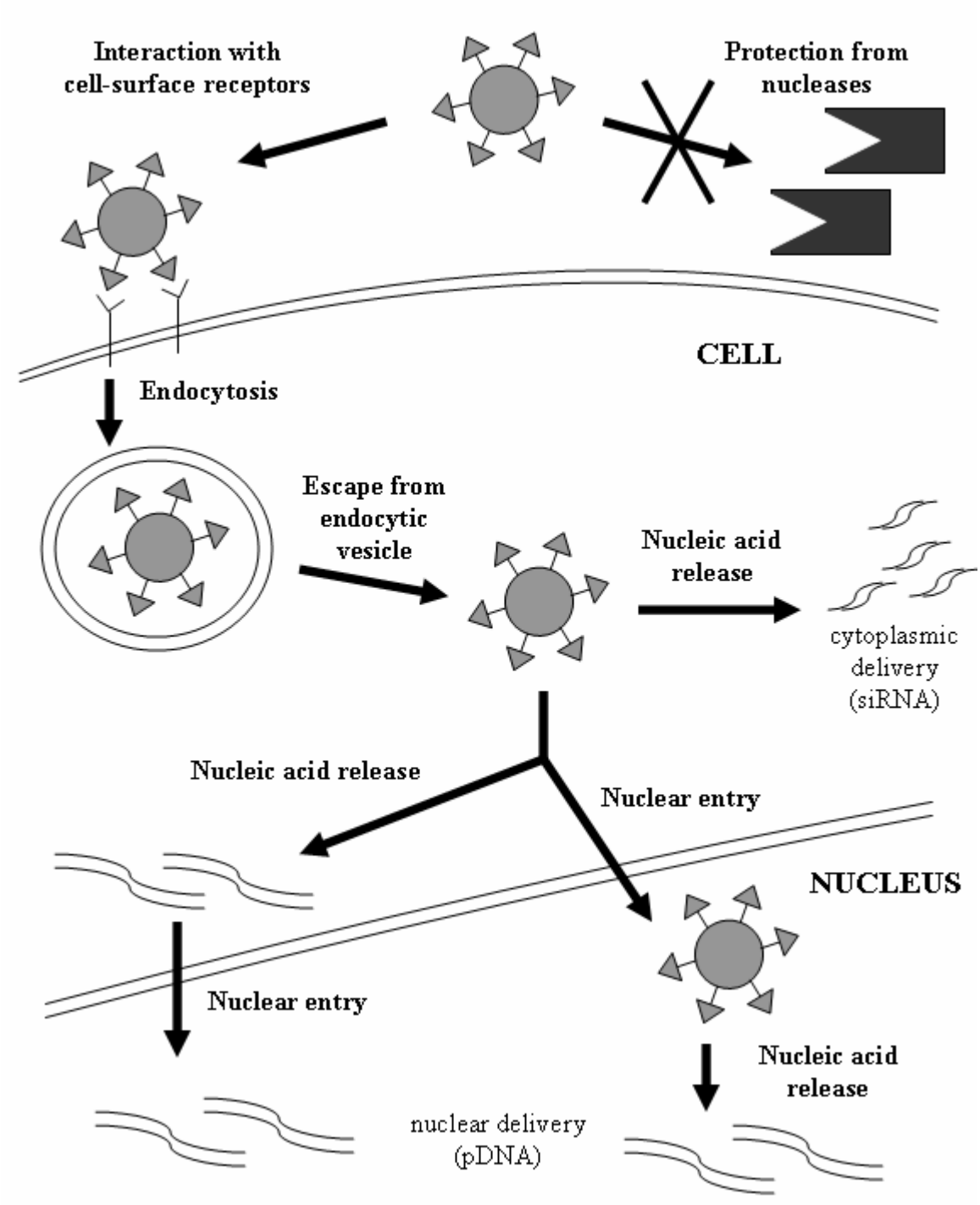

Figure 1.1 Functions of molecular conjugates
Molecular conjugates must bind and condense nucleic acid payloads, protect nucleic acids from nuclease degradation, allow for cellular uptake, facilitate escape from endocytic vesicles, and release the nucleic acids to permit their function. It remains unclear if pDNA must be released from the vector prior to nuclear entry or should be directed to the cell nucleus within intact vector-pDNA complexes.

The development of molecular conjugates has followed an additive process where the perceived challenges are addressed by a variety of modifications, the most successful of which are then incorporated into existing systems. Initially, existing materials were evaluated for their ability to bind and condense nucleic acids and mediate transfection of cultured cells [1-3]. These early non-viral systems showed little in vivo applicability due to shortcomings such as high toxicity, instability to physiological salt and serum, and poor transfection efficiency. However, the synthetic nature of non-viral systems allows for facile, well-defined modification, facilitating incorporation of new components to address specific barriers to delivery. Early attempts to improve transfection efficiency included addition of cell-targeting ligands such as transferrin [4-6] or saccharides [7-9], or addition of membrane-destabilizing peptides [2,7,10]. In an effort to boost transfection efficiency of non-viral vectors, some researchers began incorporating viral peptides [11-15] or transfecting cells in the presence of chemical agents [16-18]. To facilitate escape from the endocytic pathway, various researchers have added buffering moieties such as histidine [19-21].

These modified systems have not displayed sufficient improvements in performance, prompting synthesis of new materials designed to overcome the shortcomings of their predecessors. Various groups have sought to build vectors with fusogenic properties [22] or buffering moieties [23-24]. Other groups have constructed materials with an emphasis on reduced toxicity [25-27]. When novel materials have been found inadequate, researchers have reverted to an additive approach, modifying the new materials with functionalities similar to those that had previously been added to the first generation of materials [28].

A considerable challenge in the field of molecular conjugates is building a workable system that exploits the combined attributes of the components without suffering losses due to the assembly of the system. Modifications of existing systems, as described above, have brightened the prospects for effective in vivo gene delivery. However, these alterations, often involving changes to the chemical structure of the delivery vectors or nucleic acids, have also affected gene delivery performance in unanticipated ways. For example, we have demonstrated that conferring salt stability to polyethylenimine-DNA complexes with a poly(ethylene glycol) coating dramatically changes the morphology of the endocytosed entities and significantly reduces the resulting gene expression in vitro [29].

As molecular conjugates are designed to contain a combination of functional components, it is likely that engineered systems for non-viral gene delivery will eventually be constructed. The additive approach to vector development is giving way to a systems approach where the functional environment of and the various barriers to delivery are simultaneously considered in the materials design. For example, the initial emphasis on identifying materials that bind and condense nucleic acids may have underappreciated the importance of their subsequent intracellular release [30]; attention has now turned to vectors with a weaker binding strength [31] or whose chemical structure or nucleic acid condensation is disrupted following cellular uptake [32-38]. The need for a systems approach extends to in vitro investigations, as modifications intended for in vivo applicability can significantly affect both in vitro and in vivo performance [29].

The objective of this thesis is to develop a more comprehensive understanding of non-viral gene delivery particles' interaction with and behavior within cells. This work facilitates and promotes a systems approach to vector development by providing an improved mechanistic understanding of the process of non-viral gene transfer in vitro.

Weaknesses of an additive approach to vector development are apparent in the next two chapters, which describe multiple, correlated effects of simple modifications to delivery systems. Chapter 2 demonstrates that subtle modifications to the chemical structure of non-viral vectors can have significant and possibly inseparable effects on both transfection efficiency and toxicity. In Chapter 3, it is shown that PEGylation for extracellular salt-stabilization of non-viral gene delivery particles has a significant impact on the uptake and intracellular trafficking of these particles.

The subsequent three chapters demonstrate the value of a systems approach by characterizing the complex function of pH-buffering components in non-viral gene delivery. Incorporation of such components has been a popular strategy in the additive approach to vector development, motivated largely by examples of improved transfection efficiencies from non-viral vectors with pH-buffering capacity and by the enhanced transfection efficiency of many non-viral vectors in the presence of chloroquine. Chapter 4 of this thesis evaluates and quantifies the function of pH-buffering components in non-viral gene delivery vectors, and in Chapter 5, chloroquine and a number of its chemical analogues are studied in an effort to define its effects on transfection and to further describe the role of pH buffering. Chapter 6 further explores the role of pH-buffering components by examining delivery behavior of analogous vectors with and without

intracellular pH-buffering capacity: a cyclodextrin-containing polymer and its imidazole-terminated variant.

Chapter 7 reviews current understanding of intracellular barriers to non-viral gene delivery in the context of this report's emphasis on a systems approach to vector development. Chapter 8 offers recommendations for future work.

1.2 References

1. Felgner PL, Gadek TR, Holm M, Roman R, Chan HW, Wenz M, Northrop JP, Ringold GM, Danielsen M (1987) Lipofection: a highly efficient, lipid-mediated DNA-transfection procedure. Proc. Natl. Acad. Sci. USA 84:7413-7.
2. Haensler J, Szoka FC (1993) Polyamidoamine cascade polymers mediate efficient transfection of cells in culture. Bioconjug. Chem. 4:372-9.
3. Boussif O, Lezoualc'h F, Zanta MA, Mergny MD, Scherman D, Demeneix B, Behr J-P (1995) A versatile vector for gene and oligonucleotide transfer into cells in culture and in vivo: polyethylenimine. Proc. Natl. Acad. Sci. USA 92:7297-301.
4. Cotten M, Langle-Rouault F, Kirlappos H, Wagner E, Mechtler K, Zenke M, Beug H, Birnstiel ML (1990) Transferrin-polycation-mediated introduction of DNA into human leukemic cells: stimulation by agents that affect the survival of transfected DNA or modulate transferrin receptor levels. Proc Natl Acad Sci USA 87:4033-7.
5. Wagner E, Zenke M, Cotten M, Beug H, Birnstiel ML (1990) Transferrin-polycation conjugates as carriers for DNA uptake into cells. Proc. Natl. Acad. Sci. USA 87:3410-4.
6. Zenke M, Steinlein P, Wagner E, Cotten M, Beug H, Birnstiel ML (1990) Receptor-mediated endocytosis of transferrin-polycation conjugates: an efficient way to introduce DNA into hematopoietic cells. Proc. Natl. Acad. Sci. USA 87:3655-9.
7. Midoux P, Mendes C, Legrand A, Raimond J, Mayer R, Monsigny M, Roche AC (1993) Specific gene transfer mediated by lactosylated poly-L-lysine into hepatoma cells. Nucl. Acids Res. 21:871-8.
8. Erbacher P, Roche AC, Monsigny M, Midoux P (1995) Glycosylated polylysine/DNA complexes: gene transfer efficiency in relation with the size and the sugar substitution level of glycosylated polylysines and with the plasmid size. Bioconjug Chem. 6:401-10.
9. Zanta MA, Boussif O, Adib A, Behr JP (1997) In vitro gene delivery to hepatocytes with galactosylated polyethylenimine. Bioconjug Chem. 8:839-44.
10. Plank C, Oberhauser B, Mechtler K, Koch C, Wanger E (1994) The influence of endosome-disruptive peptides on gene transfer using synthetic virus-like gene transfer systems. J. Biol. Chem. 269:12918-24.
11. Curiel DT, Agarwal S, Wagner E, Cotton M (1991) Adenovirus enhancement of transferrin–polylysine mediated gene delivery. Proc. Natl. Acad. Sci. USA 88:8850–8854.
12. Cristiano RJ, Smith LC, Woo SLC (1993) Hepatic gene therapy: adenovirus enhancement of receptor-mediated gene delivery and expression in primary hepatocytes. Proc. Natl. Acad. Sci. USA 90:2122–2126.
13. Wagner E, Zatloukal K, Cotten M, Kirlappos H, Mechtler K, Curiel DT, Birnstiel ML (1992) Coupling of adenovirus to transferrin–polylysine/DNA complexes greatly enhances receptor mediated gene delivery and expression of transfected genes. Proc. Natl. Acad. Sci. USA 89:6099–6103.

14. Cotten M, Wagner E, Zatloukal K, Phillips S, Curiel DT, Birnstiel ML (1992) High-efficiency receptor-mediated delivery of small and large (48 kilobase) gene constructs using the endosome-disruption activity of defective or chemically inactivated adenovirus particles. Proc. Natl. Acad. Sci. USA 89:6094–6098.
15. Wagner E, Plank C, Zatloukal K, Cotton M, Birnstiel ML (1992) Influenza virus hemagglutinin HA-2 N-terminal fusogenic peptides augment gene transfer by transferrin–polylysine–DNA complexes: toward a synthetic virus-like gene-transfer vehicle. Proc. Natl. Acad. Sci. USA 89, 7934–7938.
16. Erbacher P, Roche AC, Monsigny M, Midoux M (1996) Putative role of chloroquine in gene transfer into a human hepatoma cell line by DNA/lactosylated polylysine complexes. Exp. Cell Res. 225:186-94.
17. Zauner W, Kichler A, Schmidt W, Sinski A, Wagner E (1996) Glycerol enhancement of ligand-polylysine/DNA transfection. BioTechniques 20:905-13.
18. Kollen WJW, Schembri FM, Gerwig GJ, Vliegenthart JFG, Glick MC, Scanlin TF (1999) Enhanced efficiency of lactosylated poly-L-lysine-mediated gene transfer into cystic fibrosis airway epithelial cells. Am. J. Respir. Cell Mol. Biol. 20:1081-6.
19. Midoux P, Monsigny M (1999) Efficient gene transfer by histidylated polylysine/pDNA complexes. Bioconjug. Chem. 10:406-11.
20. Pichon C, Roufai MB, Monsigny M, Midoux P (2000) Histidylated oligolysines increase the transmembrane passage and the biological activity of antisense oligonucleotides. Nucl. Acids Res. 28:504-12.
21. Kumar VV, Pichon C, Refregiers M, Guerin B, Midoux P, Chaudhuri A (2003) Single histidine residue in head-group region is sufficient to impart remarkable gene transfection properties to cationic lipids: evidence for histidine-mediated membrane fusion at acidic pH. Gene Ther. 10:1206-15.
22. Wyman TB, Nicol F, Zelphati O, Scaria PV, Plank C, Szoka FC (1997) Design, synthesis, and characterization of a cationic peptide that binds to nucleic acids and permeabilizes bilayers. Biochemistry 36:3008-17.
23. Pack DW, Putnam D, Langer R (2000) Design of imidazole-containing endosomolytic biopolymers for gene delivery. Biotechnol. Bioeng. 67:217-23.
24. Ihm JE, Han KO, Han IK, Ahn KD, Han DK, Cho CS (2003) High transfection efficiency of poly(4-vinylimidazole) as a new gene carrier. Bioconjug Chem. 14:707-8.
25. Gonzalez H, Hwang SJ, Davis ME (1999) New class of polymers for the delivery of macromolecular therapeutics. Bioconjug. Chem. 10:1068-74.
26. Putnam D, Gentry CA, Pack DW, Langer R (2001) Polymer-based gene delivery with low cytotoxicity by a unique balance of side-chain termini. Proc. Natl. Acad. Sci. USA 98:1200-5.
27. Lim YB, Han SO, Kong HU, Lee Y, Park JS, Jeong B, Kim SW (2000) Biodegradable polyester, poly[alpha-(4-aminobutyl)-L-glycolic acid], as a non-toxic gene carrier. Pharm Res. 17:811-6.
28. Pun SH, Davis ME (2002) Development of a nonviral gene delivery vehicle for systemic application. Bioconjug. Chem. 13:630-9.

29. Mishra S, Webster P, Davis ME (2004) PEGylation significantly affects cellular uptake and intracellular trafficking of non-viral gene delivery particles. Eur. J. Cell Biol. 83:97-111.
30. Schaffer DV, Fidelman NA, Dan N, Lauffenburger DA (2000) Vector unpacking as a potential barrier for receptor-mediated polyplex gene delivery. Biotechnol. Bioeng. 67:598-606.
31. Koping-Hoggard M, Varum KM, Issa M, Danielsen S, Christensen BE, Stokke BT, Artursson P (2004) Improved chitosan-mediated gene delivery based on easily dissociated chitosan polyplexes of highly defined chitosan oligomers. Gene Ther. 11:1441-52.
32. Koh JJ, Ko KS, Lee M, Han S, Park JS, Kim SW (2000) Degradable polymeric carrier for the delivery of IL-10 plasmid DNA to prevent autoimmune insulitis of NOD mice. Gene Ther. 7:2099-104.
33. Pichon C, LeCam E, Guerin B, Coulaud D, Delain E, Midoux P (2002) Poly[Lys-(AEDTP)]: a cationic polymer that allows dissociation of pDNA/cationic polymer complexes in a reductive medium and enhances polyfection. Bioconjug. Chem. 13:76-82.
34. Forrest ML, Koerber JT, Pack DW (2003) A degradable polyethylenimine derivative with low toxicity for highly efficient gene delivery. Bioconjug. Chem. 14:934-40.
35. Choi JD, MacKay JA, Szoka FC (2003) Low-pH-sensitive PEG-stabilized plasmid-lipid nanoparticles: preparation and characterization. Bioconjug. Chem. 14:420-9.
36. Carlisle RC, Etrych T, Briggs SS, Preece JA, Ulbrich K, Seymour LW (2004) Polymer-coated polyethylenimine/DNA complexes designed for triggered activation by intracellular reduction. J. Gene Med. 6:337-44.
37. Li W, Huang Z, MacKay JA, Grube S, Szoka FC (2005) Low-pH-sensitive poly(ethylene glycol) (PEG)-stabilized plasmid nanolipoparticles: effects of PEG chain length, lipid composition and assembly conditions on gene delivery. J. Gene Med. 7:67-79.
38. Read ML, Singh S, Ahmed Z, Stevenson M, Briggs SS, Oupicky D, Barrett LB, Spice R, Kendall M, Berry M, Preece JA, Logan A, Seymour LW (2005) A versatile reducible polycation-based system for efficient delivery of a broad range of nucleic acids. Nucleic Acids Res. 33:e86.

CHAPTER 2: STRUCTURAL EFFECTS OF CARBOHYDRATE-CONTAINING POLYCATIONS ON GENE DELIVERY: CYCLODEXTRIN TYPE AND FUNCTIONALIZATION[†]

2.1 Abstract

Linear cationic β-cyclodextrin (β-CD)-based polymers can form polyplexes with plasmid DNA and transfect cultured cells. The effectiveness of the gene delivery and the cellular toxicity has been related to structural features in these polycations. Previous β-CD polycations were prepared from the cocondensation of $6^A,6^D$-dideoxy-$6^A,6^D$-diamino-β-CD monomers with other difunctionalized monomers such as dimethyl suberimidate (DMS). Here, the type of CD and its functionalization are varied by synthesizing numerous $3^A,3^B$-dideoxy-$3^A,3^B$-diamino-β-and γ-CD monomers. Both alkyl-and alkoxy-diamines are prepared in order to vary the nature of the spacing between the CD and the primary amines in the monomers. These diamino-CD-monomers are polymerized with DMS to yield amidine-based polycations. The nature of the spacer between the CD-ring and the primary amines of each monomer is found to influence both molecular weight and polydispersity of the polycations. When these polycations are used to form polyplexes with plasmid DNA, longer alkyl regions between the CD and the charge centers in the polycation backbone increase transfection efficiency and toxicity in BHK-21 cells, while increasing hydrophilicity of the spacer (alkoxy versus alkyl) provides for lower toxicity. Further, γ-CD-based polycations are shown to be less toxic than otherwise identical β-CD-based polycations.

[†] Reprinted with permission from Bioconjug. Chem. 2003, 14, 672-678. Copyright 2003 American Chemical Society.

2.2 Introduction

Numerous nonviral gene delivery studies are involved in elucidating the relationships between vector structure and transfection efficiency by modifying promising systems and assaying their performance. This ongoing research has demonstrated the significant influence of polycation structure on efficiency of gene delivery. Poly-(ethyleneimine)s (PEIs) are a widely studied class of polycations for gene delivery. PEI molecular weight has been shown to affect both cytotoxicity and transfection efficiency [1,2]. The charge density [1] and degree of branching [3] in the PEI backbone also significantly alter transfection efficiency in vitro. Furthermore, substituents grafted onto PEI affect the interaction of PEI with DNA as well as PEI/DNA polyplex interactions with cells [4-6 and references therein]. Ionenes are another class of gene delivery vehicles whose structure has been related to stability of interaction with DNA [7] and to transfection efficiency [8]. Structure-function studies have also been undertaken with systems based on chitosan [9], polylysine [10], linear poly(amidoamine)s [11], polysaccharide-oligoamine conjugates [12], and other vectors. It is clear from these reports that minor changes in structure of the gene delivery vehicle can have dramatic effects on the gene delivery efficiency and toxicity of the vector.

We have prepared families of linear, β-cyclodextrin-containing polycations (βCDPs) and have shown that these polymers can be used as gene delivery vectors [13, 14]. Cyclodextrins (CDs) are cup-shaped molecules formed of cyclic oligomers of glucose. Cyclodextrins comprised of 6, 7, and 8 glucopyranose units are called α-, β-, and γ-CD, respectively (β-CD is represented in Figure 2.1). There are three distinct hydroxyls per glucopyranose unit; two secondary carbons and one primary carbon bear

these hydroxyls and are labeled C(2), C(3), and C(6), respectively (Figure 2.1). The glucopyranose units are denoted alphabetically starting with "A" and proceeding around the cyclodextrin ring (Figure 2.1).

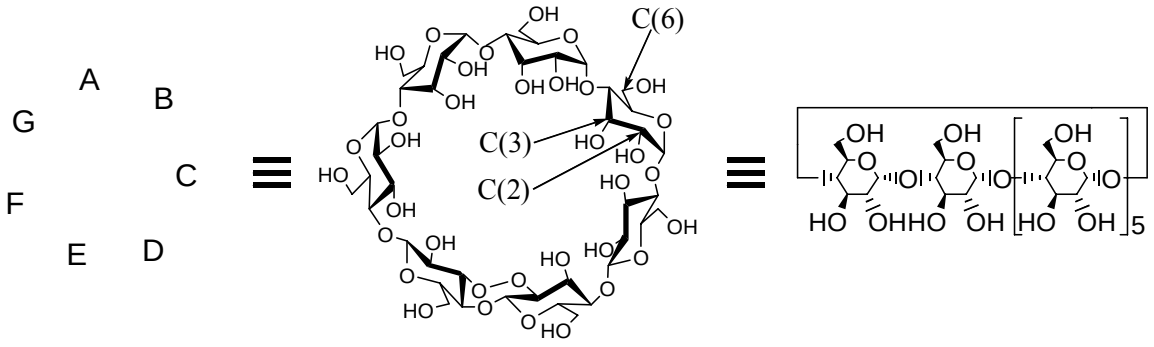

Figure 2.1 Representations and labeling of β-cyclodextrin

Initial structure-function studies with βCDPs demonstrated the importance of intercharge spacing to transfection efficiency and toxicity [14]. Significant effects on transfection efficiency were observed when the interamidine distance was reduced by just 2 Å. Upon the basis of this finding, we initiated a more complete structure-function investigation using linear, cyclodextrin-containing polycations. In part 1 of our study, we showed that cellular toxicity was related to the distance of the charge center from the carbohydrate unit (whether it be a cyclodextrin or trehalose) and that increasing polycation hydrophilicity provides decreasing toxicity [15]. Part 2 of our work revealed that the type of charge center can dramatically change the delivery efficiency [16]. With the βCDPs, amidine charge centers give greater gene delivery than quaternary ammonium charge centers. Here, we vary the type of cyclodextrin (β and γ) and the

functionalization at the cyclodextrin, i.e., $3^A,3^B$-dideoxy-$3^A,3^B$-diamino-β-and γ-CD, as compared to the previously used $6^A,6^D$-dideoxy-$6^A,6^D$-diamino-β-CD, to prepare a distinct series of linear, cyclodextrin-containing polycations. Additionally, we report the effects of spacer length between the cyclodextrin and the charge center in order to make direct comparisons between otherwise identical β-and γ-CD-based polyamidines. The polycations were characterized and assayed for plasmid DNA (pDNA) binding, polyplex size and ζ-potential, and in vitro transfection efficiency and toxicity.

2.3 Materials and methods

2.3.1 Polycation synthesis

β-and γ-cyclodextrins were purchased (Wacker Biochem Corp., Adrian, MI) and dried in vacuo at 120 °C overnight before use. Chlorosulfonic acid (Alfa Aesar; Ward Hill, MA) was distilled before use. Dimethyl suberimidate, 2HCl (DMS) was purchased from Pierce Endogen (Rockford, IL) and used without further purification. All other reagents were obtained from commercial suppliers and were used as received. Ion-exchange chromatography was run on a Toyopearl SP-650M (TosoHaas; Montgomeryville, PA) column (NH_4^+ form), and products were eluted with aqueous ammonium bicarbonate up to 0.4 M. Thin-layer chromatography was performed on Silica Gel 60 F 254 plates (EM Separations Technology; Gibbstown, NJ), and the amino compounds were eluted with 5:3:3:1 n-PrOH:AcOEt:H_2O:NH_3(aq) and visualized by reaction with ninhydrin. Matrix-assisted, laser desorption/ionization time-of-flight mass spectroscopy (MALDI-TOF-MS) was performed on a PerSeptive Biosystems Voyager DE PRO BioSpectrometry Workstation in the positive ion mode using a 2,5-

dihydroxybenzoic acid matrix. NMR spectra were recorded on a Bruker AMX500 spectrometer as dilute solutions of either D_2O or DMSO-d_6. Dialysis was conducted with a 3500 molecular weight cutoff regenerated cellulose dialysis cassette (Pierce Endogen).

Synthesis of benzophenone-3,3′-disulfonyl chloride (Scheme 2.1, "1"). Benzophenone (26.06 g, 0.143 mol) was added in small portions to 190 mL (2.86 mol) of freshly distilled chlorosulfonic acid under an argon atmosphere. The solution was then heated to 120 °C with reflux. After 20 h at 120 °C, the cooled solution was added slowly to about 1000 g of ice in a 2 L Erlenmeyer flask. The slurry was poured into a separatory funnel, then extracted with chloroform (350 mL, then 300 mL) and washed with saturated $NaHCO_3$ (200 mL), water (200 mL), and saturated NaCl (200 mL, twice). The chloroform was removed under reduced pressure. The yellow solid obtained was recrystallized twice from chloroform/hexanes. First-crop yielded 30 g of off-white crystals; second-crop yielded 5.4 g. (65% yield). Anal. ($C_{13}H_8Cl_2O_5S_2$) C, H, Cl, S.

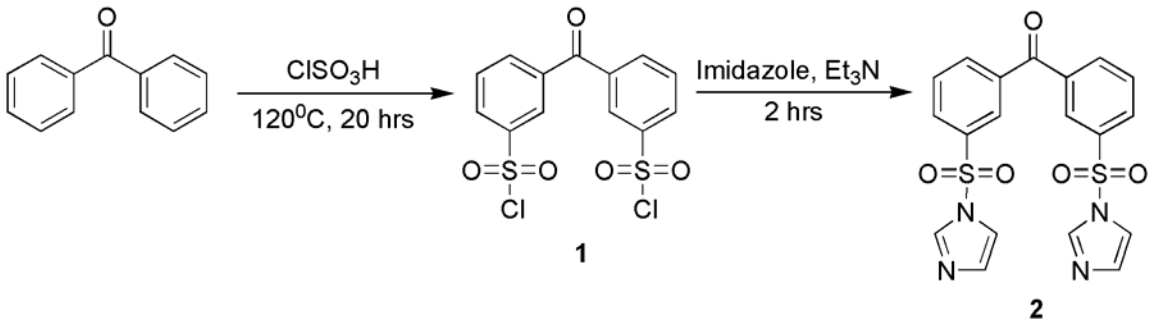

Scheme 2.1 Synthesis of benzophenone-3,3'-disulfonyl chloride

Synthesis of benzophenone-3,3′-disulfonyl imidazole (Scheme 2.1, "2"). Benzophenone-3,3′-disulfonyl chloride (13 g, 34.3 mmol) was dissolved in 150 mL of chloroform. Imidazole (4.95 g, 72.7 mmol) and Et_3N (10.2 mL, 73.2 mmol) were added.

After 30 min of stirring, 50 mL of dichloromethane was added to the slurry and allowed to stir for an additional 30 min. About 200 mL of dichloromethane was required to homogenize the reaction slurry, which was then washed with water (200 mL, twice) and dried with sodium sulfate. Benzophenone-3,3′-disulfonyl imidazole was recrystallized from dichloromethane/ethyl acetate giving 13.9 g of colorless needles (92% yield). Anal. ($C_{19}H_{14}N_4O_5S_2$) C, H, N, S. NMR data were in agreement with published chemical shifts [17].

Synthesis of cyclodextrin polycations (Scheme 2.2, "6a-d" and "7a-d"). Syntheses of $2^A,2^B$-disulfonated β-cyclodextrin (3a) [17] and $2^A,2^B$-disulfonated γ-cyclodextrin (3b) [18] were carried out according to literature methods. NMR and mass spectra data were in agreement with published values [17, 18].

Syntheses of $3^A,3^B$-di(aminoalkylamino)-β- and $3^A,3^B$-bis(aminoalkoxyamino)- γ-cyclodextrins (Scheme 2.2, "4a-d" and "5a-d") were carried out as exemplified by the following procedure: Synthesis of 5c. Hexamethylenediamine (5.89 g, 50.7 mmol) was dissolved in 35 mL of degassed water. 3b (1.50 g, 0.88 mmol) was added at once and stirred at 37 °C under nitrogen for 19 h. The reaction was further carried out at 70 °C for 3 h then concentrated under reduced pressure. Cyclodextrins were precipitated with 11:1 ace-tone:methanol and collected by filtration. Ion-exchange chromatography yielded the pure product (855 mg, 54% yield). MALDI-TOF-MS $[M+H]^+$) 1493.7.

The polycations were prepared as exemplified by the following procedure: Synthesis of 7c. 5c (100 mg, 54.7 μmol) and DMS (15.5 mg, 56.7 μmol) were taken up in 108 μL of 0.5M Na_2CO_3 and stirred for 13 h. Acidification with 1 N HCl to pH 2.0 followed by exhaustive dialysis yielded 58.4 mg of a white powder (56% yield).

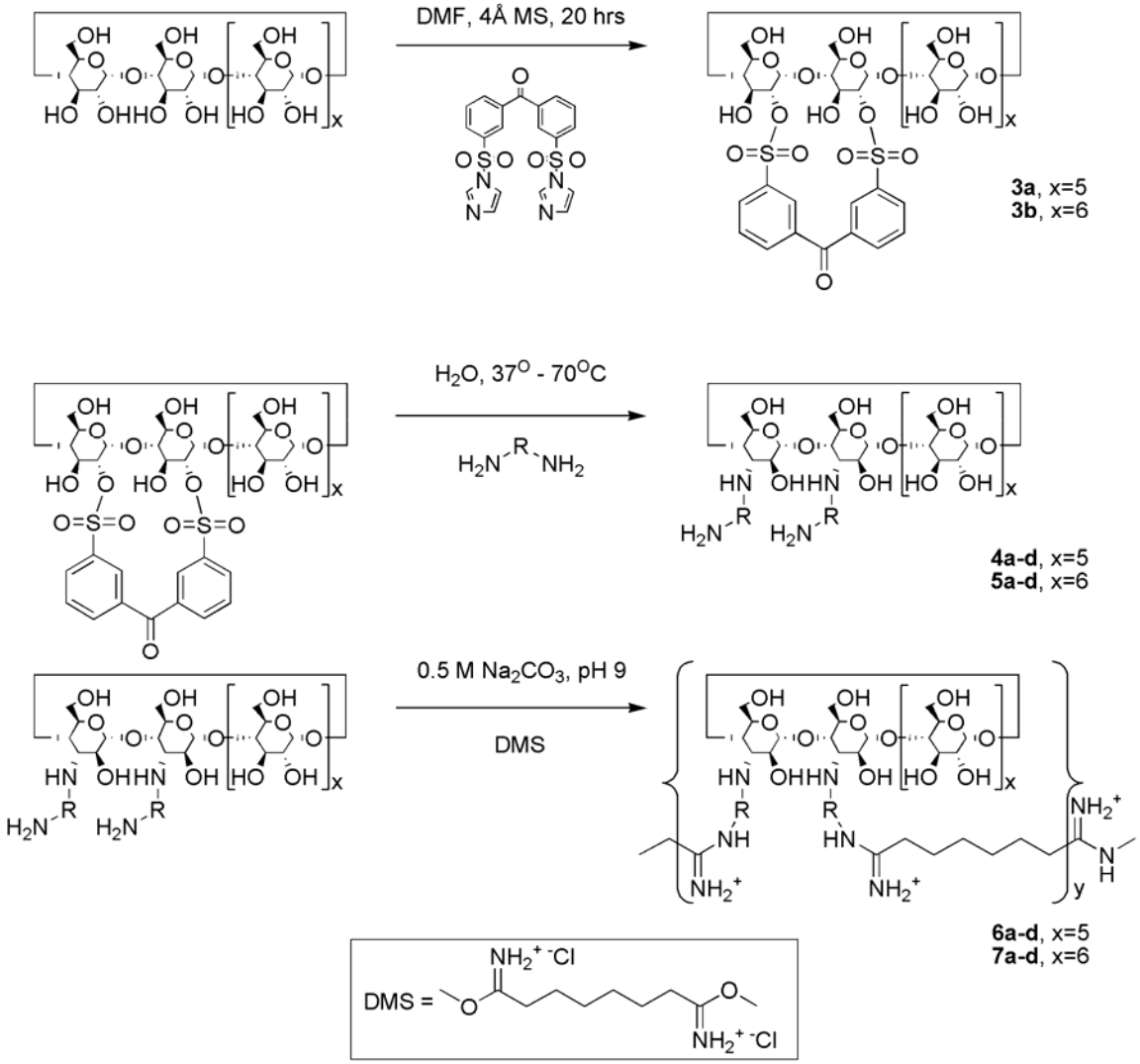

H_2N–R–NH_2	diamino-β-CD	diamino-γ-CD	β-CD-polycation	γ-CD-polycation
H_2N–(CH$_2$)$_2$–NH_2	**4a**	**5a**	**6a**	**7a**
H_2N–(CH$_2$)$_4$–NH_2	**4b**	**5b**	**6b**	**7b**
H_2N–(CH$_2$)$_6$–NH_2	**4c**	**5c**	**6c**	**7c**
H_2N–(CH$_2$)$_2$–O–(CH$_2$)$_2$–O–(CH$_2$)$_2$–NH_2	**4d**	**5d**	**6d**	**7d**

Scheme 2.2 Synthesis of cyclodextrin polycations

2.3.2 Light scattering and molecular weight determination

The specific refractive index (RI) increment, dn/dc, of each polycation was determined by fitting a linear curve to plots of RI versus concentration (five data points per polycation). Polycations were then analyzed on a Hitachi D6000 HPLC system equipped with an ERC-7512 RI detector and a Precision Detectors PD2020/DLS light scattering detector using a PL aquagel-OH column (Polymer Laboratories, Amherst, MA). The eluent was 0.8 M ammonium acetate with 0.05% sodium azide, adjusted to pH 2.8 with phosphoric acid and flowing at 0.7 mL/min. RI values were measured on a Carl Zeiss refractometer (Max Erb Instrument Co., Burbank, CA) in the same eluent as used for HPLC analysis.

2.3.3 Plasmid DNA

Plasmid pGL3-CV (Promega, Madison, WI) was amplified with the DH5R strain of E. coli (Gibco BRL, Gaithersburg, MD) and purified using the Ultra-mobius 1000 kit (Novagen; Madison, WI). This plasmid encodes the firefly luciferase gene under control of the SV40 promoter.

2.3.4 Polyplex formation and characterization

Polyplexes were formulated by adding polycation solutions in dH_2O to an equal volume of plasmid DNA (pDNA) in dH_2O (0.05 mg/mL final pDNA concentration) and incubating for 30 min. Desired charge ratios were achieved by using appropriate concentrations of polycation solution. Each polycation was examined for its ability to bind pDNA through a gel electrophoresis assay using a 0.8% agarose gel (30 μg ethidium

bromide/50 mL TAE buffer). Particle size and ζ-potential of polyplexes were analyzed using a ZetaPALS instrument (Brookhaven Instruments, Holtsville, NY).

2.3.5 Cell culture and transfections

BHK-21 cells were maintained at 37 °C in 5% CO_2 atmosphere in Dulbecco's Modified Eagle's Medium supplemented with 10% fetal bovine serum, 100 U/mL penicillin, 0.1 mg/mL streptomycin, and 0.25 μg/mL amphotericin B (Gibco BRL). For transfections, cells were seeded at 50000 cells/well in 24-well plates. Trypan blue exclusion was used to verify cell viability above 95%. At 1 day, cells were exposed to 200 μL of serum-free medium containing 1 μg of pGL3-CV plasmid pre-assembled with CD-containing polycations at various charge ratios. After 4 h, polyplex solutions were removed from the cells and replaced with 1 mL of regular growth medium. For measurement of luciferase activity and toxicity, cells were lysed 2 days after transfection with 1X Cell Culture Lysis Reagent (Promega). The Luciferase Assay System (Promega) was used to measure luciferase activity of cell lysates on a Monolight 2010 luminometer (Becton Dickinson Biosciences; San Jose, CA). Total protein content of cell lysates was assessed with the DC Protein Assay (Bio-Rad, Hercules, CA) that is a derivative of the Lowry assay.

2.4 Results

2.4.1 Polycation synthesis and characterization

β-and γ-CDs were selectively difunctionalized through a stapling reaction with benzophenone-3,3′-disulfonyl imidazole (Scheme 2.1). These intermediates react with various alkyl- and alkoxy-diamines to yield $3^A,3^B$-bis(aminoalkylamino)-CDs with various spacing groups between the carbohydrate ring and the primary amine (Scheme 2.2). The difunctionalized amino-CD monomers were polymerized with DMS to give polycations with properties shown in Table 2.1. The choice of CD-comonomer influences the polymerization with DMS; polymerization yield increases with distance between the cyclodextrin ring and the primary amine on the CD-monomer. Similar yield trends were observed for otherwise identical β-and γ-CD polycations. CD-monomers with fewer than four methylenes between the cyclodextrin and primary amine yielded polycations with an average degree of polymerization (DOP) of 5 or 6, while those synthesized from monomers with over four spacer methylenes produced an average DOP of 7 or 8. An increase in polydispersity accompanied the increase in polycation length.

Polycation	Polymerization Yield (%)	dn/dc (mL/g)	M_w (kDa)	M_w/M_n	Average degree of polymerization
6a	32	0.1029	10.0	1.1	6
6b	44	0.1406	8.1	1.3	5
6c	61	0.1515	13.9	1.7	8
6d	74	0.1322	13.0	1.4	7
7a	32	0.1085	9.3	1.1	5
7b	47	0.1386	9.6	1.4	5
7c	56	0.1237	14.7	1.6	8
7d	58	0.1279	13.3	1.3	7

Table 2.1 Effect of cyclodextrin comonomer structure on polymerization

2.4.2 Polyplex formation and characterization

To demonstrate polycation interaction with pDNA, polyplexes were formulated and run on a 0.8% agarose gel at a range of charge ratios. Polycations 6a and 7a did not completely retard DNA below a charge ratio of 1.5, while 6b-d and 7b-d retarded DNA at charge ratios of 0.5 and above (Figure 2.2). The diameter of polycation/pDNA polyplexes varied between 100 and 150 nm, while the associated ζ-potentials were all found to be positive (Table 2.2).

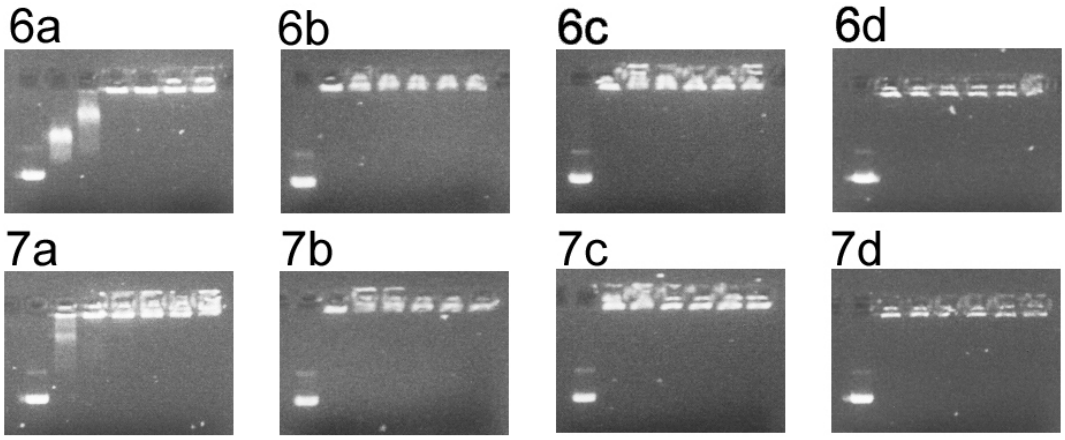

Figure 2.2 Agarose gel electrophoresis of polycation/pDNA complexes
For each polycation, complexes were formulated at charge ratios (±) of 0, 0.5, 1.0, 1.5, 2.0, 2.5, and 3.0 and run in order of increasing charge ratio (left to right) on a 0.8% agarose gel.

Polycation	Particle diameter (nm)	ζ-potential (mV)
6a	121.5 ± 1.3	12.5 ± 0.3
6b	96.4 ± 1.1	6.4 ± 1.1
6c	107.7 ± 0.9	16.7 ± 1.7
6d	88.2 ± 6.9	27.7 ± 1.0
7a	124.1 ± 1.6	23.3 ± 0.5
7b	118.6 ± 23.9	17.5 ± 3.0
7c	153.3 ± 1.7	9.6 ± 1.1
7d	102.9 ± 1.0	30.7 ± 1.4

Table 2.2 Particle sizing and ζ-potential of polycation/pDNA complexes formulated at charge ratio of 5±

2.4.3 In vitro transfection efficiency

In vitro transfection efficiency to BHK-21 cells was assessed in triplicate at charge ratios (+/-) of 2, 4, 6, 8, 10, 15, and 20. Lysates of transfected cells were assessed for luciferase activity by measuring the relative light units (RLU) normalized by total protein content (Figure 2.3). Among the diaminoalkyl-CD analogues, 6a-c and 7a-c, increased spacer length produced greater transfection efficiency, with more pronounced enhancements between the a and b variants in each series. The diaminoalkoxy-CD analogues, 6d and 7d, demonstrated intermediate levels of luciferase expression, below that achieved with the b analogues. Generally speaking, the β-CD and γ-CD polycations with identical spacers produced similar luciferase gene expression.

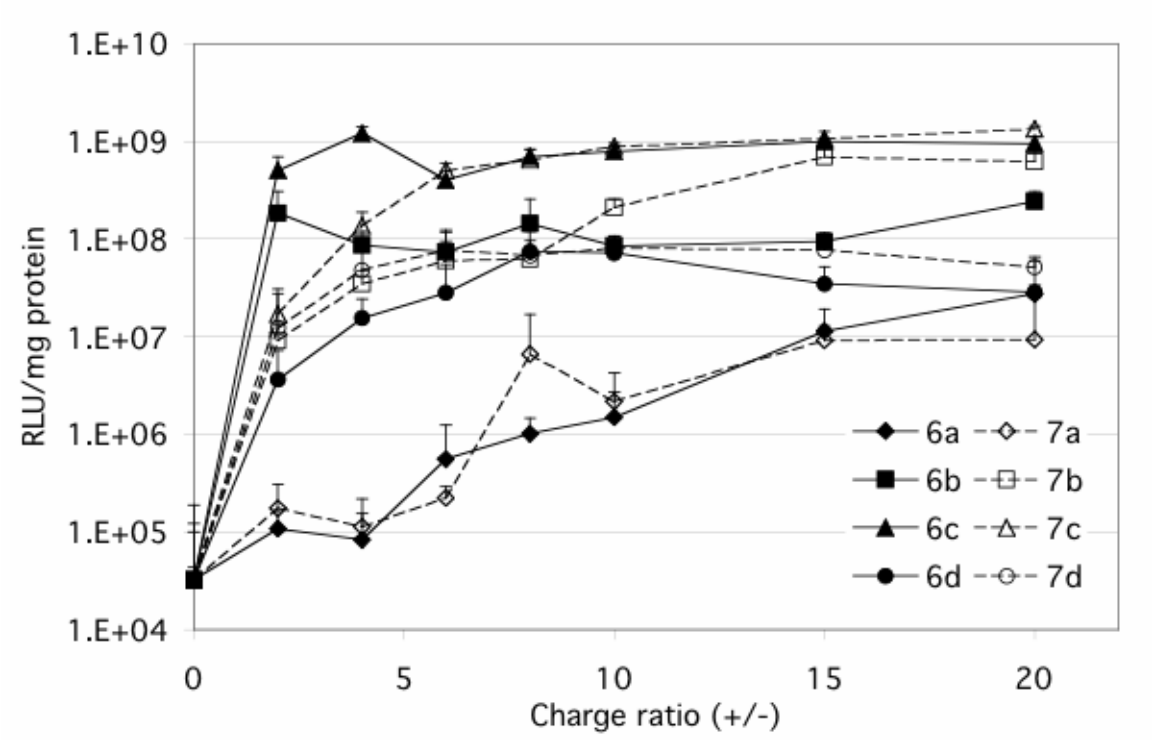

Figure 2.3 Tranfection efficiency as a function of charge ratio for cyclodextrin-polycation/pDNA complexes
Complexes were formulated at various charge ratios and exposed to BHK cells in serum-free medium for 4 h. 48 h after exposure, the cells were assayed for luciferase activity. Charge ratio of 0 indicates naked pDNA.

2.4.4 In vitro cellular toxicity

The total protein content of cell lysates was used as a measure of polyplex and/or polycation toxicity (Figures 2.4 and 2.5). The fractional cell survival of transfected cells was assessed by comparison to untransfected cells. Among the charge ratios investigated, polycations 6a-c and 7a-c demonstrated a marked decrease in cell viability with increased spacer length; 6d and 7d were essentially nontoxic at the concentrations employed. For the b and c analogues, cell viability decreased with increasing charge ratio and was worse for the β-CD polycations than for the γ-CD polycations. The toxicity of each polycation was independent of the presence of pDNA, as determined by comparison of polyplex-transfected cells with those exposed to an equal amount of polycation alone (Figure 2.5).

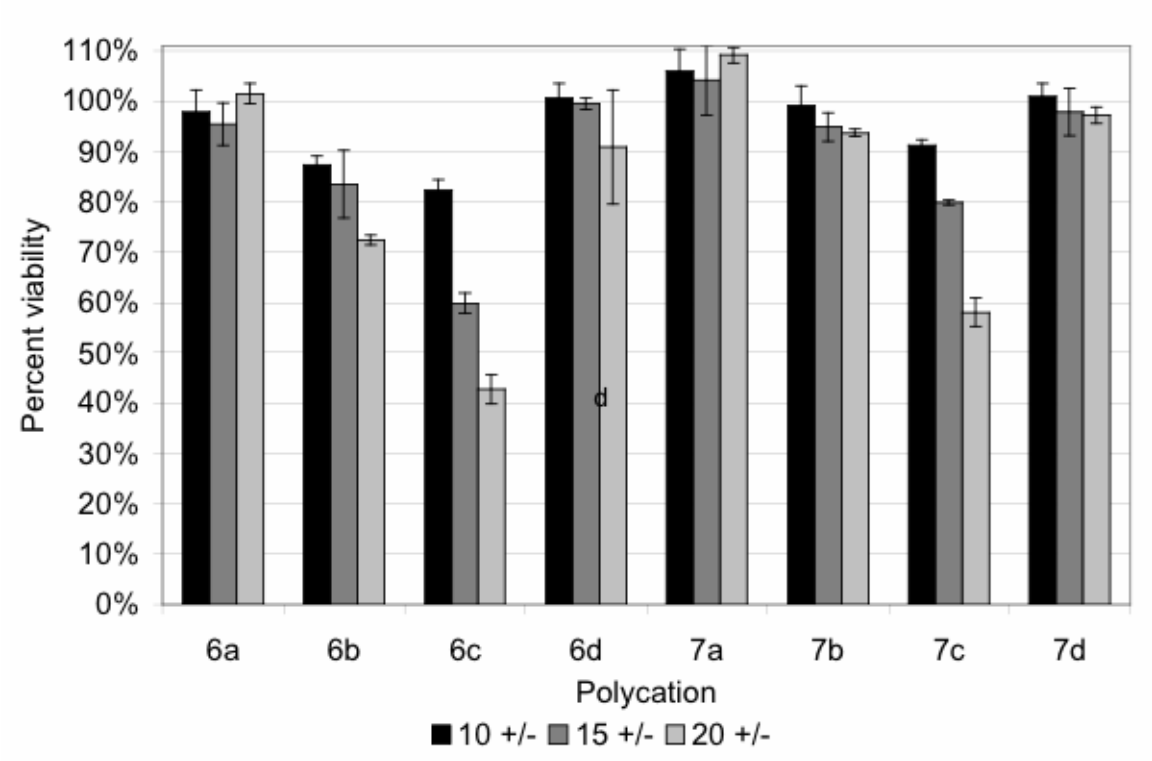

Figure 2.4 Cell viability to exposure of polycation/pDNA complexes
Cells were assayed for viability 48 h after exposure to complexes formulated at various charge ratios; data were normalized with respect to untreated cells.

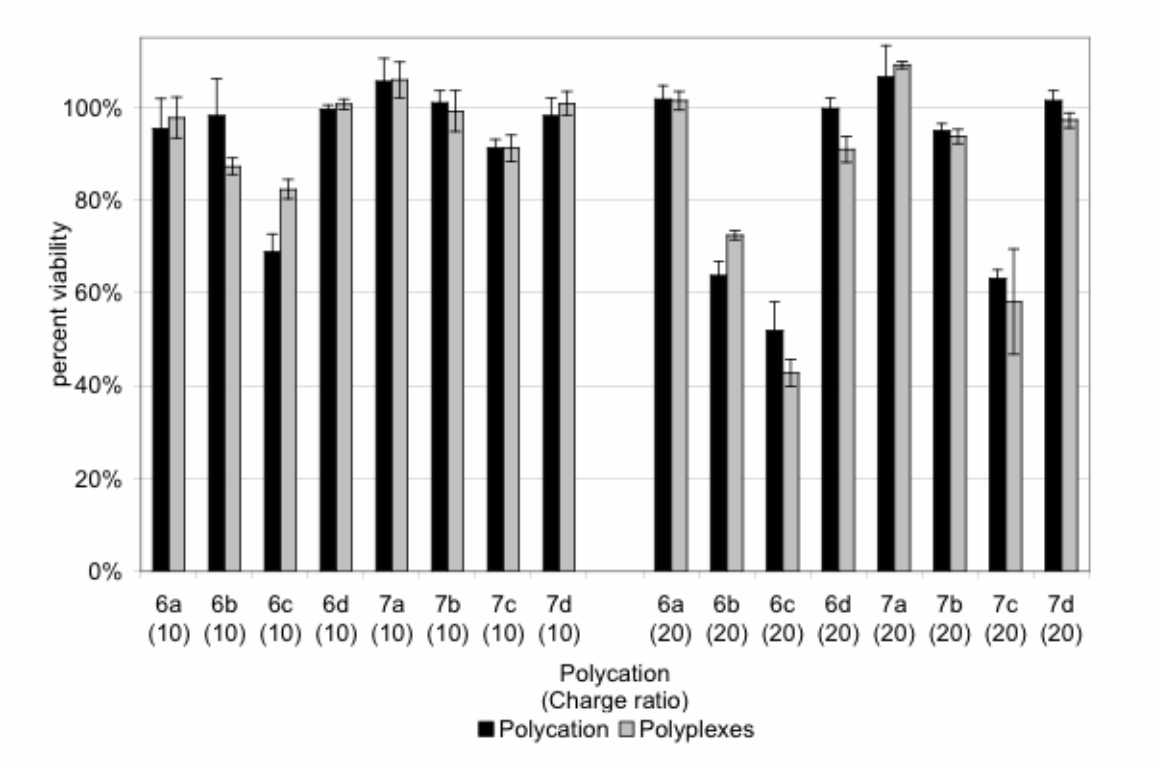

Figure 2.5 Toxicity comparison of polycation alone and polycation/pDNA complexes
Cells were exposed to polycation alone or to an equal amount of polycation complexed with pDNA; "charge ratio" for polycation alone merely represents amount of polycation. Total protein concentrations in cell lysates were used as measure of viability; data were normalized using values for untreated cells.

2.5 Discussion

Previous studies of β-cyclodextrin-containing polycations (βCDPs) have demonstrated the importance of polycation structure to cellular toxicity and in vitro transfection efficiency. The effect of interamidine distance [14] has been elucidated, as has the importance of using a bulky cyclodextrin instead of a smaller carbohydrate such as trehalose [15]. Here, we investigated the relevance of cyclodextrin ring size by studying otherwise identical series of β-and γ-cyclodextrin polycations. Within each series, the length and character of the spacer between the cyclodextrin ring and the amidine charge center were varied to understand the importance of these additional variables in our system. Such an approach allows the direct evaluation of the effect of cyclodextrin-type on in vitro transfection efficiency and cellular toxicity as well as providing further insights into the role of charge spacing along the polycationic backbone. For in vivo application of the polycations described in this report, modifications are required to impart salt and serum stability. Methodologies for modifying similar cyclodextrin-based polycations for in vivo use are available in an earlier publication [20].

The β-and γ-CD-based series of polycations follow remarkably similar trends in the DOP. DOP is found to increase with distance between the reactive primary amines of the CD-monomers and the cyclodextrins themselves. As the number of methylenes between the cyclodextrin and primary amine increases, an increase in DOP is observed with an accompanying increase in polydispersity. All polycations shown here have an average DOP between 5 and 8, corresponding to an average of 10-16 amidine charge centers per polycation chain. Assuming these differences in DOP do not significantly

affect polycation performance, a direct correlation may be made between polycation structure and the observed performance.

Previous work demonstrated that the transfection efficiency and toxicity achieved with CD-containing polycations is affected by the presence of cyclodextrins and by the alkyl chain length between charge centers [14,15]. Here, it is demonstrated that the transfection efficiency and toxicity of a related set of polycations is affected by the structure of the spacer separating the CD ring from the charge centers and, to a lesser degree, the type of CD used.

Diaminoalkyl-CD polycations 6a-c and 7a-c exhibit a marked increase in transfection efficiency as the spacer length increases, particularly with the increase from 2 to 4 methylene units. Dramatic differences between the a and b analogues are observed despite only a small change in polycation structure (a 2 Å increase in distance between the cyclodextrin and the amidine charge center). A smaller but significant increase in transfection efficiency is observed between the b and c analogues. Polycations 6a and 7a gave low levels of luciferase expression that gradually increased with increasing charge ratio. Optimum expression levels observed with these two polycations were of the same order as transfection efficiencies seen with polycations 6b, 6c, 7b, and 7c at the lowest charge ratios. Having reached relatively high transfection efficiencies at the lowest investigated charge ratios, polycations 6b, 6c, 7b, and 7c did not display the steady and marked increase with charge ratio seen with 6a and 7a. Beyond a charge ratio of 6±, only 7b demonstrated a significant increase in luciferase expression.

The least effective polycations, 6a and 7a, are also observed to require the highest charge ratio to completely retard pDNA in the electrophoresis assay. Previous work with

CD-containing polycations has shown a correlation between relative binding efficiency and transfection efficiency [15]. The reduced binding efficiency associated with decreased spacer length may result from the bulky cyclodextrins impeding the access of polycation amidines to pDNA phosphates.

The presence of CDs in the polycation backbone gives a dramatic reduction in toxicity of β-CD-containing polycations [13-16]. In part 1 of our study [15], 6^A,6^D-dideoxy-6^A,6^D-diamino-β-CDs were studied, while 3A,3B-dideoxy-3A,3B-diamino-β- and γ-CDs are investigated here. The transfection and toxicity assays employed in this series of papers do not indicate any advantages of functionalization of the CD at the C(3)-position over functionalization at the C(6)-position. In part 1 it was shown that longer spacer lengths between the CD and the charge center result in increased toxicity, which is in agreement with the result that polycations 6a-c and 7a-c demonstrate an increase in toxicity as the CD-amidine distance is increased. These results suggest that there is a toxicity-mitigating influence of the CD on the cationic center, regardless of the site of CD-derivatization. The CD may be affecting the interaction of the amidine charge centers with intracellular entities through its steric bulk and/or large sphere of hydration and thus lowering the toxicity of amidine-containing polycations. The bulkiness of the CD also hinders access of polycation amidines to pDNA phosphates. Since CD bulkiness and/or sphere of hydration correlate with the trends in both toxicity and transfection efficiency, the observation that decreases in toxicity are associated with decreases in transfection efficiency and effective pDNA binding strength are self-consistent.

The diaminoalkoxy-CD polycations 6d and 7d demonstrate an intermediate level of transfection efficiency and insignificant toxicity. Although this polycation pair pro-

vides the largest spacing between the CD and amidine residues among polycations in this study, the hydrophilic nature of the alkoxy spacer likely enlarges the effective hydration sphere around the cyclodextrin ring. In addition, the alkoxy spacer has more flexibility than alkyl spacers. These factors somehow mitigate the toxicity of polycations 6d and 7d. The change in transfection efficiency as a function of charge ratio is also intermediate relative to the diaminoalkyl-CD polycations; RLU/mg protein readings with polycations 6d and 7d rose gradually up to a charge ratio of 6±, above which no increase is observed. Each polycation produced measurable luciferase expression above background levels; the luciferase activities of untreated cells and cells treated with polycation alone are roughly 5×10^3 RLU/mg protein (data not shown), while the luciferase activity of cells treated with pDNA alone is roughly 5×10^4 RLU/mg protein. For comparison, BHK-21 cells were transfected with complexes of pDNA formulated with 25 kDa branched polyethylenimine or with βCDP6 [14]. Polyethylenimine complexes at an N/P of 5 were found to give luciferase activity of 5×10^9 RLU/mg protein (data not shown). βCDP6 complexes produced 2×10^8 RLU/mg protein at a charge ratio of 10± (data not shown).

Here, analogous β-and γ-CD-containing polycations produced similar levels of gene expression, with the exception that polycations 6b and 6c outperform their γ-CD-containing analogues 7b and 7c at charge ratios of two and four; these differences do not persist as the charge ratio is increased. At higher charge ratios, toxicity differences between the β-CD-containing polycations 6b and 6c and the γ-CD-containing analogues become apparent, with the γ-CD-containing polycations being less toxic. It is again interesting to note the correlation between enhanced transfection efficiency and increased toxicity.

The peripheral diameter of γ-CD is about 17.5 Å while that of β-CD is about 15.4 Å [19], highlighting the importance of even small variations in the CD-containing polycation system to in vitro performance. Since the polycation backbone goes through adjacent sugar residues of the cyclodextrin ring in the case of the β-and γ-CD polycations discussed in this report, the linear backbone structure varies minimally between the two. However, the remainder of the cyclodextrin-ring, which can be considered pendant to the backbone, is certainly larger in the case of γ-over β-CD.

Reineke and Davis showed that trehalose-based polyamidines are more toxic than those based on β-CD [15]. Here, CD-containing polycations demonstrate an increase in toxicity with an increase in distance between the CD and the amidine charge center and with a decrease in the size of the CD-ring. Together, these results are consistent with the hypothesis that the size of the carbohydrate moiety and its associated sphere of hydration (overall increase in hydrophilicity) mitigate the toxicity of the amidine-based polycations.

We have described the synthesis and characterization of a family of cyclodextrin-containing polycations and demonstrated significant and clear effects of polycation structure on in vitro gene expression efficiency and cellular toxicity against BHK-21 cells. The structure of diaminated cyclodextrins was found to influence both the molecular weight and polydispersity of polycations resulting from reaction of these compounds with dimethyl suberimidate. Longer alkyl regions in the polycation backbone increased transfection efficiency and toxicity, while increasing hydrophilicity was toxicity-reducing. Further, γ-CD polycations were shown to be less toxic than otherwise identical β-CD polycations.

2.6 References

1. Jeong JH, Song SH, Lim DW, Lee H, Park TG (2001) DNA transfection using linear poly(ethylenimine) prepared by controlled acid hydrolysis of poly(2-ethyl-2-oxazoline). J. Control. Release 73:391-399.
2. Godbey WT, Wu KK, Mikos AG (1999) Size matters: Molecular weight affects the efficiency of poly(ethylenimine) as a gene delivery vehicle. J. Biomed. Mater. Res. 45:268-275.
3. Remy J-S, Abdallah P, Zanta MA, Boussif O, Behr J-P, Demeneix B (1998) Gene transfer with lipospermines and polyethylenimines. Adv. Drug Deliv. Rev. 30:85-95.
4. Fischer D, von Harpe A, Kunath K, Petersen H, Li Y, Kissel T (2002) Copolymers of ethylene imine and N-(2-hydroxyethyl)-ethylene imine as tools to study effects of polymer structure on physicochemical and biological proper-ties of DNA complexes. Bioconjug. Chem. 13:1124-1133.
5. Petersen H, Fechner PM, Martin AL, Kunath K, Stolnik S, Roberts CJ, Fischer D, Davies MC, Kissel T (2002) Polyethylenimine-graft-poly(ethylene glycol) copolymers: Influence of copolymer block structure on DNA complexation and biological activities as gene delivery system. Bioconjug. Chem. 13:845-854.
6. Kircheis R, Wightman L, Wagner E (2001) Design and gene delivery activity of modified polyethylenimines. Adv. Drug Deliv. Rev. 53:341-358.
7. Zelikin AN, Izumrudov VA (2002) Polyelectrolyte complexes formed by calf thymus DNA and aliphatic ionenes: Unexpected change in stability upon variation of chain length of ionenes of different charge density. Macromol. Biosci. 2:78-81.
8. Zelikin, AN, Putnam D, Shastri P, Langer R, Izumrudov VA (2002) Aliphatic ionenes as gene delivery agents: Elucidation of structure-function relationship through modification of charge density and polymer length. Bioconjug. Chem. 13:548-553.
9. Koping-Hoggard M, Tubulekas I, Guan H, Edwards K, Nilsson M, Varum KM, Artursson P (2001) Chitosan as a nonviral gene delivery system. Structure-property relationships and characteristics compared with polyethyl-enimine in vitro and after lung administration in vivo. Gene Ther. 8:1108-1121.
10. Ohsaki M, Okuda T, Wada A, Hirayama T, Niidome T, Aoyagi H (2002) In vitro gene transfection using dendritic poly(L-lysine). Bioconjug. Chem. 13:510-517.
11. Jones NA, Hill IRC, Stolnik S, Bignotti F, Davis SS, Garnett MC (2000) Polymer chemical structure is a key determinant of physicochemical and colloidal proper-ties of polymer-DNA complexes for gene delivery. BBA-Gene Struct. Expr. 1517:1-18.
12. Azzam T, Eliyahu H, Shapira L, Linial M, Barenholz Y, Domb AJ (2002) Polysaccharide-oligoamine based conjugates for gene delivery. J. Med. Chem. 45:1817-1824.
13. Gonzalez, H., Hwang, S. J., and Davis, M. E. (1999) New class of polymers for the delivery of macromolecular thera-peutics. Bioconjug. Chem. 10:1068-1074.
14. Hwang SJ, Bellocq NC, Davis ME (2001) Effects of structure of β-cyclodextrin-containing polymers on gene delivery. Bioconjug. Chem. 12:280-290.

15. Reineke TM, Davis ME (2003) Structural effects of carbohydrate-containing polycations on gene delivery. 1. Carbohydrate size and its distance from charge centers. Bioconjug. Chem. 14:247-254.
16. Reineke TM, Davis ME (2003) Structural effects of carbohydrate-containing polycations on gene delivery. 2. Charge center type. Bioconjug. Chem. 14:255-261.
17. Teranishi K (2000) Practicable regiospecific bifunction-alization on the secondary face of α-and β-cyclodextrins. Chem. Commun. 14:1255-1256.
18. Teranishi K, Hisamatsu M, Yamada T (2000) Regiospecific synthesis of 2A,2B-disulfonated γ-cyclodextrin. Tetrahedron Lett. 41:933-936.
19. Szejtli J, Ed. (1988) Cyclodextrin Technology, Kluwer Academic Publishers, Dordrecht.
20. Pun SH, Davis ME (2002) Development of a nonviral gene delivery vehicle for systemic application. Bioconjug. Chem. 13:630-639.

CHAPTER 3: PEGYLATION SIGNIFICANTLY AFFECTS CELLULAR UPTAKE AND INTRACELLULAR TRAFFICKING OF NON-VIRAL GENE DELIVERY PARTICLES[†]

3.1 Abstract

In vitro studies of non-viral gene delivery vectors are typically not performed at physiological conditions, and thus may not provide meaningful results for in vivo investigations. We determine if polycation-plasmid DNA complexes (polyplexes) exploited for in vitro studies behave similarly to variants more applicable to in vivo use by examining their cellular uptake and trafficking. Branched polyethylenimine (25 kD) or a linear β-cyclodextrin-containing polymer are each used to formulate polyplexes, which can be PEGylated (PEG: poly(ethylene glycol)) to create particles stable in physiological salt concentrations. Particle size, cellular uptake, intracellular trafficking, and reporter gene expression are reported for polyplexes and for their PEGylated variants. PEGylation confers salt stability to particles but produced a reduction in luciferase expression. Examination of in vitro particle internalization by transmission electron microscopy shows unmodified polyplexes entering cells as large aggregates while PEGylated particles remain small and discrete, both outside and within cells. Unmodified and PEGylated particles enter cells through the endocytic pathway and accumulate in a perinuclear region. Immunolabeling reveals unpackaged exogenous DNA in cell cytoplasm and nuclei. It appears all particle types traffic towards the nucleus within vesicles and undergo degradation in vesicles and/or cytoplasm, and

[†] Reprinted with permission from Euro. J. Cell Biol. 2004, 83, 97-111.

eventually some exogenous DNA enters the nucleus, where it is transcribed. In comparing polyplexes and their PEGylated variants, significant differences in particle morphology, cellular uptake, and resultant expression suggest that in vitro studies should be conducted with particles prepared for physiological conditions if the results are to be relevant to in vivo performance.

3.2 Introduction

Non-viral gene delivery vectors have the potential to be used in therapeutic applications. These delivery vehicles avoid the DNA size limitations and immunogenicity that are possible with viral vectors, and benefit from straightforward formulation with easily manufactured, relatively low cost materials. Cationic lipids and cationic polymers are among the broad classes of materials that have shown utility in non-viral gene delivery; they both self-assemble with nucleic acids, condensing them to an appropriate size for delivery into cells.

The discovery of promising candidate vectors, e.g., polyethylenimine (Figure 1a), and identification of the various barriers to their use has been followed by more rationally designed modifications to existing materials and the development of new lipids and polymers. An example of the latter approach with cationic polymers is a vector containing β-cyclodextrin (Figure 1b) that was developed in our laboratories [1,2] and reveals extremely low toxicity both in vitro and in vivo.

a

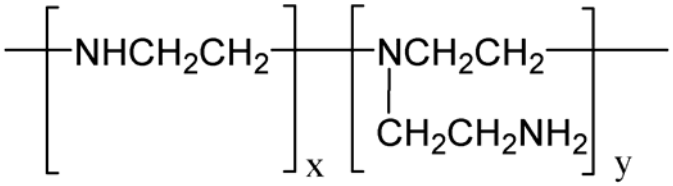

b

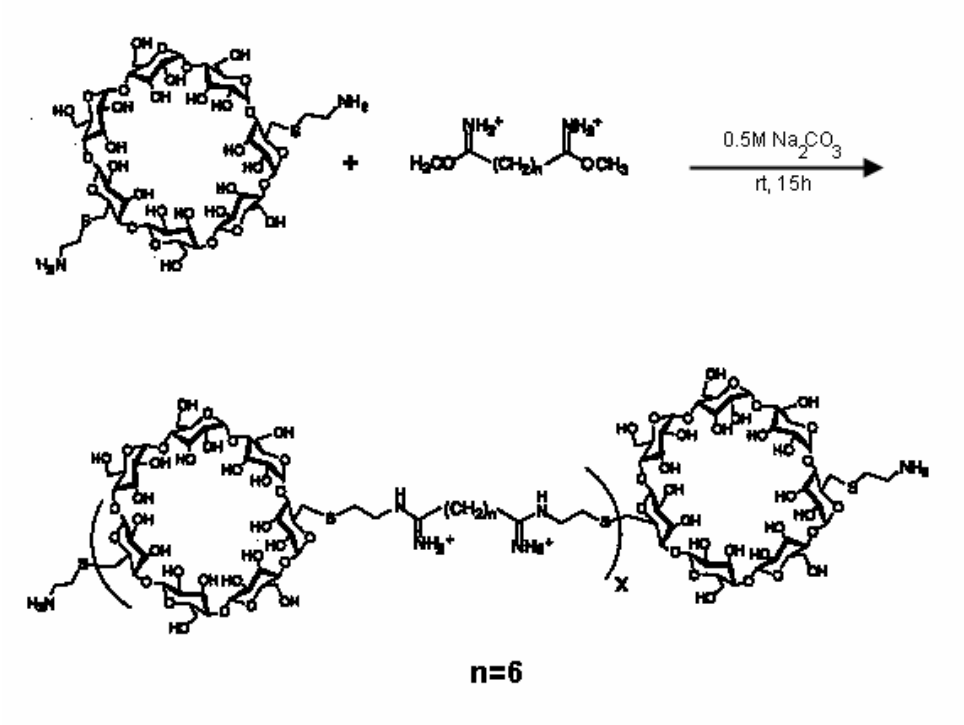

Figure 3.1 Non-viral gene delivery vectors
(a) Branched polyethylenimine, bPEI. (b) Reaction of difunctionalized β-cyclodextin and dimethylsuberimidate to produce a linear, β-cyclodextrin-containing polymer, βCDP.

Polycation-nucleic acid complexes (polyplexes) prepared with polycations such as branched polyethylenimine (bPEI) or the β-cyclodextrin-containing polymer (βCDP) have been studied extensively in vitro. These polyplexes bear a positive surface charge and aggregate in the presence of physiological salt concentration (150 mM) and/or serum

proteins. Steps to provide salt stabilization and protection against interactions with serum proteins are necessary for polyplexes to be applicable for in vivo use. Thus, non-viral gene delivery particles appropriate for in vivo use are significantly different from the unmodified polyplexes that are typically employed for in vitro studies. To prepare non-viral gene delivery formulations that are stable in the presence of physiological salt concentrations, we and others have incorporated hydrophilic polymers such as poly(ethylene glycol) (PEG), either before [3-6] or after [3,7] vector complexation with the nucleic acid.

Here, we investigate the physicochemical properties of unmodified polyplexes and their PEGylated variants and examine how these particles interact with and traffic in cultured cells. bPEI polyplexes were PEGylated through grafting of a reactive PEG molecule to free amine groups [7] while βCDP polyplexes were PEGylated through formation of inclusion complexes between a PEG-containing conjugate and the cyclodextrin moieties of the polymer [3] (Figure 3.2).

We monitored the size, zeta potential, and salt stability of these particles, and administered them to cultured cells for examination by transmission electron microscopy. The particles were further characterized by quantifying uptake of plasmid DNA (pDNA) and measuring expression of a delivered reporter gene. Collectively, these methods provide visual and quantitative means to characterize the particles and their interactions with cells in vitro. Our results demonstrate that the PEGylated particles encounter and enter cells in a manner distinct from that of unmodified polyplexes. As such, we suggest that the behavior of unmodified polyplexes in vitro will have limited relevance to the expected in vivo behavior of their salt-stabilized and physiologically relevant variants.

Further, our observations suggest a plausible process by which pDNA delivery results in measurable gene expression.

a

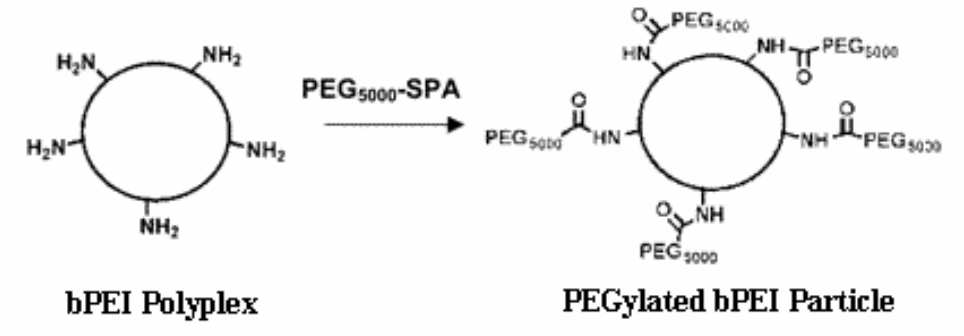

b

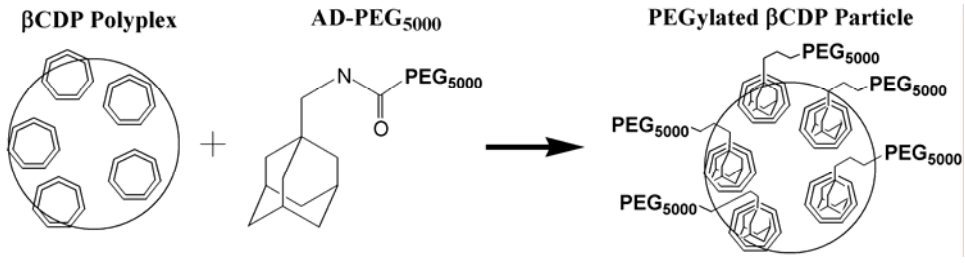

Figure 3.2 Preparation of PEGylated particles
Polyplexes were prepared and subsequently PEGylated. (a) bPEI polyplexes were PEGylated through grafting of a succinimidyl propionate (SPA)-PEG_{5000} conjugate to free amines of bPEI [7]. (b) βCDP polyplexes were PEGylated using an adamantane-PEG_{5000} conjugate [3]. The terminal adamantane is able to form inclusion complexes with β-cyclodextin in the polymer.

3.3 Materials and methods

3.3.1 Polyplex formulation and PEGylation

Branched 25 kD polyethylenimine (bPEI) was obtained from Aldrich (Milwaukee, WI). The beta-cyclodextrin-containing polymer (βCDP) and an adamantane-PEG_{5000} conjugate (AD-PEG) were synthesized as described previously [3]. The DNA plasmid pGL3-Control Vector (5256 bp) was obtained from Promega (Madison, WI) and amplified by Elim Biopharmaceuticals (Hayward, CA). Solutions of bPEI (0.067 mg/mL in 20 mM HEPES, 5% glucose) [8] and βCDP (1.03 mg/mL in dH_2O) were prepared, and polyplexes were formulated by adding polycation solution to an equal volume of pDNA (0.1 mg/mL in same solution) and incubating at room temperature for 30 minutes. bPEI polyplexes were PEGylated by addition of 4 mg methoxy-PEG_{5000}-succinimidyl propionate (Nektar, San Carlos, CA; 20 mg/mL in dH_2O) per microgram pDNA [7]. βCDP polyplexes were PEGylated by addition of 35 μg AD-PEG (100 mg/mL in dH_2O) per microgram pDNA [3]. Polyplex solutions were left at room temperature for an additional 30 minutes following PEGylation.

3.3.2 Particle sizing and zeta potential

The particle size and zeta potential of polyplexes were analyzed using a ZetaPALS instrument (Brookhaven Instruments, Holtsville, NY). Polyplex solutions were diluted 40X in dH_2O immediately before particle sizing and zeta potential measurements. To investigate effects of salt on particle size, measurements were paused briefly for the addition of 0.11 volumes of 10X phosphate-buffered saline (PBS) (Invitrogen, Carlsbad, CA) such that the final solution contained 1X PBS.

3.3.3 Cell culture and transfections

BHK-21 cells were maintained at 37°C in 5% CO_2 atmosphere in Dulbecco's Modified Eagle's Medium supplemented with 10% fetal bovine serum, 100 U/mL penicillin, 0.1 mg/mL streptomycin, and 0.25 g/mL amphotericin B (Invitrogen). Exclusion of trypan blue (Invitrogen) was used to confirm cell viability above 95%.

One day prior to transfection, cells were plated at a density of $5x10^4$ cells/mL in 6-well plates (electron microscopy, 5 mL/well), Lab-Tek 4-well chambered coverslips (Nalge-Nunc, Rochester, NY) (confocal microscopy, 1 mL/well), or 24-well plates (flow cytometry and luciferase assay, 1 mL/well). For transfection, polyplex solutions were diluted 10X in pre-warmed Opti-MEM serum-free medium (Invitrogen). The entire volume of regular medium was aspirated from the cells and replaced with one-fifth that volume of polyplex-containing serum-free medium (5 μg DNA/mL). For sample timepoints beyond four hours, the polyplex-containing medium was aspirated at four hours and replaced with regular growth medium equal to the original volume.

3.3.4 Transmission electron microscopy

At increasing timepoints after transfection, the medium was aspirated and the cells were rinsed with PBS. Cells were fixed with 2% glutaraldehyde in 100 mM sodium cacodylate with 2% sucrose, collected by scraping, and pelleted by centrifugation. Cell pellets were post-fixed in osmium tetroxide, dehydrated in ethanol, and embedded in Epon-Spurr resin. Thin sections were prepared on an Ultracut S ultramicrotome (Leica Microsystems, Deerfield, IL), contrasted with uranyl acetate and lead citrate, and imaged

on a BioTwin CM120 transmission election microscope (FEI, Hillsboro, OR) operating at 80 kV.

3.3.5 Flow cytometry and luciferase assay

For flow cytometry, pDNA was labeled prior to polyplex formation with YOYO-1 (Molecular Probes, Eugene, OR) at a density of 1 dye molecule per 100 bp DNA. Labeled polyplexes were used to transfect cells as described, and four hours after transfection, the polyplex-containing medium was aspirated and the cells were collected using trypsin-EDTA (Invitrogen). Cells were washed (10 U/mL DNase, 3 mM $MgCl_2$ in Hank's buffered saline solution (HBSS)), suspended in propidium iodide-containing buffer (HBSS, 2.5 mg/mL bovine serum albumin, 0.01 mg/mL propidium iodide), and analyzed on a FACScalibur instrument (Becton Dickinson, Franklin Lakes, NJ) with a 488 nm excitation line. Samples were initially gated by forward and side scatter, and viable cells were assayed for YOYO-1 fluorescence. Luciferase assays were conducted in triplicate, 48 hours after transfection, as previously described [9].

3.3.6 Rhodamine labeling of polymer termini

βCDP and tetramethylrhodamine isocyanate (2:1 mole TRITC:βCDP) were dried under vacuum for 30 min. in a flask wrapped with aluminum foil. DMSO was added under argon and the mixture was stirred for 30 min. at room temperature. EDC (1:1) and NHS (1:1) were added to the solution, which was kept in dark and under argon for 24 h and then dialyzed against water for 72 h in a Spectra/Pro 7 10,000 MWCO membrane (Fisher Scientific, Hampton, NH) in an aluminum-foiled 4 L beaker. Water was changed

6-8 times until it acquired no color with prolonged dialysis, after which the polymer solution was lyophilized to yield a red, dry solid.

3.3.7 Confocal microscopy

For laser scanning confocal microscopy, pDNA was labeled prior to polyplex formation with YOYO-1 at a density of 1 dye molecule per 100 bp DNA. Polyplexes were formulated with unlabeled or rhodamine-labeled βCDP and administered to cells. At selected timepoints after transfection, cells were rinsed with PBS and fixed with 4% formaldehyde in 100 mM HEPES. After 15 minutes, the fixative was removed; the cells were rinsed twice with PBS, and left in a third PBS wash. Microscopy was conducted at the Caltech Biological Imaging Center using a Zeiss 410 laser scanning confocal microscope set up from an inverted Axiophot microscope. Excitation wavelengths of 488 nm and 568 nm were used for YOYO-1 and rhodamine, respectively. YOYO-1 was detected with a 515-540 nm band pass filter and rhodamine was detected with a 580-620 nm band pass filter. The labeled polyplexes' fluorescence properties were verified with a fluorimeter system (Photon Technology International, Monmouth Junction, NJ).

3.3.8 Post-embedding immunolabeling experiments with electron microscopy

For immunolabeling experiments, pDNA was labeled with the LabelIT biotin-labeling kit (Mirus, Madison, WI) at a density of roughly 10 labels per plasmid and purified by ethanol precipitation. Polyplexes were formulated with βCDP and administered to cells. At desired timepoints after transfection, the medium was aspirated and the cells were rinsed with PBS. Cells were fixed with 4% formaldehyde in 200 mM

HEPES, collected by scraping, and pelleted by centrifugation. Cell pellets were infiltrated in 2.3 M sucrose, frozen by immersion in liquid nitrogen, freeze substituted at -80°C with dry methanol, and embedded at -50°C in Lowicryl HM20 resin (Electron Microscopy Sciences, Fort Washington, PA). Thin sections were prepared on an Ultracut S ultramicrotome and immunolabled with a mouse anti-biotin primary antibody (Sigma, St. Louis, MO), a rabbit anti-mouse secondary antibody (Organon Technika, Durham, NC), and colloidal gold (10 nm)-labeled protein A (University of Utrecht, The Netherlands). 1X PBS containing 10% fetal calf serum was used as the blocking solution, and immunolabeled sections were contrasted with uranyl acetate and lead citrate and imaged on a BioTwin CM120 transmission election microscope operating at 80 kV. Immunolabeling of control samples prepared without biotin-labeled pDNA was used to determine appropriate concentrations for antibody and colloidal gold labeling. An iterative process was used to minimize background labeling from gold-labeled protein A alone, the secondary antibody and gold-labeled protein A together, and finally both antibodies and gold-labeled protein A together.

3.4 Results

3.4.1 PEGylation confers salt stability to polyplexes

bPEI polyplexes were prepared at an N/P ratio of 5/1 and PEGylated by subsequent addition of a 10:1 weight:weight ratio of methoxy-PEG_{5000}-SPA (methoxy-PEG_{5000}-SPA:bPEI). βCDP polyplexes were prepared at an N/P ratio of 5/1 and PEGylated by subsequent addition of a 1:1 mol ratio of AD-PEG_{5000} (adamantane:cyclodextrin). Dynamic light scattering was used to monitor the size and salt stability of the particles (Figure 3.3). When diluted in water, both bPEI and βCDP polyplexes are roughly 100 nm in size. The PEGylated particles show a slightly higher diameter (ca. 110 nm) than the polyplexes. Upon addition of 0.1 volume 10X phosphate-buffered saline (PBS), the measured size of the unmodified polyplexes steadily increased, indicating aggregation of polyplexes. The PEGylated particles did not aggregate in the presence of PBS; thus, the PEGylation methods employed here conferred salt stability to the particles. Both unmodified and PEGylated polyplexes had positive zeta potentials in dH_2O; bPEI polyplexes showed a more significant reduction in surface charge upon PEGylation than did βCDP polyplexes (Figure 3.4).

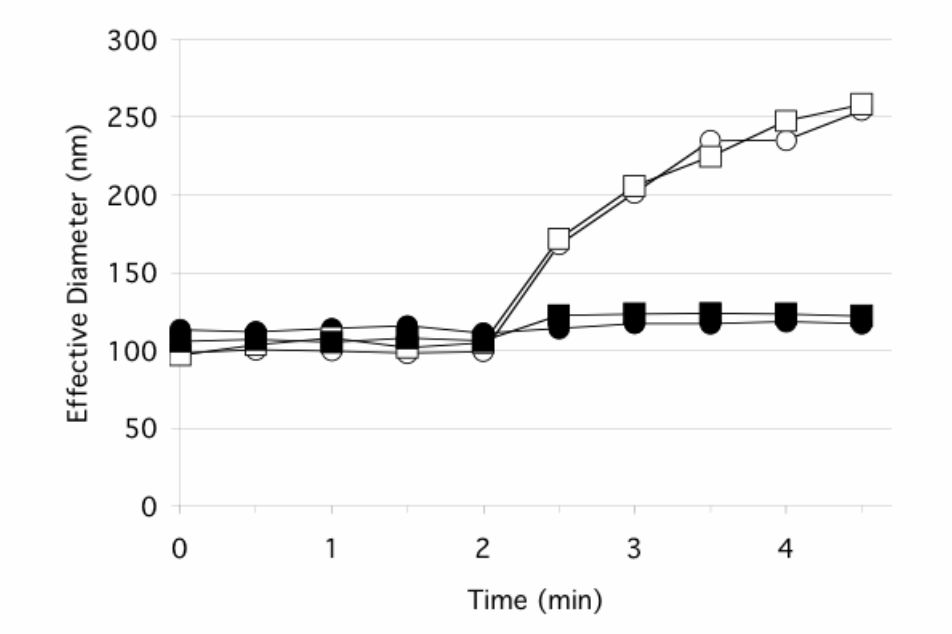

Figure 3.3 Particle sizing by dynamic light scattering
Dynamic light scattering was used to assess polyplex size. After initial dilution in water, unmodified polyplexes were observed to be slightly smaller than their PEGylated variants. After 2 minutes, measurements were paused for addition of 0.11 volumes 10X phosphate-buffered saline (PBS). The aggregation of unmodified polyplexes in 150 mM salt was observed as a steady increase in polyplex size. The size of PEGylated polyplexes remained stable in salt. bPEI polyplexes (□), PEGylated bPEI particles (■), βCDP polyplexes (○), PEGylated βCDP particles (●).

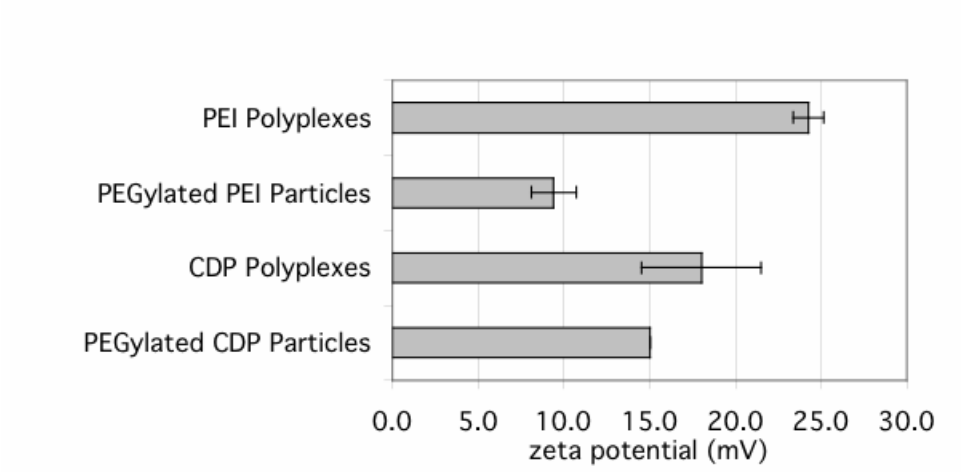

Figure 3.4 Zeta potential of polyplexes
The surface charge of polyplexes was measured using a phase analysis light scattering instrument. PEGylation produced only a slight decrease in the zeta potential of polyplexes. Samples run in triplicate. Error bar for PEGylated βCDP particles is too small to be observable in this figure.

3.4.2 Electron microscopy shows distinctive particles entering and within cells

Particle interactions with and uptake by cultured cells were visualized using transmission electron microscopy. Intact polyplexes were easily identifiable by comparison with control samples. Unmodified polyplexes were seen as irregular aggregates roughly 300-500 nm in diameter. The 100-nm polyplexes observed by light scattering in water are likely the rounded components in some of the aggregates. In contrast, PEGylated particles were visualized as discrete, individual entities on the order of 100 nm in diameter, consistent with the size observed by light scattering.

Aggregates of unmodified polyplexes were found to be associated with cell surfaces, and invaginations of cell surfaces often conformed to these polyplex aggregates (Figures 3.5a-3.5b, 3.6a-3.6c). Also, the cell membrane often appeared noticeably thicker and darker in the immediate proximity of the polyplexes, a possible indication of clathrin accumulation on the cytoplasmic face of the cell membrane. Polyplexes were observed intracellularly as large aggregates, and as the time between the initial exposure to polyplexes and the cells' fixation was increased from 0.5 to 24 hours, an increasing number of polyplex aggregates appeared in the vicinity of the cell nucleus.

Most intracellular, polyplex-containing vesicles conformed to the aggregates' shape and contained little to no void space beyond that occupied by the aggregates (Figures 3.5c-3.5f, 3.6d-3.6i). The increasing size of the aggregates closer to the nucleus suggested an aggregation of polyplex aggregates was occurring. These TEM observations of polyplex aggregates are similar to those reported for lipopolyamine-DNA complexes administered to cells [10].

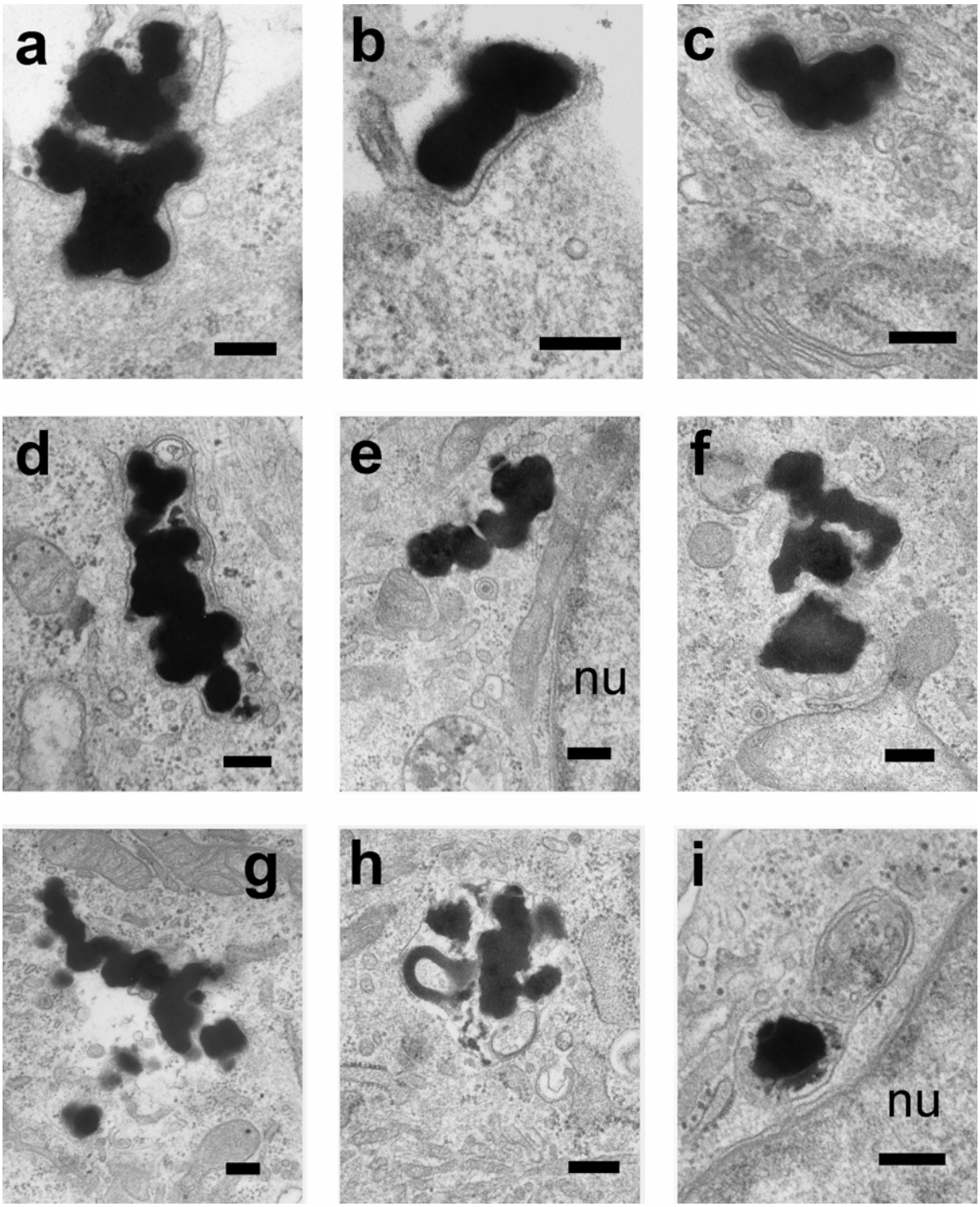

Figure 3.5 TEMs of bPEI polyplexes

BHK-21 cells were exposed to bPEI polyplexes and prepared for TEM imaging. Polyplexes appear as large aggregates and are seen associated with cell membranes, often directly with invaginations of these cell membranes (a-b). The cytoplasmic face of these membranes often appeared thicker and darker near the polyplexes, possibly indicating clathrin accumulation (a-b). The large aggregates proceed into cells in large vesicles that conform to the shape of the aggregates (c-d). At later times, polyplexes are more commonly found in the periphery of the cell nucleus and some are observed in the

cytoplasm without surrounding membranes (e-g). Also, the structure of some aggregates appears to be degrading (h-i). Bars, 200 nm. Cell nucleus, nu.

Intact membranes were not observed to surround all intracellular polyplex aggregates. In some cases, the surrounding cytoplasm extended directly to the observed aggregates (Figures 3.5f, 3.6k-3.6m), whereas in other cases the aggregates bordered void spaces (Figures 3.5g, 3.6j-3.6k, 3.6n). Intact polyplexes or their aggregates were not observed within any cell nucleus. Some polyplexes appeared to be disassembling, with less distinct and defined borders than most aggregates (Figures 3.5g-3.5i, 3.6q-3.6r). These degrading polyplexes were found more commonly within vesicles than free in cytoplasm.

PEGylated bPEI particles consistently appeared as discrete, individual particles roughly 100 nm in diameter. Extracellularly, these particles were primarily distributed irregularly across small stretches of cell membranes. Individual particles could be seen in invaginations of the membrane or in small vesicles in the immediate vicinity of the membrane (Figures 3.7a-3.7d). Moving away from the cell membrane towards the nucleus, larger vesicles distributed in the cytoplasm contained increasing numbers of the distinct, identifiable particles (Figures 3.7e-3.7i). The vesicles had variable diameters and enclosed moderate numbers of individual particles that were packed loosely together. As with the unmodified polyplexes, some PEGylated bPEI particles were not contained within vesicle membranes (Figures 3.7l-3.7n, 3.7p-3.7r). Again, the surrounding cytoplasm at times extended directly to the observed particles. No PEGylated bPEI particles were observed within a cell nucleus.

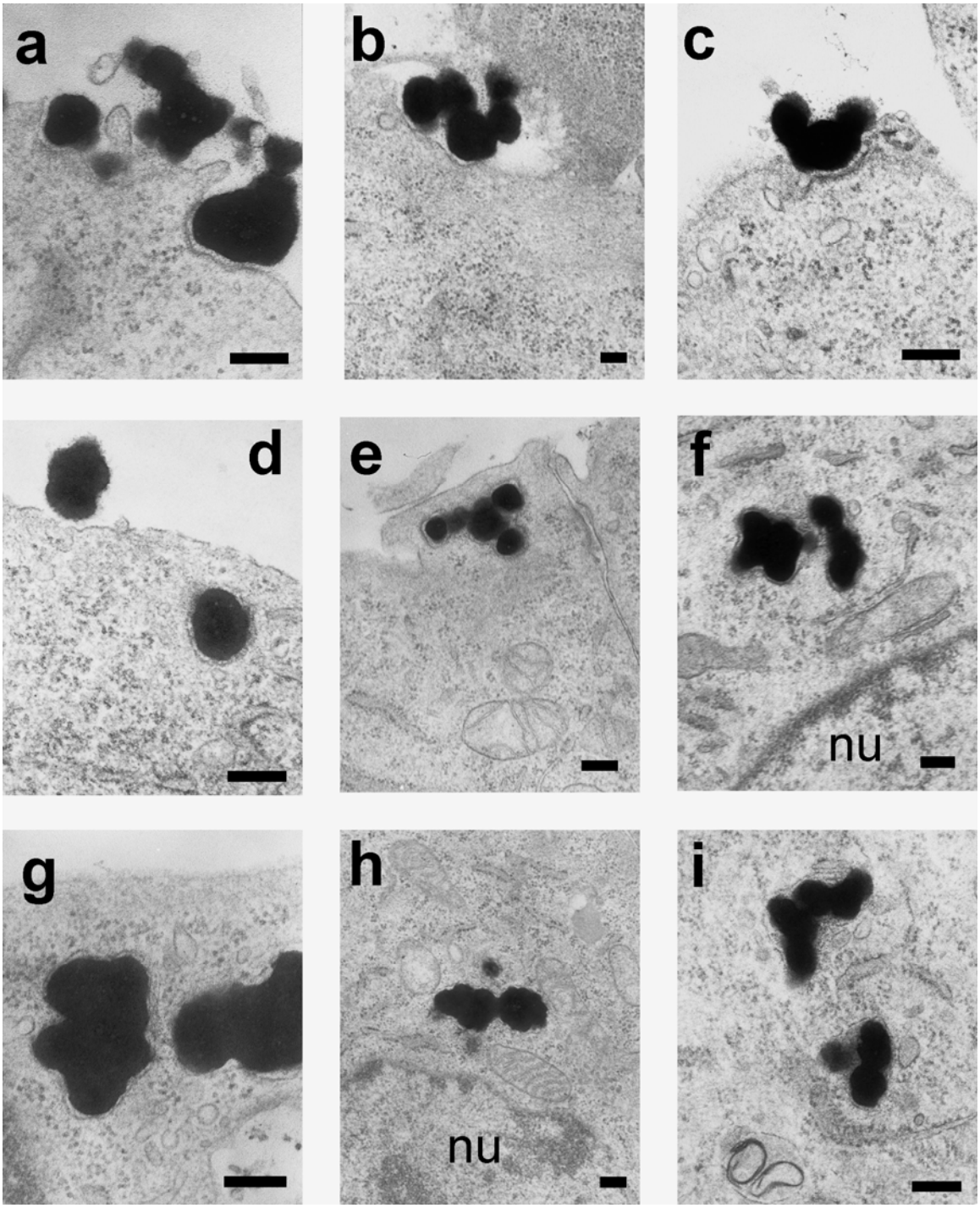

Figure 3.6 TEMs of βCDP polyplexes

BHK-21 cells were exposed to βCDP polyplexes and prepared for TEM imaging. The results were similar to those obtained with bPEI polyplexes. βCDP polyplexes appear as large aggregates and are seen associated with cell membranes, often directly with invaginations of these cell membranes (a-c). The cytoplasmic face of these membranes often appeared thicker and darker near the polyplexes, possibly indicating clathrin accumulation (a-c). The aggregates proceed into cells in large vesicles that conform to the aggregates' shape (d-i). Some membranes do not fully surround the polyplexes (h-i).

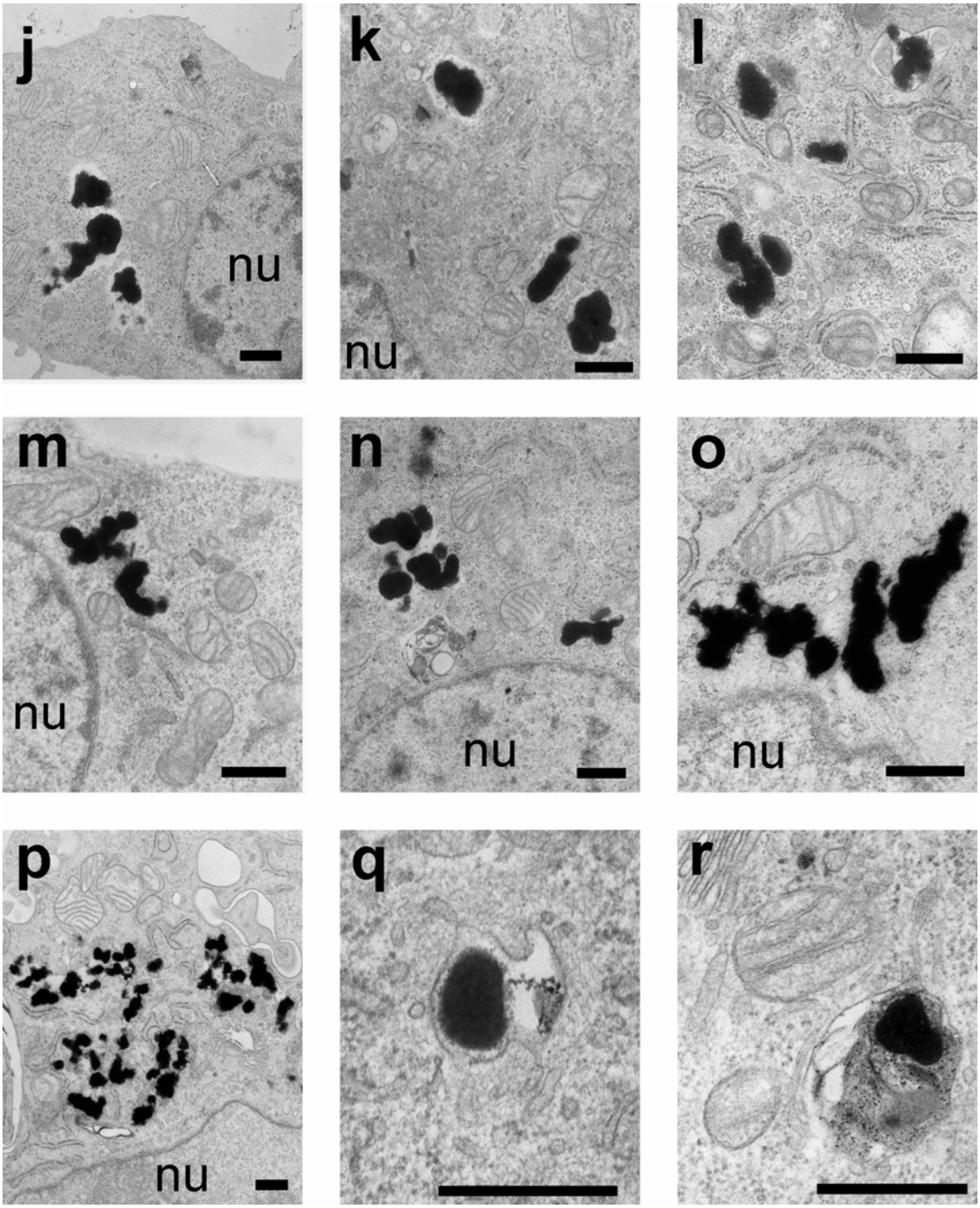

(*Figure 3.6, continued*) At later times, many polyplexes are observed in the cytoplasm without surrounding membranes (j-n). The cytoplasm appears to contact the polyplexes in some cases, whereas in others there is a void space between the polyplexes and the surrounding cytoplasm. Later timepoints show an accumulation of polyplexes in a perinuclear region (o-p). As with bPEI polyplexes, some βCDP polyplexes appear to be undergoing degradation (q-r). Bars for (a-i), 200 nm. Bars for (j-r), 500 nm. Cell nucleus, nu.

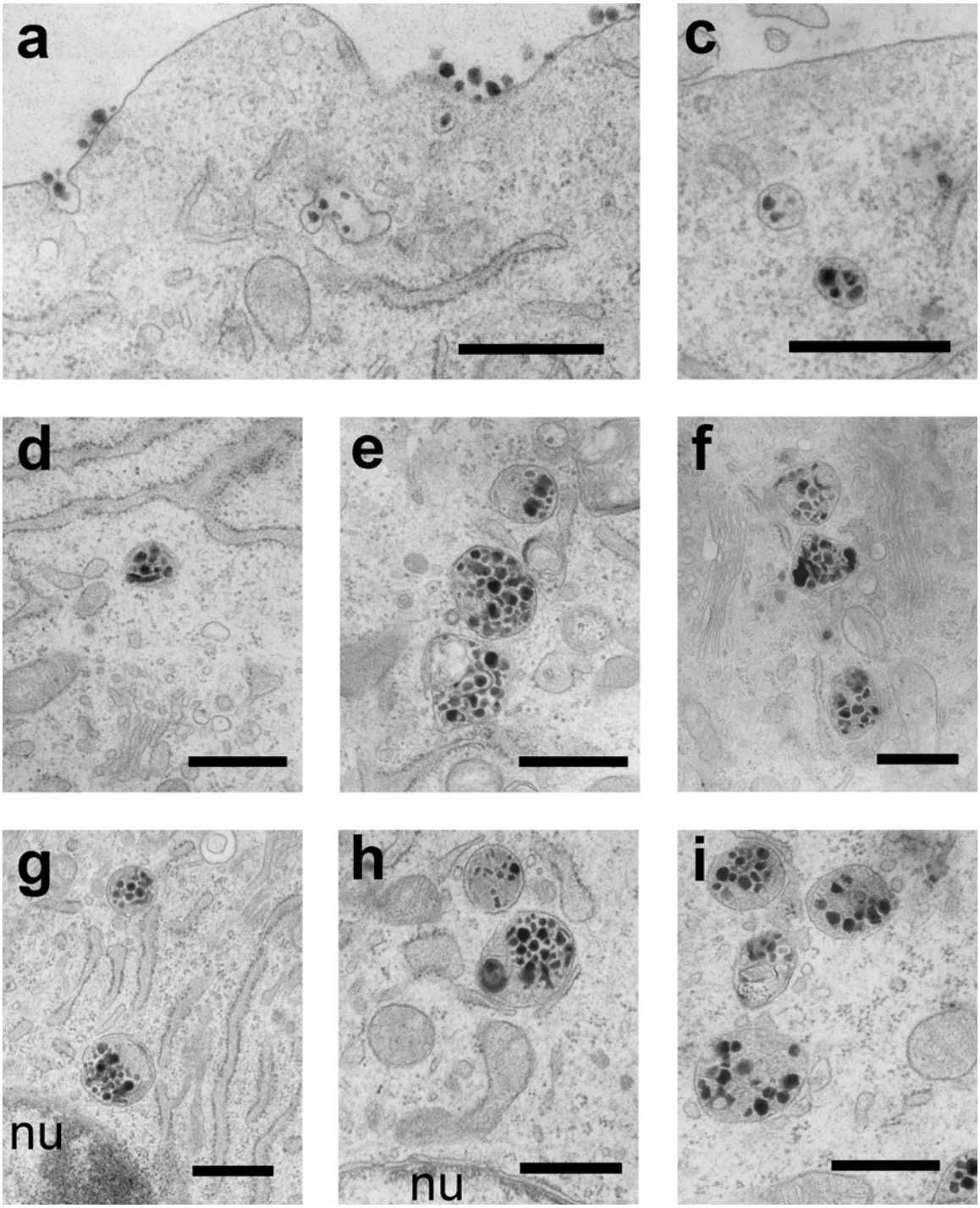

Figure 3.7 TEMs of PEGylated bPEI particles

PEGylated bPEI particles appear as small, discrete entities roughly 100 nm in diameter. Individual particles are distributed unevenly across small stretches of cell membranes and occasionally can be seen in invaginations of the membrane or in small vesicles in the immediate vicinity of the membrane (a-d). Most intracellular PEGylated bPEI particles are contained within circular vesicles in moderate numbers and continue to appear as

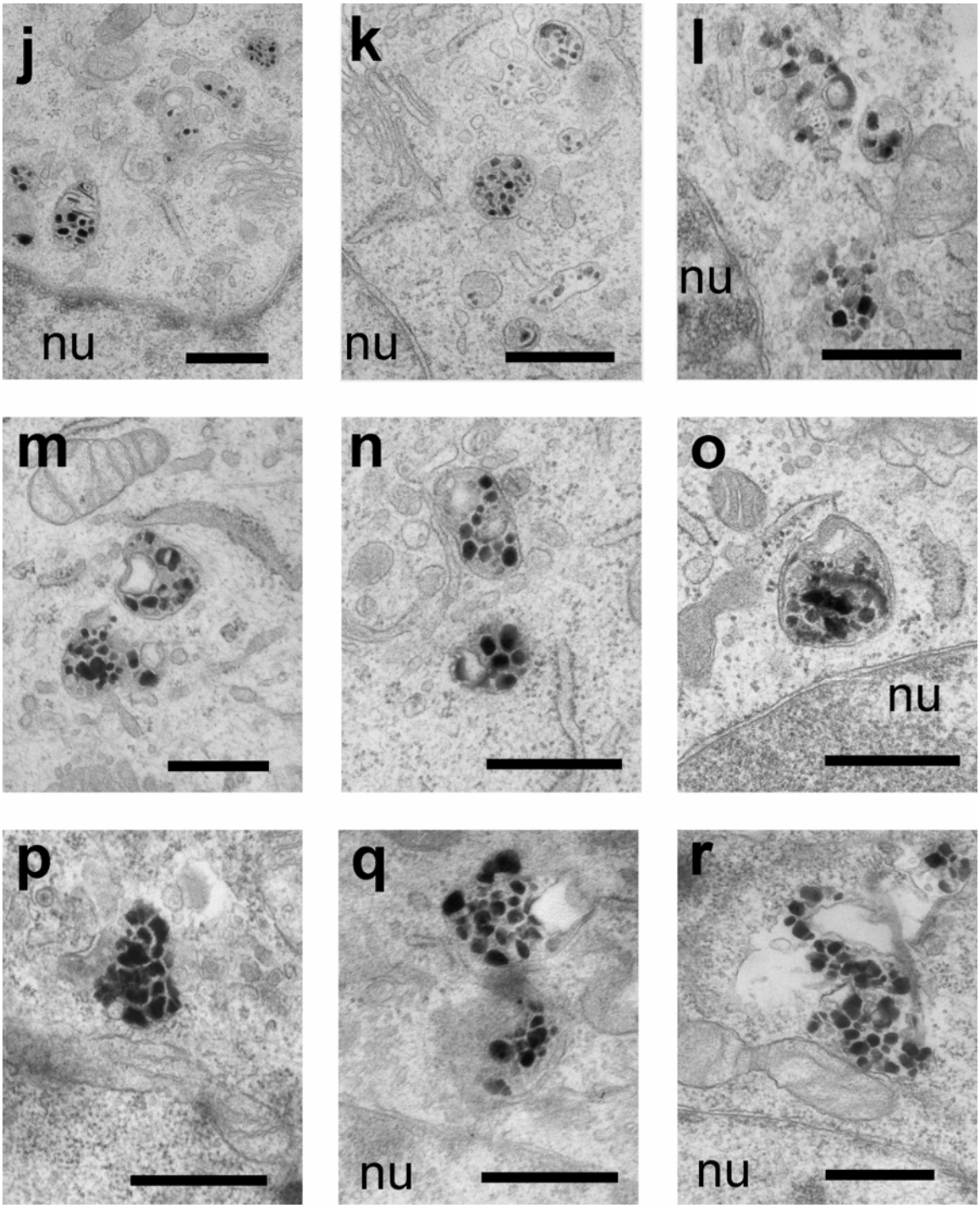

(*Figure 3.7, continued*) distinct, individual particles (e-i). At later times, large vesicles filled with these PEGylated particles collect in a perinuclear location (g-h). Bars for (a-i), 500 nm. The particles fill many vesicles near the cell nucleus, while other vesicles contain smaller numbers of particles or contain particles of more irregular appearance (j-o). In some cases, collections of particles are seen in the absence of surrounding membranes (j-l, p-r). Bars for (j-r), 500 nm. Cell nucleus, nu.

In contrast to the PEGylated bPEI particles, PEGylated βCDP particles have not been identified within cells. Beyond the absence of polyplexes, untransfected cells and cells exposed to either pDNA alone or βCDP alone appeared identical to transfected cells.

3.4.3 Volume density analysis confirms accumulation of polyplexes in cells

To verify the apparent accumulation of polyplexes in cells, volume density analysis [11] was undertaken for βCDP polyplexes. A lattice was overlaid on a randomly collected sampling of images, and the fraction of vertices on polyplexes was compared with the fraction of vertices on cell cytoplasm. This process was repeated for cells fixed at four different timepoints. The results showed a linear increase over time in the intracellular space occupied by βCDP polyplexes (Figure 3.8).

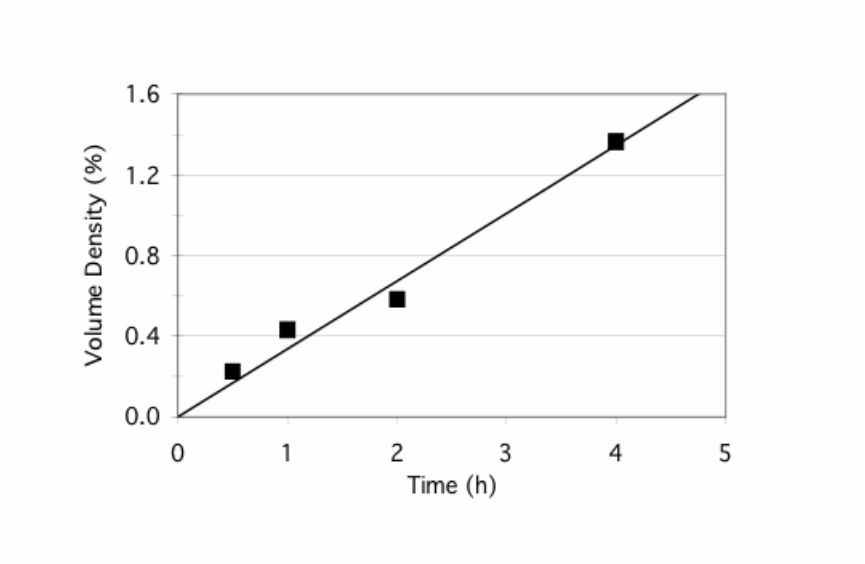

Figure 3.8 Volume density estimate for βCDP polyplexes
The intracellular space occupied by βCDP polyplexes in electron micrographs is seen to increase as the time after the initial exposure of cells to polyplexes increases. Data were collected from 21 micrographs for each timepoint.

3.4.4 Flow cytometry provides a measure of pDNA uptake

Flow cytometry analysis provided a relative measure of pDNA uptake to cells (Figure 3.9). Delivery of YOYO-1-labeled pDNA by bPEI or βCDP increased the mean cellular fluorescence by two orders of magnitude above untransfected or non-complexed pDNA controls. PEGylation of bPEI particles did not inhibit their uptake, as the mean fluorescence of transfected cells was slightly greater than that obtained with the unPEGylated counterpart. The PEGylated βCDP particles, however, showed significantly reduced uptake relative to the unmodified βCDP polyplexes; the mean fluoresence of transfected cells was only one order of magnitude above that of the controls. Rather than indicating reduced uptake from every cell, the reduced mean cellular fluorescence results from a sharp drop in the number of cells exhibiting the highest levels of pDNA uptake.

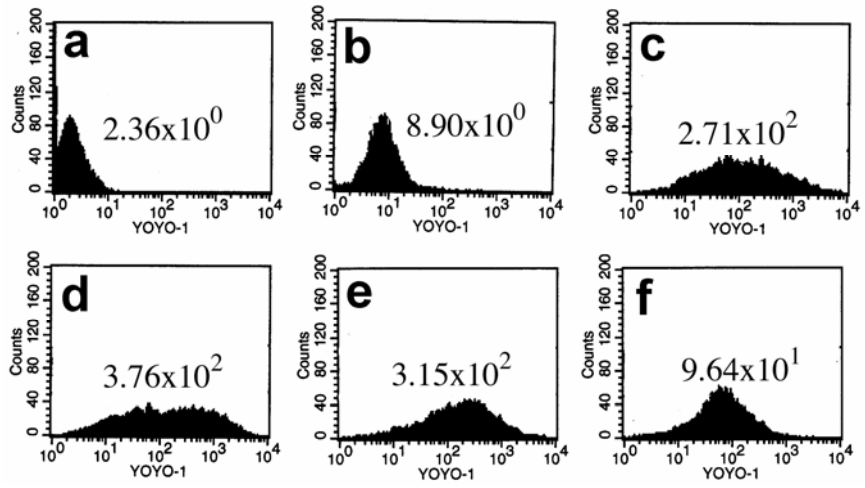

Figure 3.9 Uptake of fluorescently labeled DNA by flow cytometry
Plasmid DNA labeled with YOYO-1 was administered to cells using various means. Four hours after initial exposure, cells were collected, washed, and analyzed for YOYO-1 fluorescence by flow cytometry. Untransfected cells (a) and cells treated with naked DNA (b) have low levels of fluorescence. bPEI polyplexes (c) and PEGylated bPEI particles (d) both deliver significant amounts of pDNA to cells. PEGylated βCDP particles (f) show markedly less uptake than pDNA complexed to βCDP (e). Number indicates mean fluorescence. Samples are for duplicate measurements.

3.4.5 PEGylation of polyplexes reduces expression of a delivered reporter gene

The DNA plasmid pGL3-Control Vector expresses firefly luciferase under the control of the SV40 promoter. In vitro transfections with this plasmid showed that polyplexes prepared with bPEI or βCDP produced luciferase expression levels 2-3 orders of magnitude above that achieved by pDNA alone (Figure 3.10). Both types of PEGylated particles produced expression levels less than 1 order of magnitude greater than levels produced by pDNA alone.

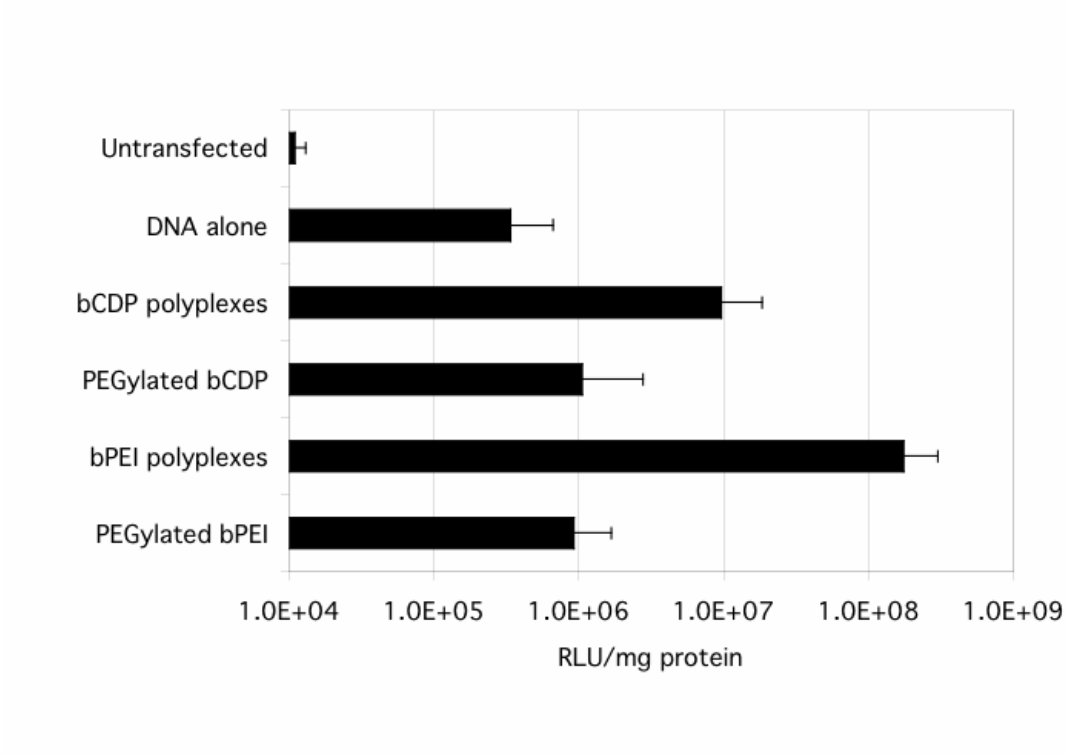

Figure 3.10 Assay for expression of delivered reporter gene
pDNA encoding the gene for firefly luciferase was administered to BHK-21 cells. The naked pDNA, polyplexes, or PEGylated polyplexes were exposed to cells for 4 hours in serum-free medium, after which the polyplex solutions were replaced with regular medium. Two days after transfection, cells were lysed and cell lysates were assayed for luciferase activity. Polyplexes produce significant levels of luciferase expression, but PEGylation of polyplexes reduces the observed luciferase activity nearly to the level achieved with naked pDNA.

3.4.6 Confocal microscopy indicates most pDNA remains associated with βCDP

Laser scanning confocal microscopy was used to visualize delivery of βCDP polyplexes (Figure 3.11). In samples containing YOYO-1-labeled pDNA and unlabeled βCDP, YOYO-1-labeled DNA was easily identifiable, distributed in a punctate manner on or within cells. In samples containing rhodamine-labeled βCDP and YOYO-1-labeled pDNA, the rhodamine signal appeared in a punctate pattern as observed for YOYO-1-labeled pDNA in the previous samples. However, there was no discernible YOYO-1 signal.

Examination of complexes on a fluorimeter indicated that the YOYO-1 signal is quenched in complexes formed between YOYO-1-labeled pDNA and the rhodamine-labeled βCDP (Figure 3.12). Dissociation of complexes by addition of sodium dodecyl sulfate restored the YOYO-1 signal, indicating that the YOYO-1 signal should be seen for unpackaged, labeled pDNA within cells.

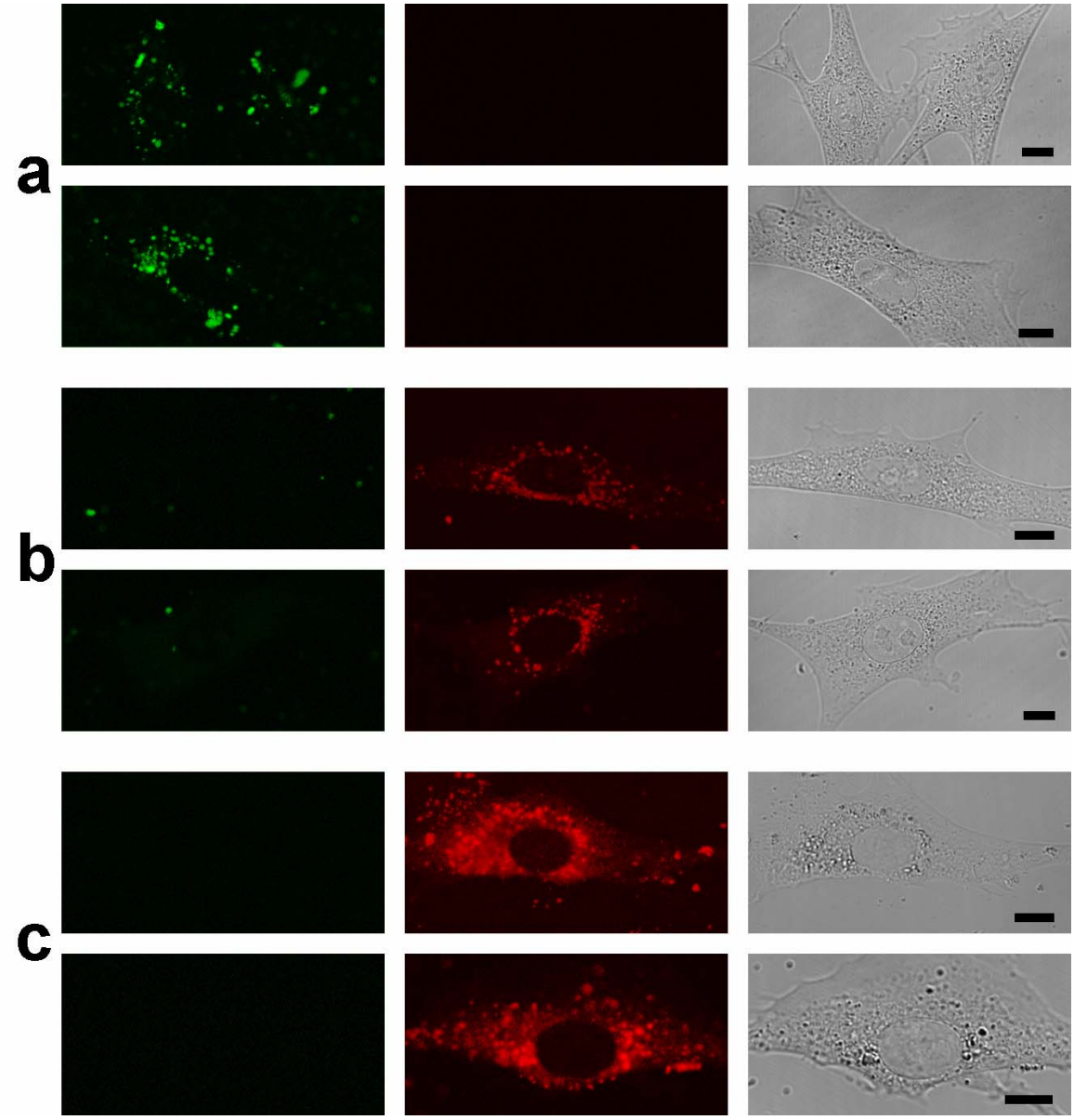

Figure 3.11 Confocal microscopy images
BHK-21 cells were exposed to βCDP polyplexes and examined by laser scanning confocal microscopy. Left, Ex=488 nm and Em=515-540 nm. Center, Ex=568 nm and Em=580-620 nm. Right, brightfield image. For YOYO-1-labeled pDNA and unlabeled βCDP (a), a punctate YOYO-1 signal is visible in cells. For YOYO-1-labeled pDNA and rhodamine-labeled βCDP (b), the YOYO-1 signal is no longer visible and a punctate rhodamine signal appears. For unlabeled pDNA and rhodamine-labeled βCDP (c), a punctate rhodamine signal appears as in the previous sample. Diffuse cytoplasmic staining in rhodamine channel indicates free rhodamine-labeled βCDP. Bars, 10 μm.

a

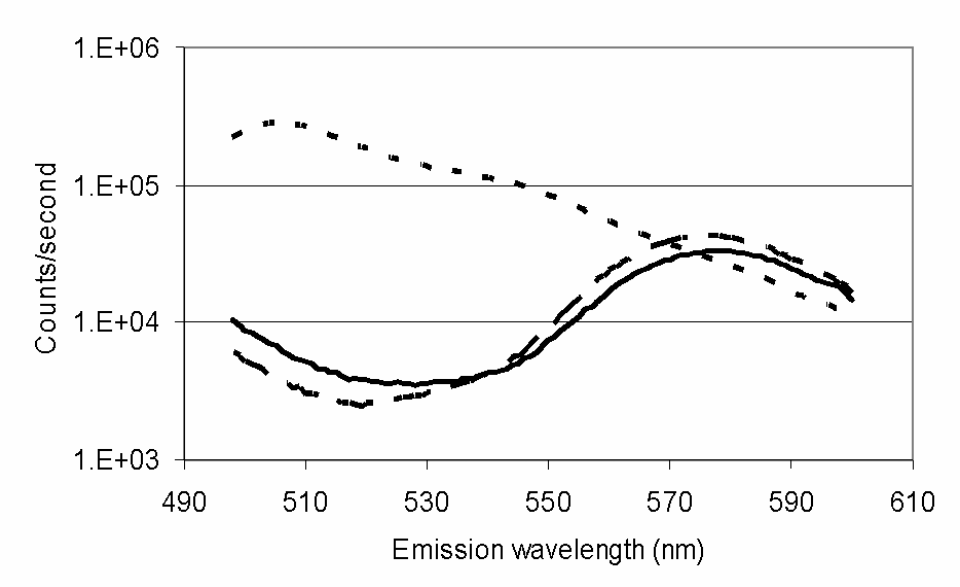

b

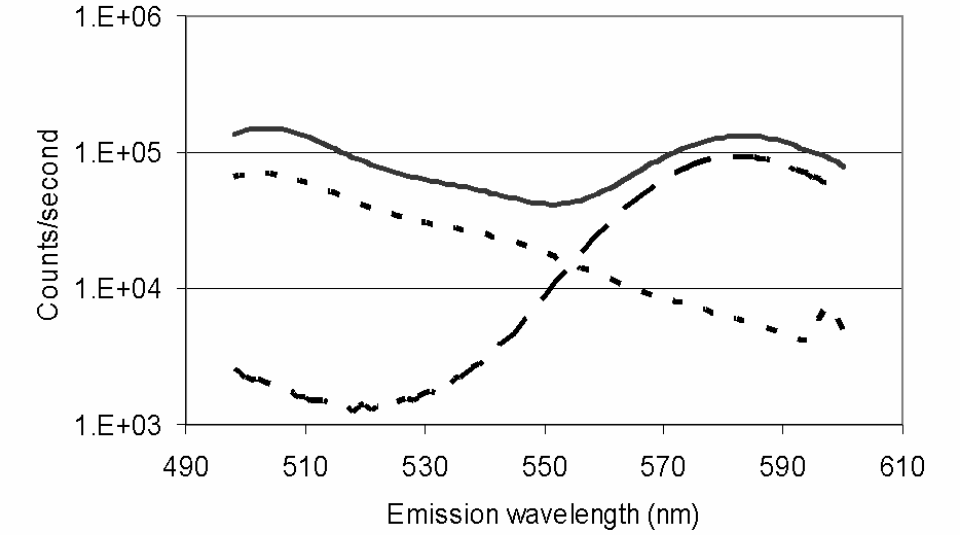

Figure 3.12 Fluorescence of labeled polyplexes

βCDP polyplexes were formulated by adding either unlabeled βCDP or rhodamine-labeled βCDP to either unlabeled pDNA or YOYO-1-labeled pDNA. The polyplexes were examined on a fluorimeter using an excitation wavelength of 488 nm. In water, singly-labeled polyplexes display expected emission spectra, but the YOYO-1 fluorescence is quenched in doubly-labeled polyplexes (a). Dissociation of doubly-labeled polyplexes by addition of an equal volume of 1% sodium dodecyl sulfate restored the fluorescence of the YOYO-1-labeled pDNA (b). Unlabeled βCDP + YOYO-1-labeled pDNA (short dashes), rhodamine labeled βCDP + unlabeled pDNA (long dashes), rhodamine-labeled βCDP + YOYO-1-labeled pDNA (solid line).

3.4.7 Unpackaged intracellular pDNA can be visualized with immunolabeling

Examination of immunolabeled sections successfully demonstrated the presence of intracellular pDNA not contained in βCDP polyplexes. In cells transfected with biotin-labeled pDNA complexed with βCDP, polyplexes were consistently labeled with numerous gold particles, indicating successful immunolabeling of biotin in polyplexes (Figures 3.13a-3.13d). Clusters of roughly 5-10 gold particles were also seen outside of polyplexes in some cells (Figures 3.13c-3.13g). Most often circular in arrangement, gold clusters in the cytoplasm did not display an obvious distribution relative to the cell membrane or nucleus. In a few cells, gold clusters were found in the nucleus (Figure 3.13g). Neither gold clusters nor gold-labeled polyplexes were observed in samples transfected with unlabeled pDNA complexed with βCDP; similarly, cells transfected with biotinylated pDNA and βCDP showed no colloidal gold labeling when incubated with only secondary antibody and gold-labeled protein A (not shown). These controls suggest that the gold clusters and the prominent labeling of polyplexes indicate specific labeling of biotin.

Figure 3.13 Visualization of intracellular pDNA by immunolabeling
Biotin-labeled pDNA was delivered to cells by means of βCDP polyplexes. TEM sample preparation included anti-biotin immunolabeling with colloidal gold. Polyplexes are

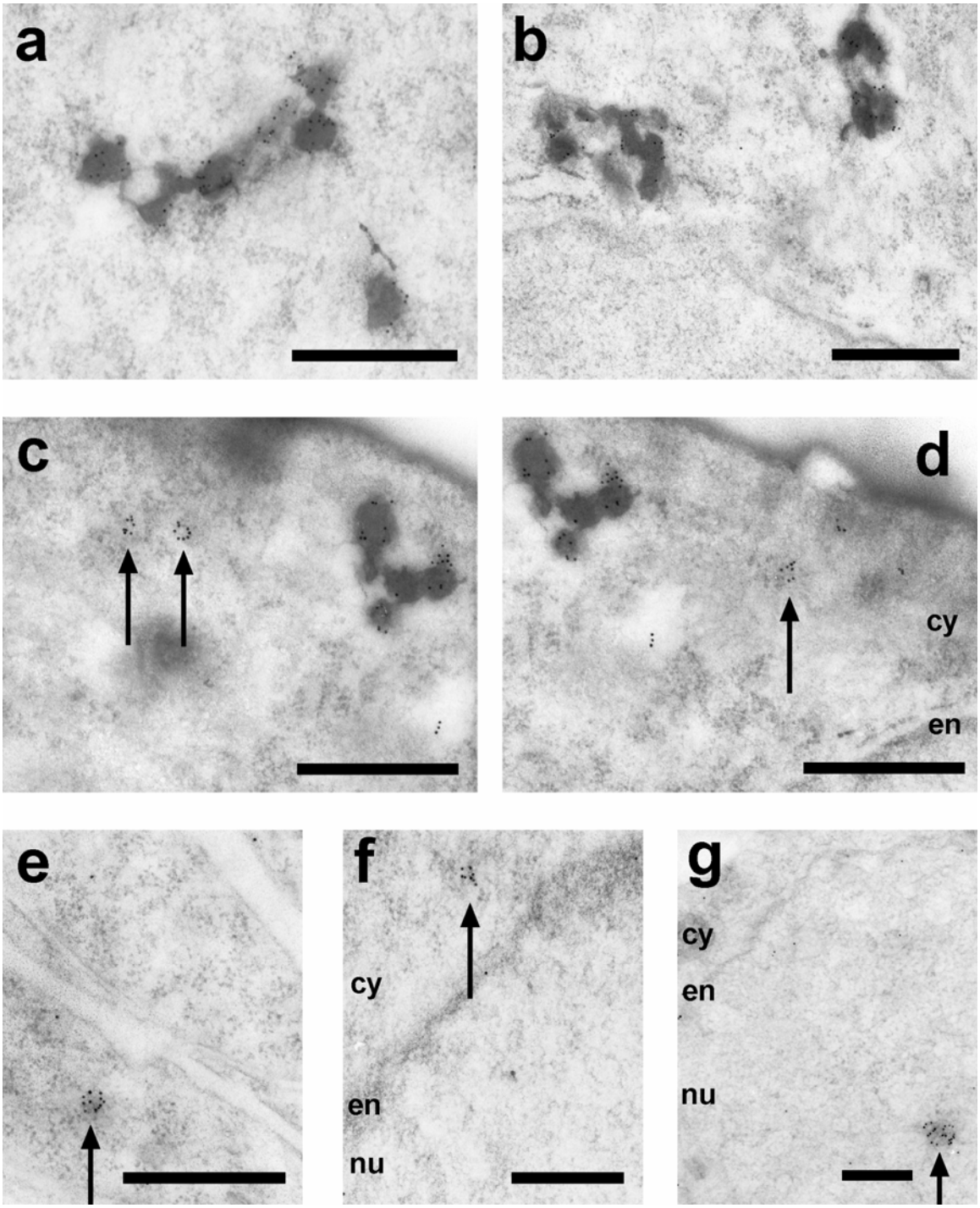

(*Figure 3.13, continued*) consistently labeled with numerous gold particles (a-d). In addition, some cells contain clusters of colloidal gold outside of polyplexes (c-g, arrows), an indication of intracellular pDNA that has unpackaged from polyplexes. A few of the intracellular gold clusters are within a cell nucleus (g). Equivalently immunolabeled samples that had been transfected with βCDP polyplexes containing unlabeled pDNA do not show colloidal gold labeling of polyplexes or colloidal gold clustering (not shown). Bars, 500 nm. Cytoplasm, cy; nuclear envelope, en; cell nucleus, nu.

3.5 Discussion

Exposure to physiological salt concentrations transforms unmodified polyplexes with diameters of 100 nm into 300-500 nm-wide aggregates. This aggregation process takes place in solution, before polyplexes enter cells. Thus, it is likely that unmodified polyplexes transfect adherent cells more successfully than suspension cells in vitro because the aggregates of unmodified polyplexes can simply sediment onto adherent cells [8,12,13], a scenario far removed from that which polyplexes would encounter in vivo.

Modification with PEG is an effective means of stabilizing polyplexes against physiological salt. PEGylated particles are only slightly larger than their unmodified variants, and as expected, retain a small positive zeta potential that is reduced from the higher values obtained with polyplexes. This surface charge can be controlled with additional components [3]. Consistent with published results, flow cytometry did not show uptake inhibition of bPEI polyplexes PEGylated with a 10/1 (w/w) PEG/PEI ratio [14]. The similar levels of uptake between unmodified and PEGylated bPEI complexes are interesting given the fact that the cells are clearly encountering particles of quite different size, surface coating, and morphology.

The difference in uptake inhibition between bPEI and βCDP polyplexes cannot be explained by differences in the surface charge of the PEGylated variants, as PEGylated bPEI particles were observed to have a lower zeta potential than PEGylated βCDP particles. The flow cytometry data suggest that PEGylation inhibits the uptake of βCDP polyplexes, but this reduction in uptake is not sufficient to explain our inability to observe intracellular PEGylated βCDP particles by TEM. Intracellular particles are clearly observed by confocal microscopy (not shown). Thus, it is likely that PEGylated

βCDP particles are not revealed by - or are disassociated by - the staining techniques employed here for electron microscopy.

Association of gene delivery particles with clathrin-like structures, visualization of intracellular particles contained in vesicles, and gradual progression of particles towards a perinuclear location together confirm that polyplexes enter cells by and proceed through the endocytic pathway. As they approach the cell nucleus, polyplex aggregates appear to grow in size, while vesicles containing PEGylated bPEI particles show increasing numbers of particles. These observations suggest that multiple polyplex-containing or particle-containing vesicles fuse to concentrate the polyplexes in perinuclear vesicles.

Using confocal microscopy, Sonawane et al. recently indicated that intact bPEI polyplexes are released from endosomes but are unlikely to be transported into the cell nucleus [15]. Here, electron microscopy results show that bPEI polyplexes, βCDP polyplexes, and PEGylated bPEI particles are all found free in the cytoplasm (Figures 3.5f-3.5g, 3.6j-3.6k, 3.6m-3.6n, 3.7l-3.7n, 3.7p-3.7r) and are not found as intact entities in cell nuclei. The significant levels of gene expression achieved with unmodified polyplexes indicate that some pDNA reaches the site of transcription, i.e., the cell nucleus. Thus, some degree of pDNA-polycation dissociation occurs before the pDNA is transcribed. Our observations of intracellular polyplexes that appear to be in the process of disassembly (Figures 3.5g-3.5i, 3.6q-3.6r) and of unpackaged pDNA in the cytoplasm (Figures 3.13c-3.13f) demonstrate that the dissociation can occur prior to pDNA entering the nucleus.

Post-embedding immunolabeling with colloidal gold is a proven means of visualizing intracellular biotin-labeled nucleic acids [16]; this technique was successfully used here to visualize unpackaged intracellular and intranuclear pDNA. The demonstration of βCDP polyplex dissociation outside of the cell nucleus raises the question of how the pDNA is eventually delivered to the nucleus. Diffusion of pDNA in cytoplasm is severely restricted [17,18]. Nuclear delivery may occur through events associated with cell division [19-22] or through pDNA association in cytoplasm with newly synthesized proteins that are bound for the nucleus [23-26]. Confocal microscopy of βCDP samples did not reveal pDNA that was not associated with the polymer, and in the immunolabeling experiments, gold clusters appeared only infrequently in the cell nucleus. Thus, we believe that despite the measurable levels of gene expression, only small amounts of pDNA - below our detection limit by confocal microscopy - are delivered to the cell nucleus by transfections with βCDP.

PEGylation led to significantly reduced expression of the luciferase reporter gene with both polycations. For the case of βCDP polyplexes, at least part of the loss in expression may be attributable to the reduced uptake of the PEGylated variants. With either polycation, PEGylation does not reduce the level of uptake or the level of luciferase expression to that of pDNA alone. For bPEI polyplexes, the severe reduction in luciferase expression with PEGylation occurred despite similar levels of pDNA uptake to cells. PEGylation and/or reaction to primary amines on the surface of bPEI polyplexes may impair the “proton sponge” effect [15,27], a significant factor in the effectiveness of bPEI as a delivery vector. For both bPEI and βCDP, unmodified polyplexes may escape from intracellular vesicles more readily because of the manner in which aggregated

polyplexes fill vesicles and contort their membranes. In contrast, vesicles containing PEGylated bPEI particles are generally smooth and circular in appearance, even as the vesicles contain increasing numbers of particles. Finally, the observation of PEGylated bPEI particles as small, discrete entities within intracellular vesicles indicates that PEGylation confers stability to these particles even intracellularly. The reduction in luciferase expression might also result if the PEGylation stability is associated with a reduction in intracellular DNA unpackaging from polyplexes.

The development of non-viral gene delivery vectors for therapeutic applications must take into account the vectors' eventual exposure to physiological environments. PEGylation is a common and effective means of conferring salt stability to polyplexes. However, as shown here, unmodified polyplexes and PEGylated particles encounter cells as substantially different entities and behave differently upon cell entry. Thus, in vitro characterizations of unmodified polyplexes likely provide limited conclusions about in vivo performance of the PEGylated variants. Such in vitro studies will carry more significance if the materials examined have physiological relevance. Further, in vivo application of non-viral vectors will require particles that are stable against physiological salt and serum concentrations and are specifically targeted. Given the results presented here, it is worthwhile to consider if particle alterations necessary to meet in vivo requirements also significantly impact in vitro performance. In summary, our observations suggest the need for further investigation of the intracellular mechanisms of gene delivery with particles that are appropriately modified for in vivo application.

3.6 Acknowledgment

I am grateful to Jeremy Heidel for synthesis of the adamantane-PEG5000 conjugate and for conducting the particle sizing and luciferase assay, Jianjun Cheng for synthesis of the rhodamine-labeled polymer, and Siva Wu for assistance with electron microscopy and for conducting the volume density estimation.

3.7 References

1. Gonzalez H, Hwang SJ, Davis ME (1999) New class of polymers for the delivery of macromolecular therapeutics. Bioconjug. Chem. 10:1068-1074.
2. Hwang SJ, Bellocq NC, Davis ME (2001) Effects of structure of β-cyclodextin-containing polymers on gene delivery. Bioconjug. Chem. 12:280-290.
3. Pun SH, Davis ME (2002) Development of a nonviral gene delivery vehicle for systemic application. Bioconjug. Chem. 13:630-639.
4. Kwok KY, McKenzie DL, Evers DL, Rice KG (1999) Formulation of highly soluble poly(ethylene glycol)-peptide DNA condensates. J. Pharm. Sci. 88:996-1003.
5. Petersen H, Fechner PM, Martin AL, Kunath K, Stolnik S, Roberts CJ, Fischer D, Davies MC, Kissel T (2002) Polyethylenimine-graft-poly(ethylene glycol) copolymers: influence of copolymer block structure on DNA complexation and biological activities as gene delivery system. Bioconjugate Chem. 13:845-854.
6. Kursa M, Walker GF, Roessler V, Ogris M, Roedl W, Kircheis R, Wagner E (2003) Novel shielded transferrin-polyethylene glycol-polyethylenimine/DNA complexes for systemic tumor-targeted gene transfer. Bioconjug. Chem. 14:222-231.
7. Ogris M, Brunner S, Schuller S, Kircheis R, Wagner E (1999) PEGylated DNA/transferrin-PEI complexes: reduced interaction with blood components, extended circulation in blood and potential for systemic gene delivery. Gene Therapy 6:595-605.
8. Ogris M, Steinlein P, Kursa M, Mechtler K, Kircheis R, Wagner E (1998): The size of DNA/transferrin-PEI complexes is an important factor for gene expression in cultured cells. Gene Therapy 5:1425-1433.
9. Popielarski SR, Mishra S, Davis ME (2003) Structural effects of carbohydrate-containing polycations on gene delivery. 3. Cyclodextrin type and functionalization. Bioconjug. Chem. 14:672-678.
10. Labat-Moleur F, Steffan A-M, Brisson C, Perron H, Feugeas O, Furstenberger P, Oberling F, Brambilla E, Behr J-P (1996) An electron microscopy study into the mechanism of gene transfer with lipopolyamines. Gene Therapy 3:1010-1017.
11. Gundersen HJG, Bagger P, Bendtsen TF, Evans SM, Korbo L, Marcussen N, Moller A, Neilsen K, Nyengaard JR, Pakkenberg B, Sorensen FB, Vesterby A,

West MJ (1988) The new stereological tools: disector, fractionator, nucleator, and point sampled intercepts and their use in pathological research and diagnosis. APMIS 96:857-881.

12. Boussif O, Zanta MA, Behr J-P (1996) Optimized galenics improve in vitro gene transfer with cationic molecules up to 1000-fold. Gene Ther. 3:1074–1080.
13. Zou SM, Erbacher P, Remy JS, Behr J-P (2000) Systemic linear polyethylenimine (L-PEI)-mediated gene delivery in the mouse. J. Gene Med. 2:128-134.
14. Ogris M, Steinlein P, Carotta S, Brunner S, Wagner E (2001) DNA/polyethylenimine transfection particles: influence of ligands, polymer size, and PEGylation on internalization and gene expression. AAPS PharmSci 3:E21.
15. Sonawane ND, Szoka FC, Verkman AS (2003) Chloride accumulation and swelling in endosomes enhances DNA transfer by polyamine-DNA polyplexes. J. Biol. Chem. 278:44826-44831.
16. Beltinger C, Saragovi HU, Smith RM, LeSauteur L, Shah N, DeDionisio L, Christensen L, Raible A, Jarett L, Gewirtz AM (1995) Binding, uptake, and intracellular trafficking of phosphorothioate-modified oligodeoxynucleotides. J. Clin. Invest. 95:1814-1823.
17. Lukacs GL, Haggie P, Seksek O, Lechardeur D, Freedman N, Verkman AS (2000): Size-dependent DNA mobility in cytoplasm and nucleus. J. Biol. Chem. 275:1625-1629.
18. Lechardeur D, Lukacs GL (2002) Intracellular barriers to non-viral gene transfer. Curr. Gene Ther. 2:183-194.
19. Wilke M, Fortunati E, Van Den Broek M, Hoogeveen A, Scholte B (1996) Efficacy of a peptide-based gene delivery system depends on mitotic activity. Gene Ther. 3:1133–1142.
20. Brunner S, Sauer T, Carotta S, Cotton M, Saltik M, Wagner E (2000) Cell cycle dependence of gene transfer by lipoplex, polyplex and recombinant adenovirus. Gene Ther. 7:401-407.
21. Brunner S, Furtbauer E, Sauer T, Kursa M, Wagner E (2002) Overcoming the nuclear barrier: cell cycle independent nonviral gene transfer with linear polyethylenimine or electroporation. Mol. Ther. 5:80-86.
22. Ludtke JJ, Sebestyen MG, Wolff JA (2002) The effect of cell division on the cellular dynamics of microinjected DNA and dextran. Mol. Ther. 5:580-588.
23. Boulikas, T (1997) Nuclear localization signal peptides for the import of plasmid DNA in gene therapy. International J. of Oncology 10:301-309.
24. Dean DA (1997) Import of plasmid DNA into the nucleus is sequence specific. Exp. Cell Res. 230:293-302.
25. Wilson GL, Dean BS, Wang G, Dean DA (1999) Nuclear import of plasmid DNA in digitonin-permeabilized cells requires both cytoplasmic factors and specific DNA sequences. J. Biol. Chem. 274:22025-22032.
26. Mesika A, Grigoreva I, Zohar M, Reich Z (2001) A regulated, NFκB-assisted import of plasmid DNA into mammalian cell nuclei. Mol. Ther. 3:653-657.
27. Behr J-P (1994) Gene transfer with synthetic cationic amphiphiles: prospects for gene therapy. Bioconjug. Chem. 5:382-389.

CHAPTER 4: SINGLE CELL KINETICS OF INTRACELLULAR, NON-VIRAL, NUCLEIC ACID DELIVERY VEHICLE ACIDIFICATION AND TRAFFICKING[†]

4.1 Abstract

Mechanistic understanding of the intracellular trafficking of non-viral nucleic acid delivery vehicles remains elusive. A live, single cell-based assay is described here that is used to investigate and quantitate the spatiotemporal, intracellular pH microenvironment of polymeric-based nucleic acid delivery vehicles. Polycations such as polyethylenimine (PEI), poly-L-lysine (PLL), beta-cyclodextrin-containing polymers lacking or possessing imidazole termini (CDP or CDP-imid), and cyclodextrin-grafted PEI (CD-PEI) are used to deliver an oligonucleotide containing a single fluorophore with two emission lines that can be employed to measure the pH. Delivery vehicles were also sterically stabilized by addition of poly(ethylene glycol) (PEG) and investigated. The intracellular trafficking data obtained via this new methodology show that vectors such as PEI and CDP-imid can buffer the endocytic vesicles while PLL and CDP do not. Additionally, the PEGylated vectors reveal the same buffering capacity as their unstabilized variants. Here, the live cell, spatiotemporal mapping of these behaviors is demonstrated and, when combined with cell uptake and luciferase expression data, shows that there is not necessarily a correlation between buffering capacity and gene expression.

[†] Reprinted with permission from Bioconjug. Chem. 2005, 16, 986-994. Copyright 2005 American Chemical Society.

4.2 Introduction

Recent difficulties and costs with viral delivery vectors have helped to renew interest in replacing these systems with biocompatible, polymeric vectors for gene delivery and potential gene therapy in humans [1,2]. Although viruses can be useful for ex vivo gene delivery, they present many problems for systemic, in vivo use, including stimulation of immune responses, potential pathogenicity, lack of designable targeting to specific tissues and cell types, and cost of manufacturing. By comparison, polymeric vectors can be prepared so that they do not elicit an immune response and are capable of carrying nucleic acids of virtually any size. Additionally, synthetic delivery vehicles can be targeted to specific cells using appropriate ligands [3-6].

Improving the delivery efficiency remains a major challenge in non-viral nucleic acid delivery. For effective delivery, the vector must first reach the cell of interest. Once internalized by receptor-mediated endocytosis, the delivery system should actively transport the nucleic acid out of the endocytic pathway and allow for movement into the nucleus. At some point during the delivery process, the non-viral vector must release the nucleic acid payload, although it is unclear where unpackaging should occur to enable the most effective delivery. Thus, the synthetic vector must perform multiple functions for effective intracellular trafficking [7-9].

An important portion of the intracellular trafficking of non-viral delivery vehicles is their behavior in the endocytic pathway. The vehicles enter into this pathway by endocytosis and must escape in order to avoid degradation by the lysosomal system [10-12]. Little is known about the spatiotemporial pH changes that the vectors face as they travel intracellularly or how these changes affect delivery and expression [13,14].

Certain polymers, such as polyethyleneimine (PEI), are said to exhibit a "proton sponge" effect since they have titratable amine groups (pKa values in the range of 4-7) and have the ability to buffer pH changes as endocytic vesicles acidify [15]. Other polymers, such as poly-L-lysine (PLL) or beta-cyclodextrin-containing polymers (CDP), do not possess this ability [16]. It is not well understood how the delivery vectors respond to pH changes in the endocytic pathway and how those responses affect export to the cytoplasm to allow the cytoplasmic transport and nuclear delivery of the nucleic acid.

Prior studies examining endosomal pH changes utilized flow cytometry to look at averages of hundreds of cells simultaneously for different types of polyplexes (PLL and PEI) [10,17] or employed an indirect approach that depended on colocalization of dextrans [18]. Here, we develop a new methodology to monitor in single cells the spatiotemporial pH experienced by nucleic acids delivered using polymeric delivery vehicles. Our work differs from previous nucleic acid delivery studies in that we employ a single pH-sensitive fluorophore, SNARF-4F, directly conjugated to the nucleic acid of interest. This method avoids concerns about relative labeling density or interactions between multiple fluorophores, makes no assumptions regarding colocalization, and directly evaluates the pH microenvironment of the nucleic acid of interest. While valuable, previous studies involving average values from numerous cells do not offer the specificity of the single cell approach described below. Also, gene delivery particles that are in different locations in the cell or are endocytosed at different times cannot be distinguished by cell averaging methods. In contrast, the single cell analysis method we present here using laser scanning confocal microscopy allows for direct examination of uptake of delivery particles in single cells in real time. Particles at different locations in

the cell can easily be identified, and pH differences quantified, as transport of such particles from the periphery of the cell towards the nucleus can take on the order of tens of minutes.

Identifying pH differences as a function of delivery particle chemical composition and location within the cell will be important for better understanding of how trafficking occurs and may assist in the design process and search for more efficient delivery vectors. Here, we show that the pH microenvironment can be correlated to transfection progression and particle location through direct visualization. This method allows for monitoring of the entire pathway, from early internalization onwards, and for direct visualization in real time to measure individual differences among cells.

4.3 Materials and methods

4.3.1 Labeled oligonucleotide and delivery vectors

A 21-base RNA phosphorothioate oligonucleotide was synthesized (Caltech Biological Synthesis Facility, Pasadena, CA) with sequence 5'-GACGUAAACGGCCACAAGUUC-3'. The 5' end of the oligonucleotide was capped with the 5'-amino modifier 5 (Glen Research, Sterling, VA), supplying a 5' terminal primary amine to which an NHS-ester of the SNARF-4F fluorophore could be reacted. To carry out this reaction, the dry oligonucleotide was re-suspended in phosphate-buffered saline (pH 7.4). The pH-sensitive fluorescent molecule SNARF-4F-carboxylic acid (Molecular Probes, Eugene, OR) was converted to an NHS-ester by reaction with 1-ethyl-3-(3-dimethylaminopropyl)carbodiimide hydrochloride (EDC) (1:1 molar eq.) and N-hydroxysulfosuccinimide (sulfo-NHS) (5:1 molar eq.) in MES buffer (pH 6.0) for 15

minutes. Subsequently, the oligonucleotide was added to the reaction mixture (10:1 molar eq., SNARF-4F:oligonucleotide) and reacted for 2 hours at room temperature in the dark. The SNARF-4F-labeled oligonucleotide was purified from unreacted SNARF-4F with CentriSep 20 columns (Princeton Separations, Adelphia, NJ). In multiple reactions, the yield of labeled oligonucleotide was 50-60%.

The beta-cyclodextrin-containing polycation (CDP) and imidazole-terminated beta-cyclodextrin-containing polycation (CDP-imid) were synthesized as described previously [19]. Solutions of these cyclodextrin-containing polycations were prepared at 2.06 mg/mL in dH2O. 25 kD branched polyethylenimine (bPEI) (Aldrich, Milwaukee, WI) solution was formulated at 0.067 mg/mL in 20 mM HEPES buffer with 5% glucose. Poly-L-lysine (Sigma) solution was prepared at 0.06 mg/mL in 0.3 M NaCl. Cyclodextrin-grafted linear polyethylenimine (CD-PEI) was synthesized as described previously [20] and a solution formulated at 10 mg/mL in dH_2O. Lipofectamine (Invitrogen) was diluted to 0.025 mg/mL in Opti-MEM serum-free medium (Gibco/Invitrogen).

4.3.2 Formulation and PEGylation of complexes

To formulate labeled complexes, the SNARF-4F-labeled oligonucleotide was diluted in dH2O to a concentration of 0.1 mg/mL. Polycation-oligonucleotide complexes were prepared by adding a polycation solution (as described above) to an equal volume of SNARF-4F-oligonucleotide. Complexes were then incubated at room temperature for 30 minutes. These conditions produce complexes at an N/P ratio of 10/1 for CDP and CDP-imid, 5/1 for bPEI, and 3/1 for poly-L-lysine. Lipoplexes were prepared by adding

lipofectamine at a concentration of 25 μg/mL in Opti-MEM to the nucleic acid at a concentration of 10 μg/mL in Opti-MEM.

For PEGylation of CDP complexes, an adamantane-poly(ethylene glycol)5000 conjugate (AD-PEG) was prepared as previously described [19]. CDP complexes and CDP-imid complexes were salt-stabilized by the addition of 35 micrograms AD-PEG (100 mg/mL in dH2O) per microgram oligonucleotide. bPEI complexes were salt-stabilized by addition of 4 micrograms methoxy-PEG5000-succinimidyl propionate (Nektar, San Carlos, CA; 20 mg/mL in dH2O) per microgram oligonucleotide. Solutions were incubated at room temperature for an additional 30 minutes after PEGylation. For examples of these types of PEGylation methods and results of stabilization within cells see [21].

4.3.3 Cell culture

HeLa cells were grown in 10-cm culture dishes (Becton Dickinson) at 37ºC in a humid 5% CO2 atmosphere. Each dish held 10 mL of growth media, which consisted of DMEM with 10% fetal bovine serum, 100 units/mL penicillin, 100 units/mL streptomycin, 10 mM HEPES, 0.1 mM non-essential amino acids, and 2 mM L-glutamine (Irvine Scientific, Santa Ana, CA). The cells were passaged once a week and plated onto glass-bottom tissue culture plates (Labtek) for each imaging experiment. The total medium volume per well was 0.7 mL after seeding, and the cells were incubated for 24 hours before transfection.

4.3.4 Fluorescence microscopy

An inverted Zeiss LSM 510 META confocal microscope was used for all fluorescence and brightfield measurements. A 63x oil objective (NA 1.4) was employed for all measurements. Excitation of the SNARF fluorophore was achieved with the 543 nm line of the He-Ne laser line supplied with the microscope. The fluorescence signal was detected by the photomultiplier tubes within the META detector after passing through a variable confocal pinhole set to 2 Airy units (chosen to maximize the S/N ratio while minimizing out-of-plane light). The META detector allows for the emitted wavelengths to be separated into ~10 nm bins of light. For the SNARF fluorophore, the collected emission light was separated into 3 distinct bins: 569-601 nm, 601-633 nm, and 633-687 nm.

4.3.5 pH Calibration Assay

Buffers with pH = 4.2, 5.0, 6.0, 7.0, and 8.0 were prepared as follows: The pH 4.2 and pH 5 buffers were made by adjusting the pH of a 0.2 M potassium acetate solution to the appropriate pH with glacial acetic acid. The pH 6.0 buffer was prepared by mixing 1.2 mL of 1 M Na_2HPO_4 and 8.8 mL of 1 M NaH_2PO_4. The pH 7.0 buffer was formulated by mixing 5.8 mL of 1 M Na_2HPO_4 and 4.2 mL of 1 M NaH_2PO_4. The pH 8.0 buffer was prepared by mixing 9.3 mL of 1 M Na_2HPO_4 and 0.7mL of 1 M NaH_2PO_4. The pH of these latter three buffers was adjusted with 6 M NaOH. To determine the pH calibration curve, PLL, CDP, and PEGylated CDP particles were incubated as follows: 2 μL of each polyplex solution (prepared as described above) were added to 100 μL of each buffer and allowed to equilibrate for at least three hours. Each sample was then imaged

under the microscope, as described, and the intensity measurements for each of the three bins were collected. The intensity values were normalized with respect to the middle bin (601-633 nm emission light) to generate calibration curves for the different pH values. The ratios of the intensity values of the 633-687 emission bin divided by those of the 569-601 emission bin do not differ significantly for all three types of particles at the same pH values; hence, we are able to use these ratios to determine intracellular pH.

4.3.6 In vitro transfection imaging

After 24 hours, the growth medium in each well was removed and replaced with an equal amount of Opti-MEM medium. 2 μL of delivery particle containing solution were then added to each well and placed in a 37 ºC incubator for 2 hours to allow for sufficient uptake. The cells were then imaged at 37 ºC, with the fluorescence emission collected into 3 channels as previously described. Cells with delivery particles at different locations and stages of transport were imaged to generate a "pH map" of the cell. Fluorescence intensity ratios were then calculated and compared to the calibrated pH values to determine the intracellular pH environment for each of the individual signals.

4.3.7 Plasmid uptake and expression

The firefly-luciferase-expressing DNA plasmid pGL3-Control Vector (5256 bp) (Promega, Madison, WI) was amplified using the Ultramobius 1000 kit (Novagen, Madison, WI). One day prior to transfection, HeLa cells were plated at a density of 5×10^4 cells/mL in 24-well plates (1 mL/well). For transfection, polyplex solutions were

diluted 10X in pre-warmed Opti-MEM serum-free medium (Invitrogen), while lipoplex solutions were applied as formulated (in Opti-MEM). Uptake was assessed four hours after transfection as described previously [21]. Briefly, cells were transfected in duplicate with YOYO-1-labeled plasmid DNA, and the YOYO-1 fluorescence of viable cells was measured four hours after transfection using a FACScalibur instrument (Becton Dickinson, Franklin Lakes, NJ). Expression of firefly luciferase was assayed as previously described [22]. Briefly, the polyplex-containing medium was aspirated four hours after transfection and replaced with regular growth medium equal to the original volume, and luciferase assays were conducted in triplicate 48 hours after transfection.

4.4 Results

4.4.1 Fluorescence pH assay

The emission spectrum of SNARF-4F varies as a function of pH and has two peaks, one at 575 nm that increases in intensity as the pH declines, and one at 650 nm that increases in intensity as the pH increases; the crossover occurs at ~620 nm (Figure 4.1a). Thus, SNARF-4F can be used alone to monitor the pH in the range of 4-8, precisely the region useful for following the intracellular trafficking involving the endocytic pathway. SNARF-4F was conjugated to the 5' end of an RNA phosphorothioate oligonucleotide and the pH sensitivity of the conjugate was observed whether the labeled oligonucleotide was free in solution or was bound by a cationic polymer and condensed into delivery particles. SNARF-4F signals are approximately the same pH value independent of whether it is free in solution, conjugated to the nucleic acid, or bound in a delivery vehicle (Figure 4.1b). The labeled oligonucleotide was used to prepare particles with a variety of non-viral gene delivery vectors; for most systems examined, the resulting particles were ~100±25 nm in size (Figure 4.2), and the oligonucleotide exhibited stability against serum when packaged in the delivery particles (data not shown). The intracellular trafficking of these fluorescently-labeled particles was monitored in cultured cells as described below.

To measure pH changes in cells via confocal microscopy, a META attachment was employed to separate the fluorescence emission into three wavelength bins (569-601, 601-633, and 633-687 nm). In order to generate a pH calibration curve, PLL and PEGylated CDP particles were prepared with the SNARF-4F RNA conjugate, incubated in buffers with pH ranging from 4.2-8.1, and directly visualized under the

a

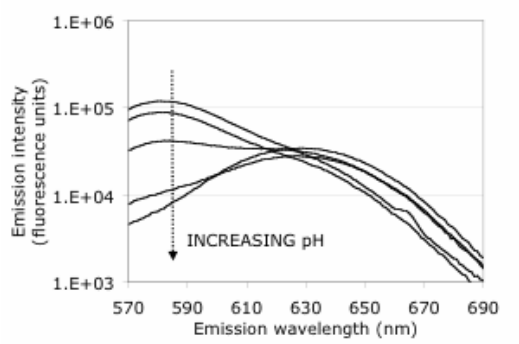

b

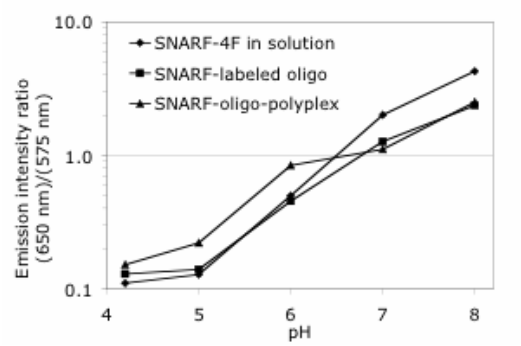

c

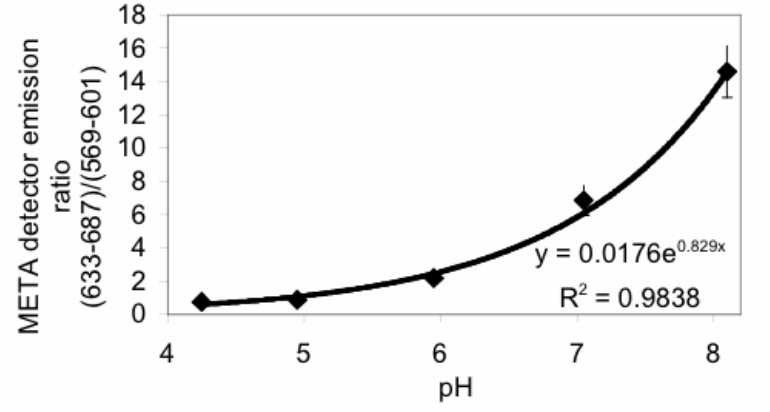

Figure 4.1 Fluorescence of SNARF-4F

(a) Fluorescence emission spectra of SNARF-4F as a function of pH. At low pH values, the peak at 575 nm is prominent, while the peak at 650 nm is low. As the pH rises, the 575 nm peak decreases in intensity, while the 650 nm peak rises to a maximum. pH measurements were taken in buffers with pH of 4.2, 5, 6, 7, and 8.

(b) Ratio of emission intensities for SNARF-4F dye, assessed via fluorimeter. Attaching the dye to oligonucleotides or complexing the labeled oligonucleotides into particles does not appreciably change the emission spectrum of the dye, compared to free dye in solution.

(c) From the fluorescence microscope, mean fluorescence signal from 633-687 nm divided by signal from 569-601 nm for SNARF-4F as a function of pH for different particles in buffered solutions.

microscope. The pH of the environment was quantified by measuring the SNARF-4F emission in all three bins and sequentially calculating the ratios of all three bins compared to one another. The ratios did not differ significantly for PLL and PEGylated CDP particles in solution, and the data were combined to generate a single calibration curve. It was determined that the 633-687/569-601 nm ratio was the most sensitive to pH changes. An exponential curve was fit to these data points to determine an equation for calculating pH from the fluorescence intensity ratios, which was then used to determine intracellular endosomal pH values (Figure 4.1c).

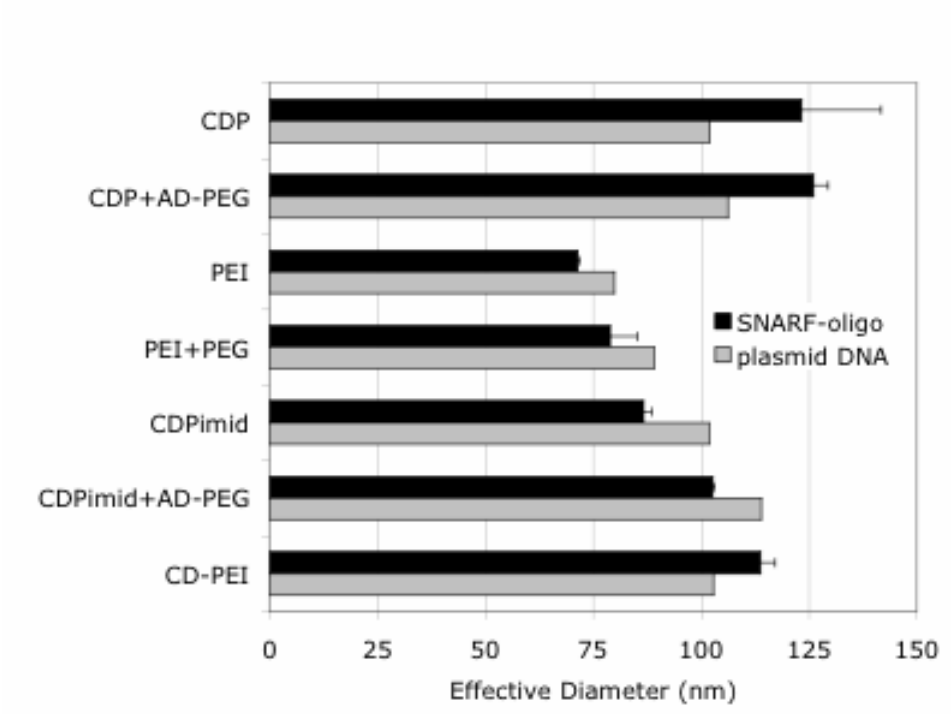

Figure 4.2 Average diameters of the various particles used in this study
Dynamic light scattering was employed to measure the effective diameters of the particles formulated. Most of these particles were formulated with an average effective diameter between 75-125 nm. Complexation of the polycation to either the SNARF-oligonucleotides or plasmid DNA resulted in particles of similar size.

By labeling the nucleic acids, and not the delivery vectors, the assay determines the pH environment of the delivered nucleic acids whether bound to the delivery vector or free in solution. It is relatively straightforward to directly visualize the SNARF-4F fluorescence when it is in a particle (Mishra et al. show high resolution TEM and fluorescent confocal microscopy results that confirm vesicle containment of intact particles using some of the vector systems employed here [21]), as the signal appears as a round cluster. Figure 4.3 shows an example of intact PLL polyplexes after 4 hours incubation and PEI polyplexes after 24 hours incubation imaged within different regions of the cell. The pH is depicted colorimetrically in this image; those polyplexes experiencing a lower pH environment appear more strongly blue colored whereas those experiencing a higher pH appear more strongly red colored. Diffuse staining indicative of unpackaged SNARF-oligonucleotide was not observed in these experiments, suggesting that unpackaged conjugate is diluted below the detection limit.

4.4.2 Intracellular pH measurements

HeLa cells were exposed to the delivery particles for 2 hours to allow for uptake and trafficking. While this time may seem long for endocytic processes, numerous reports have indicated that particle uptake and trafficking is notably slower [6, 10]. The media was then replaced to remove most of the free particles in solution, and the cells were incubated for up to 24 hours before imaging. Because of the direct nature of our assay, it is not necessary to completely remove the free particles; in fact, particles that have entered more recently can be visualized and the endosomal pH values individually quantitated.

a

b

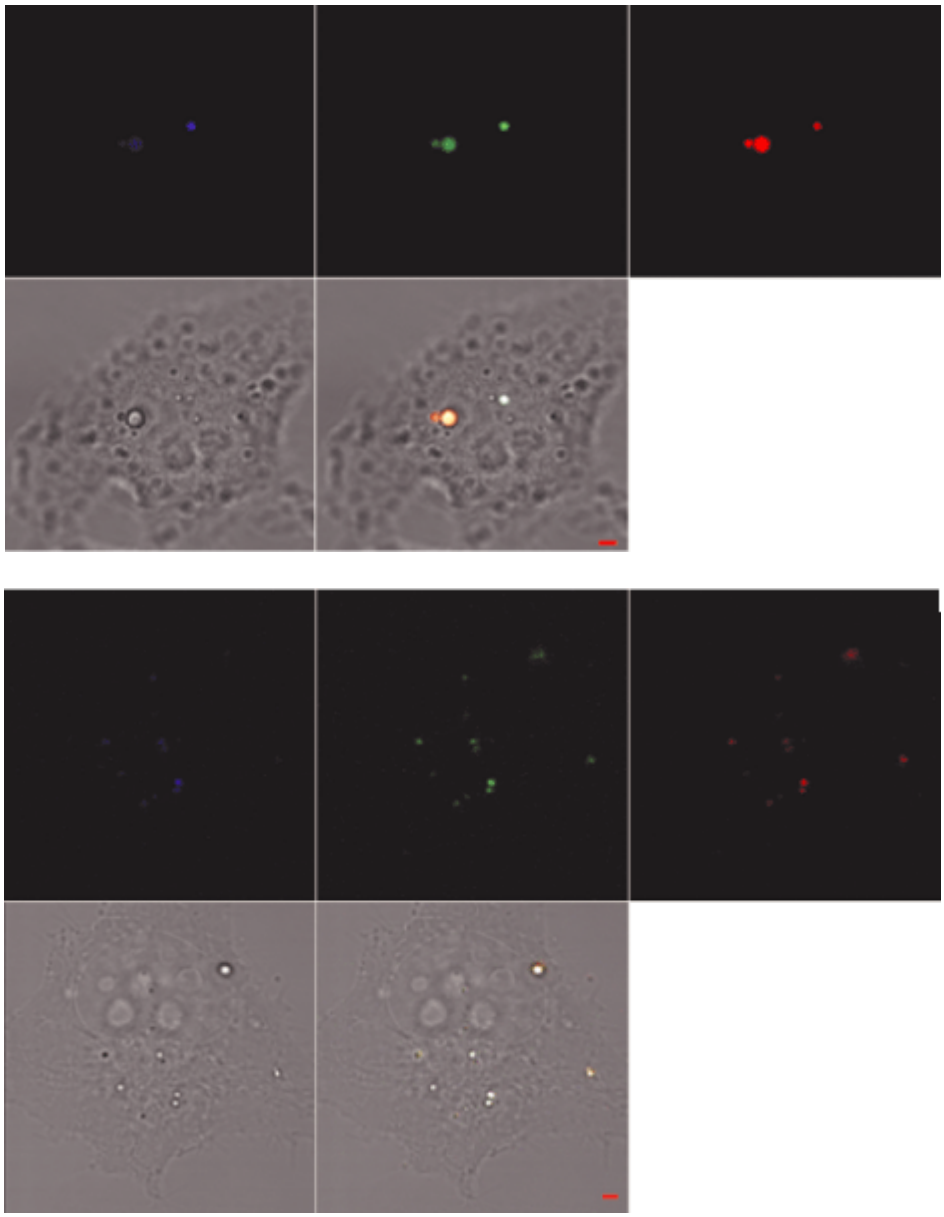

Figure 4.3 Examples of SNARF-oligo particles observed within cells
In the top row of these images, the left image represents the 569-601 nm channel, the center the 601-633 nm channel, and the right the 633-687 nm channel. (a) Image of PLL particles within cells after two hours incubation. In this case, the large spot has not acidified, while the smaller one to the right has acidified to pH 4.5. This image illustrates the inherent cell-cell variability of the uptake process, indicating that acidification does not occur uniformly or in a set time window. (b) Image of PEI particles in a cell after 24 hours incubation. The spots below the nucleus are at ~ pH 6, while the large one in the upper right corner is still at pH 7.5, suggesting that the particles in the upper right may have entered much later than the others. Scale bars = 1 μm.

A major advantage of direct visualization is that different regions of an individual cell can be quantitated separately and not averaged into a bulk measurement. We have found that early in the transfection process (less than 4 hours), there appear to be regional differences in pH values within the cell (Figures 4.3 and 4.4). Specifically, the cytoplasm can be divided into three regions – region I: within 2 μm of the cell membrane; region II: the cytoplasmic region between the other regions; and region III: within 2 μm of the nuclear membrane. We did not observe intact particles or labeled nucleic acids within the nucleus for any imaging condition. This is not unexpected for the CDP delivery systems, as Mishra et al. have shown that intact particles do not enter the nucleus (only released nucleic acids can be visualized in the nuclear compartment) [21].

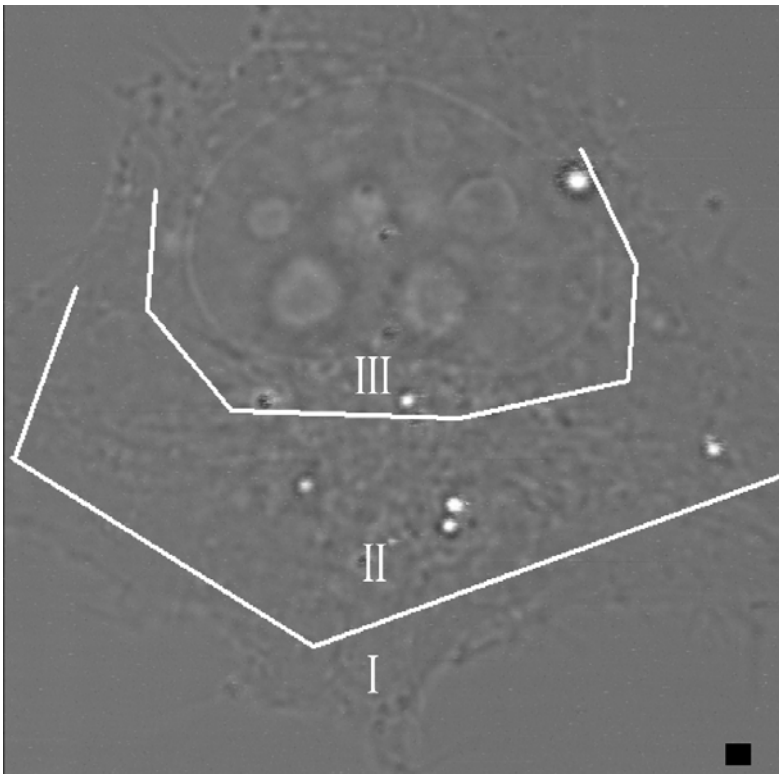

Figure 4.4 A schematic of a cell depicting the three regions described in the text
Region I is the area of the cell within 2 μm of the cell membrane, region III is the region within 2 μm of the nucleus, and region II depicts the area in between. Scale bar = 1 μm.

As the particles are first internalized, their pH is uniformly high in region I for all examined classes of delivery vectors; however, the pH drops for PLL, CDP, and lipofectamine particles as they travel towards the nucleus (Figures 4.5 and 4.6). The reduction in pH for PLL is rather rapid and is complete by 2 hours after initial incubation for those particles that reach region II. For the CDP vector, particles in region I are still at neutral pH after four hours, those in region II are at an average pH of 6.1 with significant variability in pH, while those close to the nucleus have acidified by four hours to an average pH of 5.2. Lipofectamine particles also display such an acidification, reaching an average pH of 4.6 by 16 hours. Again, the average value does not tell a complete story; certain particles in region II have fully acidified, while others are slower to do so.

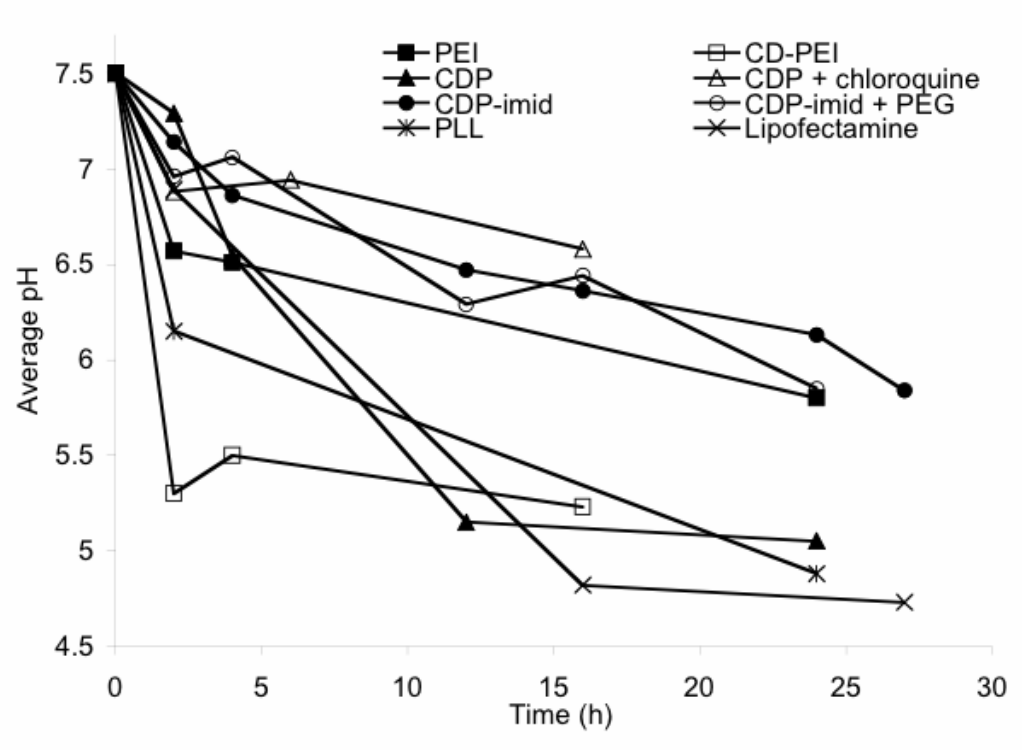

Figure 4.5 Plots of average pH of all cells and regions as a function of time

a

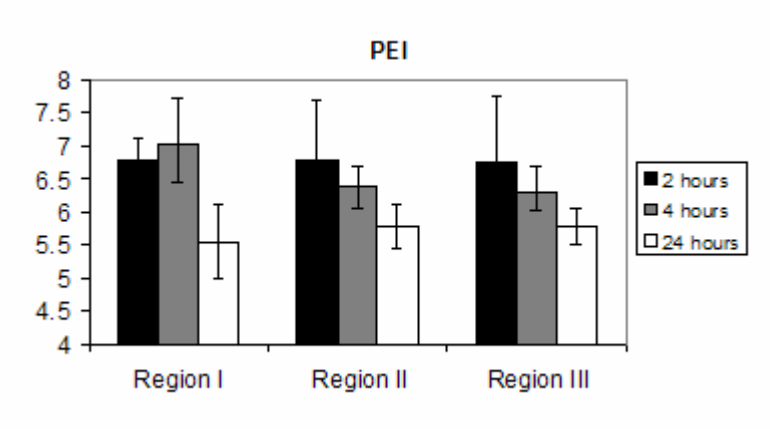

b

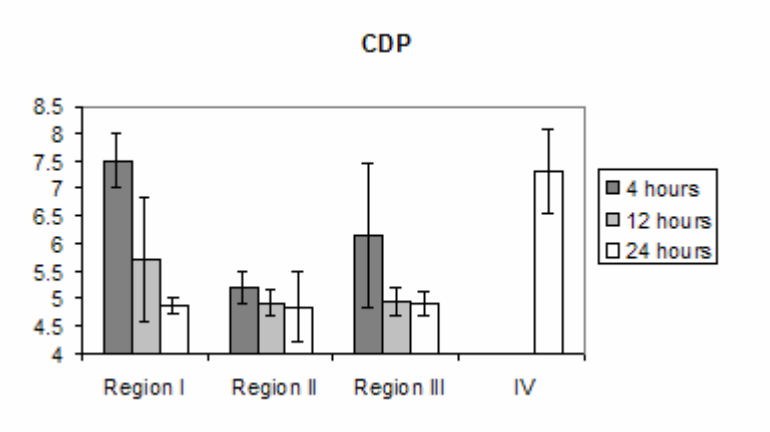

c

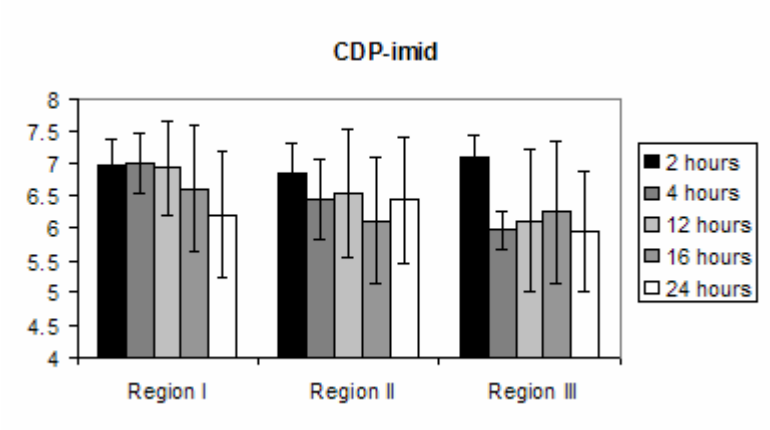

Figure 4.6 Regional pH values as a function of time and region within the cell
As seen with PEI (a), CDP (b), and CDP-imidazole (c) particles, particles experience intracellular pH variability across regions. For non-buffering systems such as CDP, differences are pronounced at earlier times.

In contrast, PEI particles display relatively consistent pH values for each time point, independent of region. Over time, the PEI particles do acidify from pH ~6.6 to pH ~5.8; however, the decrease is not as prominent as for PLL or CDP, which have acidified in all three regions by 24 hours. Even at this time point, however, there are still a few cells (~1-4%) that show particles that are not acidified, possibly because they have entered the cells only recently; these particles are indicated as being in region IV (Figure 4.6). CD-PEI exhibits acidification to pH ~5.5 rather quickly, even in region I. However, it does not fully acidify below this pH, even after 16 hours.

Although CDP particles do not buffer pH, modifications can be introduced to allow for buffering capacity. Conjugation of an imidazole group to the polymer termini produces CDP-imid, a vector that displays a limited buffering of pH. The acidification of CDP-imid particles occurs gradually, and even after 16 hours, the average endosomal pH was ~6.3. Further acidification was observed to occur, with the average pH reaching ~6 by 24 hours. Administration of chloroquine in conjunction with CDP particles resulted in a comparable buffering effect, with the pH remaining at ~6.6 even after 16 hours.

Three types of particles (CDP, CDP-imid, PEI) permitted facile comparison between PEGylated and unPEGylated variants. Interestingly, differences between PEGylated and unPEGylated variants of the same polyplex type were minor. For instance, at 16 hours after transfection, the average pH for PEGylated CDP-imid was ~6.4, while it was ~6.3 for the unPEGylated CDP-imid (Figure 4.4). Similar results were obtained for the other types of particles at each time point (data not shown).

4.4.3 Transfection data

To explore the implications of the buffering behavior on the gene delivery efficiency of the examined delivery vectors, the delivery of luciferase plasmid DNA was employed. The examined delivery vectors generate similarly-sized particles regardless of whether they are used to condense the SNARF-labeled oligonucleotide or plasmid DNA (Figure 4.2). The gene delivery activity of the various delivery vectors was assessed by transfecting cells with firefly luciferase-expressing plasmid DNA and assaying for luciferase expression (Figure 4.7).

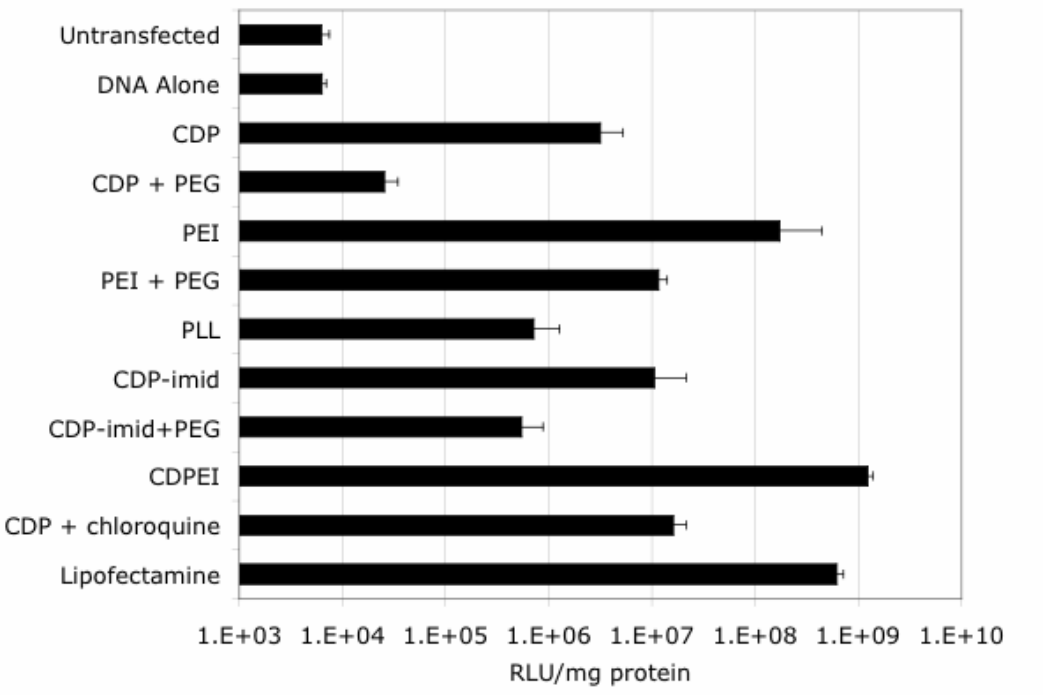

Figure 4.7 Gene delivery efficiency for each of the particles used in this study
The delivery vectors were complexed with plasmid DNA encoding luciferase, and used to transfect HeLa cells. The relative luciferase expression varies markedly for each type of particle. In general, stabilizing particles through PEGylation resulted in lower luciferase expression.

DNA uptake by cells was quantified using fluorescently-labeled plasmid DNA and analysis by flow cytometry (Figure 4.8). The cellular fluorescence intensity can be correlated with relative uptake of plasmid DNA because the fluorescent label used (YOYO-1) was shown on a fluorimeter to be pH-insensitive (data not shown).

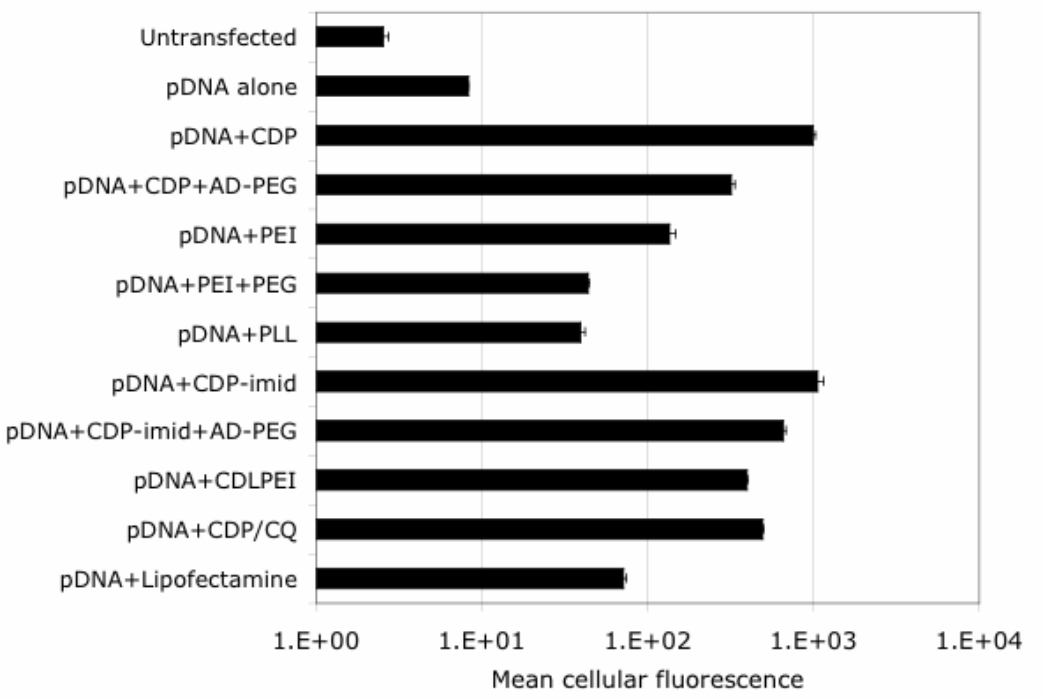

Figure 4.8 Measure of DNA uptake for each type of particle
Fluorescently labeled plasmid DNA was complexed with each type of delivery vector, and administered to HeLa cells. After four hours, the cells were collected and analyzed by flow cytometry. The mean cellular fluorescence was used as a measure of DNA uptake.

4.5 Discussion

The fluorescence-based pH assay described herein provides the ability to follow and track individual particles within cells over time and thus gives insight into the nature of their trafficking within the cell. The development of this methodology was enabled by the facile labeling of the oligonucleotide and by the preservation of the label's pH sensitivity even when the conjugated oligonucleotides were condensed into delivery particles. Here, only a single fluorophore is used per nucleic acid molecule, thus avoiding the issue of uneven labeling (of nucleic acids or within particles) that can be present with two-fluorophore experiments.

Individual cells are examined in this assay, and particles residing in different zones within a given cell can be visualized and their local pH environment examined. Specifically, a "pH map" of the delivery vectors can be determined as a function of the time-dependent spatial locations (i.e., close to the cell membrane, near the nucleus, or in between) of the vectors as they traverse the cell. The relevance of this approach is demonstrated, for example, by the small percentage of cells showing PEI particles in region IV (those that are not acidified even after 24 hours). In a bulk assay, this information would be lost, with such individual differences combined into a statistical average. Here, we directly access spatiotemporal information and use it to refine models of intracellular trafficking of delivery particles.

The current model of delivery vehicle transport through the cell suggests that the particles are first internalized within endosomal compartments, after which the compartments mature from early endosomes to late endosomes and finally to lysosomes; the pH of these compartments progressively declines until reaching pH ~4.5 [10,17,23].

Our results support this model of trafficking through the endocytic pathway by demonstrating and quantifying the reduction in pH experienced by delivered nucleic acids as they move through the cell. The ability of the delivery vehicles to circumvent or alter the steps of the endocytic pathway is of interest for understanding how efficiencies and transport rates are affected. Specifically, those particles that contain titratable amines at pH values between approximately 4 and 7 (such as PEI) are thought to buffer the endosomal compartments and prevent maturation into lysosomes. The buffering thus affects delivery. It is believed that those polymers that can buffer act as "proton sponges" and promote osmotic swelling and lysis of endosomes. This lysis is speculated to allow endocytic pathway release that thus improves delivery efficiency [11,15].

In general, these models have been developed without an assessment of the spatial and temporal localization of the relevant pH changes. Each endosome is an individual entity and acidifies at a different rate that is dependent upon cell type and other factors. Here, we specifically examine acidification within HeLa cells and find that spatial differences are prominent for CDP and PLL particles at early times (before 4 hours). When these particles have trafficked for more than 12 hours, they reach a pH of roughly 4.8-5.0 and show little difference regardless of position within the cell. These low pH values suggest that the endosomes have fully acidified and are at the lysosomal stage. For PEI, the spatial localization is less important than temporal differences, and the pH values are relatively constant throughout the cell for a given time point. After 24 hours, the pH is ~5.8, indicating that full acidification does not occur. For CDP-imid particles, the pH values are also relatively constant throughout the cell for a particular time point;

the imidazole group acts to buffer the pH (relative to CDP particles) and the pH remains above 6 for almost 24 hours (similar to PEI).

The uptake, intracellular trafficking, and gene delivery efficiency of PEGylated gene delivery particles differs from that of their unPEGylated variants [21]. Comparing PEGylated CDP, PEGylated CDP-imid, and PEGylated PEI particles to their unPEGylated variants, we observe no significant differences in the extent or kinetics of acidification. This result indicates the PEG coating does not affect acidification or progression through the endocytic pathway. Retention of buffering capacity with the PEGylated particles is significant because systemic, in vivo administraton of non-viral gene delivery particles will require PEGylation or other means of salt-stabilization.

The relatively high delivery efficiency of PEI has been linked to its ability to act as a "proton sponge," and there is evidence to support this hypothesis [11,15,24,25]. Improvements in non-viral transfection efficiency in the presence of chloroquine have also provided credence to the "proton sponge" hypothesis. It is shown here that chloroquine confers significant buffering activity to a vector system that otherwise readily acidifies. However, by comparing vectors with and without pH buffering capacity, it is clear that buffering capacity alone does not necessarily correlate with gene delivery efficiency. Despite similar pH buffering capacity, the three types of PEGylated particles generate reduced expression relative to their unPEGylated variants. The terminal imidazole group confers significant pH buffering capacity to CDP-imid that is not present for CDP; at the charge ratio examined here, the buffering activity does not correlate with significant improvements in transfection efficiency. Conversely, the significant buffering capacity of PEI is not seen in CD-PEI, but both vectors give strong

expression, consistent with published results [20]. The lack of correlation between buffering and gene expression has been observed by others [13,26]. Forrest et al. revealed that acetylated PEI gave both reduced buffering capacity and improved transfection efficiency relative to unmodified PEI [26]. (The buffering capacity of both CD-PEI and this acetylated PEI is reduced because some amine groups of PEI have been converted to other functionalities [20,26].) Also, recent reports have shown that new polymeric vectors designed with buffering capacity do not necessarily perform well as gene delivery vectors [13,27].

The data gathered here by a single-cell approach can be analyzed in aggregate for comparison with prior studies that have utilized flow cytometry to compile aggregate data. Our results in HeLa cells and those of Akinc and Langer in NIH 3T3 cells [17] both indicate that PEI shows a strong buffering capacity relative to PLL. This is consistent with a simple model where the titratable amines of PEI that are not present on PLL confer buffering capacity. In contrast, Forrest and Pack observed almost the opposite behavior, with PEI showing little to no buffering capacity as a function of cell line and PLL particles showing sharp variability as a function of cell line [10], including almost no reduction in pH in HepG2 cells even 15 hours after transfection. Of note, fluorescently-labeled nucleic acids were utilized in our study and that of Akinc and Langer, while Forrest and Pack conducted their experiments by fluorescently-labeling the delivery vectors.

It has been widely observed that chloroquine treatment produces increases in transfection efficiency for many types of non-viral gene delivery particles [16,28], as seen in this study with CDP particles. The mechanism of this improvement is unclear.

One possibility is that high intracellular or intravesicular concentrations of chloroquine induce the unpackaging of delivered nucleic acids from delivery vectors [28,29]. Chloroquine is also known to buffer the vesicles of the endocytic pathway [30], and this buffering may inhibit the transfer of endocytosed gene delivery particles to lysosomes. Our results do not resolve the questions surrounding this mechanism, but they do show that chloroquine treatment inhibits acidification of intracellular CDP particles in HeLa cells. In the bulk assay of Akinc and Langer, chloroquine buffered the average pH of PLL particles in NIH 3T3 cells. In contrast to our results, their data included a sharp fluctuation where the average pH of the intracellular PLL particles dropped abruptly to pH ~4 in the first two hours before rising upward in the next two hours [17]. The kinetics of chloroquine uptake may differ for the two cell lines. Although Forrest and Pack did not observe buffering by PEI, their bulk assay showed significant buffering when PEI transfection was accompanied by chloroquine [10].

When acidification of endocytic vesicles is buffered by gene delivery particles, the vesicles still progress through the endocytic pathway. PEI, for example, is shown here to demonstrate strong buffering capacity in a gene delivery particle. Lecocq et al. used centrifugation methods to show that intracellular PEI eventually colocalizes with the lysosomal marker cathepsin C [31]. Kichler et al. observed that in vitro reporter gene expression was impaired when endosome acidification was inhibited with bafilomycin A1, indicating that, despite its buffering activity, PEI relies on the acidification process for transfection [32]. Similarly, Singh et al. histidylated two cationic lipids to confer pH buffering and found that gene delivery with these lipids was less efficient in the presence of bafilomycin A1 [33].

Single-cell methods can supply new information on intracellular trafficking that will be useful in the design of improved gene delivery vectors. For example, various researchers have sought to enhance intracellular vector unpackaging by preparing acid-labile polycation-DNA particles [14,34]. A detailed description of the spatial and temporal pH changes experienced by these particles in cells would indicate the probable intracellular location(s), timing, and extent of the particle degradation, thus facilitating refinement of the pH-sensitive vectors.

The compact, intense clusters of SNARF-4F fluorescence observed within cells are assumed to represent nucleic acids contained within vesicles. The small size of the SNARF-oligonucleotide suggests that the fluorescent signal from unpackaged intracellular oligonucleotides would appear diffuse. The absence of such diffuse staining could indicate that the majority of delivered nucleic acids remained within the delivery particles [21]. Alternatively, the unpackaged oligonucleotide may present a signal so diffuse that it is below the detection limit, or it may be rapidly degraded and/or expelled from cells.

One question that arises is why there might be any particles still remaining in region I (near the cell membrane) at 12 or even 24 hours after transfection. One plausible explanation is that these particles have entered only a few hours earlier and have not had time to acidify. Particles in this category might have been stuck on the outer surface for hours before being endocytosed. However, this does not fully explain the existence of very low pH endosomes near the cell membrane. A second possibility is that such endosomes are trafficking very slowly towards the nucleus, or are traveling in a random trajectory and have fully acidified but happen to be close to the membrane when imaged.

The particles must be transported along microtubules within endosomes in order to navigate the cytoplasm; the trajectories of these endosomes are often stochastic [35,36].

The advantages of the method presented here include the ability to directly visualize each cell and follow the internalization and endosome trafficking of delivery vehicles over time. This approach avoids or minimizes some of the problems of bulk imaging by flow cytometry that include quantitation of dead cells, presence of particles on the surface of the cell, and suppression of variability by intracellular region. The dynamics of the uptake and acidification process can be quantitated in both time and space, and any escape or other behavior can be monitored. By analyzing single cells, any variability in the process can be revealed and not buried in the overall average. This variability is especially evident at early times, as particles in certain spatial regions exhibit a broad range of pH values. We can also measure and segregate small subpopulations that would otherwise be combined into the statistical mean. Through the use of this assay, individual cells can be tracked for hours, and the spatial and temporal pH profile can be analyzed to better understand intracellular trafficking of non-viral gene delivery vectors. In summary, this new methodology has yielded data from which we have carried out further analyses of prior experiments performed in aggregate, quantified the differences in buffering capacity among a variety of delivery vectors, revealed that PEGylation does not significantly affect buffering capacity, and verified that chloroquine can confer buffering to gene delivery particles. The results presented here raise further questions about the role of pH buffering in the endocytic pathway and its importance to gene delivery efficiency.

4.6 References

1. Davis ME (2002) Non-viral gene delivery systems. Curr. Opin. Biotechnol. 13:128-131.
2. Godbey WT, Mikos AG (2001) Recent progress in gene delivery using non-viral transfer complexes. J. Control. Release 72:115-125.
3. Boussif O, Lezoualc'h F, Zanta MA, Mergny MD, Scherman D, Demeneix B, Behr JP (1995) A versatile vector for gene and oligonucleotide transfer into cells in culture and in vivo: polyethylenimine. Proc. Natl. Acad. Sci. USA 92:7297-7301.
4. Luo D, Saltzman WM. (2000) Synthetic DNA delivery systems. Nat. Biotechnol. 18:33-37.
5. Stayton PS, Hoffman AS, Murthy N, Lackey C, Cheung C, Tan P, Klumb LA, Chilkoti A, Wilbur FS, Press OW (2000) Molecular engineering of proteins and polymers for targeting and intracellular delivery of therapeutics. J. Control. Release 65:203-220.
6. Godbey WT, Wu KK, Mikos AG. (1999) Tracking the intracellular path of poly(ethylenimine)/DNA complexes for gene delivery. Proc. Natl. Acad. Sci. USA 96:5177-81.
7. Bieber T, Meissner W, Kostin S, Niemann A, Elsasser HP. (2002) Intracellular route and transcriptional competence of polyethylenimine-DNA complexes. J. Control. Release 82:441-454.
8. Remy-Kristensen A, Clamme JP, Vuilleumier C, Kuhry JG, Mely Y (2001) Role of endocytosis in the transfection of L929 fibroblasts by polyethylenimine/DNA complexes. Biochim. Biophys. Acta 1514:21-32.
9. Hwang SJ, Davis ME (2001) Cationic polymers for gene delivery: designs for overcoming barriers to systemic administration. Curr. Opin. Mol. Ther. 3:183-191.
10. Forrest ML, Pack DW (2002) On the kinetics of polyplex endocytic trafficking: implications for gene delivery vector design. Mol. Ther. 6:57-66.
11. Sonawane ND, Szoka FC, Verkman AS (2003) Chloride accumulation and swelling in endosomes enhances DNA transfer by polyamine-DNA polyplexes. J. Biol. Chem. 278:44826-44831.
12. Akinc A, Lynn DM, Anderson DG, Langer R (2003) Parallel synthesis and biophysical characterization of a degradable polymer library for gene delivery. J. Am. Chem. Soc. 125:5316-5323.
13. Funhoff AM, van Nostrum CF, Koning GA, Schuurmans-Nieuwenbroek NM, Crommelin DJ, Hennink WE (2004) Endosomal escape of polymeric gene delivery complexes is not always enhanced by polymers buffering at low pH. Biomacromolecules 5:32-39.
14. Choi JS, MacKay JA, Szoka FC (2003) Low-pH-sensitive PEG-stabilized plasmid-lipid nanoparticles: preparation and characterization. Bioconjug. Chem. 14:420-429.
15. Behr JP (1997) The proton sponge: A trick to enter cells the viruses did not exploit. Chimia 51:34-36.

16. Gonzalez H, Hwang SJ, Davis ME (1999) New class of polymers for the delivery of macromolecular therapeutics. Bioconjug. Chem. 10:1068-1074.
17. Akinc A, Langer R (2002) Measuring the pH environment of DNA delivered using nonviral vectors: implications for lysosomal trafficking. Biotechnol. Bioeng. 78:503-508.
18. Chen QR, Zhang L, Luther PW, Mixson AJ (2002) Optimal transfection with the HK polymer depends on its degree of branching and the pH of endocytic vesicles. Nucleic Acids Res. 30:1338-134.
19. Davis ME, Pun SH, Bellocq NC, Reineke TM, Popielarski SR, Mishra S, Heidel JD (2004) Self-assembling nucleic acid delivery vehicles via linear, water-soluble, cyclodextrin-containing polymers. Curr. Med. Chem. 11:179-197.
20. Pun SH, Bellocq NC, Liu A, Jensen G, Machemer T, Quijano E, Schluep T, Wen S, Engler H, Heidel J, Davis ME (2004) Cyclodextrin-modified polyethylenimine polymers for gene delivery. Bioconjug. Chem. 15:831-840.
21. Mishra S, Webster P, Davis ME (2004) PEGylation significantly affects cellular uptake and intracellular trafficking of non-viral gene delivery particles. Eur. J. Cell. Biol. 83:97-111.
22. Popielarski SR, Mishra S, Davis, ME (2003) Structural effects of carbohydrate-containing polycations on gene delivery. 3. Cyclodextrin type and functionalization. Bioconjug. Chem. 14:672-678.
23. Sonawane ND, Thiagarajah JR, Verkman AS (2002) Chloride concentration in endosomes measured using a ratioable fluorescent Cl- indicator: evidence for chloride accumulation during acidification. J. Biol. Chem. 277:506-5513.
24. Akinc A, Thomas M, Klibanov AM, Langer R (2005) Exploring polyethyleneimine-mediated DNA transfection and the proton sponge hypothesis. J. Gene Med. 7:657-663.
25. Fukushima S, Miyata K, Nishiyama N, Kanayama N, Yamasaki Y, Kataoka K (2005) PEGylated polyplex micelles from triblock catiomers with spatially ordered layering of condensed pDNA and buffering units for enhanced intracellular gene delivery. J. Am. Chem. Soc. 127:2810-2811.
26. Forrest ML, Meister GE, Koerber JT, Pack DW (2004) Partial acetylation of polyethylenimine enhances in vitro gene delivery. Pharm. Res. 21:365-371.
27. Dubruel P, Christiaens B, Rosseneu M, Vandekerckhove J, Grooten J, Goossens, V, Schacht E (2004) Buffering properties of cationic polymethacrylates are not the only key to successful gene delivery. Biomacromolecules 5:379-388.
28. Erbacher P, Roche AC, Monsigny M, Midoux P (1996) Putative role of chloroquine in gene transfer into a human hepatoma cell line by DNA/lactosylated polylysine complexes. Exp. Cell. Res. 225:186-194.
29. Allison JL, O'Brien RL, Hahn FE (1965) DNA: reaction with chloroquine. Science 149:1111-1113.
30. Maxfield FR (1982) Weak bases and ionophores rapidly and reversibly raise the pH of endocytic vesicles in cultured mouse fibroblasts. J. Cell. Biol. 95:676-681.
31. Lecocq M, Wattiaux-De Coninck S, Laurent N, Wattiaux R, Jadot M (2000) Uptake and intracellular fate of polyethylenimine in vivo. Biochem. Biophys. Res. Commun. 278:414-418.

32. Kichler, A., Leborgne, C., Coeytaux, E., and Danos, O. (2001) Polyethylenimine-mediated gene delivery: a mechanistic study. J. Gene. Med. 3:135-144.
33. Singh RS, Goncalves C, Sandrin P, Pichon C, Midoux P, Chaudhuri A (2004) On the gene delivery efficacies of pH-sensitive cationic lipids via endosomal protonation: a chemical biology investigation. Chem. Biol. 11:713-723.
34. Walker GF, Fella C, Pelisek J, Fahrmeir J, Boeckle S, Ogris M, Wagner E (2005) Toward Synthetic Viruses: Endosomal pH-Triggered Deshielding of Targeted Polyplexes Greatly Enhances Gene Transfer in vitro and in vivo. Mol. Ther. 11:418-425.
35. Kulkarni RP, Wu DD, Davis ME, Fraser SE (2005) Quantitating intracellular transport of polyplexes by spatio-temporal image correlation spectroscopy. Proc. Natl. Acad. Sci. USA 102:7523-7528.
36. Suh J, Wirtz D, Hanes J (2003) Efficient active transport of gene nanocarriers to the cell nucleus. Proc. Natl. Acad. Sci. USA 100:3878-3882.

CHAPTER 5: CHLOROQUINE (CQ), ITS CHEMICAL ANALOGUES, AND THEIR EFFECTS ON NON-VIRAL GENE DELIVERY

5.1 Abstract

The presence of chloroquine (CQ) dramatically enhances transfection efficiency of many types of polyplexes (complexes of nucleic acids and polycations). The mechanism of this action is not well understood and has not been extensively investigated. Here, a number of CQ analogues are synthesized, with variations either on the alkyl amino side chain or on the aromatic ring, in order to develop a structure-function correlation among CQ and its analogues in non-viral, polycation-based gene delivery.

It was found that the tertiary amino moiety is important to CQ's enhancement of gene expression, as its removal eliminates the enhancement. Further, the enhancement is dramatically affected by changes to the aromatic ring. Quinacrine (QC), a CQ analogue with a tricyclic aromatic acridinyl structure, shows much higher cytotoxicity than CQ and can enhance transfection similarly to CQ at a concentration 10 times lower. N^4-(7-Chloro-4-pyridinyl)-N^1,N^1-diethyl-1,4-pentanediamine (CP), a CQ analogue with a pyridinyl aromatic ring, gives lower cytotoxicity than CQ but has no effect on gene expression. Transfection in the presence of N^4-(7-trifluoromethyl-4-quinolinyl)-N^1,N^1-diethyl-1,4-pentanediamine (CQ7a), a 7-trifluoromethyl CQ analogue, shows luciferase activity one order of magnitude higher than in the presence of CQ at same concentration (200 μM), while transfection in the presence of N^4-(4-quinolinyl)-N^1, N^1-diethyl-1,4-pentanediamine (CQ7b), a 7-H CQ analogue, shows no effect on transfection.

CQ and CQ7a both demonstrate activity in buffering the pH experienced by polyplexes within the endocytic pathway, but CQ7a is more potent in enhancing gene transfer. CQ7a has higher binding affinity to DNA than CQ as well as a greater tendency to competitively displace the polycation from polyplexes at an achievable intracellular concentration. These findings suggest that in addition to pH-buffering activity, CQ's competitive displacement of polycations and its own interaction with nucleic acids are important to its enhancement of gene expression in non-viral nucleic acid delivery systems.

5.2 Introduction

The intracellular transport of polycation/DNA complexes (polyplexes) involves their cellular uptake, release from the endocytic pathway into the cytoplasm, and delivery of DNA to the cell nucleus. To achieve transgene expression, polyplexes must overcome several extra- and intracellular barriers [1]. A large body of literature suggests that entrapment of polyplexes in the endocytic pathway, and their resulting degradation in lysosomes, represents a major impediment to transfection efficiency [1-3].

Significant increases in gene expression with many non-viral gene delivery systems are observed when chloroquine (CQ) is present during the transfection [4-8]. We have observed increased transfection efficiency in the presence of CQ in our studies using cyclodextrin-containing polycations (CDP) for the delivery of nucleic acids [9-14]. Although CQ has been widely used as a transfection enhancement reagent, the mechanism by which CQ enhances gene expression remains unclear. CQ is a weak base with pK_a's of 8.1 and 10.2 [15], and can buffer the luminal pH of endosomes [16,17].

This activity could improve transfection efficiency by facilitating DNA release from the endocytic pathway (as it may generate swelling and destabilization of endosomes) [18] or by inhibiting lysosomal enzyme degradation [19,20]. Such hypotheses are supported by the observation that polyethyleimine (PEI), itself known to buffer endosomes, does not benefit from the presence of CQ [7,21]. Noting that CQ interacts with DNA [7,22,23], others have suggested that CQ may increase the transfection efficiency by facilitating dissociation of DNA from polyplexes [7].

Here we attempt to understand the mechanism of CQ-induced increases in gene expression by designing several CQ analogues (Figure 5.1) and studying gene transfer in the presence of these compounds. By correlating the chemical structures of CQ analogues with their contributions to gene transfer, information on the role of CQ is obtained. A similar structure-property approach has been applied to understand the mechanism of CQ's antimalarial activity [24-27].

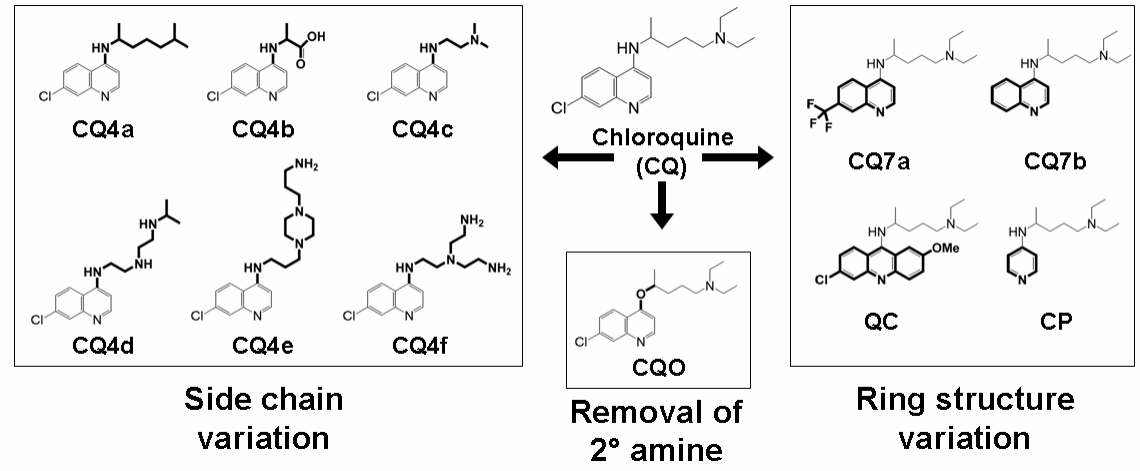

Figure 5.1 Chemical structures of chloroquine and analogues
A series of chloroquine analogues were synthesized to study the effects of variations in side chain, variations in ring structure, or removal of the secondary amine.

5.3 Materials and methods

Chemicals reagents were purchased from Sigma-Aldrich (St. Louis, MO) and used without further purification unless otherwise indicated. NMR spectra were collected on Varian 300 MHz and Inova 500 MHz spectrometers. Chloroquine (CQ) and quinocrine (QC) were purchased from Sigma.

5.3.1 Polycation

A linear β-cyclodextrin-containing polymer (CDP) was synthesized and used for condensing DNA in this study. The synthesis of CDP has been described in detail elsewhere [9,10]. The average molecular weight of the polycation used in this study is 6000 Da. The structure of CDP is shown in Scheme 5.1. Each repeat unit contains two positively-charged amidine groups that can efficiently bind and condense DNA [10].

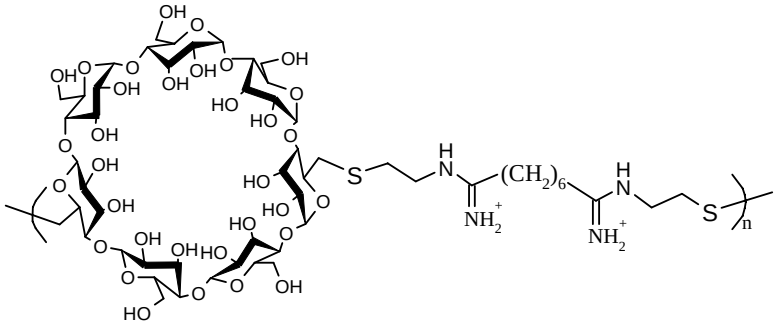

Scheme 5.1 Structure of CDP

5.3.2 Synthesis of CQ analogues

Chloroquine (CQ) is a quinoline analogue with a chloro group at the 7-position and an alkyl amino group at the 4-position (Figure 5.1). CQ analogues with side alkyl amino side chain variation were synthesized via substitution reaction of an appropriate amine and 4,7-dichloroquinoline. CQ analogues of ring-size variations and ring-substituent variations were synthesized similarly using an appropriate quinoline or pyridine derivative as starting materials.

Synthesis of CQ4a. A mixture of 4,7-dichloroquinoline (619 mg, 3.1 mmol) and 1,5-dimethylhexylamine (3.1 g, 23.7 mmol) was heated at 100 °C for 1 h and then at 155 °C for 3 h. The reaction was monitored by TLC to ensure the completion of reaction. Unreacted amines were distilled under vacuum and could be reused. The resulting brownish residue was applied to a silica gel flash column and a solvent mixture ($CHCl_3$/CH_3OH /Et_3N (25/1/1)) was used as eluent. CQ4a was isolated in 64% yield after combining elution fractions. CQ4a was further purified by crystallization ($CHCl_3$ and hexane) to give 120 mg (13% yield) of white solid. ^1H NMR ($CDCl_3$) δ 8.52 (1H, d), 7.95 (1H, d), 7.64 (1H, s), 7.37 (1H, d), 6.42 (1H, d), 4.78 (1H, br), 3.71 (1H, m), 1.67 (2H, m), 1.59 (1H, m), 1.43 (2H, m), 1.32 (3H, d), 1.23 (2H, d), 0.87 (6H, d). ESI-MS: expected M 264, found $[M+H]^+$ 265.

Synthesis of CQ4b. 4,7-Dichloroquinoline (1.98g, 10 mmol) and L-alanine (1.78 g, 20 mmol) were heated in the presence of phenol (8 g) for one hour at 160 °C. The solution was poured into a solution mixture of 10% KI (30 mL) and ethyl ether (30 mL). The aqueous layer was then washed with ether layer (3×30 mL). The combined ether layer was extracted once with 10% KI (30 mL). The pH of the combined aqueous phase

was adjusted to 7. The aqueous solution was let uncovered for slow evaporation at room temperature. After about 24 h, white crystals were filtered and dried under vacuum (1.25g, 55%). ^{1}H NMR ($CDCl_3$) δ 8.43 (1H, m), 8.33 (1H, m), 7.76 (1H, s), 7.56 (1H, m), 6.66 (1H, m), 4.26 (1H, m), 1.66 (3H, d)

Synthesis of CQ4c. CQ4c was synthesized using the same method as CQ4a with corresponding amine (26%). ^{1}H NMR ($CDCl_3$) δ 8.53 (1H, d), 7.94 d (1H, d), 7.70 (2H, m), 7.36 (1H, m), 5.92 (1H, br.), 3.28 (2H, t), 2.68 (2H, t), 2.30 (6H, s)

Synthesis of CQ4d. 4,7-Dichloroquinoline (0.62g) and excess N1-isopropyl-diethylenetriamine (2 mL) was heated at 100 °C for 1 h and then at 155 °C for additional 3 h. TLC analysis indicated that 4,7-Dichloroquinoline was completely consumed after 4 h. Unreacted amine was distilled at 85-110 °C using a Kugelrohr apparatus under a vacuum of approximately 50 millitorr. The remaining brown oil was transferred to a silica gel flash column. A solvent mixture (CH_2Cl_2/CH_3OH/NH_4OH (70/28/2), 200 mL) was used as eluent, followed by another eluent (CH_2Cl_2/CH_3OH/NH_4OH (5/20/4), 200 mL). Three fractions were isolated and analyzed by ^{1}H NMR (data not shown). The second fraction (Rf=0.1 in CH_2Cl_2/NH_4OH/CH_3OH (40/1.5/80)) was found to be CQ4d with some impurities. All of the fractions were combined and transferred to another silica gel column and eluted ($CHCl_3$/CH_3OH /Et_3N (10/1/1), 200 mL). Clean fractions were combined. Solvents were removed by vacuum to give a slight yellow oil (35%). ESI-MS: expected M=306, found $[M+H]^{+}$=307. ^{1}H NMR (CD_3CD) δ 8.52 (1H, d), 7.94 (1H, d), 7.70 (1H, d), 7.35 (1H, m), 6.32 (1H, d), 5.98 (1H, br.), 3.36 (2H, m), 3.06 (2H, m), 2.80 (3H, m), 2.07 (2H, m), 1.07 (6H, d).

Synthesis of CQ4e. 4,7-Dichloroquinoline (0.5g) and excess 1,4-piperazine-dipropanamine (5 mL) were heated at 135 °C for 12 h. TLC analysis indicated that 4,7-Dichloroquinoline was completely consumed. Unreacted amine was distilled at 85-110 °C using a Kugelrohr apparatus under a vacuum of approximately 50 millitorr. The remaining brown oil was transferred to a silica gel flash column. A solvent mixture (CH_2Cl_2/CH_3OH/NH_4OH (70/28/2), 800 mL) was used as eluent, followed by elution in CH_2Cl_2/CH_3OH/NH_4OH ((5/20/4), 200 mL) and CH_3OH/NH_4OH ((1/1), 200 mL). Three different compounds were observed on TLC (CH_2Cl_2/CH_3OH/NH_4OH (5/20/4)) and each was analyzed by ^1H NMR (data not shown). The fraction with Rf=0.33 was found to be CQ4e. The combined fractions were transferred to another column and eluented with ($CHCl_3$/CH_3OH /Et_3N (10/1/1), 200 mL). Clean fractions were obtained and combined. Solvents were removed under vacuum to give a colorless oil (31%). ESI-MS: expected M=361, found $[M+H]^+$=362. ^1H NMR (CD_3CD) δ 8.35 (1H, d), 8.07 (1H, d), 7.77 (1H, d), 7.39 (1H, m), 6.53 (1H, d), 3.39 (2H, d), 2.41-2.69 (14H, m), 1.93 (2H, m), 1.64 (2H, m).

Synthesis of CQ4f. 4,7-Dichloroquinoline (0.68g) and excess of Tris-(2-aminoethyl)-amine (5 mL) were heated at 135 °C for 12 h. TLC analysis indicated that 4,7-Dichloroquinoline was completely consumed. Unreacted amine was distilled at 85-110 °C using a Kugelrohr apparatus under a vacuum of approximately 50 millitorr. The remaining brown oil was transferred to a silica gel flash column. A solvent mixture (CH_2Cl_2/CH_3OH/NH_4OH (70/28/2), 800 mL) was used as eluent, followed by elution with CH_2Cl_2/CH_3OH/NH_4OH ((5/20/4), 200 mL) and CH_3OH/NH_4OH ((1/1), 200 mL). Three different compounds were observed on TLC (CH_2Cl_2/CH_3OH/NH_4OH (5/20/4))

and each was analyzed by ^{1}H NMR (data not shown). The fraction with Rf=0.2 was found to be CQ4f. The combined fractions were transferred to another column and eluented with ($CHCl_3$/CH_3OH/NH_4OH (20/5/1), 200 mL). Clean fractions were obtained and combined. Solvents were removed under vacuum to give a colorless oil (15%). ESI-MS: expected M=307, found $[M+H]^+$=308. ^{1}H NMR (CD_3CD) δ 8.50 (1H, d), 7.98 (1H, m), 7.92 (1H, d), 7.32 (1H, m), 6.69 (1H, br), 6.35 (1H, d), 3.36 (2H, m), 2.85 (6H, m), 2.63 (4H, m), 1.59 (4H, br).

Synthesis of CQ7a. 4-chloro-7-trifluoromethyl quinoline (0.5g, 2.16 mmole) and 2-amino-5-diethylaminopentane (2.61 g, 15.7 mmole) were heated together at 100 °C for 1 hour and then 155 °C for 4.5 hours. Reaction was then cooled to room temperature and excess unreacted amine was removed by Kugelrohr distillation at 120 °C under vacuum. The remaining brown crude oil was then dissolved in $CHCl_3$ and purified by preparative TLC using $CHCl_3$/CH_3OH/Et_3N (25/1/1) as an eluent to yield a colorless oil (32%). ^{1}H NMR (CD_3OD) δ 8.62 (1H, d), 8.23 (1H, d), 7.91 (1H, m), 7.58 (1H, m), 6.52 (1H, d), 5.55 (1H, m), 3.75 (1H, m), 2.56 (6H, m), 1.80 (2H, m), 1.67 (2H, m), 1.36 (3H, d), 1.06 (6H, d).

Synthesis of CQ7b. CQ7b was synthesized using the same method as CQ4a using 4-chloroquinoline and 2-amino-5-diethylaminopentane (10%). ^{1}H NMR (CD_3OD) δ 8.53 (1H, d), 7.97 (1H, d), 7.76 (1H, d), 7.61 (1H, m), 7.40 (1H, m), 6.42 (1H, d), 5.21 (1H, br), 3.75 (1H, m), 2.50 (6H, m), 1.76 (2H, m), 1.62 (2H, m), 1.31 (3H, d), 1.08 (6H, d).

Synthesis of CP. 4-Chloropyridine hydrochloride (1.0g, 6.66 mmole) and 2-amino-5-diethylaminopentane (8.06 g, 50.88 mmole) were heated at 100^{o}C for 1 hour, 155^{o}C for 3 hours, and 135^{o}C for 16 hours. Reaction was then cooled to room

temperature and the unreacted excess amine was removed by Kugelrohr distillation of the crude reaction mixture at 120°C under vacuum. The remaining crude brown oil was then dissolved in $CHCl_3$ and purified by preparative TLC using $CHCl_3/CH_3OH/NH_4OH$ (5/1/0.2) as an eluent to yield a colorless oil (24%) ^{1}H NMR (CD_3OD) δ 8.14 (1H, dd), 6.37 (1H, dd), 4.44 (1H, br), 3.51 (1H, m), 2.54 (4H, m), 2.41 (2H, m), 1.18-1.54 (4H, m), 1.19 (3H, d), 1.02 (6H, t).

Synthesis of CQO. NaH (60% dispersion in mineral oil, 0.234 g, 5.84 mmole) was added to a flame-dried round bottom. Anhydrous DMF (16.1 mL) was added to the flask under N_2. To this suspension was added dropwise a solution of N,N-diethyl-2-aminoethanol (0.71 mL, 5.35 mmole) in DMF (16.1 mL) and the resulting mixture was stirred 30 minutes (gas evolution had stopped). A solution of 4,7-dichloroquinoline (0.96 g, 4.87 mmole) in DMF (14.6 mL) was then added to the reaction. Reaction was complete after 30 minutes as monitored by TLC. The reaction mixture was then poured into 200 mL water. The product was extracted with EtOAc (3 × 100mL). The organic layer was then dried over Na_2SO_4, filtered, and concentrated in vacuo to give the title compound in 95% yield (1.29 g). ^{1}H NMR (CD_3OD) δ 8.14 (1H, dd), 6.37 (1H, dd), 4.44 (1H, br), 3.51 (1H, m), 2.54 (4H, m), 2.41 (2H, m), 1.18-1.54 (4H, m), 1.19 (3H, d), 1.02 (6H, t). 1D-NOE experiments confirmed the positioning of the amino substituent.

5.3.3 Cell culture and transfection experiments

Plasmid pGL3-CV (Promega, Madison, WI) containing the luciferase gene under the control of the SV40 promoter was amplified by E. coli strain DH5α and was then

purified using the Ultramobius 1000 plasmid kit (Novagen, San Diego, CA). HepG2 and HeLa cells were purchased from the ATCC (Rockville, MD). Cells were cultured according to recommended procedures using Minimum Essential Medium (HepG2) or Dulbecco's Modified Eagle's Medium (HeLa), with 2 mM L-glutamine, 1.5 g/L sodium bicarbonate, 0.1 mM non-essential amino acids, 1.0 mM sodium pyruvate, and 10% fetal bovine serum. Media and supplements were purchased from Gibco BRL (Gaithersburg, MD). Cells were transfected in serum-reduced medium with CDP/pDNA polyplexes as described previously, in the presence of CQ or CQ analogues at various concentrations. Determination of cell viability and total protein concentration was conducted by a modified Lowry protein assay, also described previously [1].

For cell transfection and luciferase assay, cells were plated at 5×10^4 cells/well in 24-well plates 24 h in advance. Immediately prior to transfection, cells were rinsed once with PBS (pH 7.4), and 200 μL of Optimem (Gibco) was added to each well. pGL3-CV (1 μg, 5 μL of a 0.2 μg/μL solution in DNAse-free water) was mixed with an equal volume of polymer (5 μL of 24.9 mg/mL freshly prepared CDP solution in DNAse-free water) to give charge ratio 5±. 185-190 μL of Optimem and an appropriate amount of CQ (or CQ analogues) solution were mixed with CDP/pDNA complexes (10 μL) to give a final volume of 200 μL. These solutions were immediately transferred to each well. After 4 h of incubation (37 °C, 5% CO_2), the media in each well was replaced with 1 mL of culture media. After another 44 h, the media was removed by aspiration. Cells were washed twice with PBS (pH 7.4) before addition of 100 μL of 1x cell culture lysis buffer (Promega). Cell lysates were analyzed for luciferase activity with luciferase assay

reagent (Promega). Light units were integrated over 10 s in duplicate with a luminometer (Monolight 2010, Analytical Luminescence Laboratory, San Diego, CA).

The amount of protein in cell lysates obtained 48 h after transfection was used as a measure of cell viability. Protein levels of transfected cells were determined by the DC Protein Assay (Bio-Rad, Hercules, CA) and normalized with protein levels of cells transfected with naked DNA. A protein standard curve was run with various concentrations of bovine IgG (Bio-Rad) in cell culture lysis buffer.

5.3.4 Uptake of polyplexes in the absence or presence of CQ analogues

pDNA was prepared for fluorophore binding by reacting with Label-IT Amine (Mirus, Madison, WI). After 1 hour at 37 °C, the amine-terminated DNA was recovered by precipitation with ethanol, then incubated overnight with Alexa-fluor-488 NHS ester (Molecular Probes, Eugene, OR). The labeled DNA was purified by precipitation with ethanol. The percentage of pDNA labeling was determined to be 3.3 wt% by measuring the fluorescence intensity of labeled DNA ($\lambda_{excitation}$ 488 nm; $\lambda_{emission}$ 535 nm) using a Spectrafluor Plus plate reader (Tecan, Durham, NC) and comparing with a standard curve.

Labeled pDNA was condensed with CDP prior to being administered to HepG2 cells at a concentration 5 μg DNA/mL culture medium (same concentration as in gene transfection study). Uptake was terminated at 30 min and at 2 hours. Cells were treated with 0.25% trypsin, washed with phosphate-buffered saline and Hanks balanced salt solution, and analyzed by fluorescence-activated cell sorting (FACS).

5.3.5 Uptake and intracellular accumulation of CQ, CQ7a, and CQ7b

HepG2 cells (2×10^6 cells) were incubated at 37 °C in 2 mL Opti-MEM (pH 7.4) without or with pDNA/CDP (3 pmol/20 nmol) in the presence of 100 μM of CQ, CQ7a or CQ7b. After incubation in a humidified atmosphere (95% air, 5% CO_2) for scheduled time, the medium was removed; cells were washed three times with cold PBS containing 100 μM of corresponding CQ analogue, washed three more times in cold PBS, and then lysed by 20 min incubation in 1 mL of 1x cell culture lysis buffer. The lysates was diluted with 1 mL NaOH (0.1N), and 80 μL of such solution was analyzed on a Spectrafluor Plus plate reader (Tecan) at excitation wavelength of 360 nm and emission wavelength of 465 nm. The resulting fluorescence results were converted to concentrations of CQ or CQ analogues using a standard curve. The cellular concentration of CQ or CQ analogues was calculated assuming a cell volume of 3×10^{-6} μL [5].

5.3.6 Interaction of pDNA with CQ analogues

Varying amounts of pDNA were added to a 20 μM solution of CQ or CQ analogues, giving pDNA concentrations between 0 and 150 nM. UV absorbance of the mixture was recorded on a Cary 3G UV-Vis spectrophotometer (Varian, Palo Alto, CA) at room temperature.

5.3.7 Electrophoretic mobility of pDNA in the presence of CQ analogues

Each polycation was examined for its ability to bind pDNA through gel electrophoresis experiments as previously described [9,10]. pGL3-CV (5 μL of a 0.2 μg/μL solution in DNAse-free water) was mixed with an appropriate amount of CQ,

CQ7a, or CQ7b. Each solution was incubated for approximately 10 min. Loading buffer (5 μL) was added to each sample, followed by an appropriate volume of Borax buffer (0.025 M, pH 8.4) to give a final volume of 25 μL for each sample. 10 μL of such mixture was transferred into the wells of a 0.5% agarose gel (6 μg of ethidium bromide/100 mL TAE buffer (40 mM Tris-acetate, 1 mM EDTA)) and electrophoresed.

5.3.8 Displacement of DNA from polyplexes by CQ analogues

pGL3-CV (2 μg, 0.6 pmol) in 10 μL of DI water was complexed with CDP (24 μg, 4 nmol) in 10 μL. The solution was diluted by adding 80 μL PBS and kept for 30 min at 25 °C. The effect of CQ or CQ analogues on the stability of the complexes was studied as described [28] by increasing the concentration of CQ or CQ analogues upon adding 100 μL of a solution containing twice as much as the concentrations of interest. After a further 30 min at 25 °C, each solution was passed through a Pall Life Science Supor Membrane (100 nm) presoaked and rinsed with a solution containing the equivalent concentration of the CQ analogues. 40 μL of the filtrate was mixed with 40 μL of 5.6 μM 4,6-diamidino-2-phenylindole, dihydrochloride (DAPI). The amount of unpackaged DNA was determined from the fluorescence intensities ($\lambda_{excitation}$ 350 nm; $\lambda_{emission}$ 465 nm) of the DAPI-containing filtrate solution [7]. The percentage of pDNA dissociated from polyplexes was calculated according to $(I_f-I_0)/(I_t-I_0)\times100$, where I_t is the fluorescence intensity of DAPI in the presence of the total full of pDNA, I_0 is the fluorescence intensity of DAPI in the absence of pDNA, and I_f is the fluorescence intensity of the filtrate containing dissociated pDNA.

5.3.9 Dye exclusion assay to evaluate accessibility of condensed pDNA

The accessibility of polyplexes in the presence of CQ analogues was evaluated by dye exclusion through adaption of a published procedure [30]. After formulation, polyplexes were diluted 2.5x in dH_2O. For each sample, 25 μL of polyplex solution was transferred to a well of an opaque, black 96-well plate and combined with 25 μL of CQ analogue solution at twice the concentration of interest. Separately, a 200x dilution of the supplied PicoGreen stock solution (Molecular Probes) was prepared in 10 mM HEPES buffer. After polyplex-CQ analogue solutions were incubated for 5 min at room temperature, each 50 μL sample was combined with 50 μL of PicoGreen solution and the fluorescence ($\lambda_{excitation}$ 488 nm, $\lambda_{emission}$ 535 nm) of the resulting solutions was evaluated with a Spectrafluor Plus plate reader (Tecan, Durham, NC). The percentage dye exclusion was calculated from the ratio $((F_{DNA}-F_{sample})/(F_{DNA}-F_{H2O}))$, where F_{DNA} is the fluorescence of a sample of DNA alone (no polycation), F_{sample} is the sample fluorescence, and F_{H2O} is the fluorescence of a blank (control) sample.

5.3.10 Intracellular buffering activity of CQ analogues

The activity of CDP and CDPimid in buffering the pH environment of intracellular polyplexes was evaluated using the method of Kulkarni, et al. [29]. Briefly, polyplexes were formulated between the polymer of interest and an oligonucleotide labeled with the pH-sensitive fluorophore SNARF-4F (Molecular Probes, Carlsbad, CA). HeLa cells were treated with the polyplexes and imaged using an inverted Zeiss LSM 510 META confocal microscope with a 63x oil objective (NA 1.4). Excitation of the SNARF fluorophore was achieved with the 543 nm line of the He-Ne laser line supplied with the

microscope. After passing through a variable confocal pinhole, the SNARF-4F emission was collected by the META detector in distinct wavelength bins of 569-601 nm and 633-687 nm. Using a standard curve, the relative intensity of individual signals across these bins was used to evaluate the pH environment of the corresponding intracellular polyplex(es).

5.3.11 Measure of unpackaged intracellular nucleic acids

To obtain a relative measure of intracellular nucleic acid unpackaging, HeLa cells in 24-well plates were transfected with polyplexes of CDP or CDPimid and a FITC-labeled DNA oligonucleotide (FITC-oligo). Fourteen hours after transfection, cells were collected by trypsinization and pelleted by centrifugation (6 min at 2400 rpm). Each sample was resuspended in 10 μL 1x cell culture lysis buffer (Promega) and stored at 4 °C. Controls consisted of known amounts of FITC-oligo in 1x cell culture lysis buffer. After 30 min incubation, each sample was mixed with 25 μL of 37 °C low-melting-point agarose (1% in TAE buffer) and transferred immediately to a well of an agarose gel (0.5% in 60 mL TAE buffer). The agarose gel was subjected to gel electrophoresis and imaged under UV illumination. Detection of FITC-oligo was achieved through its fluorescent signal. Migration of FITC-oligo from control samples was used to indicate the expected migration of FITC-oligo unpackaged from cells.

5.4 Results

5.4.1 Synthesis of CQ analogues

Chloroquine (CQ) is a quinoline analogue with an alkyl amino group at the 4-position (Figure 5.1). Here, a family of CQ analogues was prepared with a fixed ring structure (7-chloroquinoline) and variable side chains (CQ4a-f, CQO, Figure 5.1). CQ4a-f and CQO are readily synthesized in a one-step substitution reaction between 4,7-dichloroquinoline and the corresponding aliphatic amines [31]. A second group of CQ analogues that contained 2-amino-5-diethylaminopentane as the side chain (identical to CQ) was prepared with variable 7-substitutes on the quinoline ring (CQ7a-b) or with variable aromatic ring sizes (CP and QC). CQ7a-b and CP were synthesized via the substitution reaction between 2-amino-5-diethylaminopentane and the corresponding 4-chloroquinoline derivatives or 4-chloro pyridine, respectively. The resulting products were either crystallized or separated by column chromatography to give high purity.

5.4.2 Transfection with CQ analogues in HepG2 cells

One microgram of pGL3-CV (0.3 pmol), encoding for the luciferase gene under the control of the SV40 promoter, was complexed with CDP (12 μg, 2 nmol) at a charge ratio (5±) that gives complete DNA binding. The polyplexes were added in the presence of CQ or CQ analogues to HepG2 cells in 24-well plates. Transfection efficiencies were determined by assaying for luciferase protein activity and reported in relative light units (RLU) per milligram of total cellular protein (Table 5.1).

The observed luciferase activity increased from 4.3×10^6 RLU/mg protein in the absence of CQ to 15.6×10^6 RLU/mg protein in the presence of CQ. When the tertiary

alkyl amine side chain of CQ was replaced with either a hydrocarbon (CQ4a) or with a negatively charged carboxylate moiety (CQ4b), the luciferase activities of transfected cells were roughly the same as that in the absence of CQ (Table 1). CQ4c, a CQ analogue possessing a tertiary amine, enhances transfection to a degree similar to CQ. These observations show the importance of the terminal tertiary amine moiety of CQ for enhancing polyplex transfection efficiency. When more amine groups were introduced to the side chain of CQ (three amine groups in CQ4d-e and four amine groups in CQ4f), the maximal luciferase activities were only slightly higher than with CQ for HepG2 cells transfected in the presence of those analogues.

CQ Analogues (conc.)	RLU/mg protein (x 10^{-6})	Cell Viability (%)
None	4.3	100
CQ (200 μM)	15.6	60
CQ4a (150μM)	4.7	89
CQ4b (150 μM)	4.3	84
CQ4c (150 μM)	24.7	64
CQ4d (200 μM)	21.5	74
CQ4e (100 μM)	20.2	74
CQ4f (150 μM)	25.0	83
CQ7a (200 μM)	168.0	61
CQ7b (200 μM)	2.7	100
CP (200 μM)	6.4	85
QC (20 μM)	24.6	57

Table 5.1 Transfection of HepG2 Cells in the presence of CQ analogues
HepG2 cells were transfected for 4 h with CDP/pGL3-CV polyplexes in the absence or presence of CQ or CQ analogues. Gene expression was evaluated 48 h later by assaying the luciferase activity (in relative light units, RLU) of cell lysates. The viability of the cells was assessed by measuring the total amount of recovered protein. The CQ analogue concentrations represented in the table are those which gave the optimal increase in transfection efficiency.

Dramatic changes in luciferase activity were observed for cells transfected in the presence of CQ analogues with variations on the quinoline ring and the same side chain moiety as CQ (Table 1 and Figure 5.2). Replacement of the 7-chloro of CQ by a lipophilic trifluoro group (CQ7a) gave an order of magnitude increase in luciferase activity (15.6×10^6 RLU/mg protein for CQ to 168×10^6 RLU/mg protein for CQ7a). When the 7-substituent was removed (CQ7b), the CQ analogue completely lost the capacity for transfection enhancement. CP, a CQ analogue with a pyridinyl structure, also had no contribution to transfection. Quinacrine (QC), a CQ analogue having an acridine ring structure, enhanced transfection to a similar degree as CQ but at one-tenth the concentration. QC is more toxic than CQ; a concentration of QC higher than 50 μM leads to complete cell death.

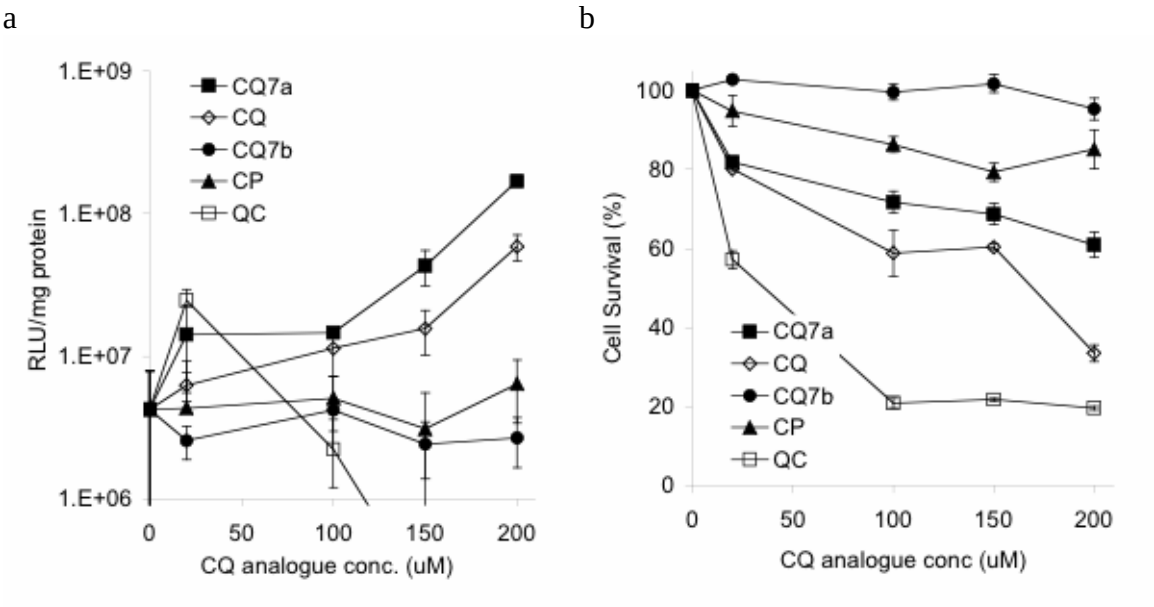

Figure 5.2 Effect of CQ analogues on transfection of HepG2 cells
HepG2 cells were transfected with CDP/pDNA polyplexes in the presence of various CQ analogues. Luciferase activity was used as a measure of transfection efficiency (a) and total protein was used as a measure of cell viability (b).

5.4.3 Cellular uptake of polyplexes in the presence of CQ analogues

Flow cytometry analysis was used to give a relative measure of pDNA uptake into cells (Figure 5.3, Table 5.2). pDNA was labeled with Alexa-fluor-488, condensed into particles with CDP, and exposed to HepG2 cells for 30 minutes or 2 hours in the presence or absence of CQ or CQ analogues. Cells were then analyzed by fluorescence-activated cell sorting (FACS). Uptake of naked pDNA was minimal, as the mean fluorescence of cells treated with naked pDNA is the same as that of as untreated cells (Table 2). Cells exposed to complexes of labeled DNA and CDP displayed increases in mean cellular fluorescence, indicating that polyplexes were internalized by cells. Similar observations of internalization have been reported elsewhere [7,32]. At both 30 min and 2 h, cells exposed to polyplexes revealed significant uptake regardless of the presence of absence of CQ or CQ analogues. 12-19% of cells at 30 min. and 65-75% of cells at 2 h contained detectable levels of fluorescently-labeled pDNA (% positive, Table 2). The presence of CQ or CQ analogues gave slightly reduced uptake relative to the case of polyplexes alone. Also, the fluorescence distribution pattern was very similar at both 30 min and 2 h for cells transfected in the presence and absence of CQ or CQ analogues. Although cells transfected in the presence of QC gave similar % positive and mean fluorescence as cells transfected in the presence of other CQ analogues, the values may not reflect actual polyplex uptake because QC is itself fluorescent at the wavelengths used for the FACS analysis (data not shown).

pDNA or Polyplexes	CQ or CQ analogue	30 min			2 h		
		% negative	% positive	Mean fluorescence	% negative	% positive	Mean fluorescence
-	-	99.2	0.8	4.1	99.7	0.3	3.45
pDNA	-	99.3	0.7	4.0	98.9	1.1	5.48
Polyplexes	-	82.8	17.5	12.9	20.9	79.3	125.7
Polyplexes	CQ	85.5	11.9	10.0	32.5	67.7	79.3
Polyplexes	CQ7b	82.2	18.8	15.0	24.7	75.5	88.3
Polyplexes	CQ7a	85.4	14.8	9.2	35.0	65.2	78.1
Polyplexes	CP	87.4	12.8	7.6	24.0	76.2	109.0

Table 5.2 Summary of flow cytometry analysis of polyplex uptake in the absence or presence of CQ analogues

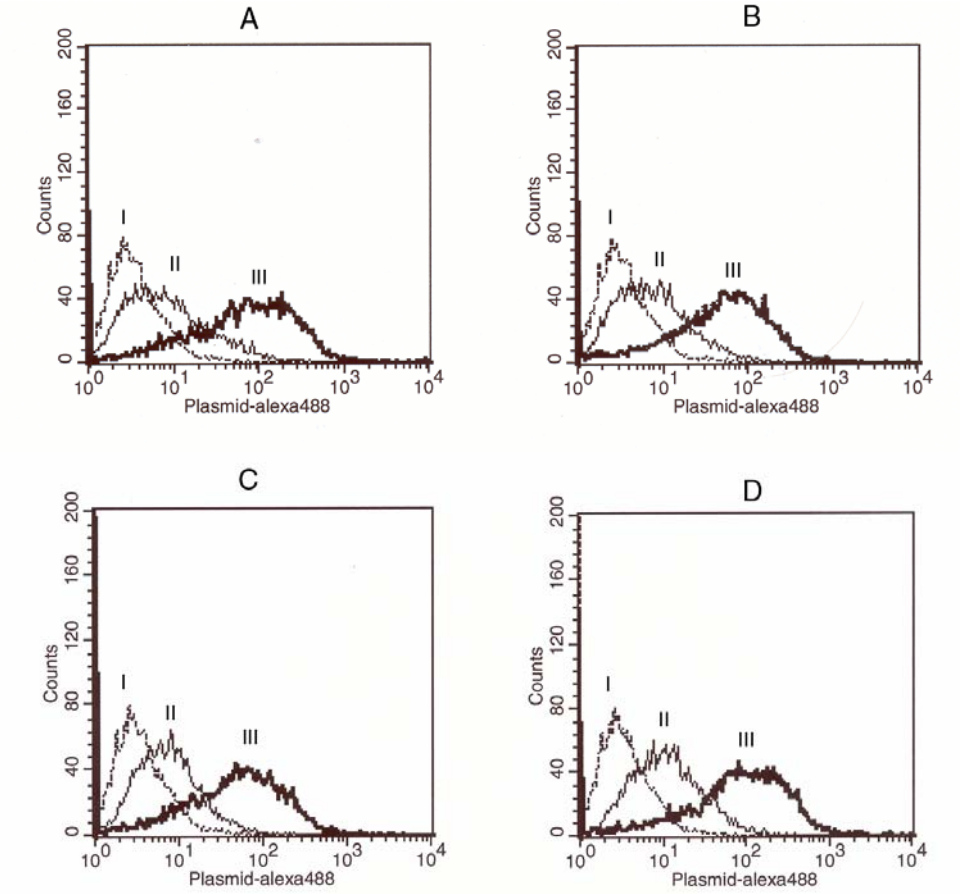

Figure 5.3 Flow cytometry analysis of polyplex uptake in the presence of CQ analogues
pDNA labeled with Alexa-fluor-488 was condensed with CDP and administered to HepG2 cells. Uptake was terminated at 30 min and 2 h and cells were analyzed by flow cytometry. Uptake of polyplexes was similar in the absence of any CQ analogue (a) or in the presence of 200 μM CQ (b), 200 μM CQ7b (c), or 200 μM CQ7a (d). The cellular fluorescence was analyzed at 0 min (I), 30 min (II), or 2 h (III).

5.4.4 Uptake and intracellular concentration of CQ analogues

CQ can penetrate the cell membrane and accumulate in acidic compartments, especially in lysosomes, in a time-dependent manner [7]. The concentration of CQ in HepG2 cells (as measured by its fluorescence in cell lysates) increased as a function of treatment time and reached nearly 12 mM following 4 h of treatment with 100 μM CQ (Figure 5.4). CQ accumulated in HepG2 cells with a cell-to-medium concentration ratio of ~100. Relative to CQ, CQ7a achieved a more rapid intracellular accumulation and reached a concentration of 11 mM in cells only 30 min after exposure to 100 μM CQ7a (Figure 5.4). Beyond this time, the intracellular concentration of CQ7a remained steady throughout the 4 h uptake study. The achieved intracellular concentrations noticeably exceeded the 0.1 mM concentration in the surrounding medium.

The uptake of CQ and CQ7a into HepG2 cells was also investigated in the presence of pDNA/CDP polyplexes. Both CQ and CQ7a exhibited strong uptake; after 4 h, intracellular concentrations were 13-15 mM, slightly higher than their concentrations in the absence of polyplexes.

When the substituent at the 7-position of CQ was removed, the resulting CQ analogue (CQ7b) showed a lower tendency to accumulate in cells. The maximum intracellular concentration of CQ7b was around 2 mM after 4 h treatment, about five times lower than that of CQ or CQ7a. These uptake analyses demonstrate that the transmembrane capability of CQ and its analogues are closely related to the substituent at the 7-position of the quinoleic ring. The trifluoromethyl group is a strong electron-withdrawing, lipophilic group, and CQ7a that contained this group showed fast cell-membrane penetration and intracellular accumulation relative to CQ.

The observed concentrations are averaged across cells; if taken into cells, CQ analogues that accept protons at the relevant pH are likely found at much greater concentrations in vesicles of the endocytic pathway. CQ is believed to accumulate in such vesicles as a result of its intravesicular protonation [33].

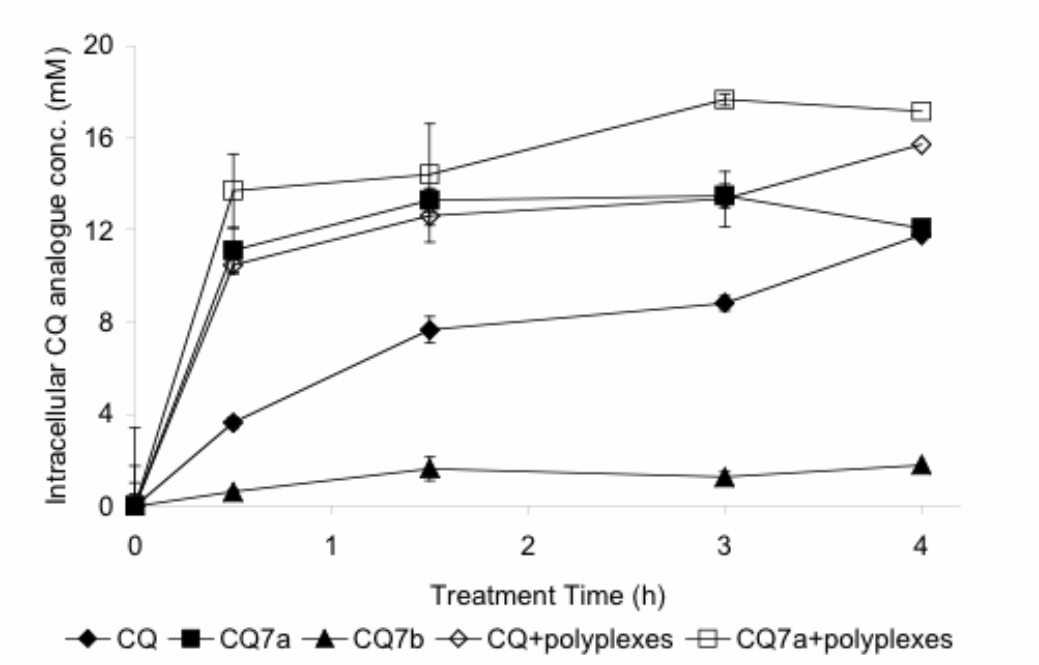

Figure 5.4 Uptake and intracellular accumulation of CQ analogues
HepG2 cells were exposed to CQ analogues (0.1 mM) in the presence or absence of polyplexes, and the fluorescence of cell lysates was used to evaluate the intracellular concentration of CQ analogues at various timepoints after initial exposure.

5.4.5 Interaction of CQ analogues with pDNA

It is well-known that CQ can bind DNA [22,34]. Previous work has indicated that CQ exists as a doubly-protonated cation in dilute aqueous solutions at physiological pH, and its binding to DNA is related to insertion of its quinoleic moiety into DNA base pairs and to electrostatic interaction between the cationic side chain and the phosphate anions along the DNA backbone [22]. The binding of CQ to DNA could lead to destabilization of the association between the plasmid and the delivery vehicle polycations [7].

The binding of CQ and its analogues to DNA was evaluated by stepwise addition of small increments of pDNA to a solution containing a constant concentration of a CQ analogue at 20 μM. As shown in Figure 5.5, progressive depression of the UV absorption peaks from the CQ analogues and a shift of these peaks towards longer wavelengths occurred with all the compounds studied. These results suggest that CQ analogues can interact with pDNA.

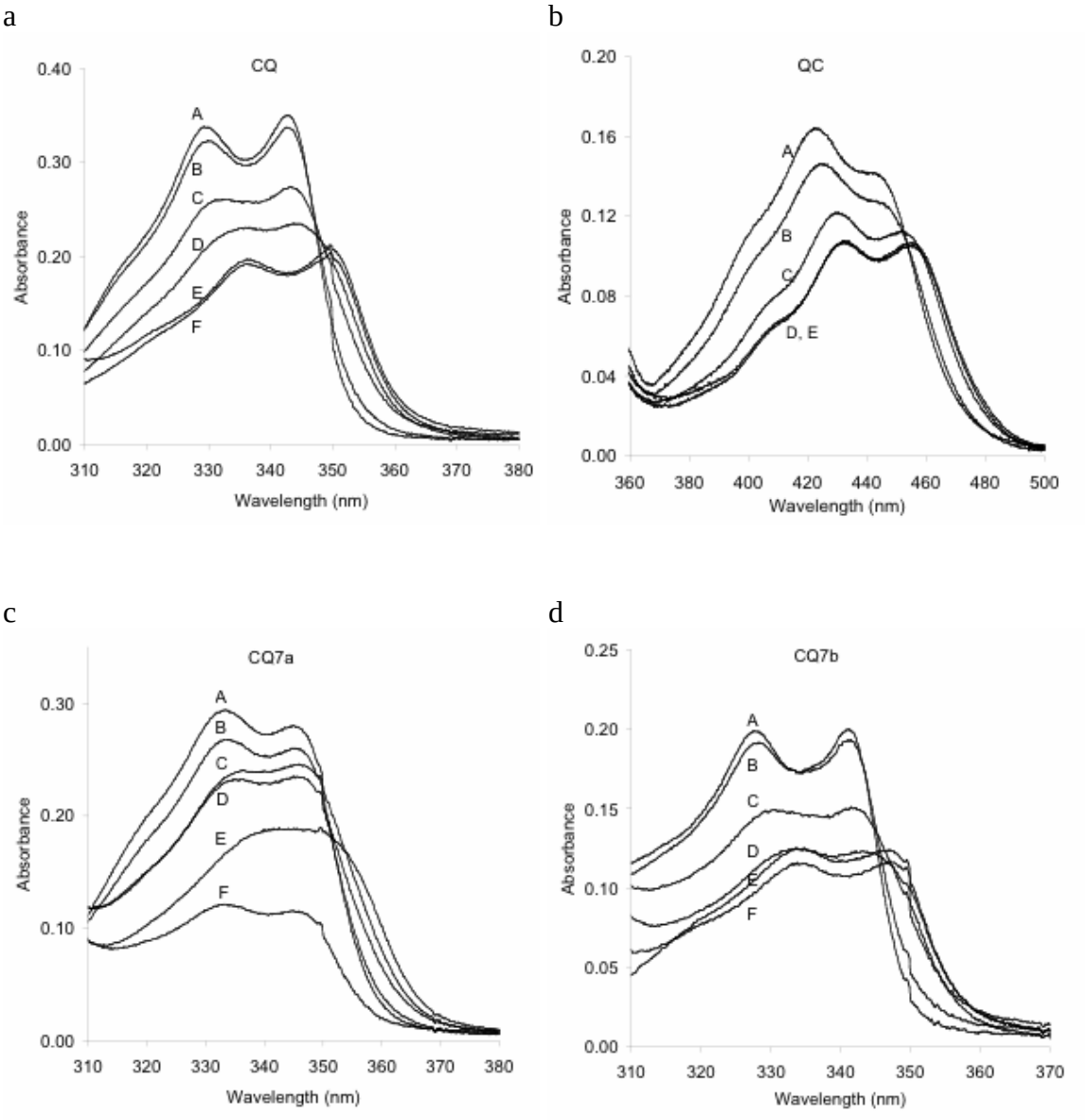

Figure 5.5 Interaction of pDNA with CQ analogues

The absorbance of CQ analogue solutions (20 μM) was monitored in the presence of varying concentrations of pDNA: 0 nM (A), 1.8 nM (B), 7.5 nM (C), 15 nM (D), 37.5 nM (E), or 150 nM (F). The CQ analogues examined – CQ (a), QC (b), CQ7a (c), and CQ7b (d) – all exhibited interactions with pDNA.

5.4.6 Electrophoretic mobility of pDNA in the presence of CQ analogues

pDNA was incubated in the presence of the CQ analogues at various concentrations, and the change of its mobility on an agarose gel was investigated (Figure 5.6). The band from pDNA treated with CQ7a at 100 μM showed essentially the same pattern as the untreated control, indicating that CQ7a had little effect on the mobility of pDNA at this concentration. pDNA treated with CQ7a at a concentration one-order of magnitude higher (1 mM) showed slightly retarded movement while the motility of the pDNA was completed prohibited when treated with CQ7a at 10 mM. For comparison, CQ7b had little effect on the pDNA retardation when treated with CQ7b at the same concentration range (0.1-10 mM). CQ at 100 μM and 1 mM did not retard pDNA, but did so slightly at 10 mM.

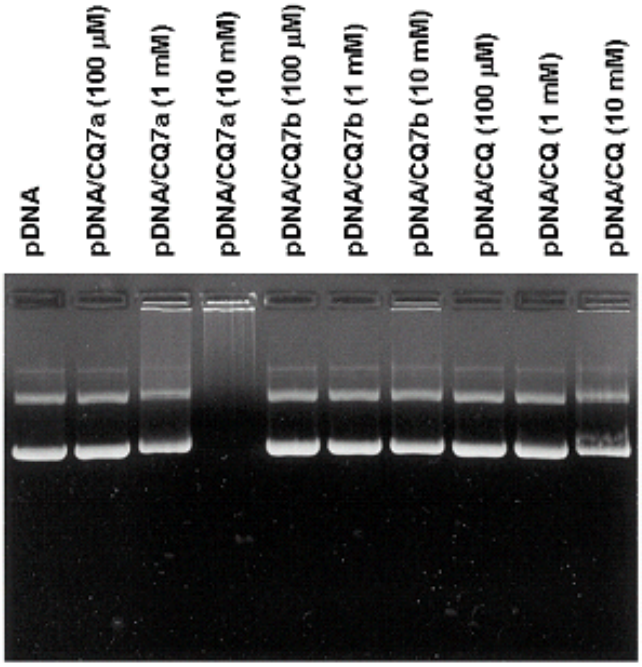

Figure 5.6 Electrophoretic mobility of pDNA in the presence of CQ, CQ7a, or CQ7b
Plasmid DNA was incubated with various concentrations of CQ analogues, loaded to an agarose gel, and subjected to electrophoresis. CQ7a showed the strongest interactions with DNA, and some interaction was also apparent with CQ.

5.4.7 DNA displacement from polyplexes by CQ, CQ7a, or CQ7b

Polyplexes can be separated from unpackaged pDNA by filtration. To assess the stability of CDP/pDNA polyplexes against CQ analogues, solutions of polyplexes and CQ analogues were filtered to remove intact polyplexes, and unpackaged pDNA in the filtrate was measured by a fluorescence method (Figure 5.7). CQ7a was able to displace 40% of total condensed pDNA at a concentration as low as 500 μM. 40-50% of the pDNA was found in the filtrate for CQ7a concentrations of 500 μM to 10mM, and over 70% of pDNA was displaced with a CQ7a concentration of 20 mM. CQ displayed weaker ability to displace pDNA than CQ7a. The pDNA displaced from the polyplexes by CQ gradually increased from 10% with 500 μM CQ to roughly 50% with 20 mM CQ. With CQ7b, less than 3% of free displaced pDNA was detected in the filtrate at a concentration of 2.5 mM or lower. The displaced pDNA gradually increased from 10% to about 30% when polyplexes were treated with 5 mM to 20 mM of CQ7b, respectively.

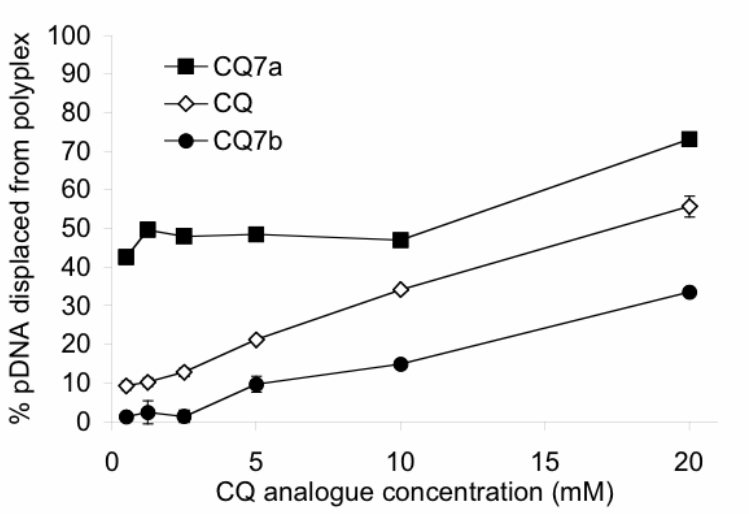

Figure 5.7 DNA displacement from polyplexes by CQ, CQ7a, or CQ7b
CDP/pDNA polyplexes were incubated with various concentrations of CQ, CQ7a, or CQ7b, then filtered to remove intact polyplexes. Displaced DNA in the filtrate was then quantified. CQ7a showed the strongest ability to displace DNA, followed by CQ.

5.4.8 Accessibility of pDNA in the presence of CQ analogues

The examinations of CQ analogue interaction with nucleic acids (and/or polyplexes) led us to focus on a smaller set of molecules for further study: CQ, CQ7a (shows strong effects on transfection and strong interactions with DNA), and CP (not effective in increasing transfection; a single-ring structure that should impede interaction with DNA). One of the motivations of our study was to elucidate the role of endocytic vesicle buffering by CQ in gene transfer; we synthesized an additional CQ analogue, CQO (where an oxygen replaces the secondary aniline at the 4 position of chloroquine), in order to examine a compound that retained CQ's interaction with nucleic acids through its dual-ring structure but had less ability to buffer the pH of endocytic compartments.

PicoGreen experiences significant fluorescence enhancement upon intercalation in nucleic acids, such that its exclusion indicates inaccessibility of the nucleic acids to intercalation [30]. This characteristic was used to evaluate the relative accessibility of pDNA in the presence of CQ analogues. Polyplexes were incubated with various concentrations of CQ analogues, combined with solutions of PicoGreen, and evaluated for fluorescence intensity (Figure 5.8). CQ7a, CQ, and CQO demonstrated enhancements in dye exclusion with increasing concentration. Dye exclusion was ~30% for 0.5 or 1 mM CQ7a and rose to almost 100% at 4 mM. Dye exclusion was ~23% for CQ (0.5 or 1 mM) and ~17% for CQO (0.5 or 1 mM), with slightly greater exclusion for CQ/CQO at 4 mM. PicoGreen was not excluded from DNA by CP.

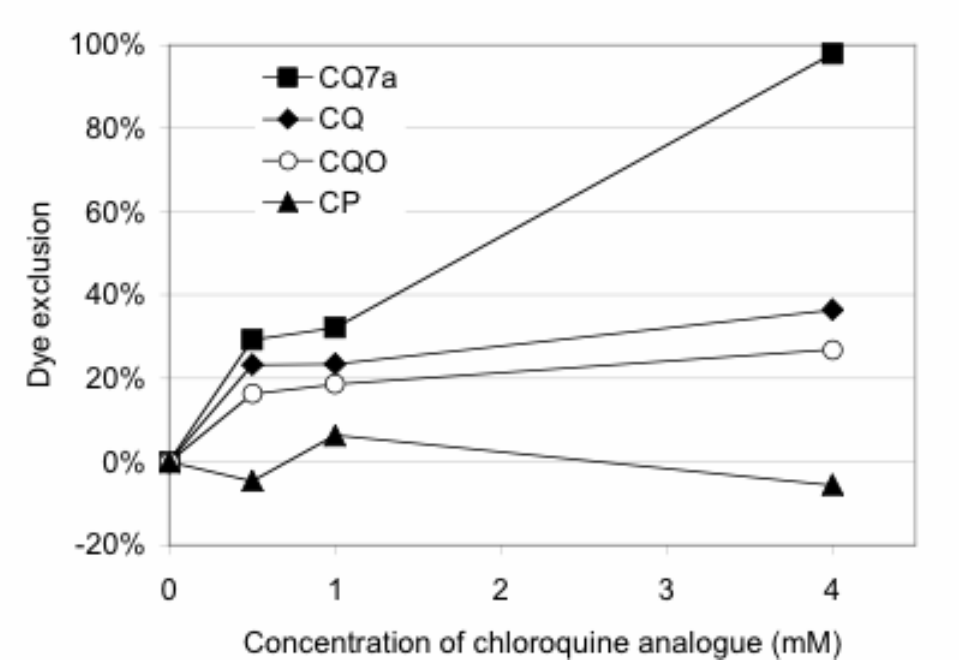

Figure 5.8 Dye exclusion from pDNA in the presence of CQ analogues
pDNA was incubated with various concentrations of CQ analogues, then combined with solutions of PicoGreen, a DNA-intercalating dye. DNA alone showed strong fluorescence, but CQ analogues produced marked increases in dye exclusion, most significantly with CQ7a.

5.4.9 Intracellular buffering activity of CQ analogues

To evaluate the actual intracellular buffering activity of CQO and other CQ analogues, we employed the method of Kulkarni, et al. [29], in which polyplexes labeled with the pH-sensitive fluorophore SNARF-4F are administered to cells and used to evaluate the local pH environment of polyplexes within individual cells. The data can be compiled in aggregate to indicate the actual buffering activity of CQ analogues within cells (Figure 5.9). By this measure, CQ and CQ7a (0.1 mM) displayed strong buffering activity relative to the absence of any CQ analogues. CQO displayed mild buffering activity, while CP exhibited none.

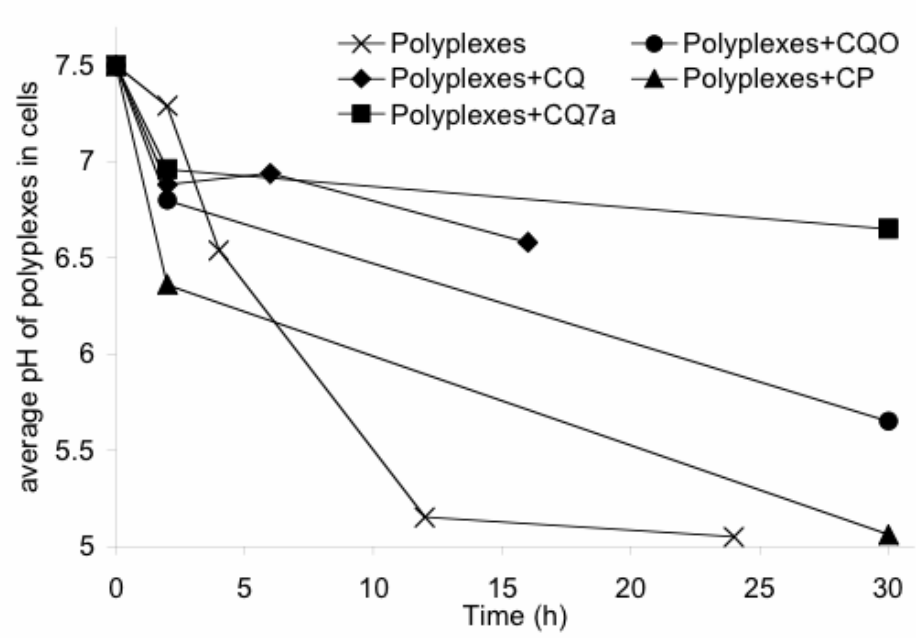

Figure 5.9 Intracellular buffering activity of CQ analogues
The ability of CQ analogues to buffer the pH experienced by CDP polyplexes was evaluated. Polyplexes containing CDP and a SNARF-4F-labeled oligonucleotide were administered to HeLa cells along with CQ analogues (0.1 mM). Confocal microscopy was used to visualize intracellular SNARF-4F-labeled polyplexes. The pH environment of the polyplexes could be evaluated using the pH-sensitivity of SNARF-4F [29]. CQ and CQ7a display strong, similar buffering activity, while CQO shows mild buffering and CP does not exhibit pH-buffering of polyplexes.

5.4.10 Transfection with CQ analogues in HeLa cells

The intracellular buffering activity of CQ analogues was evaluated in HeLa cells (Figure 5.8). To compare these results more directly with effects on transfection efficiency, HeLa cells were transfected with CDP/pDNA polyplexes in the presence or absence of the selected CQ analogues (CQ, CQ7a, CQO, and CP). The trends in the transfection levels for CQ, CQ7a, and CP in HeLa cells were consistent with transfections of HepG2 cells (Figure 5.10). Both CQ and CQ7a conferred a concentration-dependent increase in transfection efficiency; this increase was greater with CQ7a. CQO produced little to no increase in luciferase expression, and CP produced no increase.

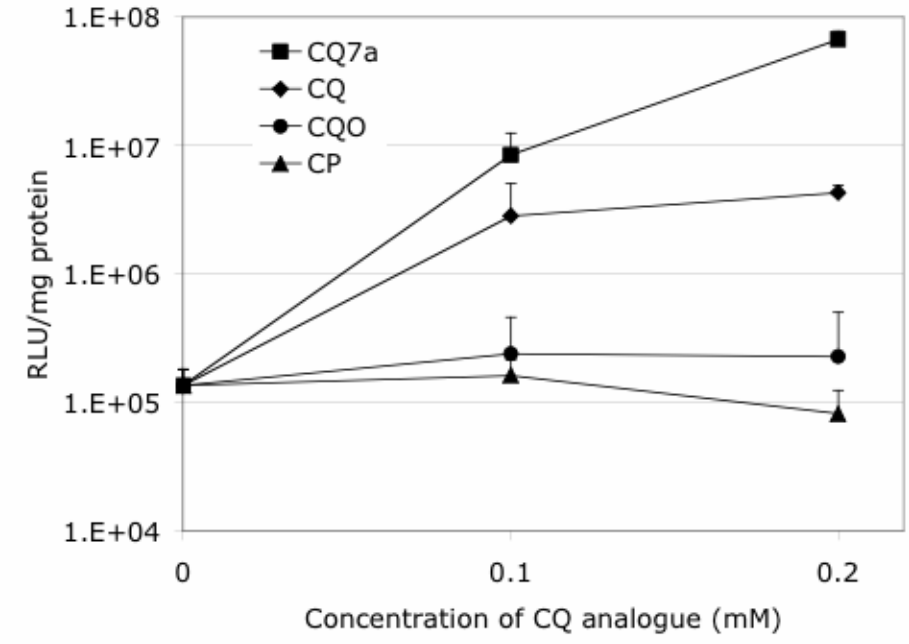

Figure 5.10 Effect of CQ analogues on transfection of HeLa cells
HeLa cells were transfected with CDP/pDNA polyplexes in the presence of various CQ analogues. Luciferase activity was used as a measure of transfection efficiency.

5.4.11 Measure of unpackaged intracellular nucleic acids following transfection in the presence of CQ analogues

The comet assay is a standard method of evaluating DNA damage [35,36]. In this assay, cells are gently lysed, embedded in an agarose gel on a glass slide or coverslip, and exposed to electrophoresis. Only damaged cellular DNA is reduced to a size that permits migration within the gel, and this damaged DNA will generate a characteristic "comet" pattern upon subsequent intra-gel labeling of nucleic acids by a fluorescent marker. The size and fluorescence intensity of the comet reflects the extent of DNA damage. By this method, individual cells may be visually evaluated for DNA damage.

We have modified this assay to produce an aggregate separation and visualization of delivered and unpackaged nucleic acids. Rather than evaluating samples on an individual-cell basis, cells are collected by centrifugation, lysed, embedded in an agarose gel, and subjected to electrophoresis in order to generate a relative measure of DNA unpackaging for a particular sample. Also, we transfect cells using nucleic acids covalently modified with a fluorescent marker rather than adding a fluorescent label after electrophoresis. Thus, we are able to distinguish exogenous (delivered) nucleic acids from cellular DNA. The "unpackaged" oligonucleotide measured by this assay is that which migrates through the agarose gel to the same extent as in the case of direct gel loading of the oligonucleotide.

HeLa cells were transfected in the presence of CQ analogues and examined by this assay. Despite the activity of CQ and CQ7a in displacing pDNA from polyplexes (Figure 5.7), samples transfected with these CQ analogues actually generate less

unpackaged (migrating) DNA than samples transfected without CQ analogues or samples transfected in the presence of CQO.

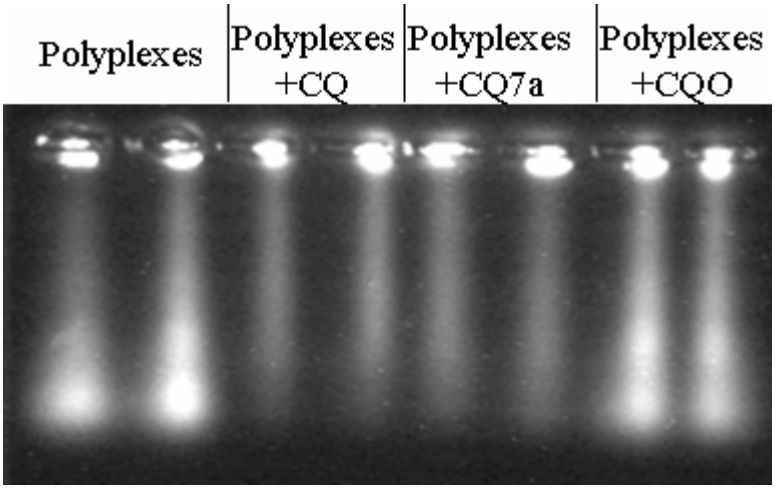

Figure 5.11 Separation of unpackaged nucleic acid from transfected cells
When cells transfected with a FITC-labeled oligonucleotide are collected, lysed, embedded in an agarose gel, and subjected to electrophoresis, migrating oligonucleotide can be detected through the fluorescence of the FITC-label. As the leading band of this oligonucleotide migrates to the same extent as oligonucleotide loaded directly to the gel (not shown), it can be interpreted to be unpackaged. Cells transfected in the presence of CQ or CQ7a produce less unpackaged (migrating) FITC-oligo than cells transfected in the absence of chloroquine analogues or in the presence of CQO.

Discussion

Chloroquine (CQ) enhances the transfection efficiency of many non-viral gene delivery vectors, but the means by which this occurs is not well established. Here, we contribute to the understanding of CQ-related increases in gene expression by studying a number of CQ analogues whose structures are designed to probe hypothesized mechanisms, i.e., pH buffering of endocytic vesicles. This is the first study to correlate the CQ structure with its function during gene transfer.

Several CQ analogues were designed and synthesized and their ability to enhance gene transfer investigated. As shown by the data in Table 5.1, the side chain structure of CQ is important to enhancing transfection. CQ4a and CQ4b, CQ analogues that lack side-chain cationic amino groups, show no effects on gene transfer. However, the side-chain amino group is not entirely responsible for CQ's activity, because transfection is not enhanced by some CQ analogues containing this group (CQ7b and CP).

CQ analogues bearing more than two amino moieties (CQ4d-f) are more basic than CQ. Expression levels in the presence of those CQ analogues are essentially the same as CQ and as a CQ analogue with only two amino moieties (CQ4c), indicating that the basicity of CQ is not the major reason for its effects on gene transfer.

The aromatic ring structure of CQ clearly contributes to its function as a transfection-enhancing agent (Figure 5.2). CP, a pyridinyl-based CQ analogue, does not increase gene expression at all, while QC, an acridine-based CQ analogue, enhances the transfection at an optimal concentration of 20 μM, ten times lower than the optimal concentration of CQ. QC and CP show higher and lower toxicity than CQ, respectively.

Therefore, both CQ's enhancement of gene expression and its toxicity are related to the aromatic ring structure.

Dramatic effects on gene expression occur with changes in the 7-substituent of the CQ aromatic ring (while maintaining the side chain of CQ). When the 7-Cl group of CQ is replaced with a proton (CQ7b), the CQ analogue loses its capacity to enhance gene expression. If a trifluoromethyl group (CQ7a) is used instead of the 7-Cl group, the transfection enhancement is markedly improved relative to enhancement by CQ (Table 5.1, Figure 5.2, Figure 5.10).

There are no significant effects on the uptake of polyplexes in the presence of the CQ analogues, and the intracellular concentrations of CQ and CQ7a are similar at 4 h (Figure 5.3). Apparently, the differences in transfection enhancement between CQ and CQ7a are not due to differences in uptake. However, CQ7b indicates that the lipophilic or the electron-withdrawing character of the 7-substituent can contribute to the uptake of CQ analogues, providing some explanation for the lack of effect on transfection efficiency by CQ7b and possibly CP. The absorbance spectra of CP and CQO do not allow their cellular uptake to be measured using the method employed for other CQ analogues.

The intracellular buffering activity of CQ, CQ7a, and CQO shows a correlation between gains in transfection efficiency and buffering of the pH experienced by polyplexes within cells (Figures 5.9, 5.10). CQO does not enhance transfection efficiency; this molecule interacts with nucleic acids in a manner similar to CQ (Figure 5.8) but displays reduced buffering activity. CQ analogues without a side chain amino group (CQ4a, CQ4b) should have reduced pH-buffering activity, and they do not reveal

the enhancement in gene expression that is seen with variants containing one or more side chain amino groups (CQ, CQ4c-f) (Table 5.1). Together, these results support the hypothesis that CQ's pH-buffering of endocytic vesicles is necessary for its contributions to transfection efficiency.

Buffering does not, however, provide a full explanation of CQ's contributions to transfection efficiency. The participation of both the side chain and the aromatic ring in increasing transfection efficiency suggests that CQ may achieve its function through multiple mechanisms. Also, the intracellular buffering by CQ and CQ7a is functionally similar, so the buffering hypothesis does not explain the significant additional increase in transfection efficiency when CQ is replaced with CQ7a. Compounds such as monensin, methylamine, spermine, and ammonium chloride are known to buffer endocytic vesicles but do not contribute to transfection efficiency [7], providing additional indication that buffering activity is not a sufficient condition for improved transfection.

CQ, CQ7a, and QC all confer sharp gains in transfection efficiency, but dramatic variations in their performance suggest that CQ's effect on transfection efficiency is related to its interactions with DNA. Parker et al. have demonstrated that CQ can bind to both DNA and RNA in vitro, an interaction which can alter the biological and physical properties of the DNA [34]. Interactions between DNA and CQ analogues are strongly associated with the aromatic structures of those ligands. Because of its acridine structure, QC exhibits strong interactions with DNA, and this molecule is a potent enhancer of gene transfer at relatively low concentration. The single aromatic ring of CP should render this molecule unable to bind DNA as effectively as its multi-ring analogues, consistent with the fact that CP does not enhance gene transfer.

In addition to ring structure, the electron-withdrawing character of the substituent at the 7-position can affect the strength of binding between CQ analogues and DNA [23]. This effect is demonstrated by gel retardation of pDNA with various concentrations of CQ, CQ7a, and CQ7b (Figure 5.6). CQ7a shows the strongest interaction with pDNA, displaying some retardation of pDNA electrophoresis at 1 mM and essentially complete retardation at 10 mM. CQ7b shows a weaker interaction with pDNA, as pDNA mobility did not change in the presence of CQ7b over a wide range of concentrations. The strength of interaction between CQ and pDNA is likely intermediate of those from CQ7a and CQ7b since CQ slightly retarded pDNA electrophoresis at 10 mM.

DNA must be dissociated from polycations in order to achieve gene expression. We have shown that CDP/pDNA polyplexes do not reach the nucleus of transfected cells, but deliver unpackaged pDNA to both the cytoplasm and cell nucleus [32]. It is likely that gene transfer is improved with enhanced intracellular unpackaging [37]. The presence of CQ analogues can destabilize polyplexes, generating unpackaged pDNA (Figure 5.7). The ability to displace pDNA from CDP decreases in the order of CQ7a, CQ, and CQ7b, corresponding to the order of binding strengths displayed by the gel retardation assay. Although cells may be exposed to relatively low concentrations of CQ analogues during transfection, intracellular accumulation drives the concentrations within cells to much higher levels (Figure 5.4). For CQ and CQ7a, these concentrations are sufficient to disrupt polyplexes. The cellular average concentrations measured here should be less still than the concentrations found in the vesicles of the endocytic pathway, where CQ accumulates within cells [33], it is therefore likely that polyplexes in the endocytic pathway will be subject to unpackaging in the presence of CQ.

The biological and physical properties of DNA can be altered when it is bound by CQ [34]. CQ7a, which displays stronger binding affinity for DNA, can be expected to have similar effects. Beyond their activity in displacing DNA from polyplexes, CQ and CQ7a appear to interact directly with nucleic acids, even when those nucleic acids have been delivered to cells (Figures 5.8, 5.11). Strong binding by numerous CQ7a molecules could alter the physical properties of pDNA and reduce the overall negative charge of its backbone via electrostatic interaction between the anionic phosphate groups of pDNA and cationic amino side chains of CQ7a. When bound by CQ, pDNA could achieve improved gene transfer due to changes in its intracellular processing or its rate of intracellular degradation [38-39].

CQ7a greatly enhances gene expression over CQ (Figures 5.1, 5.9), an effect that is not explained by intracellular buffering activity alone. The observed higher luciferase activity from transfection in the presence of CQ7a is likely due to CQ7a's greater displacement of polycations (Figure 5.8) and its stronger interactions with intracellular nucleic acids (Figures 5.6, 5.10, 5.11).

In summary, a structure-function correlation among CQ and its analogues in non-viral, polycation-based gene delivery is reported. It is demonstrated that the tertiary amino moiety of CQ is important to its enhancement of gene expression. Further, changes in the aromatic ring of CQ significantly affect its ability to enhance gene expression. A CQ analogue with a three fused aromatic ring structure (QC) shows much high cytotoxicity than CQ and can enhance transfection similarly to CQ at a concentration 10 times lower. A CQ analogue with one pyridinyl aromatic ring (CP) gives lower cytotoxicity than CQ but has no effect on gene transfer. Variation at the 7-

position of CQ dramatically changes its ability to enhance transfection. Transfection with a 7-trifluoromethyl CQ analogue (CQ7a) shows luciferase activity an order of magnitude higher than transfection with the same concentration of CQ (0.2 mM), while transfection is not affected by in the presence of a 7-H CQ analogue (CQ7b). The fused aromatic ring structure (acridinyl ring) in QC and the strong electron-withdrawing group (trifluoromethyl) in CQ7a endow these molecules with higher binding affinity to DNA. Also, the stronger intercalator, CQ7a, has a higher tendency than CQ to competitively displace the polycation from CDP/pDNA polyplexes at a concentration that is achievable intracellularly after several hours treatment. Finally, CQ and CQ7a appear to interact directly with nucleic acids in cells.

Thus, we propose that the mechanism of CQ action is three-fold (Figure 5.12). One, intracellular accumulation of CQ drives its concentration to a point at which it is able to facilitate unpackaging of nucleic acids from the polyplexes. CQ accumulates in cells to concentrations greatly exceeding that in the extracellular medium; it reaches still higher concentrations in the vesicles of the endocytic pathway, where internalized polyplexes are also delivered. Second, consistent with numerous literature reports, CQ buffers the vesicles of the endocytic pathway, helping delivered nucleic acids escape from these vesicles and/or avoid lysosomal degradation. Third, intracellular interactions between CQ and unpackaged nucleic acids contribute to gene expression. CQ can bind to the DNA via interaction with DNA bases and through electrostatic interaction with anionic phosphate groups. These interactions lead to changes in the biological and physical properties of the delivered nucleic acids, possibly altering their intracellular processing or slowing their degradation.

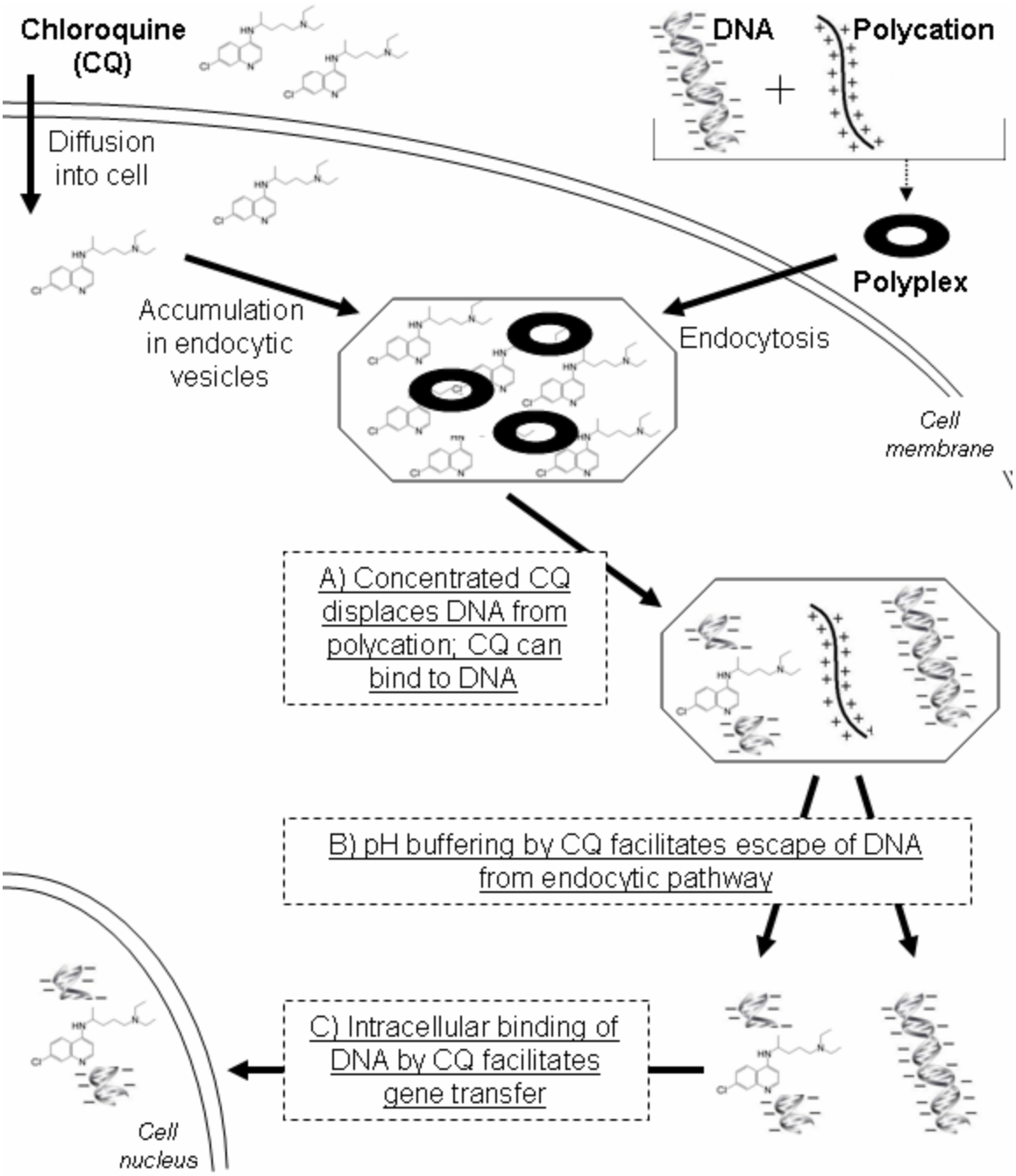

Figure 5.12 Proposed model for CQ enhancement of non-viral gene delivery

The results of this work suggest that CQ acts to increase the transfection efficiency of non-viral gene delivery vectors through three modes. First, polyplexes encounter high concentrations of CQ in the endocytic pathway, leading to enhanced unpackaging of delivered DNA. Second, CQ buffers the pH of endocytic vesicles, helping the DNA escape the endocytic pathway. Third, DNA binding by CQ also facilitates transfection, perhaps by altering the trafficking, processing, or degradation of the DNA within cells.

5.6 Acknowledgment

Many people contributed to the work in this chapter, and their efforts are very much appreciated. In particular, Jianjun Cheng and Ryan Zeidan were responsible for the synthesis of the chloroquine analogues and Rajan Kulkarni collected the data on intracellular pH-buffering activity. This work also reflects contributions from Aijie Liu, Suzie Pun, Greg Jensen, and Nathalie Bellocq.

5.7 References

1. Hwang SJ, Davis ME (2001) Cationic polymers for gene delivery: Designs for overcoming barriers to systemic administration. Curr. Opin. Mol. Ther. 3:183-191.
2. Davis ME (2002) Non-viral gene delivery systems. Curr. Opin. Biotechnol. 13:128-131.
3. Lechardeur D, Verkman AS, Lukacs GL. (2005) Intracellular routing of plasmid DNA during non-viral gene transfer. Adv Drug Deliv Rev. 57:755-67.
4. Wagner E, Zenke M, Cotton M, Beug H, Birnstiel ML (1990) Transferrin-Polycation Conjugates as Carriers for DNA Uptake into Cells. Proc. Natl. Acad. Sci. USA 87:3410-3414.
5. Zenke M, Steinlein P, Wagner E, Cotten M, Beug H, Birnstiel ML (1990) Receptor-Mediated Endocytosis of Transferrin Polycation Conjugates - an Efficient Way to Introduce DNA into Hematopoietic-Cells. Proc. Natl. Acad. Sci. USA 87:3655-3659.
6. Midoux P, Mendes C, Legrand A, Raimond J, Mayer R, Monsigny M, Roche AC (1993) Specific gene transfer mediated by lactosylated poly-L-lysine into hepatoma cells. Nucleic Acids Res. 21:871-8.
7. Erbacher P, Roche AC, Monsigny M, Midoux P (1996) Putative role of chloroquine in gene transfer into a human hepatoma cell line by DNA/lactosylated polylysine complexes. Exp Cell Res. 225:186-94.
8. Monsigny M, Roche AC, Midoux P, Mayer R (1994) Glycoconjugates as carriers for specific delivery of therapeutic drugs and genes. Adv. Drug Deliv. Rev. 14:1-24.
9. Gonzalez H, Hwang SJ, Davis ME (1999) New class of polymers for the delivery of macromolecular therapeutics. Bioconjug. Chem. 10:1068-1074.
10. Hwang SJ, Bellocq NC, Davis ME (2001) Effects of structure of beta-cyclodextrin-containing polymers on gene delivery. Bioconjug. Chem. 12:280-290.
11. Pun SH, Davis ME (2002) Development of a nonviral gene delivery vehicle for systemic application. Bioconjug. Chem. 13:630-639.

12. Reineke TM, Davis ME (2003) Structural effects of carbohydrate-containing polycations on gene delivery. 2. Charge center type. Bioconjug. Chem. 14, 255-261.
13. Reineke TM, Davis ME (2003) Structural effects of carbohydrate-containing polycations on gene delivery. 1. Carbohydrate size and its distance from charge centers. Bioconjug. Chem. 14, 247-254.
14. Popielarski SR, Mishra S, Davis ME (2003) Structural effects of carbohydrate-containing polycations on gene delivery. 3. Cyclodextrin type and functionalization. Bioconjug. Chem. 14, 672-678.
15. Irvin JL, Irvin EM (1947) Spectrophotometric and Potentiometric Evaluation of Apparent Acid Dissociation Exponents of Various 4-Aminoquinolines. J. Am. Chem. Soc. 69:1091-99.
16. Maxfield FR (1982) Weak Bases and Ionophores Rapidly and Reversibly Raise the Ph of Endocytic Vesicles in Cultured Mouse Fibroblasts. J. Cell Biol. 95:676-681.
17. Poole B, Ohkuma S (1981) Effect of Weak Bases on the Intralysosomal Ph in Mouse Peritoneal-Macrophages. J. Cell Biol. 90:665-669.
18. Sonawane ND, Szoka FC, Verkman AS (2003) Chloride accumulation and swelling in endosomes enhances DNA transfer by polyamine-DNA polyplexes. J Biol Chem. 278:44826-31.
19. Wibo M, Poole B (1974) Protein degradation in cultured cells. II. The uptake of chloroquine by rat fibroblasts and the inhibition of cellular protein degradation and cathepsin B1. J. Cell Biol. 63:430-40.
20. Poole B, Ohkuma S, Warburton MJ (1977) The accumulation of weakly basic substances in lysosomes and the inhibition of intracellular protein degradation. Acta Biol Med Ger. 36:1777-88.
21. Behr J-P (1997) The proton sponge: A trick to enter cells the viruses did not exploit. Chimia 51:34-36.
22. Allison JL, O'Brien RL, Hahn FE (1965) DNA: reaction with chloroquine. Science 149:1111-3.
23. Cohen SN, Yielding KL (1965) Spectrophotometric Studies of Interaction of Chloroquine with Deoxyribonucleic Acid. J. Biol. Chem. 240:3123-31.
24. Egan T (2001) Structure-Function Relationships in Chloroquine and Related 4-Aminoquinoline Antimalarials. Mini Reviews in Medicinal Chemistry 1:113-123.
25. Kaschula CH, Egan TJ, Hunter R, Basilico N, Parapini S, Taramelli D, Pasini E, Monti D (2002) Structure-activity relationships in 4-aminoquinoline antiplasmodials. The role of the group at the 7-position. J. Med. Chem. 45:3531-9.
26. Egan TJ, Hunter R, Kaschula CH, Marques HM, Misplon A, Walden J (2000) Structure-function relationships in aminoquinolines: effect of amino and chloro groups on quinoline-hematin complex formation, inhibition of beta-hematin formation, and antiplasmodial activity. J. Med. Chem. 43:283-91.
27. De D, Krogstad FM, Byers LD, Krogstad DJ (1998) Structure-activity relationships for antiplasmodial activity among 7-substituted 4-aminoquinolines. J. Med. Chem. 41:4918-26.
28. Erbacher P, Roche AC, Monsigny M, Midoux P (1995) Glycosylated polylysine/DNA complexes: gene transfer efficiency in relation with the size and

the sugar substitution level of glycosylated polylysines and with the plasmid size. Bioconjug Chem. 6:401-10.

29. Kulkarni RP, Mishra S, Fraser SE, Davis ME (2005) Single-cell kinetics of intracellular, nonviral, nucleic acid delivery vehicle acidification and trafficking. Bioconjug. Chem. 16:986-94.
30. Akinc A, Thomas M, Klibanov AM, Langer R (2005) Exploring polyethylenimine-mediated DNA transfection and the proton sponge hypothesis. J. Gene Med. 7:657–63.
31. De D, Byers LD, Krogstad DJ (1997) Antimalarials: Synthesis of 4-aminoquinolines that circumvent drug resistance in malaria parasites. J. Heterocyclic Chem. 34:315-20.
32. Mishra S, Webster P, Davis ME (2004) PEGylation significantly affects cellular uptake and intracellular trafficking of non-viral gene delivery particles. Eur. J. Cell Biol. 83:97-111.
33. Poole B, Ohkuma S (1981) Effect of weak bases on the intralysosomal pH in mouse peritoneal macrophages. J. Cell Biol. 90:665-9.
34. Parker FS, Irvin JL (1952) The Interaction of Chloroquine with Nucleic Acids and Nucleoproteins. J. Biol. Chem. 199:897-909.
35. Ostling O, Johanson KJ (1984) Microelectrophoretic study of radiation-induced DNA damages in individual mammalian cells. Biochem. Biophys. Res. Comm.
36. Singh NP, McCoy M, Tice RR, Schneider E (1988) A simple technique for quantitation of low levels of DNA damage in single cells. Exp. Cell Res. 175:184-91.
37. Schaffer DV, Fidelman NA, Dan N, Lauffenburger DA (2000) Vector unpacking as a potential barrier for receptor-mediated polyplex gene delivery. Biotechnol Bioeng. 67:598-606.
38. Lechardeur D, Sohn KJ, Haardt M, Joshi PB, Monck M, Graham RW, Beatty B, Squire J, O'Brodovich H, Lukacs GL (1999) Metabolic instability of plasmid DNA in the cytosol: a potential barrier to gene transfer. Gene Ther. 6:482-97.
39. Lukacs GL, Haggie P, Seksek O, Lechardeur D, Freedman N, Verkman AS (2000) Size-dependent DNA mobility in cytoplasm and nucleus. J. Biol. Chem. 275:1625-9.

CHAPTER 6: INTRODUCTION OF A TERMINAL IMIDAZOLE GROUP HAS MULTIPLE EFFECTS ON THE GENE DELIVERY BEHAVIOR OF A CYCLODEXTRIN-CONTAINING POLYCATION

6.1 Abstract

The cyclodextrin-containing polycation (CDP) is one of many non-viral gene delivery vectors that show improved transfection efficiency when modified to have pH-buffering capacity. This feature is presumed to confer enhanced ability to escape the endocytic pathway. Here, the differences in delivery behavior between CDP and its pH-buffering, imidazole-terminated variant (CDPimid) are investigated in order to elucidate the mechanism(s) by which these related materials exhibit differences in gene delivery. In cell-free assays that include dye exlusion and heparan sulfate displacement, CDP appears to have weaker binding strength with nucleic acids than CDPimid. Analysis of transfected cells, however, indicates that CDPimid more readily releases nucleic acids in the intracellular setting, suggesting that differences in transfection efficiency between CDP and CDPimid may result from factors beyond buffering activity and endosomal escape. Transfection in the presence of chloroquine analogues provides further evidence of differences in the intracellular processing of CDP and CDPimid polyplexes.

6.2 Introduction

The delivery efficiency of non-viral vectors must be improved if these materials are to achieve their therapeutic potential. A bevy of materials have been identified which are capable of condensing nucleic acids into small particles and delivering them to cells. Despite extensive uptake of exogenous nucleic acids by cells, non-viral vectors do not generate the levels of gene expression that are possible with viral vectors. Further development of non-viral vectors has been hindered by poor understanding of the intracellular fate of the gene delivery particles.

Once internalized by cells, non-viral gene delivery particles are generally deposited into the endocytic pathway and must escape in order to avoid degradation by the lysosomal system [1-6]. Little is known about the particles' intracellular trafficking or how these circumstances affect delivery and expression. However, many researchers have considered that escape from the endocytic pathway may be facilitated by exploiting the progressive acidification of its compartments [7-8]. This approach has been inspired in part by the influenza virus, in which acidic pH triggers reorganization of the hemagglutinin protein and facilitates viral escape from the endocytic pathway. The intracellular pH-buffering activity of some polymers, particularly polyethyleneimine (PEI), has been linked to increases in transfection efficiency [5,9], and the utility of pH-buffering activity in nonviral gene transfer has been supported by increases in transfection efficiency in the presence of chloroquine, a small molecule that can buffer the vesicles of the endocytic pathway.

The majority of early non-viral vectors, including poly-L-lysine or the cyclodextrin-containing polycation (CDP), do not contain any pH buffering elements

[10,11]. However, the positive aspects of these non-buffering materials (such as the low cytotoxicity of CDP) have motivated efforts to improve their gene delivery performance through rational modification. The relative effectiveness of pH-buffering vectors, most notably PEI, has prompted incorporation of buffering elements in both existing and novel non-buffering delivery vectors; these modified materials often exhibit improvements in transfection efficiency [11-15].

Modification of CDP with a terminal imidazole group has been shown to improve its transfection efficiency at low charge ratios (of most interest for systemic administration) without concomitant increases in toxicity [12]. Recent reports, however, have shown that pH-buffering activity does not always correlate with improved transfection efficiency, raising questions about the value or necessity of this feature in non-viral vectors [16-19]. Differences in delivery behavior between CDP and its pH-buffering, imidazole-terminated variant (CDPimid) were investigated in order to elucidate mechanism(s) by which these two related materials exhibit differences in gene delivery behavior. The goal of this work is to obtain further experimental evidence to evaluate the value and necessity of pH-buffering components in non-viral gene delivery systems.

6.3 Materials and methods

6.3.1 Polycations, pDNA, and polyplexes

A β-cyclodextrin-containing polycation (CDP) and its imidazole-terminated variant (CDPimid) were synthesized as described previously [12] (Figure 6.1). The DNA plasmid pGL3-CV (Promega, Madison, WI), containing the luciferase gene under the control of the SV40 promoter, was amplified by E. coli strain DH5α and purified using the Ultramobius 1000 plasmid kit (Novagen, San Diego, CA). Polyplexes were formulated at a charge ratio of 5± by adding solutions of polycation (CDP or CDPimid) (1.03 mg/mL in dH_2O) to equal volumes of nucleic acids (0.1 mg/mL in dH_2O) and incubating for 30 min. For surface modification with poly(ethylene glycol) (PEGylation), 35 μg adamantane-PEG (Ad-PEG, 100 mg/mL in dH_2O) per μg DNA was added to CDP or CDPimid polyplexes after formulation, and solutions were incubated a further 30 min [20]. 25-kD branched polyethylenimine (PEI) (Sigma, St. Louis, MO) was used to formulate polyplexes as previously described [21].

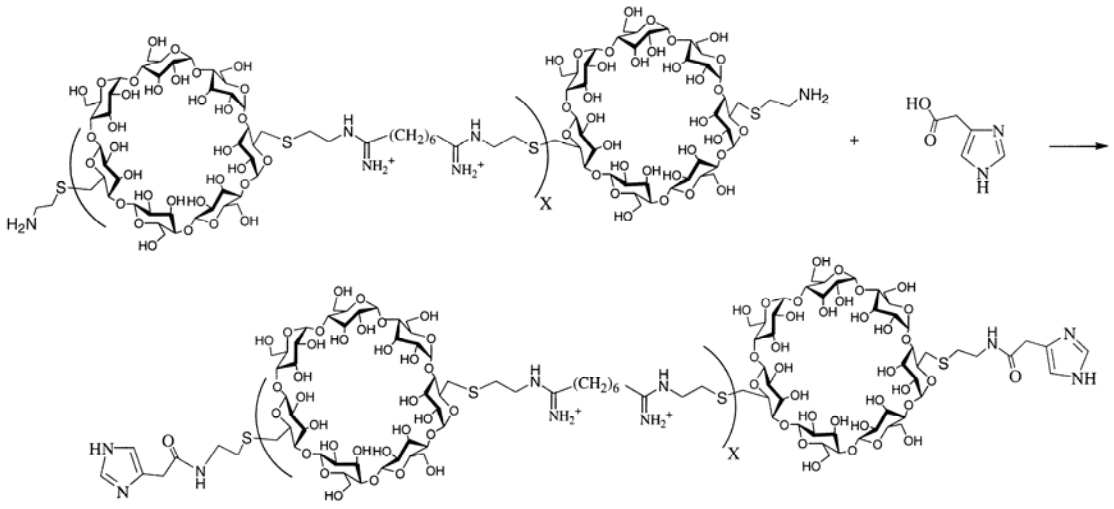

Figure 6.1 Reaction of CDP to give CDPimid
An imidazole end group can be directly conjugated to the termini of the cyclodextrin-containing polycation (CDP).

6.3.2 Cell culture and transfections

HeLa and BHK-21 cells were maintained in Dulbecco's Modified Eagle's Medium with 2 mM L-glutamine, 1.5 mg/mL sodium bicarbonate, 0.1 mM non-essential amino acids, 1.0 mM sodium pyruvate, and 10% fetal bovine serum. 293-T7 cells, which constitutively express T7 RNA polymerase, were maintained in media as above with 0.8 mg/mL geneticin (G418) [22]. The medium was purchased from Mediatech (Herndon, VA) and supplements were purchased from Gibco BRL (Gaithersburg, MD).

For evaluation of transfection efficiency through luciferase assay, cells were plated in 24-well plates at a density of 5×10^4 cells/well. Polyplexes were formulated between CDP or CDPimid and the plasmid pGL3-CV (Promega), which encodes the firefly luciferase gene under control of an SV40 promoter. One day after plating, cells were transfected in Opti-MEM serum-free medium (Invitrogen). Two days after transfection, luciferase activity of cell lysates was evaluated with the Luciferase Assay System (Promega) and total protein concentration was assessed by the DC Protein Assay (Bio-Rad, Hercules, CA).

For transfections in the presence of chloroquine analogues, immediately after polyplex-containing media was added to cells for transfection, an appropriately-sized aliquot of chloroquine analogue stock solution (5 mM) was added to the media and mixed. The chloroquine analogues investigated were chloroquine, CQ7a (trifluoromethyl- in place of chloro- at the 7 position of chloroquine), CQO (oxygen in place of secondary amine at the 4 position of chloroquine), and CP (pyridinyl aromatic ring in place of dual-ring structure in chloroquine).

6.3.3 Intracellular buffering activity of CDP and CDPimid

The activity of CDP and CDPimid in buffering the pH environment of intracellular polyplexes was evaluated using the method of Kulkarni, et al. [16]. Briefly, polyplexes were formulated between the polymer of interest and an oligonucleotide labeled with the pH-sensitive fluorophore SNARF-4F (Molecular Probes, Carlsbad, CA). HeLa cells were treated with the polyplexes and imaged using an inverted Zeiss LSM 510 META confocal microscope with a 63x oil objective (NA 1.4). Excitation of the SNARF fluorophore was achieved with the 543 nm line of the He-Ne laser line supplied with the microscope. After passing through a variable confocal pinhole, the SNARF-4F emission was collected by the META detector in distinct wavelength bins of 569-601 nm and 633-687 nm. Using a standard curve, the relative intensity of individual signals across these bins was used to evaluate the pH environment of the corresponding intracellular polyplexes.

6.3.4 Salt-induced dissociation of polyplexes

The stability of polyplexes against increasing salt concentration was evaluated by dye exclusion following a published procedure [23]. After formulation, polyplexes were diluted 5x in dH_2O. Separately, 200x dilutions of the supplied PicoGreen stock solution (Molecular Probes) were prepared in 10 mM HEPES buffer containing various concentrations of NaCl. For each sample, 50 μL of polyplex solution was transferred to a well of an opaque, black 96-well plate and combined with 50 μL of PicoGreen solution; after 10 min, the fluorescence ($\lambda_{excitation}$ 488 nm; $\lambda_{emission}$ 535 nm) of the polyplex-PicoGreen solution was evaluated using a Spectrafluor Plus plate reader (Tecan, Durham,

NC). The percentage dye exclusion was calculated from the ratio $((F_{DNA}-F_{sample})/(F_{DNA}-F_{H2O}))$, where F_{DNA} is the fluorescence of a sample of DNA alone (no polycation), F_{sample} is the sample fluorescence, and F_{H2O} is the fluorescence of a blank (control) sample.

6.3.5 Heparan sulfate displacement of nucleic acids from polyplexes

Displacement of pDNA from polyplexes by heparan sulfate was evaluated by gel electrophoresis. CDP and CDPimid polyplexes were formulated, and to 10 μL of polyplex solution was added an appropriate volume of heparan sulfate (5 mg/mL in dH_2O). After 5 min incubation at room temperature, 1 mL of loading buffer was added to each sample and the samples were transferred to a 0.5% agarose gel (30 μg ethidium bromide/50 mL TAE buffer), electrophoresed, and visualized under UV illumination.

6.3.6 Measure of intracellular nucleic acid unpackaging

To obtain a relative measure of intracellular nucleic acid unpackaging, HeLa cells in 24-well plates were transfected with 2 μg of a FITC-labeled DNA oligonucleotide (FITC-oligo) packaged in CDP or CDPimid polyplexes. At selected times after transfection, cells were collected by trypsinization and pelleted by centrifugation (6 min at 2400 rpm). Each sample was resuspended in 10 μL 1x cell culture lysis buffer (Promega) and stored at 4 °C. Control samples were prepared as solutions of known amounts of FITC-oligo in 10 μL 1x cell culture lysis buffer. After 30 min incubation, each sample was mixed with 25 μL of low-melting-point agarose solution (1% in TAE buffer, 37 °C) and transferred immediately to a well of an agarose gel (0.5% in 60 mL TAE buffer). The agarose gel was subjected to electrophoresis and then imaged under

UV illumination. Detection of FITC-oligo was achieved through its fluorescent signal. Migration of FITC-oligo from control samples was used to indicate the expected migration of unpackaged FITC-oligo from cell lysates.

6.3.7 Flow cytometry for evaluation of nucleic acid uptake

For flow cytometry, polyplexes were formulated with a FITC-labeled oligonucleotide. Labeled polyplexes were used to transfect cells as described; four hours after transfection, the polyplex-containing medium was aspirated and replaced with regular growth medium. Cells were washed (10 U/mL DNase, 3 mM $MgCl_2$ in Hank's buffered saline solution (HBSS)), suspended in propidium iodide-containing buffer (HBSS, 2.5 mg/mL bovine serum albumin, 0.01 mg/mL propidium iodide), and analyzed on a FACScalibur instrument (Becton Dickinson, Franklin Lakes, NJ) with a 488 nm excitation line. Samples were initially gated by forward and side scatter, and viable cells were assayed for FITC fluorescence.

6.3.8 Transmission electron microscopy of CDP and CDPimid polyplexes within cells

For transmission electron microscopy, BHK-21 cells were transfected with CDP/pDNA or CDPimid/pDNA polyplexes. At increasing timepoints after transfection, the medium was aspirated and the cells were rinsed with PBS. Cells were fixed with 2% glutaraldehyde in 100 mM sodium cacodylate with 2% sucrose, collected by scraping, and pelleted by centrifugation. Cell pellets were post-fixed in osmium tetroxide, dehydrated in ethanol, and embedded in Epon-Spurr resin. Thin sections were prepared on an Ultracut S ultramicrotome (Leica Microsystems, Deerfield, IL), contrasted with

uranyl acetate and lead citrate, and imaged on a BioTwin CM120 transmission election microscope (FEI, Hillsboro, OR) operating at 80 kV.

For immunolabeling experiments, pDNA was labeled with the LabelIT biotin-labeling kit (Mirus, Madison, WI) at a density of roughly 10 labels per plasmid and purified by ethanol precipitation. Polyplexes were formulated with CDP or CDPimid and administered to BHK-21 cells. At desired timepoints after transfection, the medium was aspirated and the cells were rinsed with PBS. Cells were fixed with 2% glutaraldehyde in 100 mM sodium cacodylate with 2% sucrose, collected by scraping, and pelleted by centrifugation. Cell pellets were infiltrated in 2.3 M sucrose, frozen by immersion in liquid nitrogen, freeze substituted at -80°C with dry methanol, and embedded at -50°C in Lowicryl HM20 resin (Electron Microscopy Sciences, Fort Washington, PA). Thin sections were prepared on an Ultracut S ultramicrotome and immunolabled with a mouse anti-biotin primary antibody (Sigma), a rabbit anti-mouse secondary antibody (Organon Technika, Durham, NC), and colloidal gold (10 nm)-labeled protein A (University of Utrecht, The Netherlands). 1X PBS containing 10% fetal calf serum was used as the blocking solution, and immunolabeled sections were contrasted with uranyl acetate and lead citrate and imaged on a BioTwin CM120 transmission election microscope operating at 80 kV. Immunolabeling of control samples prepared without biotin-labeled pDNA was used to determine appropriate concentrations for antibody and colloidal gold labeling. An iterative process was used to minimize background labeling from gold-labeled protein A alone, the secondary antibody and gold-labeled protein A together, and finally both antibodies and gold-labeled protein A together.

6.3.9 Polyplex accessibility in the presence of CQ, CQ7a, CP, and CQO

The accessibility of polyplex-compacted DNA in the presence of CQ analogues was evaluated by dye exclusion, through adaption of a published procedure [23]. After formulation, polyplexes were diluted 2.5x in dH_2O. For each sample, 25 μL of polyplex solution was transferred to a well of an opaque, black 96-well plate and combined with 25 μL of CQ analogue solution at twice the concentration of interest. Separately, a 200x dilution of the supplied PicoGreen stock solution (Molecular Probes) was prepared in 10 mM HEPES buffer. After polyplex-CQ analogues solutions were incubated for 5 min at room temperature, each 50 μL sample was combined with 50 μL of PicoGreen solution and the fluorescence ($\lambda_{excitation}$ 488 nm; $\lambda_{emission}$ 535 nm) of the resulting solutions was evaluated with a Spectrafluor Plus plate reader (Tecan, Durham, NC). The percentage dye exclusion was calculated from the ratio $((F_{DNA}-F_{sample})/(F_{DNA}-F_{H2O}))$, where F_{DNA} is the fluorescence of a sample of DNA alone (no polycation), F_{sample} is the sample fluorescence, and F_{H2O} is the fluorescence of a blank (control) sample.

6.4 Results

6.4.1 Transfection efficiency of CDPimid is greater than that of CDP

When used to deliver luciferase-expressing plasmid DNA to cultured cells, CDPimid generates greater levels of gene expression than CDP (Figure 6.2a). This is true for a variety of cell lines transfected with pGL3-CV, a DNA plasmid (pDNA) which should be transcribed and expressed only when available to the transcriptional machinery within the cell nucleus. 293-T7 cells (constitutively expressing the cytoplasmic T7 RNA polymerase) were employed to investigate the possibility that differences in expression result from differences in nuclear delivery. The plasmid pT7-Luc (a plasmid expressing luciferase under control of a T7 promoter) can be transcribed and expressed if delivered to the cytoplasm of 293-T7 cells [22], and its poor expression in 293 cells (lacking the T7 RNA polymerase) confirms that the polymerase is responsible for pT7-Luc expression (Figure 6.2b). The greater transfection efficiency of CDPimid versus CDP in the 293-T7/pT7-Luc system indicates that such differences arise prior to nuclear delivery.

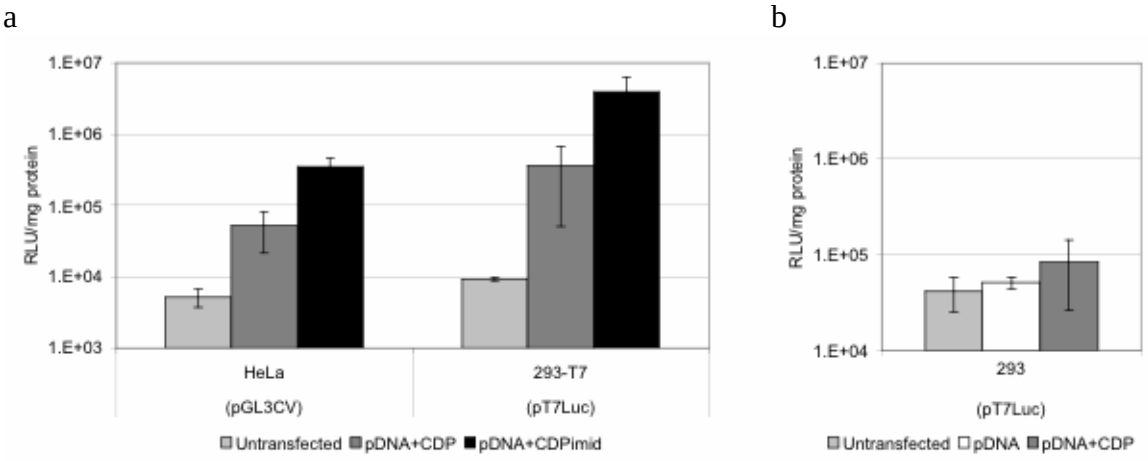

Figure 6.2 Transfection of HeLa or 293-T7 cells with CDP or CDPimid
(a) CDP or CDPimid was used to transfect HeLa cells (pGL3-CV) or 293-T7 cells (pT7-Luc) with pDNA. In each case, CDPimid generated greater luciferase expression. (b) When 293 cells are transfected with pT7-Luc, they do not show significant expression.

6.4.2 A terminal imidazole group introduces intracellular pH-buffering activity to CDP

The addition of an imidazole group to the termini of CDP is designed to impart intracellular pH-buffering capacity to the modified polycation, CDPimid. To evaluate the actual intracellular buffering activity of CDP and CDPimid, we employed the method of Kulkarni, et al. [16], where an oligonucleotide is labeled with the fluorophore SNARF-4F and used to prepare polyplexes. These polyplexes are administered to cells and the fluorescence emission of SNARF-4F is used to evaluate the local pH environment of polyplexes within individual cells. The data can be compiled in aggregate to indicate the actual intracellular buffering activity of the polycations (Figure 6.3). By this method, CDPimid demonstrates strong buffering activity relative to CDP.

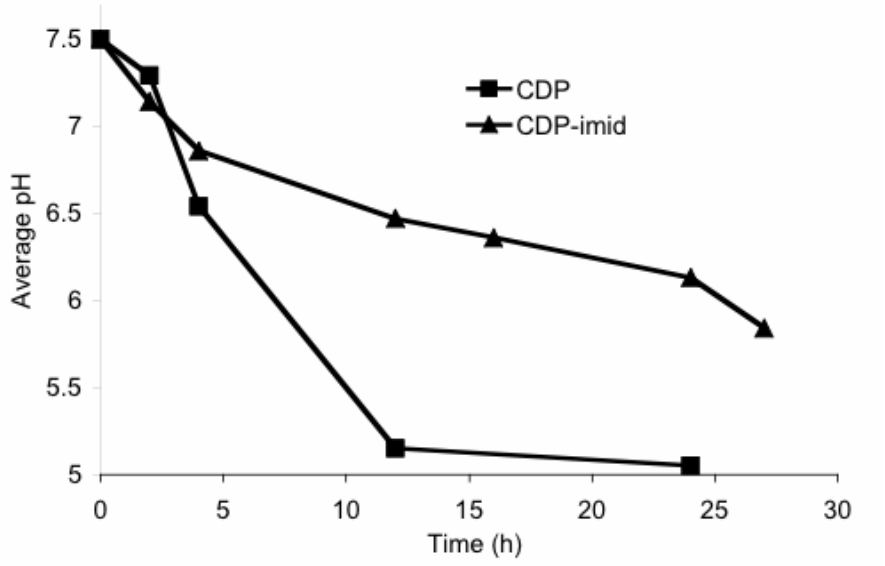

Figure 6.3 Intracellular buffering activity of CDP and CDPimid
Polyplexes containing a SNARF-4F-labeled oligonucleotide were administered to HeLa cells. Confocal microscopy was used to visualize intracellular polyplexes, whose pH environment could be calculated using the pH-sensitivity of SNARF-4F [16]. When compiled, this data gives an average intracellular pH for the delivered oligonucleotide. CDPimid displays strong buffering activity while CDP does not.

6.4.3 Exclusion of intercalating dye by CDP and CDPimid polyplexes

PicoGreen experiences significant fluorescence enhancement upon intercalation in nucleic acids, such that its exclusion indicates inaccessibility of the nucleic acids to intercalation [23]. This characteristic was used to evaluate different types of polyplexes for the relative accessibility of pDNA. Polyplexes were subjected to disruption by increasing concentrations of NaCl, then combined with solutions of PicoGreen and evaluated for fluorescence intensity. Unlike 25-kD branched polyethylenimine (PEI), which showed near complete dye exclusion without added NaCl, CDP and CDPimid gave only moderate exclusion of PicoGreen without NaCl and minimal dye exclusion at higher salt concentration (Figure 6.4a). A further study explored the reliability of observed differences between CDP and CDPimid at low NaCl concentrations; dye exclusion was less with CDP for the NaCl concentrations investigated (Figure 6.4b).

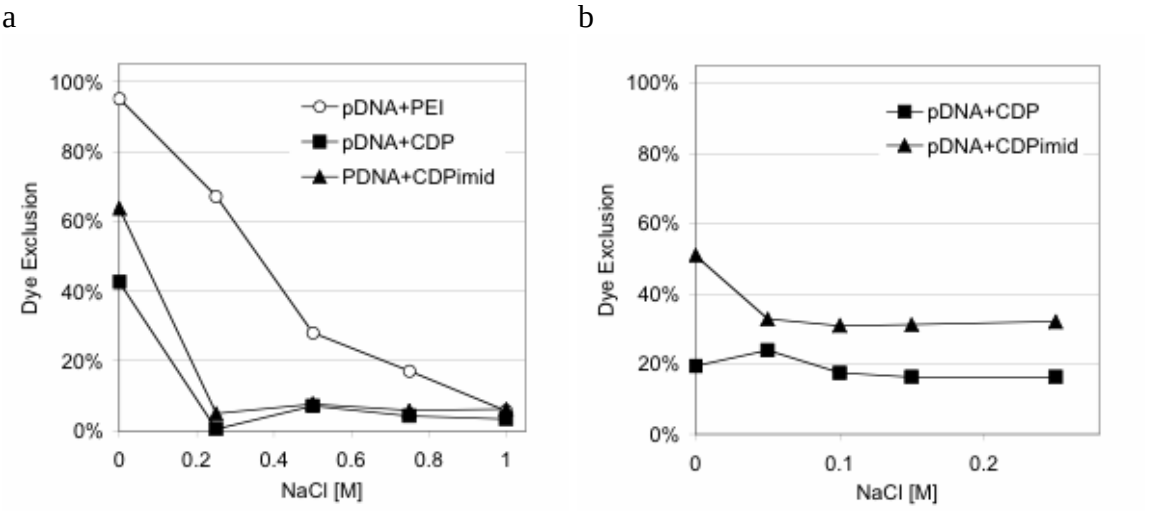

Figure 6.4 PicoGreen exclusion as a measure of salt-induced complex dissociation
The exclusion of the DNA-intercalating dye PicoGreen was used as a measure of polyplex stability against salt-induced dissocation [23]. (a) CDP and CDPimid did not exclude PicoGreen to the same extent as 25-kD branched polyethylenimine (PEI). (b) Examination of lower salt concentrations revealed that dye exclusion by CDP was consistently less than with CDPimid.

Inclusion complex formation between the PicoGreen dye and the cyclodextrin cups of CDP or CDPimid would likely impart some fluorescence to these materials. Significant fluorescence of this type would give a false impression of reduced dye exclusion, consistent with the observations of CDP and CDPimid polyplexes in the PicoGreen salt-dissociation assay. To investigate this possibility, CDP and CDPimid were incubated with PicoGreen in the absence of any DNA. The fluorescence generated by these combinations represents only 0.05% of the fluorescence enhancement seen with PicoGreen interactions with uncomplexed pDNA. Thus, the incomplete dye exclusion (measurable fluorescence) observed with CDP and CDPimid polyplexes is unlikely to be a result of PicoGreen-cyclodextrin or PicoGreen-polycation interactions.

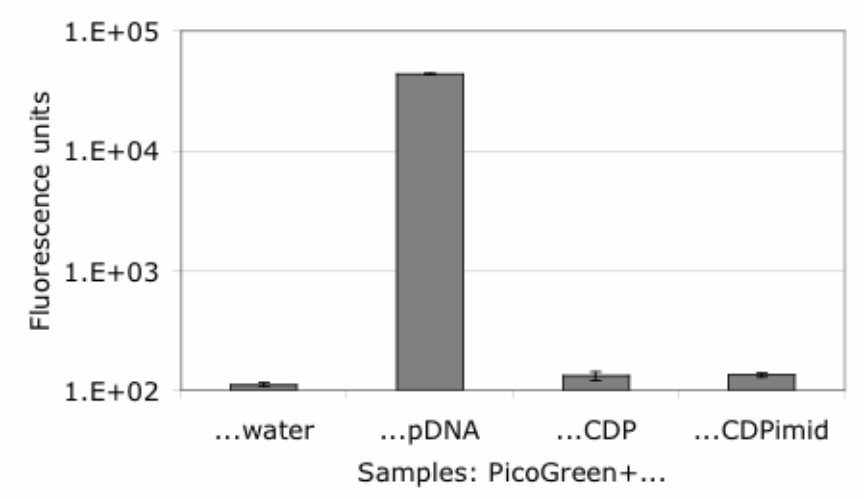

Figure 6.5 PicoGreen fluorescence with individual polyplex components
To investigate if the incomplete dye exclusion observed for CDP and CDPimid polyplexes results from PicoGreen interactions with the polycation, the dye was incubated with either pDNA alone or polycation alone. The fluorescence enhancement resulting from PicoGreen-pDNA interactions is ~2000 times the enhancement that is seen with PicoGreen-CDP or PicoGreen-CDPimid interactions.

6.4.4 CDPimid polyplexes are more resistant to heparan sulfate than CDP polyplexes

Heparan sulfate was employed to evaluate the ability of a polyanion to cause CDP or CDPimid to displace from DNA. Polyplexes were formulated, incubated with various amounts of heparan sulfate for 5 min at room temperature, and then loaded to an agarose gel and electrophoresed. Polycation-bound DNA will not migrate in the gel. At higher heparan sulfate concentrations, "free" nucleic acids could be observed due to their movement in the gel. For polyplexes formulated with a DNA oligonucleotide (Figure 6.6) or with plasmid DNA (Figure 6.7), an equivalent dose of heparan sulfate generated greater displacement with CDP than with CDPimid.

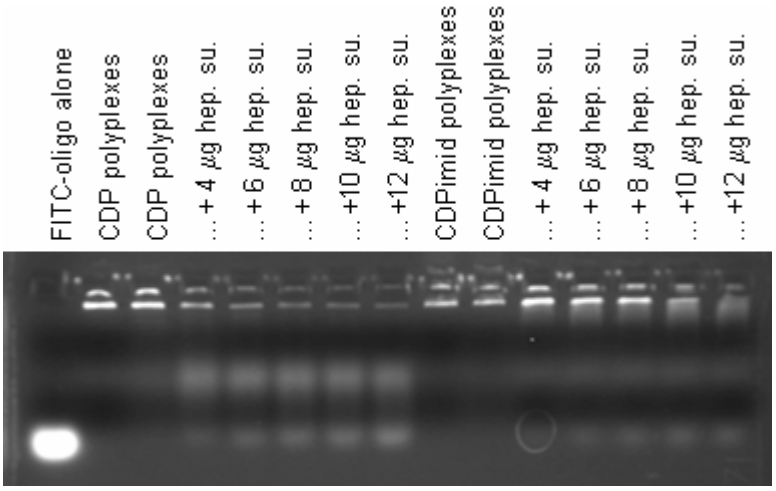

Figure 6.6 Heparan sulfate release of oligonucleotide from polyplexes
Polyplexes were prepared with a 25-mer DNA oligonucleotide (FITC-oligo) and either CDP (lanes 2-8) or CDPimid (lanes 9-15). The resulting polyplexes were incubated with increasing amounts of heparan sulfate (hep. su.) to induce oligonucleotide release. Samples were then loaded to an agarose gel and electrophoresed. With equivalent heparan sulfate loading, CDP polyplexes showed more extensive oligonucleotide release than CDPimid polyplexes.

Polyplexes are exposed to acidification when trafficking in the endocytic pathway; to test whether acidic conditions alter the relative susceptibility of CDP and CDPimid to heparan sulfate, polyplexes were acidified to pH 3 by addition of 0.1 N HCl prior to heparan sulfate incubation. Acidified polyplexes displayed an equal response to heparan sulfate as their as-formulated counterparts (Figure 6.7b).

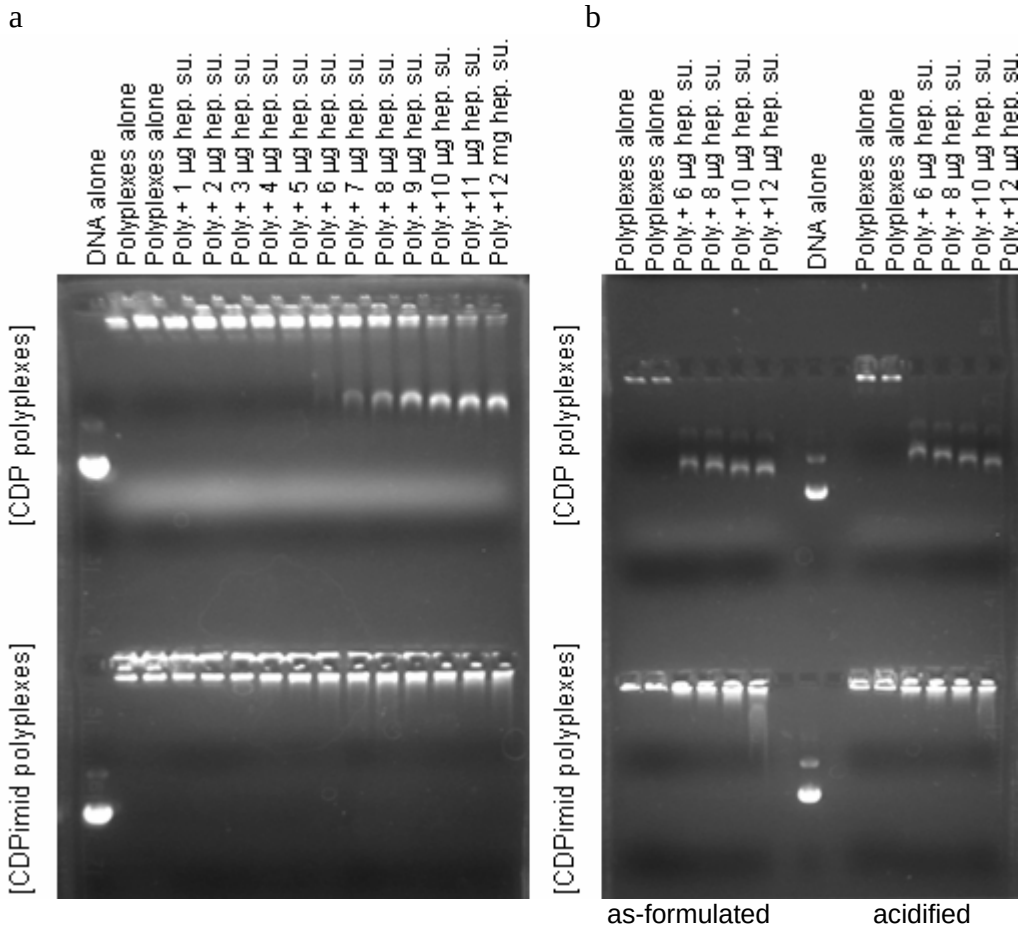

Figure 6.7 Heparan sulfate release of pDNA from polyplexes
CDP/pDNA (top row) and CDPimid/pDNA (bottom row) polyplexes (Poly.) were incubated with increasing amounts of heparan sulfate (hep. su.) to induce pDNA release. Samples were then loaded to an agarose gel and electrophoresed. (a) With equivalent heparan sulfate loading, CDP polyplexes showed more extensive pDNA release than CDPimid polyplexes. (b) Equivalent results were obtained for polyplexes incubated with heparan sulfate (left) or polyplexes acidified to pH 3 and then incubated with heparan sulfate (right).

6.4.5 Transmission electron microscopy shows CDPimid gives enhanced unpackaging and accessibility of delivered DNA relative to CDP

CDP or CDPimid polyplexes were delivered to cultured cells and visualized using transmission electron microscopy (Figures 6.8, 6.9). Intact polyplexes were easily identifiable, appearing as irregular aggregates roughly 300-500 nm in diameter. Some aggregates are composed of smaller rounded components (likely the as-formulated polyplexes readily observable by light scattering in water [10,12,16]).

Most intracellular vesicles containing CDP polyplexes conformed to the aggregates' shape and contained little to no void space or other material (Figures 6.8d-i). In contrast, vesicles containing CDPimid polyplexes occasionally enclosed portions of void space (Figures 6.9c-d) or large amounts of material separate from the aggregates (Figures 6.9b-c,e-i). It is unclear if this accompanying material is derived from or is independent of the polyplex aggregates.

As the time between the initial exposure to CDP polyplexes and the cells' fixation was increased from 0.5 to 24 h, aggregates of CDP polyplexes increasingly appeared in the vicinity of the cell nucleus (Figure 6.8). The larger size of aggregates closer to the nucleus suggested an aggregation of polyplex aggregates was occurring. Only a small minority of CDP polyplexes appeared to be disassembling (6.8q-r). These degrading polyplexes, with less distinct and defined borders than most aggregates, were found more commonly within vesicles than free in cytoplasm.

In contrast, CDPimid polyplexes were observed undergoing significant unraveling in intracellular vesicles at 4 or 8 h after initial transfection (Figure 6.9). Various loops and swirls extend from the central mass of some CDPimid polyplexes (Figure 6.9g-i).

Also, some cells contain swirls or ring structures in the absence of larger aggregates; these features may be found either within larger vesicles (Figure 6.9g,j) or filling vesicles entirely (Figure 6.9k-l). A fuzzy or hairy surface characterizes many aggregates (Figure 6.9c-d,f) and many of the loops, swirls, and rings (Figure 6.9g-l).

Both CDP and CDPimid polyplexes could be observed in the absence of surrounding membranes. Aggregates were observed either in direct contact with the surrounding cytoplasm (Figures 6.8k-m, 6.9f,j) or bordering void spaces (Figures 6.8j-k,n). Intact polyplexes or their aggregates were not observed within any cell nucleus.

In order to visualize unpackaged intracellular pDNA, CDP or CDPimid was used to deliver biotin-labeled pDNA to cells. Subsequently, TEM samples were prepared using anti-biotin immunolabeling with colloidal gold. Intracellular CDP and CDPimid polyplexes are both labeled by this method, but the numbers and density of gold particles per polyplex or aggregate are generally less with CDP than with CDPimid (6.10a, 6.11a-g). The CDPimid polyplexes can be seen in cells as large, heavily gold-labeled entities.

Immunolabeling of unpackaged pDNA within cells generates clusters of colloidal gold separate from polyplexes. For both CDP and CDPimid, these clusters are found both in the cytoplasm (Figures 6.10c-e, 6.11h) and in the cell nucleus (6.10f-h, 6.11i). Qualitative differences were not apparent among the colloidal gold clusters for the two types of polyplexes, either in their intracellular distribution or overall prevalence.

Cells transfected with unlabeled pDNA and subjected to equivalent preparation and immunolabeling do not reveal colloidal gold labeling of polyplexes or colloidal gold clustering (not shown).

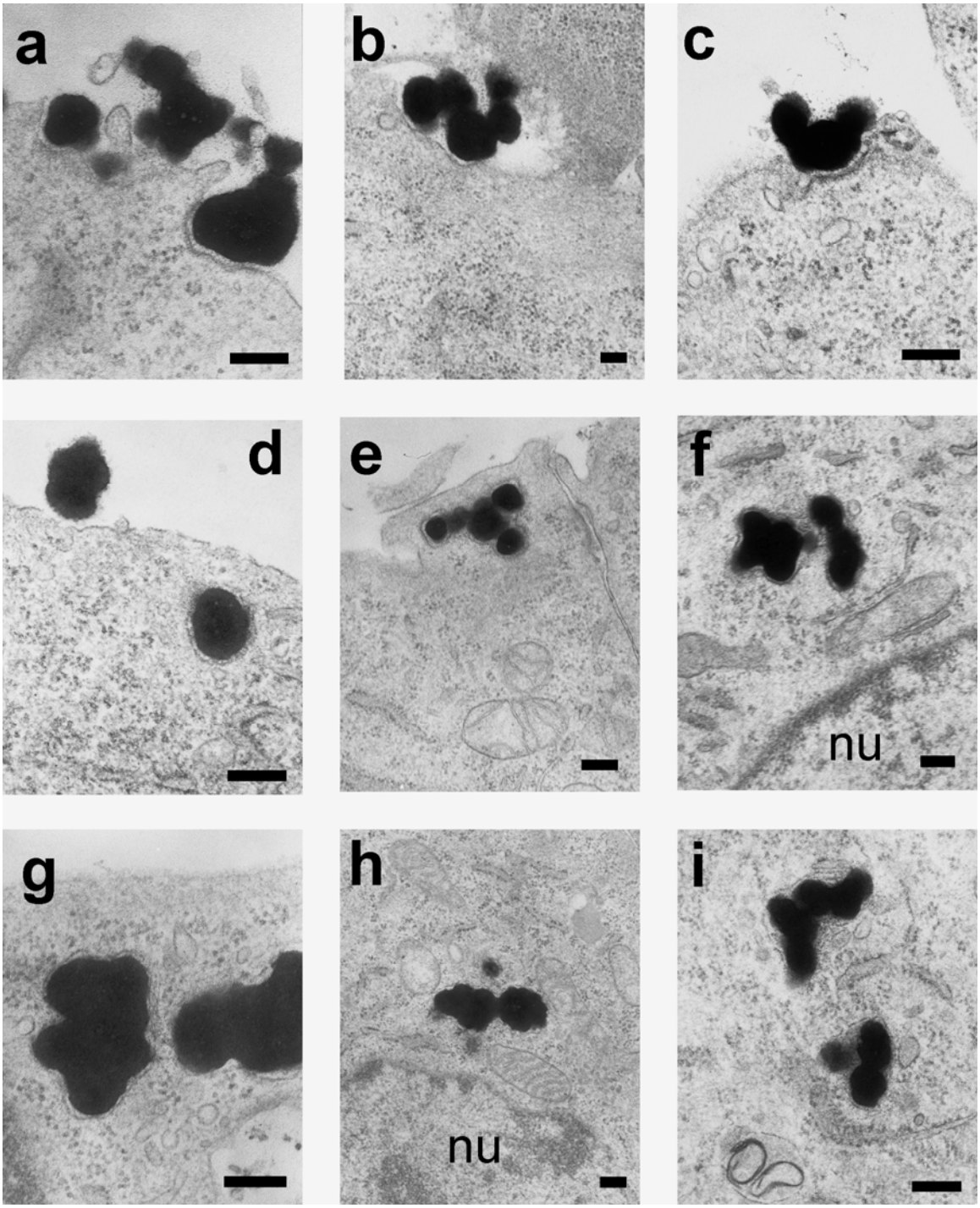

Figure 6.8 TEMs of CDP polyplexes
BHK-21 cells were exposed to CDP polyplexes and prepared for TEM imaging. The polyplexes appear as large aggregates and are seen associated with cell membranes, often directly with invaginations of these cell membranes (a-c). The aggregates proceed into cells in large vesicles that conform to the shape of the aggregates (d-i). Some polyplexes are not completely surrounded by membranes (h-i). Bars for (a-i), 200 nm.

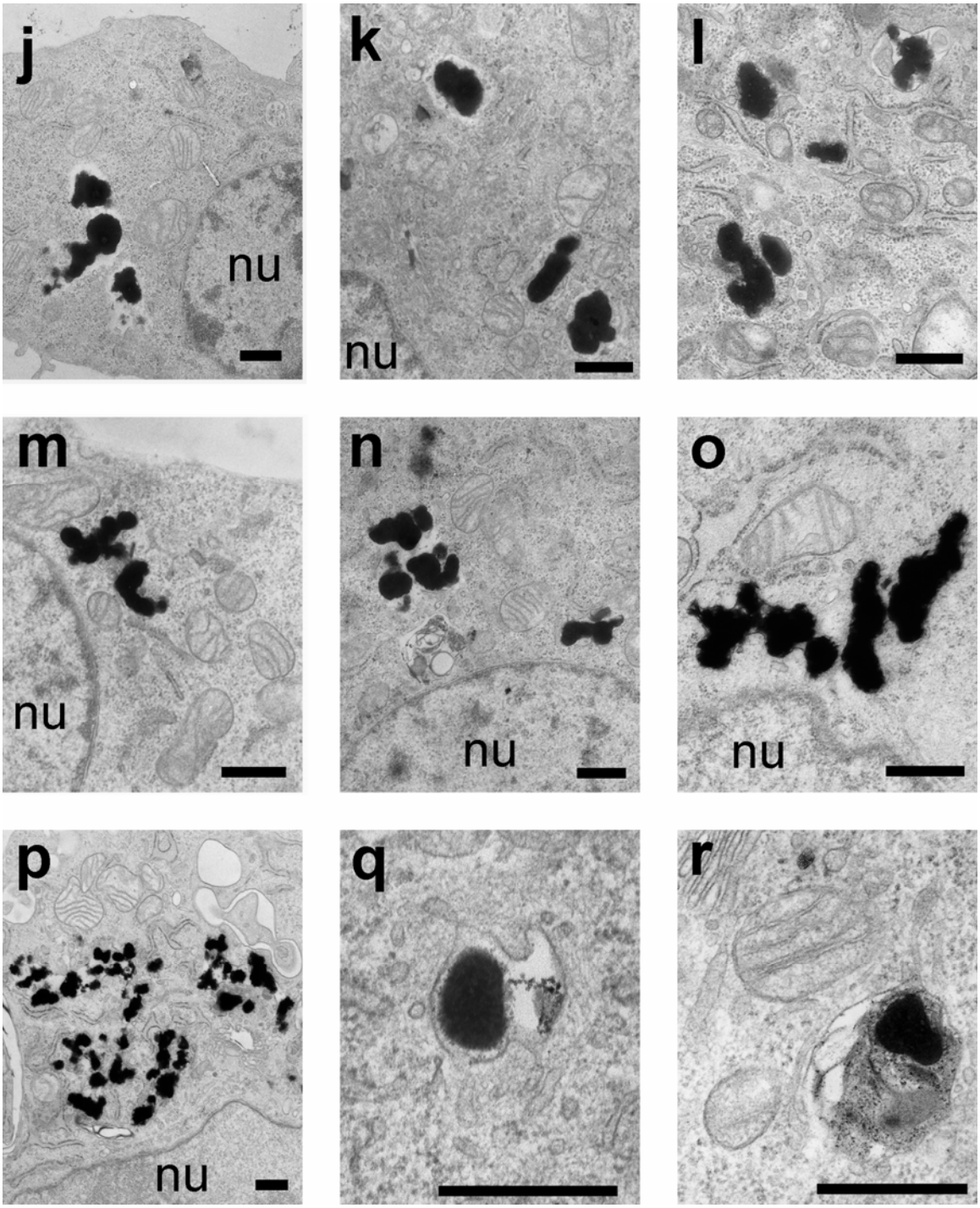

(*Figure 6.8, continued*) At later times, many polyplexes are observed in the cytoplasm without surrounding membranes (j-n). The cytoplasm appears to contact the polyplexes in some cases, whereas in others there is a void space between the polyplexes and the surrounding cytoplasm. Later timepoints show an accumulation of polyplexes in a perinuclear region (o-p). Some CDP polyplexes appear to be undergoing degradation (q-r). Bars for (j-r), 500 nm. Cell nucleus, nu.

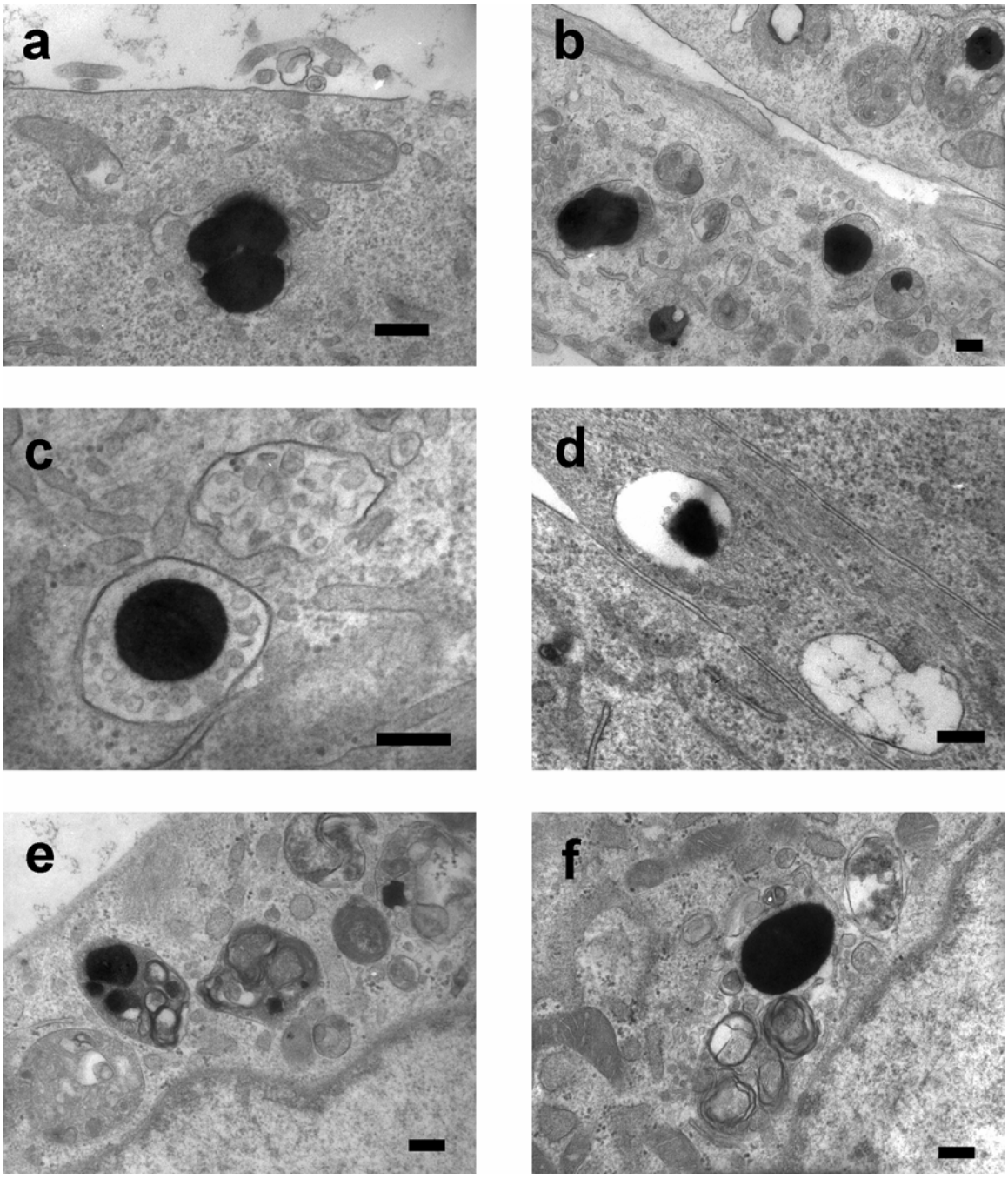

Figure 6.9 TEMs of CDPimid polyplexes
BHK-21 cells were exposed to CDPimid polyplexes and prepared for TEM imaging. As with CDP, intracellular CDPimid polyplexes appear as large aggregates within vesicles (a-b). The vesicles containing these aggregates do not necessarily conform to the aggregates' shape (b-d). Vesicles containing polyplex aggregates also appear to have a variety of other contents (b-c,e-i). Some aggregates have a fuzzy exterior (c-d,f) and not all aggregates are contained within vesicles (f). Bars for (a-f), 200 nm.

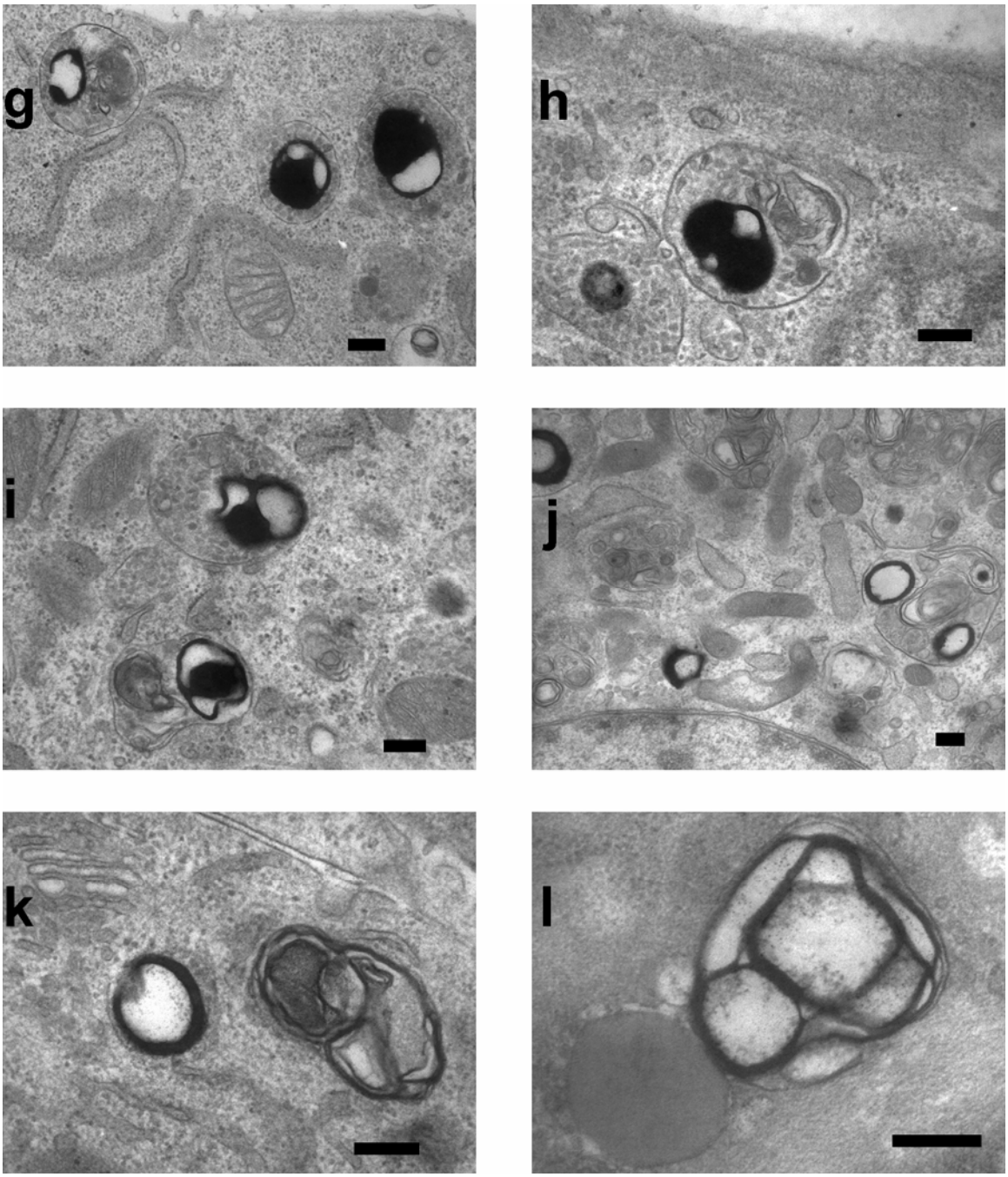

(*Figure 6.9, continued*) To a much greater extent than CDP polyplexes, CDPimid polyplexes appear to be degrading within vesicles. Various loops and swirls are observed emanating from the aggregates (g-i). In other cases, circular or oval ring structures or swirls are observed in the absence of larger aggregates, either contained within larger vesicles (g,j) or filling vesicles entirely (k-l). As with the aggregates, many of the loops, swirls, and rings appear fuzzy or hairy (g-l). Bars for (g-l), 200 nm.

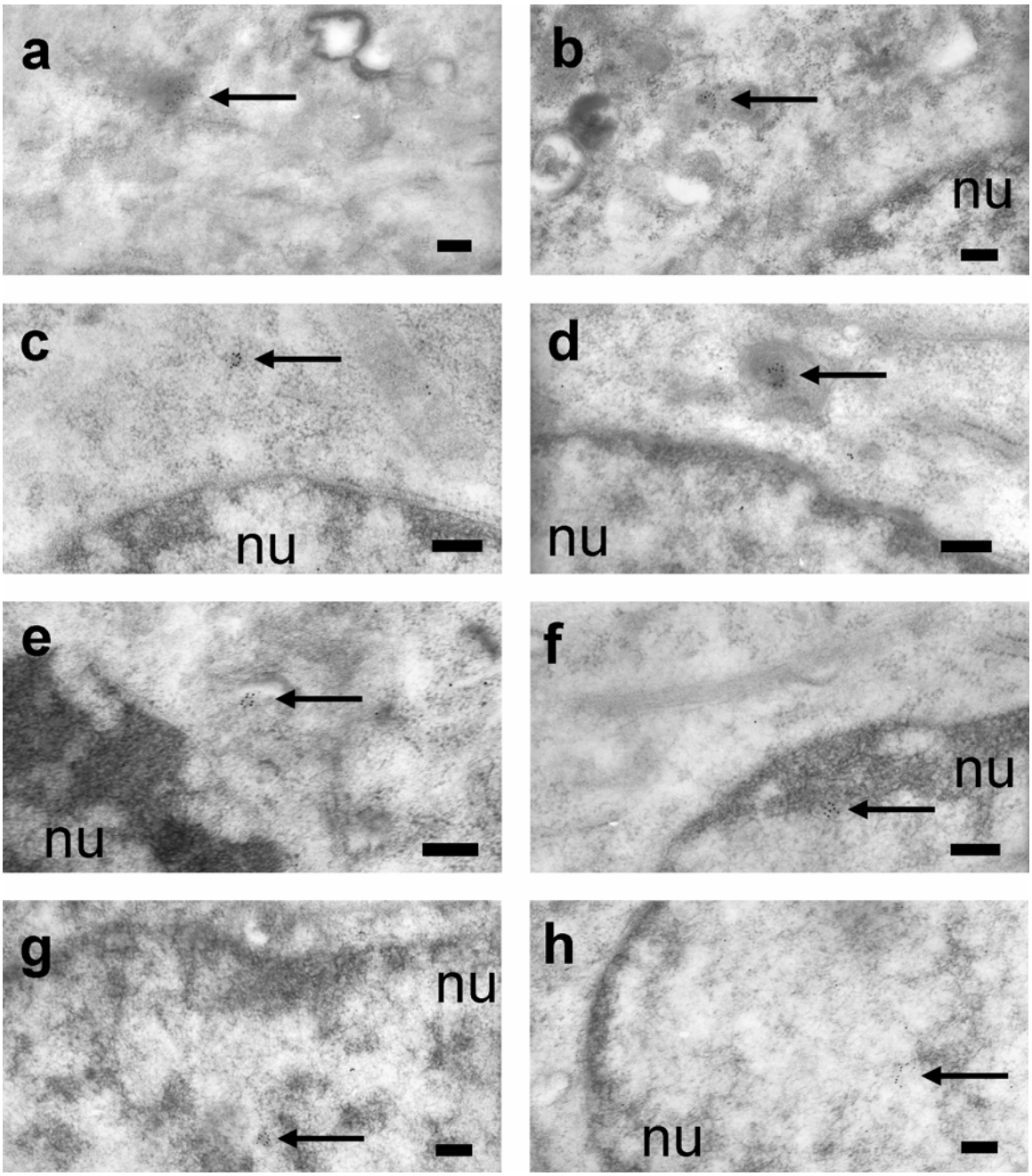

Figure 6.10 Immunolabeling to detect intracellular DNA delivered by CDP
Biotin-labeled pDNA was delivered to cells in CDP polyplexes, and TEM samples were prepared using anti-biotin immunolabeling with colloidal gold. Clusters of colloidal gold (arrows) can be found outside of polyplexes (c-h), an indication of unpackaged intracellular pDNA. Some of the intracellular gold clusters are within a cell nucleus (f-h). When CDP is used to transfect cells with unlabeled pDNA and samples are equivalently prepared and immunolabeled, there is no colloidal gold labeling of polyplexes or colloidal gold clustering (not shown). Bars, 200 nm. Cell nucleus, nu.

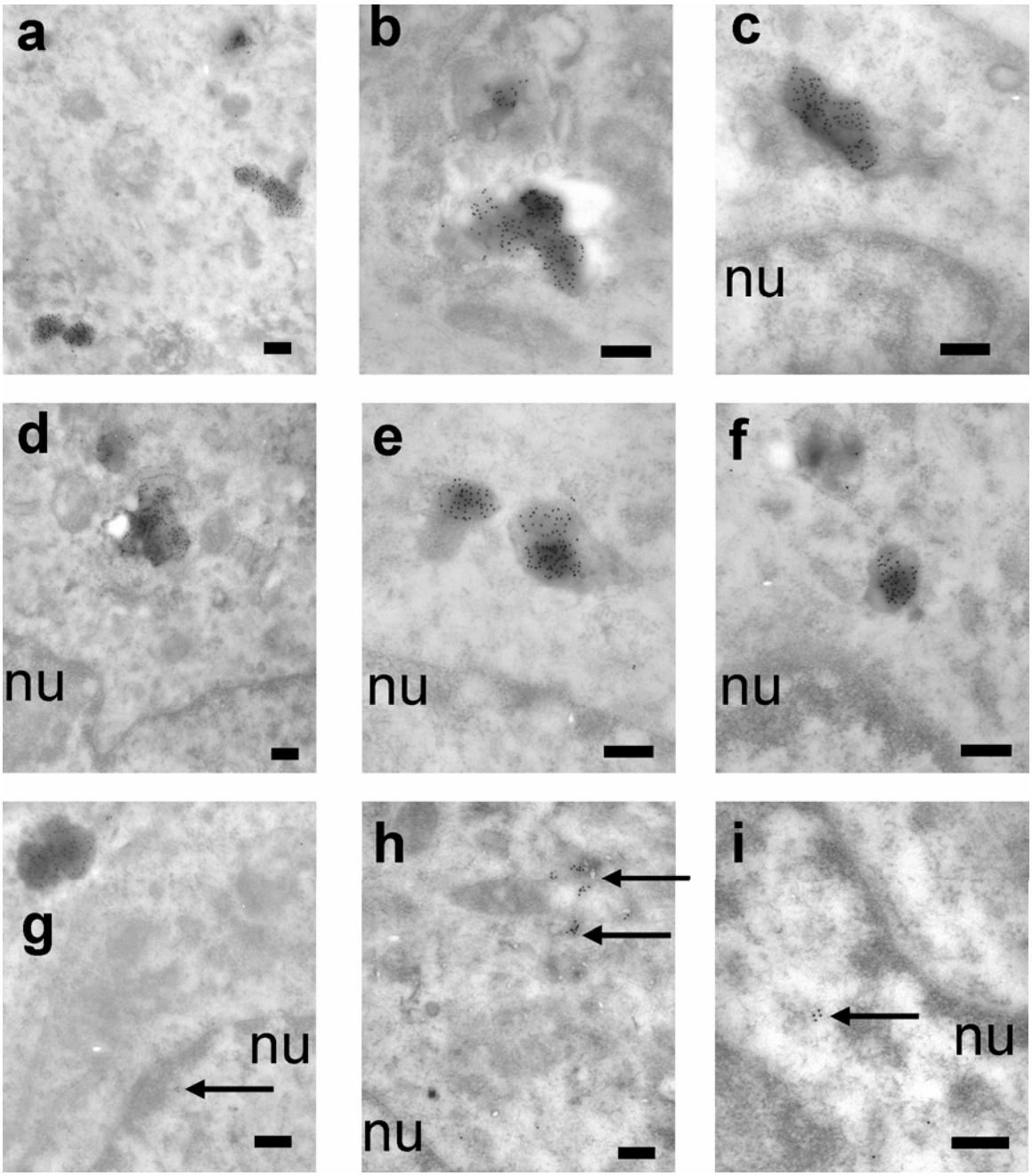

Figure 6.11 Immunolabeling to detect intracellular DNA delivered by CDPimid
Biotin-labeled pDNA was delivered to cells in CDPimid polyplexes, and TEM samples were prepared using anti-biotin immunolabeling with colloidal gold. Large, heavily gold-labeled entities (polyplexes or their aggregates) are readily observed (a-g), and the intensity of polyplex labeling (numbers of gold particles) for CDPimid polyplexes generally exceeds that observed with CDP. As with CDP polyplexes, clusters of colloidal gold (arrows) outside of polyplexes (h-i) reveal intracellular pDNA that has unpackaged from polyplexes. Such gold clusters are found in cytoplasm (h) or the cell nucleus (i). Bars, 200 nm. Cell nucleus, nu.

6.4.6 CDPimid produces more unpackaged intracellular DNA than CDP

The comet assay is a standard method of evaluating DNA damage [24,25]. In this assay, cells are gently lysed, embedded in an agarose gel on a glass slide or coverslip, and exposed to electrophoresis. Only damaged cellular DNA is reduced to a size that permits migration within the gel, and this damaged DNA will generate a characteristic "comet" pattern upon subsequent intra-gel labeling of nucleic acids by a fluorescent marker. The intensity of the comet reflects the extent of DNA damage. By this method, individual cells may be visually evaluated for DNA damage.

We have modified this assay to produce an aggregate separation and visualization of delivered and unpackaged nucleic acids. Rather than evaluating samples on an individual-cell basis, cells are collected by centrifugation, lysed, embedded in an agarose gel, and subjected to electrophoresis in order to generate a relative measure of DNA unpackaging for a particular sample. Also, rather than adding a fluorescent label after electrophoresis, we transfect cells using nucleic acids that have been covalently modified with a fluorescent marker. Thus, we are able to distinguish exogenous (delivered) nucleic acids from cellular DNA. The "unpackaged" oligonucleotide measured by this assay is that which migrates through the agarose gel to the same extent as in the case of direct gel loading of the oligonucleotide. Polyplexes suspended in 1X lysis buffer alone do not generate this migrating DNA, suggesting that the DNA unpackaging that allows for electrophoretic migration has occurred within cells.

As measured by this assay, CDPimid consistently generates greater amounts of unpackaged nucleic acids (Figures 6.12-6.14). This is true for a variety of timepoints ranging from 6 to 44 h after the initial transfection, and is true whether the polycations

are used to deliver a DNA oligonucleotide (Figures 6.12, 6.14) or siRNA (Figure 6.13). PEGylation of polyplexes does not alter this effect, as PEGylated CDPimid particles generate greater levels of migrating DNA than CDP polyplexes or their PEGylated variant (Figure 6.14). PEI was also examined in siRNA delivery and did not produce a signal representing unpackaged nucleic acid (Figure 6.13).

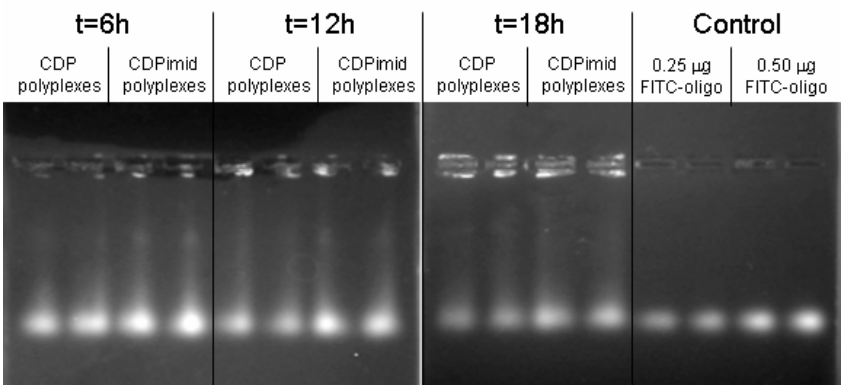

Figure 6.12 Unpackaging of DNA delivered to HeLa cells by CDP or CDPimid
CDP or CDPimid was used to transfect HeLa cells, which were evaluated after 6, 12, or 18 h for unpackaged, FITC-labeled DNA oligonucleotide. At all timepoints examined, CDPimid samples showed more unpackaged DNA than CDP samples.

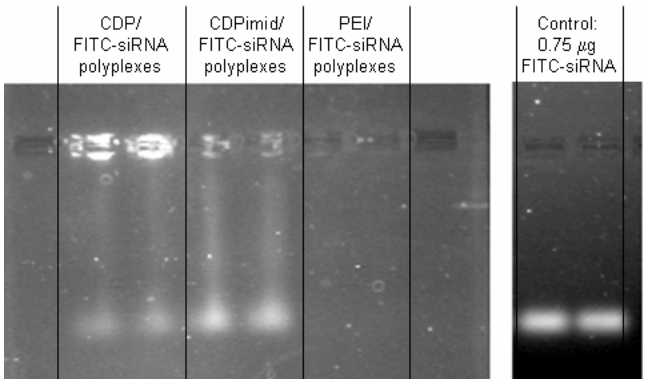

Figure 6.13 Unpackaging of siRNA delivered to HeLa cells by CDP, CDPimid, or PEI
CDP, CDPimid, or 25-kD branched polyethylenimine (PEI) was used to transfect HeLa cells, which were evaluated after 16 h for the levels of unpackaged, FITC-labeled siRNA. CDPimid samples showed more unpackaged nucleic acid than CDP samples. The PEI samples did not generate an unpackaged siRNA signal.

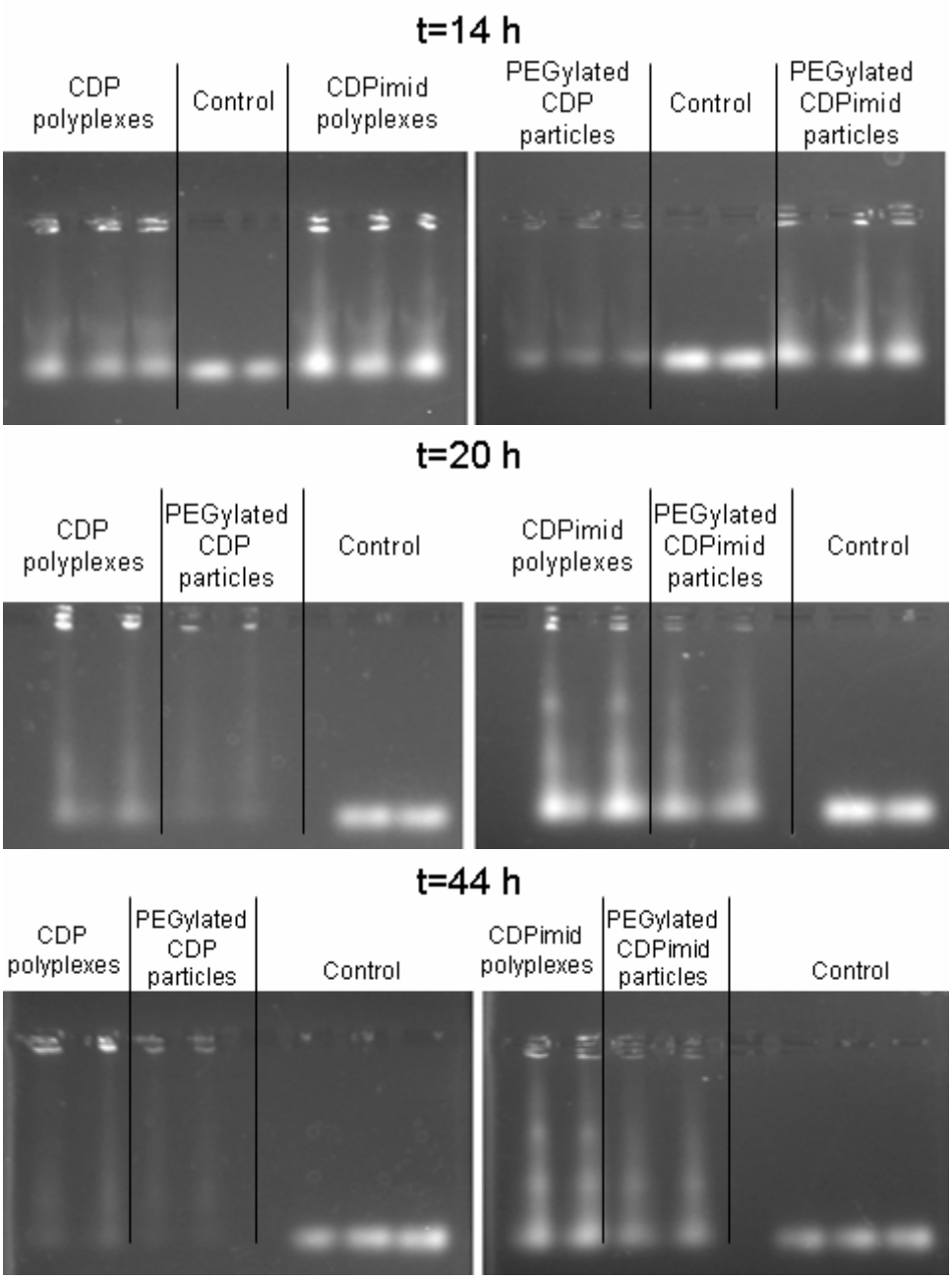

Figure 6.14 Unpackaging of DNA oligo delivered to HeLa cells by CDP or CDPimid or their PEGylated variants

CDP, CDPimid, or their PEGylated variants were used to transfect HeLa cells, which were evaluated after 14, 20, or 44 h for the levels of unpackaged, FITC-labeled DNA oligonucleotide. At all timepoints examined, the greatest amount of unpackaged DNA was seen with CDPimid samples, followed by samples transfected with PEGylated CDPimid particles. CDP and PEGylated CDP particles also show unpackaged DNA, but in lesser amounts.

6.4.7 Uptake of CDP and CDPimid polyplexes is similar but not equivalent

Rather than indicating differences in intracellular processing, differences in the amounts of unpackaged intracellular DNA with CDP and CDPimid could simply reflect differences in the total amount of DNA delivered to cells. Flow cytometry was used to evaluate the cellular uptake and retention of a FITC-labeled DNA oligo delivered to HeLa cells with CDP or CDPimid polyplexes or with their PEGylated variants (Table 6.1). All particles showed strong uptake to cells, with over 98% of cells registering positive at both examined timepoints. CDPimid samples generated greater fluorescence than CDP samples. However, CDPimid buffers the pH experienced by delivered nucleic acids whereas CDP does not (Figure 6.3), irrespective of PEGylation [16], and the fluorescence of FITC is quenched at lower pH. Thus, the observed differences in the flow cytometry data do not necessarily represent enhanced uptake with CDPimid.

Nucleic acid	Delivery vector	20 h		44 h	
		% cells FITC-positive	Mean fluorescence	% cells FITC-positive	Mean fluorescence
-	-	0.50	3.41	0.05	2.83
FITC-oligo	CDP	99.33	3109.80	99.11	1291.04
FITC-oligo	CDP+Ad-PEG	99.56	1398.83	98.12	579.79
FITC-oligo	CDPimid	99.67	6920.65	99.41	4465.41
FITC-oligo	CDPimid+Ad-PEG	99.79	6770.88	99.87	3829.96

Table 6.1 Summary of flow cytometry analysis
A FITC-labeled oligonucleotide (FITC-oligo) was used to formulate CDP, PEGylated CDP, CDPimid, or PEGylated CDPimid particles. HeLa cells were transfected with the particles and evaluated after 20 h or 44 h for FITC fluorescence by flow cytometry. All types of particles gave rise to strong fluorescence at the timepoints examined, although CDP particles did not generate as much fluorescence as CDPimid particles. Data represent the mean of duplicate samples.

6.4.8 CDP and CDPimid transfection are not equally affected by chloroquine analogues

HeLa cells were transfected with CDP/pDNA or CDPimid/pDNA polyplexes in the presence or absence of selected analogues of chloroquine (CQ). The trends in the expression levels were consistent in that CQ and (to a greater extent) CQ7a conferred marked improvements in transfection efficiency, while CQO and CP were not as beneficial (Figure 6.15). However, improvements in transfection efficiency with CQ and CQ7a were noticeably greater for CDP polyplexes than for CDPimid polyplexes, and strong effects with CDPimid were seen only with 0.2 mM CQ or CQ7a.

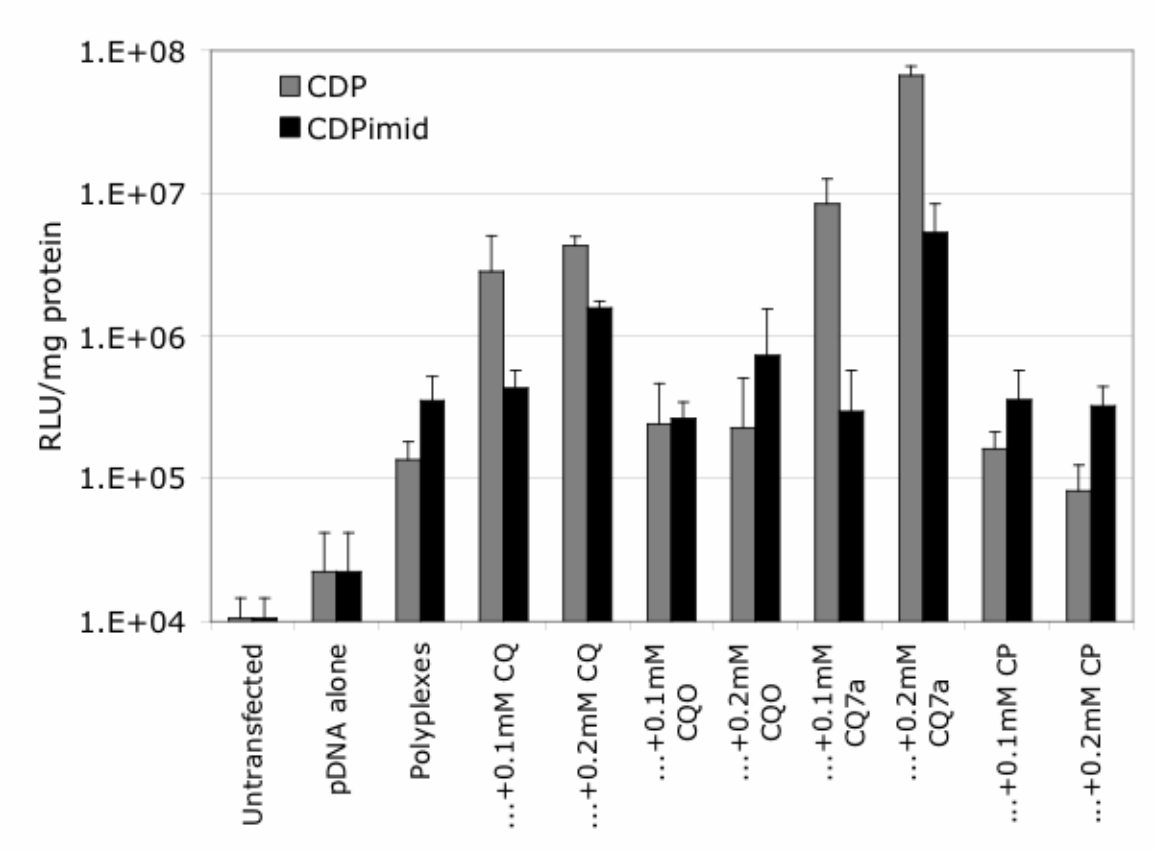

Figure 6.15 Effect of chloroquine analogues on transfection by CDP and CDPimid
HeLa cells were transfected with CDP or CDPimid polyplexes in the presence of various analogues of chloroquine (CQ). Luciferase activity was used as a measure of transfection efficiency. CQ and CQ7a gave the greatest increases in transfection efficiency, and such increases were greater with CDP polyplexes than with CDPimid polyplexes.

6.4.9 Dye exclusion with CDP and CDPimid polyplexes is similarly affected by chloroquine analogues

While CQ and CQ7a contribute significantly to the transfection efficiency of both CDP and CDPimid, greater enhancements in the case of CDP raise CDP-mediated expression to levels beyond CDPimid-mediated expression in the presence of CQ and CQ7a. Dye exclusion was used to compare the relative accessibility to chloroquine analogues of DNA in CDP and CDPimid polyplexes (Figure 6.16). As-formulated CDP and CDPimid polyplexes do not exhibit full exclusion of the DNA intercalating dye PicoGreen, but increasing concentrations of strong DNA-binding chloroquine analogues can restrict this access and generate increased dye exclusion. Here, trends in dye exclusion were similar for each polyplex type, reflecting similar accessibility of DNA to chloroquine analogues.

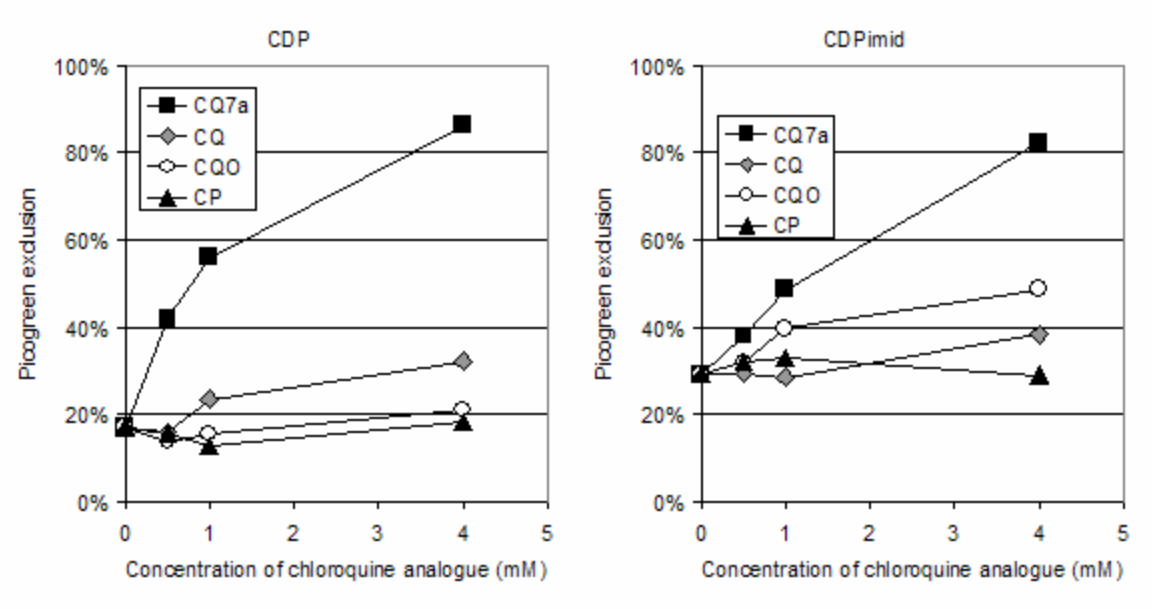

Figure 6.16 Polyplex exclusion of PicoGreen in the presence of chloroquine analogues
The exclusion of the DNA-intercalating dye PicoGreen was used to indicate the relative accessibility of pDNA in CDP or CDPimid polyplexes to chloroquine analogues.

6.5 Discussion

Modification of CDP with terminal imidazole groups successfully introduces intracellular pH-buffering activity to this non-viral gene delivery vector (Figure 6.3). The new polycation, CDPimid, displays improved transfection efficiency in a variety of cultured cell lines (Figure 6.2). It is found that CDP and CDPimid give similarly strong DNA uptake (Table 6.1) and that CDPimid also gives improved performance in cells with a cytoplasmic expression system (Figure 6.2), indicating that the improvements in transfection efficiency with CDPimid result from phenomena within cells but prior to delivery to the cell nucleus. These results are consistent with the hypothesis that the improved performance of the pH-buffering CDPimid results from enhanced escape from endocytic vesicles.

CDP has a relatively low degree of polymerization (~6), such that end-group modification may affect its chemical and biological properties and the properties of its polyplexes. Direct quantification of the polycation-DNA binding strength for CDP and CDPimid by isothermal titration calorimetry is not possible due to the nature of the polycations' amidine charge centers. Thus, indirect methods are applied to evaluate the relative binding strength of these two vectors with nucleic acids. In cell-free assays, CDP appears bound more weakly to nucleic acids than CDPimid. CDP polyplexes display weaker dye exclusion than CDPimid polyplexes (Figure 6.4) and are more susceptible to induction of DNA release by heparan sulfate (Figures 6.6, 6.7).

Despite these observations, CDPimid appears to facilitate greater intracellular release of delivered nucleic acids than CDP. CDP polyplexes within cells generally appear in transmission electron microscopy (TEM) as large, well-defined aggregates that

grow larger (due to collection or aggregation of existing aggregates) over the initial 24 hours after transfection (Figure 6.8). In contrast, extensive unraveling and disassembly of intracellular CDPimid polyplexes is observed only 4 or 8 hours after initial transfection (Figure 6.9). Immunolabeling of delivered DNA shows that CDP and CDPimid both produce unpackaged DNA, but the intensity with which CDPimid polyplexes are labeled (under equivalent conditions) suggests that the DNA within these polyplexes may be more accessible than that of CDP polyplexes (Figure 6.10-6.11). Further, a novel modification of the comet assay shows that CDPimid generates greater amounts of unpackaged nucleic acids than CDP, irrespective of the polyplexes' PEGylation (Figures 6.12-6.14).

The mechanism behind the enhanced intracellular unpackaging observed with CDPimid is unclear. Dye exclusion indicates that the terminal imidazole groups do not inhibit polycation-DNA interactions (Figure 6.4). Polyplexes may undergo changes in the binding between polycation and nucleic acid as they traffic in the endocytic pathway, particularly as the imidazole groups carry out their pH-buffering function and become protonated. The observed disassembly of CDPimid polyplexes in intracellular vesicles would support this hypothesis. Although no changes in DNA release were observed for polyplexes acidified prior to heparan sulfate treatment (Figure 6.7b), immersion in the electrophoresis buffer would mask differences if the DNA release with heparan sulfate is reversible. Efforts to conduct the gel electrophoresis at acidified pH were not successful.

As implied by the experiments with heparan sulfate, intracellular factors may be responsible for polyplex disassembly. If so, the response of CDP and CDPimid polyplexes to heparan sulfate treatment may not reflect their susceptibility to the relevant

intracellular factors. A further possibility is that differences in the intracellular distribution of polyplexes and polyplex-disrupting factors are related to the differences in unpackaging. If the pH-buffering of CDPimid facilitates its escape from the endocytic pathway and polyplex disruption occurs primarily in the cytoplasm, CDPimid should generate more unpackaged DNA. This hypothesis is undermined by numerous TEM observations of CDPimid polyplexes disassembling within intracellular vesicles.

Additional information on the intracellular behavior of CDP and CDPimid polyplexes arises from their differing responses to treatment with chloroquine analogues. Chloroquine (CQ) and (to a greater extent) its analogue CQ7a contribute significantly to the transfection efficiency of non-viral vectors, although they show stronger effects on CDP than on CDPimid (Figure 6.15). The enhancements likely result from the ability of CQ and CQ7a to facilitate unpackaging of delivered DNA, buffer the pH of the endocytic pathway, and bind to unpackaged DNA within cells (see Chapter 5).

CDPimid, CQ, and CQ7a independently display similar intracellular pH-buffering activity [16], so it is likely that CQ and CQ7a contribute to transfection efficiency of CDPimid by improving unpackaging and/or by binding the released DNA. In this case, it is not immediately clear why the transfection efficiency of CDP would surpass that of CDPimid in the presence of CQ or CQ7a. CDP polyplexes with CQ, CDP polyplexes with CQ7a, or CDPimid polyplexes (with or without CQ or CQ7a) should be similarly pH-buffered. CDPimid produces more unpackaged intracellular DNA than CDP, and CQ or CQ7a would not necessarily reverse this situation (such that CDP polyplexes with CQ or CQ7a give greater unpackaging than CDPimid polyplexes with CQ or CQ7a).

One possibility is that CQ gives greater displacement and is better able to bind unpackaged DNA with CDP than with CDPimid due to the spatiotemporal intracellular distribution of CQ and of the polyplexes. Protonation of CQ is believed to drive its accumulation in endocytic vesicles [26], where it can interact with endocytosed polyplexes. CQ-mediated polyplex disruption and CQ binding of unpackaged nucleic acids may very well occur within these vesicles. If the pH-buffering by CDPimid limits the supply of protons necessary to drive accumulation of CQ in endocytic vesicles, or if CDPimid polyplexes more readily escape the endocytic pathway and release their DNA cargo, there may be reduced opportunity for interactions between CQ and the polyplexes and/or between CQ and the delivered DNA. Thus, CQ (and also CQ7a) would not produce the same enhancements in transfection efficiency with CDPimid that are observed with CDP.

In conclusion, we have used a range of methods to investigate differences in the gene delivery behavior of CDP and its imidazole-terminated variant, CDPimid. As hypothesized, the imidazole modification of CDP confers intracellular pH-buffering activity that is correlated with an increase in transfection efficiency. The pH-buffering activity is hypothesized to facilitate escape from the endocytic pathway. It was also observed that CDPimid generates greater amounts of unpackaged intracellular nucleic acids than CDP, making the mechanism of CDPimid's increased transfection efficiency less clear. The increased unpackaged intracellular DNA with CDPimid was not consistent with measures indicating that CDPimid binds nucleic acids more strongly than CDP, emphasizing the need to evaluate the behavior of non-viral gene delivery vectors in their functional environments. The characterization of gene delivery behavior with CDP

and CDPimid reinforces the notion that non-viral gene delivery involves complex systems, where simple modifications can have unanticipated consequences.

6.6 Acknowledgment

I am grateful to Patrick Midoux for kindly supplying the 293-T7 cells and the plasmid pT7-Luc, to Rajan Kulkarni for carrying out the measures of intracellular pH-buffering activity, and to Ryan Zeidan for synthesizing the chloroquine analogues used in this study.

6.7 References

1. Bieber T, Meissner W, Kostin S, Niemann A, Elsasser HP. (2002) Intracellular route and transcriptional competence of polyethylenimine-DNA complexes. J. Control. Release 82:441-454.
2. Remy-Kristensen A, Clamme JP, Vuilleumier C, Kuhry JG, Mely Y (2001) Role of endocytosis in the transfection of L929 fibroblasts by polyethylenimine/DNA complexes. Biochim. Biophys. Acta 1514:21-32.
3. Hwang SJ, Davis ME (2001) Cationic polymers for gene delivery: designs for overcoming barriers to systemic administration. Curr. Opin. Mol. Ther. 3:183-191.
4. Forrest ML, Pack DW (2002) On the kinetics of polyplex endocytic trafficking: implications for gene delivery vector design. Mol. Ther. 6:57-66.
5. Sonawane ND, Szoka FC, Verkman AS (2003) Chloride accumulation and swelling in endosomes enhances DNA transfer by polyamine-DNA polyplexes. J. Biol. Chem. 278:44826-44831.
6. Akinc A, Lynn DM, Anderson DG, Langer R (2003) Parallel synthesis and biophysical characterization of a degradable polymer library for gene delivery. J. Am. Chem. Soc. 125:5316-5323.
7. Funhoff AM, van Nostrum CF, Koning GA, Schuurmans-Nieuwenbroek NM, Crommelin DJ, Hennink WE (2004) Endosomal escape of polymeric gene delivery complexes is not always enhanced by polymers buffering at low pH. Biomacromolecules 5:32-39.
8. Choi JS, MacKay JA, Szoka FC (2003) Low-pH-sensitive PEG-stabilized plasmid-lipid nanoparticles: preparation and characterization. Bioconjug. Chem. 14:420-429.
9. Behr JP (1997) The proton sponge: A trick to enter cells the viruses did not exploit. Chimia 51:34-36.

10. Gonzalez H, Hwang SJ, Davis ME (1999) New class of polymers for the delivery of macromolecular therapeutics. Bioconjug. Chem. 10:1068-1074.
11. Midoux P, Monsigny M (1999) Efficient gene transfer by histidylated polylysine/pDNA complexes. Bioconjug. Chem. 10:406-11.
12. Davis ME, Pun SH, Bellocq NC, Reineke TM, Popielarski SR, Mishra S, Heidel JD (2004) Self-assembling nucleic acid delivery vehicles via linear, water-soluble, cyclodextrin-containing polymers. Curr. Med. Chem. 11:179-97.
13. Midoux P, LeCam E, Coulaud D, Delain E, Pichon C (2002) Histidine containing peptides and polypeptides as nucleic acid vectors. Somat. Cell. Mol. Genet. 27:27-47.
14. Singh RS, Goncalves C, Sandrin P, Pichon C, Midoux P, Chaudhuri A (2004) On the gene delivery efficacies of pH-sensitive cationic lipids via endosomal protonation: a chemical biology investigation. Chem. Biol. 11:713-23.
15. Fukushima S, Miyata K, Nishiyama N, Kanayama N, Yamasaki Y, Kataoka K (2005) PEGylated polyplex micelles from triblock catiomers with spatially ordered layering of condensed pDNA and buffering units for enhanced intracellular gene delivery. J Am Chem Soc. 127:2810-1.
16. Kulkarni RP, Mishra S, Fraser SE, Davis ME (2005) Single cell kinetics of intracellular, nonviral, nucleic acid delivery vehicle acidification and trafficking. Bioconjug. Chem. 16:986.
17. Forrest ML, Meister GE, Koerber JT, Pack DW (2004) Partial acetylation of polyethylenimine enhances in vitro gene delivery. Pharm. Res. 21:365.
18. Dubruel P, Christiaens B, Rosseneu M, Vandekerckhove J, Grooten J, Goossens V, Schacht E (2004) Buffering properties of cationic polymethacrylates are not the only key to successful gene delivery. Biomacromolecules 5:379.
19. Funhoff AM, van Nostrum CF, Koning GA, Schuurmans-Nieuwenbroek NME, Crommelin DJA, Hennink WE (2004) Endosomal escape of polymeric gene delivery complexes is not always enhanced by polymers buffering at low pH. Biomacromolecules 5:32.
20. Pun SH, Davis ME (2002) Development of a nonviral gene delivery vehicle for systemic application. Bioconjug. Chem. 13:630-639.
21. Ogris M, Steinlein P, Kursa M, Mechtler K, Kircheis R, Wagner E (1998): The size of DNA/transferrin-PEI complexes is an important factor for gene expression in cultured cells. Gene Therapy 5:1425-1433.
22. Brisson M, Tseng WC, Almonte C, Watkins S, Huang L (1999) Subcellular trafficking of the cytoplasmic expression system. Hum Gene Ther. 10:2601-13.
23. Akinc A, Thomas M, Klibanov AM, Langer R (2005) Exploring polyethylenimine-mediated DNA transfection and the proton sponge hypothesis. J. Gene Med. 7:657–63.
24. Ostling O, Johanson KJ (1984) Microelectrophoretic study of radiation-induced DNA damages in individual mammalian cells. Biochem. Biophys. Res. Comm.
25. Singh NP, McCoy M, Tice RR, Schneider E (1988) A simple technique for quantitation of low levels of DNA damage in single cells. Exp. Cell Res. 175:184-91.
26. Poole B, Ohkuma S (1981) Effect of weak bases on the intralysosomal pH in mouse peritoneal macrophages. J. Cell Biol. 90:665-9.

CHAPTER 7: DESIGN OF NON-VIRAL GENE DELIVERY VECTORS TO OVERCOME INTRACELLULAR BARRIERS

7.1 Introduction

The intracellular barriers to efficient, non-viral gene delivery include aspects of trafficking within and escape from the endocytic pathway, unpackaging of nucleic acids from the delivery vector, mobility and persistence within cytoplasm, and delivery to the cell nucleus. By exploiting the synthetic nature of molecular conjugates, many chemical modifications have been made in an effort to address these perceived barriers. Examples include enhancement of endosomal escape with buffering components, of vector unpackaging with selectively labile vectors, of nuclease resistance with modified nucleic acids, and of nuclear delivery using targeting sequences. One area that has not been effectively addressed is the poor cytoplasmic mobility of cationic polymer-nucleic acid complexes (polyplexes) and of larger unpackaged nucleic acids. This chapter reviews recent literature on the intracellular delivery of nucleic acids by non-viral systems.

7.2 Trafficking within and escape from endocytic vesicles

A net positive surface charge facilitates facile entry of polycation-nucleic acid particles to cultured cells. Electron microscopy has been used to visualize the apparent endocytosis of pDNA complexed with cationic lipids [1] or with cationic polymers [2]. Both reports show images of gene delivery particles contained within invaginations of the cell membrane. Using polylysine-pDNA complexes, Mislick and Baldeschwieler demonstrated that this uptake occurs through binding of cationic particles to anionic cell-

surface proteoglycans [3]. The recent model of Kopatz et al. further implicates syndecans, a class of proteoglycans common to adherent cells [4]. Noting that pathogens are able to divert syndecan binding to enter cells, this model suggests that the clustering of syndecan molecules on the cell surface and their intracellular binding of actin can induce particle engulfment and cell entry. Goncalves and coworkers recently suggested that transfection efficiency is greatest when the means of uptake is clathrin-dependent endocytosis [5]; this mode of entry places limits on particle size to about 200 nm [6].

Active in all cells, nonspecific uptake through binding of proteoglycans is not useful for targeted delivery in mammals. Particles for in vivo gene delivery should incorporate ligands to target specific cell types and allow particles to enter cells through receptor-mediated endocytosis. Following uptake, the particles are delivered to the endocytic pathway. For many delivery vectors, cells transfected with fluorescently-labeled polycations and/or nucleic acids display punctate cytoplasmic staining indicative of sequestration in the endocytic pathway. Using transmission electron microscopy of cells transfected in vitro, we have observed vesicles containing intracellular polyplexes and their aggregates [2]. Vesicles of the endocytic pathway undergo active transport along intracellular microtubules. Consistent with the hypothesis of polyplex entrapment by these vesicles, Suh et al. have shown that the movement of polyethylenimine (PEI)-plasmid DNA (pDNA) complexes within cells includes an active mode that can be impaired by depolymerization of microtubules [7].

The vesicles comprising the endocytic pathway become progressively more acidic as endocytosed materials proceed towards lysosomes. There is strong evidence that endocytosed polyplexes experience this reduction in pH as they move through the

endocytic pathway. Multiple researchers have used changes in fluorescence or used confocal or electron microscopy to show polyplex components in acidic and/or endocytic compartments [2,5,8-11]. Two groups have used bulk ratiometric fluorescence assays to quanitify the acidification experienced by intracellular polyplexes. By conjugating both a pH-sensitive and a pH-insensitive label to pDNA [12] or to polycationic delivery vectors [13], these investigators were able to calculate the average pH environment of intracellular complexes made with PEI or polylysine and to show that these pH values are reduced over time. More recently, we have used a single pH-sensitive fluorophore to explored the range of pH values experienced by intracellular nucleic acids as a function of time and delivery vector [14].

These studies collectively show that many types of polyplexes proceed through the endocytic pathway and accumulate in the perinuclear region in lysosomes, where nucleases and other degradative enzymes present an undesirable environment for the delivered nucleic acids. It has been generally assumed that avoidance of lysosomes can give rise to improved gene delivery with polyplexes. This hypothesis has been supported in part by enhancements in reporter gene expression observed for transfections of many types of polyplexes in the presence of the endosomotropic agent chloroquine [15-19].

The influenza virus exploits the increasingly acidic pH of endocytic vesicles to trigger reorganization of its hemagglutinin protein and escape from the endocytic pathway. In an effort to engineer endosomal escape in non-viral gene delivery by a similar method, Kyriakides et al. developed pH-sensitive membrane-disrupting polymers [20]. Observing the strong in vitro hemolytic performance of poly(propylacrylic acid) at pH values less than 6.5, these investigators incorporated the polymer in non-viral

formulations and measured increases in reporter gene expression both in vitro and in vivo.

PEI (polyethylenimine) is one delivery vector that gives high transfection efficiencies that are unaffected by the presence of chloroquine. This observation gave rise to the "proton sponge" hypothesis, wherein PEI is naturally endosomotropic due to its numerous amine residues with pK_a values in the physiological range [21]. In this hypothesis, the amine residues of PEI are able to buffer the acidification of the endosome, thereby impeding its progression on the endocytic pathway and/or facilitating its rupture. Kichler et al. demonstrated that acidification plays a role in PEI-mediated transfection in vitro; inhibition of endosome acidification with bafilomycin A1 led to a sharp drop in reporter gene expression [22]. Akinc et al. showed that N-quaternized (and therefore non-buffering) derivatives of PEI are inferior delivery vectors [23]. The "proton sponge" hypothesis is also supported by the recent results of Sonawane and coworkers, who observed that, relative to poorly-buffering polylysine-pDNA complexes, polyplexes prepared with strongly-buffering PEI or polyamidoamine gave reduced acidification, increased swelling, improved buffering capacity, and heightened osmotic fragility of endosomes [24].

The aforementioned ratiometric fluorescence assays, however, did not fully support the "proton sponge" hypothesis for PEI. In the experiments utilizing labeled nucleic acids, PEI showed apparent buffering relative to polylysine [12, 14]; for the case of dual-labeled delivery vectors, however, the apparent buffering with PEI was restricted to only one of the three cell lines examined [13]. It was also shown recently that acetylation of PEI improved its transfection efficiency despite a concomitant reduction in

buffering capacity [25]. We have observed intact polyplexes in cytoplasm with both PEI and a non-buffering β-cyclodextrin-containing polymer, demonstrating that a buffering delivery vector is not a necessary requirement for endosomal escape of intact polyplexes [2]. Dubruel et al. have found that polymethacrylates with buffering capacity similar to polyethylenimine generate far inferior transfection, attributing this to inferior endosomal escape [26]. Funhoff et al. questioned the general applicability of the "proton sponge" hypothesis upon observing poor transfection efficiency of a new polymer with a pK_a that should supply buffering capacity [27]. Erbacher et al. further showed that chloroquine can dissociate polycations from pDNA [15]; along with preceding chapters of this report, these results suggest that vector displacement is another means by which chloroquine enhances transfection efficiency in vitro.

Despite questions about the "proton sponge" hypothesis, buffering moieties have been added to many vectors in an effort to mimic the purported endosomotropic activity of chloroquine and PEI. One such moiety is histidine, a natural amino acid whose side chain becomes protonated at pH ~6. Midoux et al. prepared a histidine-substituted polylysine that generated much greater in vitro reporter gene expression than unmodified-polylysine transfection and even unmodified-polylysine transfection in conjunction with chloroquine treatment [28]. Transfection efficiency in vitro was markedly improved with a low extent of histidine substitution and continued to improve slightly with additional histidine substitution. As with PEI-pDNA transfection, reporter gene expression in an in vitro histidylated polylysine-pDNA transfection was reduced when endosome acidification was inhibited with bafilomycin A1. While Midoux et al. used histidine substitution throughout the polylysine backbone, Davis et al. pursued an alternate

strategy of histidine substitution only at the termini of a β-cyclodextrin containing polymer [29]. Davis et al. observed that histidine substitution produced increases in in vitro reporter gene expression for the same level of pDNA delivery to cells, supporting the hypothesis that buffering moieties somehow contribute to the defeat of intracellular barriers.

Rather than applying direct histidine conjugation, some researchers have pursued buffering through incorporation of polyhistidine. Pack et al. found that the transfection efficiency of ternary complexes of pDNA, polylysine, and glycosylated polyhistidine was not significantly improved relative to simple pDNA-polylysine complexes [30]. Noting that polyhistidine had been shown to have fusogenic properties at mildly acidic pH [31], Benns and coworkers prepared a polyhistidine-graft-polylysine copolymer as a gene delivery vector. The β-galactosidase expression resulting from transfection with the copolymer was superior to that of simple polylysine [32]. The purported fusogenic contribution was limited, however, as chloroquine treatment produced further increases in transfection efficiency for both the copolymer and umodified polylysine. Although the importance of buffering thus remains in question relative to factors such as vector displacement, it is likely that buffering components offer contributions to enhanced gene delivery.

The engineering of endosomal escape processes with molecular conjugates should account for both the nature and morphology of the intravesicular polyplexes. We have used transmission electron microscopy to show that unmodified polycation-pDNA complexes enter cells as large aggregates of 3-5 times the as-formulated diameter [2]. Still-larger aggregates were observed as aggregate-containing vesicles appeared closer to

the nucleus. The membranes of these vesicles conformed to the contorted, bulbous shape of the aggregates therein. When PEI-pDNA complexes were coated with polyethylene glycol (PEG) to confer extracellular salt stability, the particles' intracellular morphology was also seen to be affected. Intracellular PEGylated particles were observed as discrete entities contained in smooth, circular vesicles, and the particles retained their as-formulated size (Fig. 7.1). The observation of unmodified polyplexes as large aggregates in intracellular vesicles may be related to the superior transfection efficiency seen with those polyplexes relative to their PEGylated variants. Only a slight swelling of the large aggregates could lead to vesicle rupture, while such is not the case with the PEGylated particles. Further studies will be needed to address these issues.

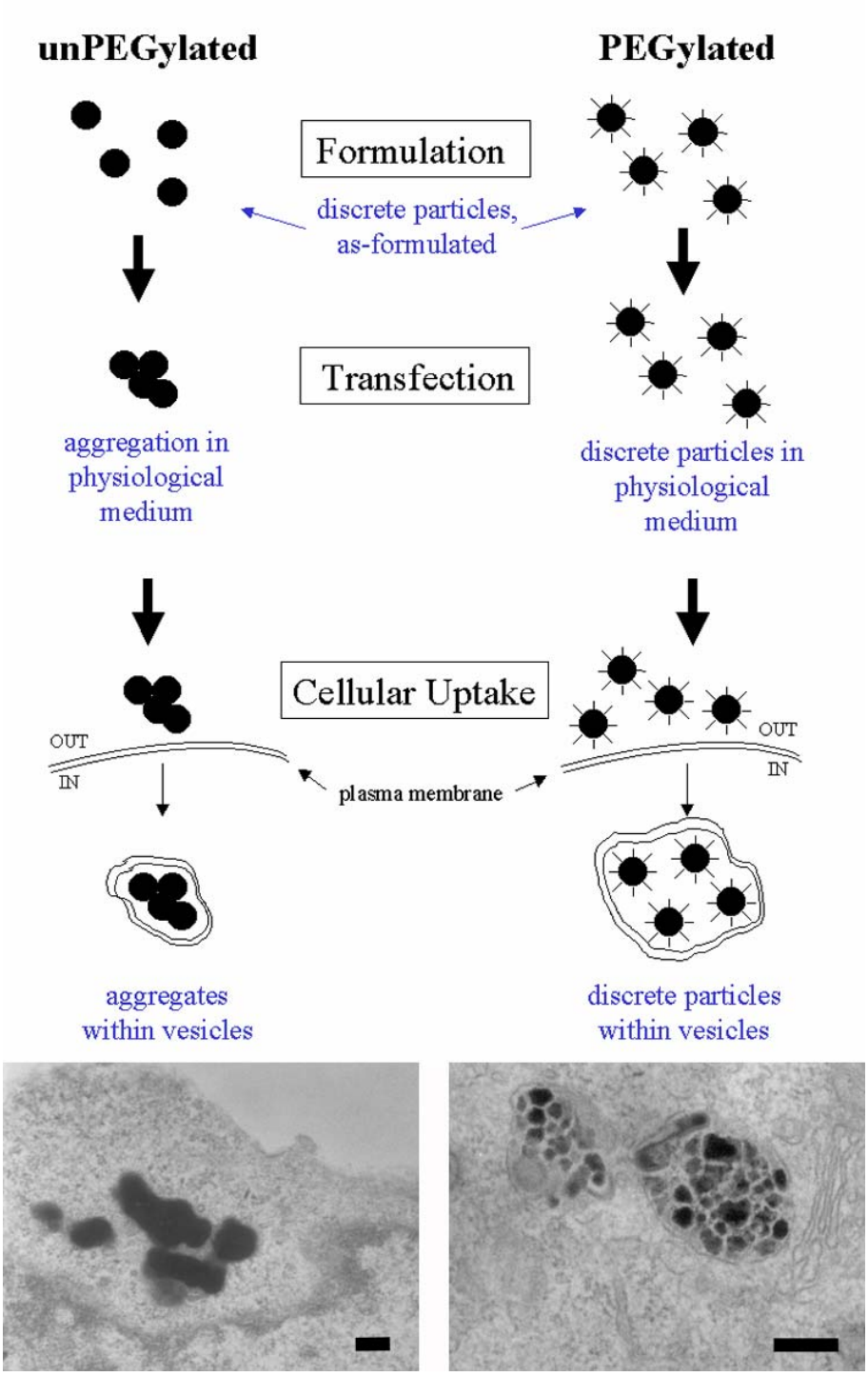

Figure 7.1 Stabilization of polyplexes affects uptake and trafficking
Unstabilized complexes aggregate in the transfection medium; these enter cells and traffic through them as large clumps. In contrast, PEGylation of non-viral complexes allows for uptake of discrete entities that remain distinct throughout the endocytic pathway. The intracellular complexes can be observed in the transmission electron microscope. Scale bars, 200 nm.

7.3 Vector unpackaging

The unpackaging of nucleic acids from delivery vectors is essential to the gene delivery process. Nucleic acids function through interactions with cellular components such as proteins and other nucleic acids, and these cellular components may remain inaccessible to nucleic acids that remain bound to delivery vectors. Reduced transcriptional activity has been observed for pDNA bound to cationic dendrimers [33] or to polylysine [34]. Prolonged binding of pDNA and more severe inhibition of its transcriptional activity are together correlated to an increase in polylysine length [34]. Koping-Hoggard et al. used chitosan to demonstrate a correlation between ease of polyplex dissociation and increases in transfection efficiency [35]. As described above, our results and those of Erbacher et al. [15] indicate that the endosomotropic agent chloroquine produces enhancements in transfection efficiency in vitro in part by dissociating the polycations from pDNA in the delivered polyplexes.

A proposed mechanism for vector unpackaging is displacement of nucleic acids by intracellular polyanions. The kinetics and ease of this unpackaging are related to the chemical structure of the delivery vector. A series of β-cyclodextrin-containing polymers prepared by Hwang et al. demonstrated a clear relationship between the polymer-pDNA binding strength and the number of methylene units separating charge centers on the polymer [36]. Itaka et al. observed that linear and branched PEI are displaced from pDNA with similar kinetics, but showed using fluorescence resonance energy transfer (FRET) that, in cells, linear PEI is displaced from pDNA far more readily than the branched variant [10]. Based on these studies, it is unlikely that polycations and/or lipid delivery systems that bind nucleic acids with sufficient strength to afford stability in vivo

will spontaneously release the nucleic acid to any great extent once inside cells. Thus, these systems should be designed so that the transition from extracellular to intracellular compartments triggers a reduction in the binding strength of the delivery vector.

Degradable delivery vectors have been designed in an effort to facilitate vector unpackaging. Various researchers have sought to construct vectors that will fall apart within cells and render the polyplexes unstable. Unfortunately, the optimal kinetics and intracellular location of this degradation are unknown, and it is difficult to predict where and how quickly a new vector will exhibit degradation. For example, Forrest et al. prepared highly cross-linked mimics of 25-kDa branched PEI by reacting 800-Da PEI with short, linear diacrylates [37]. The resulting conjugates were sensitive to hydrolysis at both near-neutral and mildly acidic pH. An intercalating-dye exclusion assay, however, showed that polyplexes produced with these conjugates did not exhibit pDNA release in vitro even after 24 h in hydrolyzing conditions. The increasingly acidic pH of endocytic vesicles can also be exploited to induce vector unpackaging. Choi et al. demonstrated that polycation-pDNA particles could be prepared with an acid-labile lipid at pH 8.5 and would rapidly degrade at pH 5.3 [38]. The pH-sensitive lipid-pDNA particles showed sharp increases in transfection efficiency relative to similar, pH-insensitive particles.

Other designs have sought to exploit the reducing environment found within cells. In an effort to provide extracellular particle stabilization that would be discarded after cellular uptake, Carlisle et al. coated PEI-pDNA polyplexes with poly[*N*-(2-hydroxypropyl)methacrylamide] through a reducible disulfide linkage [39]. The coating could be removed by reduction with dithiothreitol, and transfections with coated particles

showed that the resultant reporter gene expression could be modulated by the extent of degradable coating and the strength of the intracellular reducing environment. Rather than using disulfide bond reduction to remove a stabilizing coating, Saito and coworkers designed polyplexes to become endosomolytically active in a reducing environment [40]. The cationic DNA-binding peptide protamine and the endosomolytic protein listeriolysin O were conjugated through a disulfide bond, rendering listeiolysin O inactive. This protamine-lysteriolysin O copolymer was designed to degrade in acidic vesicles and release active listeriolysin O to facilitate the endosomal escape of the remaining polyplex. In fact, an optimized loading of listeriolysin O to the polyplexes produced pronounced enhancements in reporter gene expression.

The internal polyplex structure can also be rendered sensitive to a reducing environment. A modified polylysine vector prepared by Pichon et al. has its amine charge centers connected to the polymer backbone by disulfide bonds [41]. Polyplexes prepared with this modified polylysine can be disrupted by reduction with dithiothreitol or glutathione and exhibit improvements in transfection efficiency relative to unmodified polylysine. Miyata et al. prepared polyplexes using a thiolated PEG-polylysine copolymer, then transferred the polyplexes to an oxidative solution to crosslink the copolymers within the polyplexes [42]. Their results indicated that the extent of intrapolyplex crosslinking and the density of the polymers' cationic charge both contribute to pDNA release upon reduction of the disulfide cross-links.

Similarly, McKenzie and coworkers prepared a series of synthetic peptides as delivery vectors and observed that inclusion of cysteine residues allowed for spontaneous disulfide bond formation upon pDNA condensation [43,44]. The disulfide bond

formation conferred a reduction in particle size and stability against shear stress, and the authors ascribed increases in transfection efficiency to enhanced pDNA release upon intracellular reduction of the disulfide bonds. For these materials, variation in the number of cysteine residues can be used to control the extent of disulfide crosslinking and the resulting stability.

The reversible polymerization of liposomes presents another opportunity for preparation of degradable complexes, and polymerized lipoplexes have been designed with susceptibility to degradation by reducing conditions. Balakirev et al. used lipoic acid, a molecule containing an unstable dithiolane ring, to prepare reactive amphiphiles that polymerized under oxidative conditions to condense pDNA into small particles [45]. The researchers implicated intracellular reduction by glutathione and NAD(P)H in the improved transfection efficiency of the reducible lipoplexes.

7.4 Cytoplasmic persistence and mobility

For certain applications, it may be sufficient to ensure the nucleic acids escape from the endocytic pathway and are released from delivery vectors. RNA interference approaches, for example, are designed to function in the cytoplasm and often rely on small oligonucleotides that can readily diffuse through the cytoplasm [46]. Unfortunately, delivery to the cytoplasm is inadequate for complete genes or plasmids that must access the cell's transcriptional machinery; these materials must traverse the cytoplasm and reach the cell nucleus.

Barring direct association of polyplexes and intracellular microtubules, observations of active, microtubule-dependent intracellular transport of PEI-pDNA

complexes [7] suggest that polyplex motion in cytoplasm occurs in the context of entrapment in endocytic vesicles. Intact polyplexes are typically dense and dozens or hundreds of nanometers in diameter, and those that escape endocytic vesicles cannot be assumed to exhibit significant movement in cytoplasm or to traffic to the cell nucleus. Diffusion in the cytoplasm is restricted by the structure of the cytoskeleton and the severe crowding presented by proteins, organelles, and other macromolecules [47,48]. The apparent immobility of intact polyplexes in cytoplasm suggests that these particles can only access the cell nucleus during cell division, when there is cytoplasmic mixing and degradation of the nuclear membrane. Reports of intact polyplexes visualized in the cell nucleus are uncommon in the literature. One hypothesis describing the intracellular trafficking of polyplexes suggests that the cytoplasm presents a “dead end” for intact polyplexes due to their large size and lack of active transport mechanisms. It is reasonable to assume that current systems will undergo vector unpackaging and/or degradation before or upon deposition in the cytoplasm.

Although vector unpackaging is necessary for the eventual function of the delivered nucleic acids, its consequence in the endocytic pathway or in the cytoplasm is exposure of nucleic acids to a destructive environment. Lechardeur et al. found that cytoplasmic nucleases limit pDNA to a half-life in cytoplasm of only 50-90 min [49]. Pollard et al. confirmed these observations, finding a pDNA half-life in cytoplasm of 2 h, and suggested various means of confronting this hazard, including saturation or inhibition of cytoplasmic nucleases or the use of artificial nucleic acids that would not be susceptible to the nucleases [50]. Ribeiro et al. took a parallel approach to demonstrate that replacement of specific labile sites in pDNA can confer some resistance to nuclease

degradation without sacrificing the in vitro expression levels obtained from that pDNA [51]. Similarly, Layzer and coworkers discovered chemical modifications to siRNAs that greatly enhance the half-life in plasma without compromised efficacy in vivo [52].

The size of the nucleic acid cargo affects its intracellular mobility. Polyplexes are typically used to deliver pDNA of 5,000 or more base pairs (bp). Unpackaged pDNA of this size is unlikely to escape degradation by traversing the cytoplasm. Lukacs et al. used fluorescence recovery after photobleaching (FRAP) to measure the size-dependent diffusion of nucleic acids in cells [46]. The diffusion coefficient of linear DNA fragments in cytoplasm dropped severely as the DNA length increased from 100 to 500 bp, and fragments longer than 2000 bp exhibited little to no diffusion. More recently, it has been demonstrated that the actin cytoskeleton is largely responsible for this restricted diffusion [53]. These results suggest that, for most plasmids, diffusion alone cannot facilitate transport of unpackaged pDNA from cytoplasm into the cell nucleus.

7.5 Nuclear delivery

While the precise mechanism of intracellular trafficking remains unknown, polyplexes are able to deliver some pDNA to the cell nucleus; however, the amount is likely only a small fraction of that delivered to cells [54]. Without incorporation of components to enhance nuclear delivery, significant pDNA delivery to the cell nucleus has rarely been visualized by microscopy. In their multiple particle tracking experiments, Suh and coworkers ascribed the absence of fluorescently-labeled PEI in cell nucleus to their use of non-dividing cells [7]. Fluorescence in situ hybridization (FISH) by Langle-Rouault et al. showed unpackaged pDNA only in cytoplasm, not in the nucleus, even

though a hundredfold increase in luciferase expression had indicated the authors had successfully designed a system for improved nuclear delivery [55].

Indirect confirmation of nuclear delivery from simple polycation-pDNA particles is provided by the numerous reports of non-zero expression levels from exogenous pDNA. The expression of reporter genes indicates that some pDNA has reached the cell nucleus and been transcribed. Despite efforts at direct visualization, it remains unclear whether this pDNA reaches the nucleus in the form of polyplexes, polyplex fragments, or unpackaged pDNA. Using in vitro transfection with PEI, Godbey et al. observed fluorescently-labeled PEI and pDNA in the cell nucleus [56]. The observations were made 4 h post-transfection, and the PEI and pDNA appeared to be associated.

Using transmission electron microscopy of cells transfected in vitro, we explored the intracellular fate of polyplexes prepared with PEI or with a β-cyclodextrin-containing polymer [2]. These efforts did not reveal intact polyplexes in the cell nucleus. However, by using immunolabeling of cells transfected with biotin-labeled pDNA, we were able to visualize unpackaged pDNA in both cytoplasm and nucleus of transfected cells (Figure 7.2). In contrast to the results of Godbey et al., these observations are consistent with a hypothesis of cytoplasmic vector unpackaging followed by nuclear import of unpackaged pDNA, either intact or as digested fragments. In experiments using flow cytometry of cells transfected with fluorescently-labeled pDNA, James and Giorgio noted but discounted the possible impact of degraded pDNA [57]. It is unknown if pDNA fragments can enter the nucleus more easily than intact pDNA (a possibility supported by the aforementioned results of Lukacs and coworkers [46]) or contribute measurably to observed transfection efficiencies.

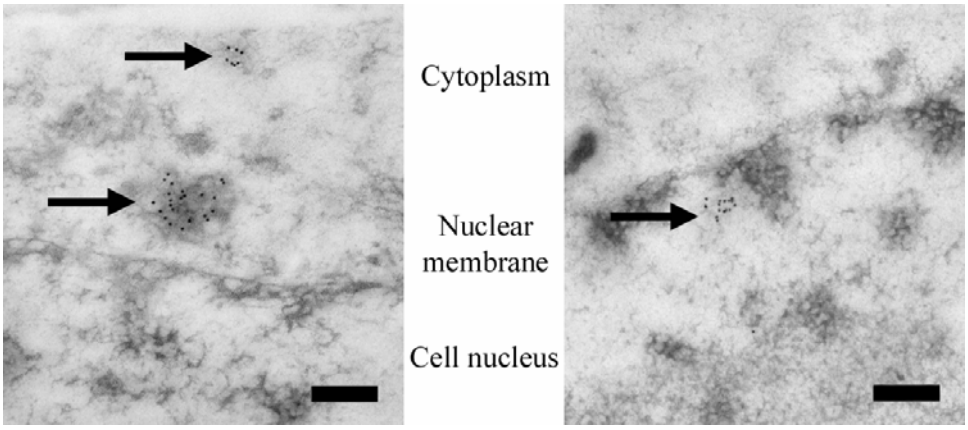

Figure 7.2 Observation of unpackaged intracellular pDNA through immunolabeling
Unpackaged intracellular nucleic acids can be visualized in the transmission electron microscope. Here, polyethylenimine was used to deliver biotin-labeled pDNA to BHK-21 cells in vitro. Cells were fixed and prepared in thin sections, and an anti-biotin antibody was used to label intracellular pDNA with colloidal gold. Clusters of gold particles (arrows) in the cytoplasm (left) or cell nucleus (right) indicate the presence of pDNA outside of intact polyplexes. Scale bars, 200 nm.

Although the mechanism of nuclear delivery is not clear, cell division appears to play a significant role. Brunner et al. and Mannisto et al. have shown that the transfection efficiencies of branched PEI and polylysine exhibit dependence on cell cycle [58, 59]. Similarly, multiple investigators have seen that mitosis produces an increase in transfection efficiency with liposomes [60-62]. Using microinjection of pDNA to cytoplasm and examining a range of pDNA doses, Ludtke et al. showed that compared to non-dividing cells, roughly twice as many dividing cells expressed a reporter gene [63]. A widely-accepted explanation for the positive correlation between transfection efficiency and cell division is that cytoplasmic pDNA can access the nucleus more easily upon the breakdown of the nuclear envelope in mitosis. As the intact actin cytoskeleton causes poor diffusivity of pDNA in cytoplasm [53], pDNA introduction to the cell nucleus may also be facilitated by cytoskeletal degradation and intracellular reorganization during cytokinesis.

In marked contrast to their work with other delivery agents, Brunner and coworkers observed that transfection with linear PEI was not affected by the cell cycle [58,64]. Consistent with this result, confocal microscopy by Wightman et al. showed pDNA association with the nucleus for linear PEI but not branched PEI [65]. Linear PEI shares its unusual cell-cycle independence with viral vectors, which can exploit viral mechanisms for nuclear delivery, and electroporation. A molecular-level explanation of how linear PEI and electroporation achieve cell-cycle independence could provide valuable insight for improving nuclear delivery of non-viral vectors.

In the design of synthetic gene delivery systems, reliance on cell division for nuclear delivery should be avoided because of the desire to target non-dividing cells in vivo. As transfection efficiency is not abolished entirely in non-dividing cells, existing systems likely achieve some nuclear delivery through one or more alternative mechanisms. Although the numerous nuclear pore complexes allow small solutes and proteins to pass freely through the nuclear envelope, pDNA (but not complexes, unless they are very small [66]) may be able to be transported into the cell nucleus through these pores via a passive or active transport mechanism. Too large to diffuse through the nuclear pore complexes by passive diffusion, karyophilic proteins are directed to the nucleus by a class of peptides known as nuclear localization signals (NLSs) [67-70]. NLS-containing proteins are carried to the cell nucleus through a nuclear pore complex in a stepwise, energy-dependent fashion. Efforts to incorporate a nuclear targeting component in a synthetic gene delivery system have focused on exploiting this natural pathway for nuclear delivery [71].

Conjugation to an NLS has been shown to enhance the nuclear delivery of carboplatin, a small molecule anticancer agent [72]. Analogously, some investigators have attempted to enhance nuclear delivery of delivered nucleic acids by direct labeling with NLSs. Sebestyen et al. utilized covalent attachment of an NLS to a linearized pDNA construct with a functional reporter gene [73]. When the construct was applied to digitonin-permeabilized cells, the NLS did not affect the resulting expression levels. These authors subsequently showed that an NLS markedly enhanced nuclear delivery of linear pDNA in microinjected cells for only DNA under 1500 bp [74]. Consistent with this result, a microinjected 900-bp linear expression cassette produced greater reporter gene expression when conjugated to the NLS. Moving beyond this size limit, Zanta et al. prepared a 3500-bp linear DNA fragment capped by a single terminal NLS [75]. When administered to cultured cells with a cationic lipid or with PEI, the NLS-labeled construct produced greater luciferase expression than an unlabeled construct or pDNA. However, the effect of the NLS was less pronounced in non-dividing cells or with increasing DNA doses.

The aforementioned reports all incorporated the NLS of the SV40 large T antigen. Early identification of this NLS has left it well-characterized in the literature, but there is no guarantee that this classical NLS is the most suitable option for non-viral delivery of nucleic acids. The wide variety of NLSs is accompanied by many independent import pathways. Although proteins directed for nuclear import are not necessarily restricted to a single pathway [68], the simultaneous function of independent pathways may indicate that certain cargoes are best suited for specific pathways [76]. Cellular nucleic acids

enter the nucleus on a distinct pathway from many proteins, as evidenced by the nuclear import of RNA-containing small nuclear ribonucleoprotein particles [77].

Rather than using the SV40 large T antigen NLS, Subramanian et al. conjugated the M9 NLS to a DNA-binding peptide and used cationic lipids to deliver the conjugate-pDNA complexes to cultured cells [78]. These M9-containing lipoplexes exhibited significant improvements in transfection efficiency relative to simple pDNA-lipid transfection, but formulations that excluded the peptide conjugate in favor of one or both of its unconjugated components also produced increases in reporter gene expression. Further, the number of peptides necessary to elicit these effects was enormous. As such, it is difficult to assess the extent to which the M9 NLS contributed to nuclear delivery through the expected mechanism. Using peptide nucleic acid (PNA) clamps to bind NLS peptides to linearized 5000-bp pDNA, Bremner et al. observed little enhancement in transfection efficiency with any of 4 NLSs: the SV40 large T antigen NLS, an extended version of this NLS, the M9 NLS, and the NLS of the human T cell leukemia virus type 1 Rex protein [79]. Only the minor increase with the extended SV40 large T antigen NLS was statistically significant.

The variable performance of NLSs in non-viral delivery could stem from multiple factors, including inhibitory interactions between NLSs and nucleic acids. The NLSs studied by Bremner et al. displayed electrostatic interactions with nucleic acids, and conjugation to pDNA impeded NLS binding to transport receptors [79]. Further, it is not clear that NLSs, whose natural function is in protein transport, can contribute to the transport of large pDNA. Another concern is a dearth of knowledge on the optimal NLS loading number and density. In their experiments with microinjected or digitonin-

permeabilized cells, Ludtke et al. observed a positive correlation between enhanced nuclear delivery and a greater number of NLSs per linear DNA construct [74]. An excessive NLS loading, however, may cause different regions of a single DNA construct to be directed simultaneously through multiple nuclear pore complexes, leaving the nucleic acid unable to enter the nucleus efficiently or entirely. Zanta et al. emphasized this point, designing their gene construct with a single, effectual NLS and estimating that the likelihood of simultaneous entry through multiple nuclear pore complexes was significantly enhanced for nucleic acids above 1000 bp [75].

Rather than incorporating an NLS, some investigators have sought to exploit the nuclear import machinery in an indirect manner. As shown by Kaneda et al., delivery of nuclear proteins concurrent with lipofection of pDNA enhances the pDNA nuclear delivery and gene expression [80]. These authors suspected that complexes of pDNA and nuclear proteins could protect pDNA from nucleases and facilitate pDNA transfer to the nucleus. Under the assumption that endogenous, newly-synthesized nuclear proteins can function in the same way, a number of investigators have proposed a “piggybacking” mechanism for pDNA delivery to the nucleus [76,81]. As newly-synthesized nuclear proteins will be in the cytoplasm and many will contain both a DNA-binding element and an NLS, this hypothesis suggests that DNA-binding elements of the nuclear proteins bind to unpackaged pDNA in the cytoplasm and carry this pDNA into the nucleus as they are carried there by the nuclear import machinery.

Dean and coworkers lent credence to the piggybacking hypothesis by demonstrating that the sequence of pDNA could affect its nuclear import, and that this import, requiring certain cytoplasmic factors, could be inhibited by restricting transport

through the nuclear pore complex [81,82]. Langle-Rouault et al. demonstrated a sequence-dependent effect using a plasmid containing the Epstein-Barr origin of replication, oriP [55]. The researchers used lipofection or microinjection to transfect a cell line that stably expressed Epstein-Barr nuclear antigen 1. Consistent with a hypothesis of enhanced nuclear delivery through interaction beween oriP and Epstein-Barr nuclear antigen 1, the oriP-containing plasmid showed a 100-fold transfection efficiency enhancement in the stably-expressing cell line. Similarly, Vacik et al. showed that expression of pDNA containing portions of the smooth muscle gamma actin promoter was markedly enhanced in cultured cells that express transcription factors specific to smooth muscle cells (SMCs) [83]. The enhanced expression was observed both in SMCs and in epithelial cells stably transfected to express an SMC serum response factor. Mesika et al. used the transcription factor NF-κB to develop a controllable method of nuclear delivery through piggybacking [84]. NF-κB is found predominantly in the cytoplasm unless its nuclear localization is activated by a particular stimulus. These investigators prepared pDNA with a repeating sequence of NF-κB binding sites, used a cationic dendrimer to transfect cells in vitro, and monitored luciferase reporter gene expression as a function of NF-κB stimulation. In the four cell lines investigated, an order of magnitude enhancement in gene expression was observed for transfection with the modified pDNA in conjunction with activation of NF-κB. Confocal microscopy verified that NF-κB activation improved nuclear delivery of the modified pDNA, leading the authors to conclude that the modified pDNA was binding NF-κB in the cytoplasm and accompanying it to the nucleus upon NF-κB activation.

For all systems, the morphology of the nucleic acids may have an impact on nuclear delivery efficiency. Studies in non-viral gene delivery tend to focus on closed circular pDNA, which is resistant to exonucleases and gives higher transfection efficiency than its linearized variant [79]. However, the best results to date with NLSs have utilized linearized nucleic acids [74,75,79]. In part, the disparate performance of circular and linearized pDNA may be due to differences in cytoplasmic mobility.

Existing non-viral delivery systems do not traverse the nuclear membrane with ease. NLSs act naturally to deliver cellular proteins to the nucleus, but the NLS function may not be transferable to larger entities such as pDNA thousands of bp in length. Further, the methods currently under study for nuclear delivery, including NLSs and piggybacking, may be severely undermined by the relative immobility of pDNA in cytoplasm if this immobility impedes the delivered nucleic acids from encountering the relevant proteins. The development of an efficient nuclear delivery method remains an area of opportunity.

7.6 Future directions

A variety of means are under development to address the intracellular barriers experienced by nucleic acids that are delivered by molecular conjugates. For example, the acidity of the endocytic pathway presents an opportunity for the engineering of endosomotropic mechanisms, and one approach to induce dissociation of polyplexes utilizes the reducing environment of the cell. Such modifications may become more effective with elucidation of the preferred time and location of endosomal escape and

vector unpackaging. Efforts to engineer improved persistence and nuclear delivery are also underway.

To date, non-viral approaches have not produced a full rival to the superior transfection efficiency of viral vectors. A particular intracellular barrier that remains to be addressed is the poor cytoplasmic mobility of larger nucleic acids. pDNA that is unpackaged from delivery vectors in the cytoplasm is likely to be degraded before it can diffuse to its place of function or to bind proteins that can confer nuclease protection and nuclear delivery. A mechanism for promoting cytoplasmic mobility, perhaps in conjunction with nuclear delivery, likely presents an opportunity for further improvements in transfection efficiency. As non-viral systems are commonly characterized by transient expression, opportunities also remain in prolonging expression. A successful approach by Nakai et al. achieved integration of exogenous pDNA by linearization; integration was further enhanced with incorporation of virally-derived inverted terminal repeats [85].

Recent research demonstrates that the intracellular trafficking of non-viral formulations is affected by the particles' morphology, size, and cellular uptake mechanism [2,5]. For example, Goncalves et al. recently demonstrated that the size of polylysine-pDNA complexes dictates whether they enter cells through clathrin-dependent or -independent pathways [5]. These authors used a variety of methods to present detailed characterizations of the materials' intracellular destination(s) and observed that clathrin-dependent internalization was more conducive to enhanced transfection. Because the physiochemical nature of the delivery formulation affects both its cellular uptake and its intracellular trafficking, progress in intracellular gene delivery requires

such elucidation of mechanisms for physiologically-relevant systems that are salt- and serum-stabilized, appropriately-sized, and targeted to specific cell types.

7.7 Conclusion: A systems approach

Among the numerous challenges of creating a non-viral delivery system exists a daunting one: the integration of the components into a workable system that combines the attributes of the components without suffering losses because of the integration. Examples of the detrimental effects of integration already exist: as shown in Chapter 3, PEGylation of polyplexes can endow them with serum stability but also greatly inhibit gene expression. The key issue is to develop delivery systems that provide the appropriate spatio-temporal functions, i.e., the system must perform particular functions in the right places at the right times to provide for effective transport of the nucleic acid to the desired site of action in mammals. This is likely to require an adaptive system, one that can sense its surroundings and respond dynamically to spatio-temporal, environmental changes. Early examples of these systems do exist [29], but much further progress employing this approach will be necessary to bring these entities from laboratory systems to practical “bedside” medicines.

7.8 References

1. Labat-Moleur F, Steffan AM, Brisson C, Perron H, Feugeas O, Furstenberger P, Oberling F, Brambilla E, Behr JP (1996) An electron microscopy study into the mechanism of gene transfer with lipopolyamines. Gene Ther. 3:1010-17.
2. Mishra S, Webster P, Davis ME (2004) PEGylation significantly affects cellular uptake and intracellular trafficking of non-viral gene delivery particles. Eur. J. Cell Biol. 83:97-111.
3. Mislick KA, Baldeschwieler JD (1996) Evidence for the role of proteoglycans in cation-mediated gene transfer. Proc. Natl. Acad. Sci. USA 93:12349-54.
4. Kopatz I, Remy JS, Behr JP (2004) A model for non-viral gene delivery: through syndecan adhesion molecules and powered by actin. J. Gene Med. 6:769-76.
5. Goncalves C, Mennesson E, Fuchs R, Gorvel JP, Midoux P, Pichon C (2004) Macropinocytosis of polyplexes and recycling of plasmid via the clathrin-dependent pathway impair the transfection efficiency of human hepatocarcinoma cells. Mol. Ther. 10:373-85.
6. Rejman J, Oberle V, Zuhorn IS, Hoekstra D (2004) Size-dependent internalization of particles via the pathways of clathrin- and caveolae-mediated endocytosis. Biochem. J 377:159-69.
7. Suh J, Wirtz D, Hanes J (2003) Efficient active transport of gene nanocarriers to the cell nucleus. Proc. Natl. Acad. Sci. USA 100:3878-82.
8. Fajac I, Allo JC, Souil E, Merten M, Pichon C, Figarella C, Monsigny M, Briand P, Midoux P (2000) Histidylated polylysine as a synthetic vector for gene transfer into immortalized cystic fibrosis airway surface and airway gland serous cells. J. Gene Med. 2:368-78.
9. Grosse S, Tremeau-Bravard A, Aron Y, Briand P, Fajac I (2002) Intracellular rate-limiting steps of gene transfer using glycosylated polylysines in cystic fibrosis airway epithelial cells. Gene. Ther. 9:1000-7.
10. Itaka K, Harada A, Yamasaki Y, Nakamura K, Kawaguchi H, Kataoka K (2004) In situ single cell observation by fluorescence resonance energy transfer reveals fast intra-cytoplasmic delivery and easy release of plasmid DNA complexed with linear polyethylenimine. J. Gene Med. 6:76-84.
11. Rosenkranz AA, Yachmenev SV, Jans DA, Serebryakova NV, Murav'ev VI, Peters R, Sobolev AS (1992) Receptor-mediated endocytosis and nuclear transport of a transfecting DNA construct. Exp. Cell Res. 199:323-9.
12. Akinc A, Langer R (2002) Measuring the pH environment of DNA delivered using nonviral vectors: implications for lysosomal trafficking. Biotechnol. Bioeng. 78:503-8.
13. Forrest ML, Pack DW (2002) On the kinetics of polyplex endocytic trafficking: implications for gene delivery vector design. Mol. Ther. 6:57-66.
14. Kulkarni RP, Mishra S, Fraser SE, Davis ME (2005) Single cell kinetics of intracellular, nonviral, nucleic acid delivery vehicle acidification and trafficking. Bioconjug. Chem. 16:986-94.
15. Erbacher P, Roche AC, Monsigny M, Midoux M (1996) Putative role of chloroquine in gene transfer into a human hepatoma cell line by DNA/lactosylated polylysine complexes. Exp. Cell Res. 225:186-94.

16. Gonzalez H, Hwang SJ, Davis ME (1999) New class of polymers for the delivery of macromolecular therapeutics. Bioconjug. Chem. 10:1068-74.
17. Midoux P, Mendes C, Legrand A, Raimond J, Mayer R, Monsigny M, Roche AC (1993) Specific gene transfer mediated by lactosylated poly-L-lysine into hepatoma cells. Nucl. Acids Res. 21:871-8.
18. Oupicky D, Carlisle RC, Seymour LW (2001) Triggered intracellular activation of disulfide crosslinked polyelectrolyte gene delivery complexes with extended systemic circulation in vivo. Gene Ther. 8:713-24.
19. Zhang X, Sawyer GJ, Dong X, Qiu Y, Collins L, Fabre JW (2003) The in vivo use of chloroquine to promote non-viral gene delivery to the liver via the portal vein and bile duct. J. Gene Med. 5:209-18.
20. Kyriakides TR, Cheung CY, Murthy N, Bornstein P, Stayton PS, Hoffman AS (2002) pH-sensitive polymers that enhance intracellular drug delivery in vivo. J Control. Release 78:295-303.
21. Behr JP (1997) The proton sponge - a trick to enter cells the viruses did not exploit. Chimia 51:34-36.
22. Kichler A, Leborgne C, Coeytaux E, Danos O (2001) Polyethylenimine-mediated gene delivery: a mechanistic study. J. Gene Med. 3:135-44.
23. Akinc A, Thomas M, Klibanov AM, Langer R (2005) Exploring polyethylenimine-mediated DNA transfection and the proton sponge hypothesis. J. Gene Med. 7:657-63.
24. Sonawane ND, Szoka FC, Verkman AS (2003) Chloride accumulation and swelling in endosomes enhances DNA transfer by polyamine-DNA polyplexes. J. Biol. Chem. 278:44826-31.
25. Forrest ML, Meister GE, Koerber JT, Pack DW (2004) Partial acetylation of polyethylenimine enhances in vitro gene delivery. Pharm. Res. 21:365-71.
26. Dubruel P, Christiaens B, Rosseneu M, Vandekerckhove J, Grooten J, Goossens V, Schacht E (2004) Buffering properties of cationic polymethacrylates are not the only key to successful gene delivery. Biomacromolecules 5:379-88.
27. Funhoff AM, van Nostrum CF, Koning GA, Schuurmans-Nieuwenbroek NME, Crommelin DJA, Hennink WE (2004) Endosomal escape of polymeric gene delivery complexes is not always enhanced by polymers buffering at low pH. Biomacromolecules 5:32-9.
28. Midoux P, Monsigny M (1999) Efficient gene transfer by histidylated polylysine/pDNA complexes. Bioconjug. Chem. 10:406-11.
29. Davis ME, Pun SH, Bellocq NC, Reineke TM, Popielarski SR, Mishra S, Heidel JD (2004) Self-assembling nucleic acid delivery vehicles via linear, water-soluble, cyclodextrin-containing polymers. Curr. Med. Chem. 11:179-97.
30. Pack DW, Putnam D, Langer R (2000) Design of imidazole-containing endosomolytic biopolymers for gene delivery. Biotechnol. Bioeng. 67:217-23.
31. Wang CY, Huang L (1984) Polyhistidine mediates an acid-dependent fusion of negatively charged liposomes. Biochemistry 23:4409-16.
32. Benns JM, Choi JS, Mahato RI, Park JS, Kim SW (2000) pH-sensitive cationic polymer gene delivery vehicle: N-Ac-poly(L-histidine)-graft-poly(L-lysine) comb shaped polymer. Bioconjug. Chem. 11:637-45.
33. Bielinska AU, Kukowska-Latallo JF, Baker JR (1997) The interaction of plasmid

DNA with polyamidoamine dendrimers: mechanism of complex formation and analysis of alterations induced in nuclease sensitivity and transcriptional activity of the complexed DNA. Biochim. Biophys. Acta 1353:180-90.

34. Schaffer DV, Fidelman NA, Dan N, Lauffenburger DA (2000) Vector unpacking as a potential barrier for receptor-mediated polyplex gene delivery. Biotechnol. Bioeng. 67:598-606.
35. Koping-Hoggard M, Varum KM, Issa M, Danielsen S, Christensen BE, Stokke BT, Artursson P (2004) Improved chitosan-mediated gene delivery based on easily dissociated chitosan polyplexes of highly defined chitosan oligomers. Gene Ther. 11:1441-52.
36. Hwang SJ, Bellocq NC, Davis ME (2001) Effects of structure of beta-cyclodextrin-containing polymers on gene delivery. Bioconjug. Chem. 12:280-90.
37. Forrest ML, Koerber JT, Pack DW (2003) A degradable polyethylenimine derivative with low toxicity for highly efficient gene delivery. Bioconjug. Chem. 14:934-40.
38. Choi JD, MacKay JA, Szoka FC (2003) Low-pH-sensitive PEG-stabilized plasmid-lipid nanoparticles: preparation and characterization. Bioconjug. Chem. 14:420-9.
39. Carlisle RC, Etrych T, Briggs SS, Preece JA, Ulbrich K, Seymour LW (2004) Polymer-coated polyethylenimine/DNA complexes designed for triggered activation by intracellular reduction. J. Gene Med. 6:337-44.
40. Saito G, Amidon GL, Lee K-D (2003) Enhanced cytosolic delivery of plasmid DNA by a sulfhydryl-activatable listeriolysin O/protamine conjugate utilizing cellular reducing potential. Gene Ther. 10:72-83.
41. Pichon C, LeCam E, Guerin B, Coulaud D, Delain E, Midoux P (2002) Poly[Lys-(AEDTP)]: a cationic polymer that allows dissociation of pDNA/cationic polymer complexes in a reductive medium and enhances polyfection. Bioconjug. Chem. 13:76-82.
42. Miyata K, Kakizawa Y, Nishiyama N, Harada A, Yamasaki Y, Koyama H, Kataoka K (2004) Block catiomer polyplexes with regulated densities of charge and disulfide cross-linking directed to enhance gene expression. J. Am. Chem. Soc. 126:2355-61.
43. McKenzie DL, Kwok KY, Rice KG (2000) A potent new class of reductively activated peptide gene delivery agents. J. Biol. Chem. 275:9970-7.
44. McKenzie DL, Smiley E, Kwok KY, Rice KG (2000) Low molecular weight disulfide cross-linking peptides as nonviral gene delivery carriers. Bioconjug. Chem. 11:901-9.
45. Balakirev M, Schoehn G, Chroboczek J (2000) Lipoic acid-derived amphiphiles for redox-controlled DNA delivery. Chem. Biol. 7:813-9.
46. Lukacs GL, Haggie P, Seksek O, Lechardeur D, Freedman N, Verkman AS (2000) Size-dependent DNA mobility in cytoplasm and nucleus. J. Biol. Chem. 275:1625-9.
47. Luby-Phelps K (2000) Cytoarchitecture and physical properties of cytoplasm: volume, viscosity, diffusion, intracellular surface area. Int. Rev. Cytol. 192:311-20.

48. Lechardeur D, Lukacs GL (2002) Intracellular barriers to non-viral gene transfer. Curr. Gene Ther. 2:183-94.
49. Lechardeur D, Sohn KJ, Haardt M, Joshi PB, Monck M, Graham RW, Beatty B, Squire J, O'Brodovich H, Lukacs GL (1999) Metabolic instability of plasmid DNA in the cytosol: a potential barrier to gene transfer. Gene Ther. 6:482-97.
50. Pollard H, Toumaniantz G, Amos JL, Avet-Loiseau H, Guihard G, Behr JP, Escande D (2001) Ca2+-sensitive cytosolic nucleases prevent efficient delivery to the nucleus of injected plasmids. J. Gene Med. 3:153-64.
51. Ribeiro SC, Monteiro GA, Prazeres DMF (2004) The role of polyadenylation signal secondary structures on the resistance of plasmid vectors to nucleases. J. Gene Med. 6:565-73.
52. Layzer JM, McCaffrey AP, Tanner AK, Huang Z, Kay MA, Sullenger BA (2004) In vivo activity of nuclease-resistant siRNAs. RNA 10:766-71.
53. Dauty E, Verkman AS (2005) Actin cytoskeleton as the principal determinant of size-dependent DNA mobility in cytoplasm: a new barrier for non-viral gene delivery. J. Biol. Chem. 9:7823-8.
54. Pollard H, Remy JS, Loussouarn G, Demolombe S, Behr JP, Escande D (1998) Polyethylenimine but not cationic lipids promotes transgene delivery to the nucleus in mammalian cells. J Biol. Chem. 273:7507-11.
55. Langle-Rouault F, Patzel V, Benavente A, Taillez M, Silvestre N, Bompard A, Sczakiel G, Jacobs E, Rittner K (1998) Up to 100-fold increase of apparent gene expression in the presence of Epstein-Barr virus oriP sequences and EBNA1: implications of the nuclear import of plasmids. J. Virol. 72:6181-5.
56. Godbey WT, Wu KK, Mikos AG (1999) Tracking the intracellular path of poly(ethylenimine)/DNA complexes for gene delivery. Proc. Natl. Acad. Sci. USA 96:5177-81.
57. James MB, Giorgio TD (2000) Nuclear-associated plasmid, but not cell-associated plasmid, is correlated with transgene expression in cultured mammalian cells. Mol. Ther. 1:339-46.
58. Brunner S, Sauer T, Carotta S, Cotten M, Saltik M, Wagner E (2000) Cell cycle dependence of gene transfer by lipoplex, polyplex and recombinant adenovirus. Gene Ther. 7:401-7.
59. Mannisto M, Ronkko S, Matto M, Honkakoski P, Hyttinen M, Pelkonen J, Urtti A (2005) The role of cell cycle on polyplex-mediated gene transfer into a retinal pigment epithelial cell line. J. Gene Med. 7:466-76.
60. Tseng WC, Haselton FR, Giorgio TD (1999) Mitosis enhances transgene expression of plasmid delivered by cationic liposomes. Biochim. Biophys. Acta 1445:53-64.
61. Mortimer I, Tam P, MacLachlan I, Graham RW, Saravolac EG, Joshi PB (1999) Cationic lipid-mediated transfection of cells in culture requires mitotic activity. Gene Ther. 6:403-11.
62. Escriou V, Carriere M, Bussone F, Wils P, Scherman D (2001) Critical assessment of the nuclear import of plasmid during cationic lipid-mediated gene transfer. J. Gene Med. 3:179-87.
63. Ludtke JJ, Sebestyen MG, Wolff JA (2002) The effect of cell division on the cellular dynamics of microinjected DNA and dextran. Mol. Ther. 5:579-88.

64. Brunner S, Furtbauer E, Sauer T, Kursa M, Wagner E (2002) Overcoming the nuclear barrier: cell cycle independent nonviral gene transfer with linear polyethylenimine or electroporation. Mol. Ther. 5:80-6.
65. Wightman L, Kircheis R, Rossler V, Carotta S, Ruzicka R, Kursa M, Wagner E (2001) Different behavior of branched and linear polyethylenimine for gene delivery in vitro and in vivo. J. Gene Med. 3:362-72.
66. Liu G, Li D, Pasumarthy MK, Kowalczyk TH, Gedeon CR, Hyatt SL, Payne JM, Miller TJ, Brunovskis P, Fink TL, Muhammad O, Moen RC, Hanson RW, Cooper MJ (2003) Nanoparticles of compacted DNA transfect postmitotic cells. J. Biol. Chem. 278:32578-86.
67. Gorlich D (1998) Transport into and out of the cell nucleus. EMBO J. 17:2721-7.
68. Mattaj IW, Engelmeier L (1998) Nucleocytoplasmic transport: the soluble phase. Annu. Rev. Biochem. 67:265-306.
69. Bednenko J, Cingolani G, Gerace L (2003) Nucleocytoplasmic transport: navigating the channel. J. Cell Biol. 162:391-401.
70. Weis K (2003) Regulating access to the genome: nucleocytoplasmic transport throughout the cell cycle. Cell 112:441-51.
71. Munkonge FM, Dean DA, Hillery E, Griesenbach U, Alton EWFW (2003) Emerging significance of plasmid DNA nuclear import in gene therapy. Adv. Drug Deliv. Rev. 55:749-60.
72. Aronov O, Horowitz AT, Gabizon A, Fuertes MA, Perez JM, Gibson D (2004) Nuclear localization signal-targeted poly(ethylene glycol) conjugates as potential carriers and nuclear localizing agents for carboplatin analogues. Bioconjug. Chem. 15:814-23.
73. Sebesteyen MG, Ludtke JJ, Bassik MC, Zhang G, Budker V, Lukhtanov EA, Hagstrom JE, Wolff JA (1998) DNA vector chemistry: the covalent attachment of signal peptides to plasmid DNA. Nat. Biotech. 16:80-5.
74. Ludtke JJ, Zhang G, Sebestyen MG, Wolff JA (1999) A nuclear localization signal can enhance both the nuclear transport and expression of 1 kb DNA. J. Cell Sci. 112:2033-41.
75. Zanta MA, Belguise-Valladier P, Behr JP (1999) Gene delivery: a single nuclear localization signal peptide is sufficient to carry DNA to the cell nucleus. Proc. Natl. Acad. Sci. USA 96:91-6.
76. Boulikas T (1997) Intl. J. Oncology 10:301.
77. Michaud N, Goldfarb D (1992) Microinjected U snRNAs are imported to oocyte nuclei via the nuclear pore complex by three distinguishable targeting pathways. J. Cell Biol. 116:851-61.
78. Subramanian A, Ranganathan P, Diamond SL (1999) Nuclear targeting peptide scaffolds for lipofection of nondividing mammalian cells. Nat. Biotech. 17:873-7.
79. Bremner KH, Seymour LW, Logan A, Read ML (2004) Factors influencing the ability of nuclear localization sequence peptides to enhance nonviral gene delivery. Bioconjug. Chem. 15:152-61.
80. Kaneda Y, Iwai K, Uchida T (1989) Increased expression of DNA cointroduced with nuclear protein in adult rat liver. Science 243:375-8.
81. Dean D (1997) Import of plasmid DNA into the nucleus is sequence specific. Exp. Cell Res. 230:293-302.

82. Wilson GL, Dean BS, Wang G, Dean DA (1999) Nuclear import of plasmid DNA in digitonin-permeabilized cells requires both cytoplasmic factors and specific DNA sequences. J. Biol. Chem. 274:22025-32.
83. Vacik J, Dean BS, Zimmer WE, Dean DA (1999) Cell-specific nuclear import of plasmid DNA. Gene Ther. 6:1006-14.
84. Mesika A, Grigoreva I, Zohar M, Reich Z (2001) A regulated, NFkappaB-assisted import of plasmid DNA into mammalian cell nuclei. Mol. Ther. 3:653-7.
85. Nakai H, Montini E, Fuess S, Storm TA, Meuse L, Finegold M, Grompe M, Kay MA (2003) Helper-independent and AAV-ITR-independent chromosomal integration of double-stranded linear DNA vectors in mice. Mol. Ther. 7:101-11.

CHAPTER 8: RECOMMENDATIONS FOR FUTURE WORK

This thesis has described the importance of a systems approach in the development of non-viral gene delivery vectors. The gene delivery particles studied here have consisted of simple complexes between nucleic acids and polycations, or such complexes modified after formulation by addition of a poly(ethylene glycol) coat. Analysis of these particles' behavior in vitro provides information about their relative performance and possible shortcomings. However, particles developed for systemic administration should be targeted to specific cell types. In many cases, therapeutic performance will require expression (with plasmid DNA) or repression (with small interfering RNA) of particular genes in certain cells of the body. Further, targeted particles will likely require lower doses than nonspecific particles to achieve the desired function. The necessity of a systems approach, as indicated by this thesis, suggests that further studies (both in vitro and in vivo) be undertaken with particles targeted to specific cells, either through addition of cell-specific ligands or through use of genes which are expressed only in certain cell types. For particles targeted using a surface ligand, the ligand itself may very well influence the gene delivery behavior and performance of the gene delivery particles. Studies characterizing the behavior of targeted, salt-stabilized, and fully-assembled particles are necessary for improved, therapeutically-relevant understanding of non-viral gene delivery.

With the difficulty in developing synthetic materials that generate therapeutically-relevant gene expression, the fate and consequences of non-viral gene delivery vectors have not been extensively investigated. The toxicity of polycationic vectors has been

addressed through development of novel materials, including the cyclodextrin-containing polycations studied in this thesis. The data presented in Chapter 2 show that the chemical structure of the delivery vector is directly related to its toxicity, offering means of developing materials with an optimized balance between gene transfer and toxicity. Such efforts would benefit from an improved understanding of the source and nature of polycation toxicity. With reduced toxicity, non-viral gene delivery systems can be applied in larger doses, allowing for improved gene transfer.

A significant impediment to non-viral gene delivery is likely the metabolic instability and poor cytoplasmic mobility of larger nucleic acids. Nucleic acids that are unpackaged from delivery vectors in the cytoplasm are likely to be sequestered or degraded before having an opportunity to carry out their function. Further improvements in transfection efficiency will likely result from improved cytoplasmic mobility and/or persistence. As vector unpackaging is required for delivered nucleic acids to function, and appears to occur prior to nuclear delivery with some of the systems examined in this thesis, these aims may best be pursued by a design which assumes (and exploits) vector unpackaging in the endocytic pathway or cytoplasm and includes additional modifications for cytoplasmic mobility and/or persistence. Sample strategies include the use of peptides or ligands to target particular intracellular destinations or the use of modified nucleic acids to inhibit degradation. Thus, there is impetus for the design of non-viral gene delivery systems that can both self-assemble upon formulation and partially unpackage after cellular uptake, allowing for polycation unpackaging from nucleic acids while maintaining intracellular targeting or protective features.